2017

Synthesis and Biological Evaluation of Gymnastatin Analogues

Felicia Mutuma
Technological University Dublin

Synthesis and biological evaluation of gymnastatin analogues

By

Miss. Felicia C. Mutuma B.Sc.

A thesis presented to

Dublin Institute of Technology for the award of

Doctor of Philosophy

Prepared under the supervision of

Dr Gráinne C. Hargaden

School of Chemical and Pharmaceutical Sciences, Dublin Institute of Technology,

Kevin St, Dublin 8

and

Dr Brendan Duffy

Centre for Research in Engineering Surface Technology, Focas Institute,

Dublin Institute of Technology, Kevin St, Dublin 8

July 2017

Abstract

A library of eight novel gymnastatin analogues has been prepared. The compounds consist of an unsaturated side chain linked to a tyrosine unit using an amide bond. The compounds have various chain lengths and degrees of conjugation. Additional functionality was added to the tyrosine unit by methylation of the acid side group to prepare methyl ester derivatives. While gymnastatins have shown promising cytotoxic activity, their mode of action is not fully understood. The prepared compounds were evaluated against the A549 cancer cell line. A selection of the compounds were further evaluated for inhibition against POLO like kinase (Plk1).

The methyl ester derivatives showed more activity than compounds containing the acid side group. It was also observed that increasing the chain length resulted in increased activity against the cancer cells. The presence of an additional alkene did not significantly improve the activity. Furthermore, preliminary results of the activity of compounds using an ELISA assay showed that the compounds containing the methyl ester side group inhibited Plk1, while compounds with the acid side group showed no inhibition.

An introduction to gymnastatins is presented in Chapter 1 of this thesis. Chapter 2 contains a review of iron oxide nanoparticles, their synthesis and applications in targeted delivery. Due to time constraints, this part of the proposed study was not carried out synthetically. The synthesis and biological evaluation of gymnastatin analogues are presented in Chapter 3 and 4 respectively. The conclusions and future work are presented in Chapter 5. Finally, Chapter 6 details the experimental procedures employed in this work.

Declaration

I certify that this thesis which I now submit for examination for PhD is entirely my own work and has not been taken from the work of others, save and to the extent that such work has been cited and acknowledged within the text of my work.

This thesis was prepared according to the regulations for postgraduate studies by research of the Dublin Institute of Technology and has not been submitted in whole or in part for an award in any Institute or University.

The work on in this thesis conforms to the principles and requirements of the DIT's guidelines for ethics in research.

Signature Date:

_____ _____

Felicia C. Mutuma

Acknowledgements

I would like to express my gratitude to my supervisors, Gráinne Hargaden and Brendan Duffy for their support and guidance over the course of my PhD.

I would also like to thank Alan Casey for all his help on the biology aspect of this project.i want to thank Martin Kitson, Annette Callaghan, Jimmy Muldoon, Hugh Byrne, Jyothi Nair and all the technicians and staff in the School of Chemistry, CREST and the Focas Institute for all their help and support over the years.

My sincere thanks also go to Sarah Rawe, Craig Hicks, Miriam Kennedy, Sandra Gannon and Laura Perdisatt for everything they taught me before and at the start of my PhD.

Finally, I would like to thank my friends and family, particularly Mum, Damian, Neil and Nicky.

Abbreviations

1D	1 Dimensional
2D	2 Dimensional
A549	Human pulmonary adenocarcinoma
AB	Alamar blue
AcOH	Acetic acid
AFM	Atomic Force Microscope
AIDS	Acquired Immune Deficiency Syndrome
AOS	Alpha-olefin sulfonate
APC/C	Anaphase Promoting Complex
ATI	Alveolar type I
ATII	Alveolar type 2
BEAS-2B	Human bronchial epithelium, normal
Boc	tert-butyloxycarbonyl
Caco-2	Human epithelial colorectal adenocarcinoma
calc'd	calculated
Cdk	Cyclin-dependent kinase
CHS	Continous hydrothermal system
CLIOs	Cross linked iron oxide nanoparticles
COSY	Homonuclear correlation spectroscopy

CST	Critical solution temperature
CT-26	colon carcinoma
CTA	Cystamine tert-acylhydrazine
d	doublet
DCC	dicyclohexylcarbodiimide
dd	doublet of doublets
ddd	doublet of doublets of doublets
dddd	doublet of doublets of doublets of doublets
DIBAL-H	Di*iso*butylaluminium hydride
DIEA	di*iso*propylethylamine
DMAP	4-Dimethylaminopyridine
DMEM	Dulbecco's modified Eagle's medium
DMF	Dimethylformamide
DMP	Dess-Martin periodinane
DMSO	Dimethyl sulfoxide
DNA	Deoxyribonucleic acid
DOX	Doxorubicin
dt	doublet of triplets
E	*E*-isomer
ED_{50}	Effective dose for 50% of a group

EDC	N-(3-Dimethylaminopropyl)-N′-ethylcarbodiimide hydrochloride
EGFR	Epidermal growth factor receptor
ELISA	Enzyme-Linked Immunosorbent Assay
EPR	Enhanced permeability retention
FA	Folic acid
FBS	Fetal bovine serume
fcc	Face centred cubic
FTIR	Fourier transform infrared spectroscopy
HeLa	Human cervix epitheloid carcinoma
HER-2	human epidermal growth factor receptor 2
HMBC	Heteronuclear multiple-bond correlation spectroscopy
HRMS	High resolution mass spectrometry
HREIMS	High resolution electron ionisation mass spectrometry
HSQC	Heteronuclear single quantum correlation
HWE	Horner–Wadsworth–Emmons
IBX	2-iodoxybenzoic acid
IONP	Iron Oxide Nanoparticles
J	coupling constant

LCMS	Liquid chromatography mass spectrometry
LHRH	Leuteinizing Hormone-Releasing Hormone
log	logarithmic/exponential
LRMS	Low resolution mass spectrometry
m	multiplet
m/z	mass to charge ratio
MDT	Magnetic drug targeting
MNP	Magnetic Nanoparticle
MRI	Magnetic Resonance Imaging
MTD	Magnetic targeted delivery
MTT	3-[4,5-dimethylthiazol-2-yl]-2,5-Diphenyltetrazolium bromide
NaH	Sodium hydride
NaOH	Sodium hydroxide
nm	Nanometers
NMR	Nuclear magnetic resonance
P	Probability
PAC	poly (*N*- isopropylacrylamide-chitosan)
PBS	Phosphate buffered saline
PEG	Poly- ethylene glycol

PEI	Poly- ethylene imine
PEO	Polyethylene oxide
PEOTMA	Poly (ethylene oxide)-trimellitic anhydride chloride
PLGA	Poly (lactide-co-glycolide
Plk	POLO like kinase
PMA	Amphiphilic polymer
ppm	parts per million
PSMA	Prostate-Specific Membrane Antigen
PTX	Paclitaxel
PVBP	Poly(4-vinylbenzylphosphonate)
PVP	Polyvinylpyrrolidone
q	quartet
qd	quartet of doublets
quin	quintet
RAFT	Reversible addition fragmentation chain transfer
RES	Reticuloendothelial system
Rf	Retention factor
Rochelles Salt	Potassium sodium tartrate tetrahydrate

ROS	Reactive oxygen species
RT	Room temperature
s	singlet
sept	septet
SPIONP	Super-paramagnetic loaded nanoparticles
STM	Scanning Tunnelling Microscope
t	triplet
td	triplet of doublets
THF	Tetrahydrofuran
TLC	Thin layer chromatography
TMS	tetramethylsilane
UATR	Universal Attenuated Total Reflectance Accessory
UV	Ulta violet
UV-vis	Ultra violet- visible
v/v	Volume per volume
VEGF	Vascular endothelial growth factor
WSC	Water soluble carbodiimide
XPS	X-ray Photoelectron Microscope
Z	*Z*-isomer

α-Fe_2O_3	Hermatite
β-CD	β-cyclodextrin
γ-Fe_2O_3	Maghemite
μM	Micromolar

Table of Contents

List of Schemes

List of Figures

List of Tables

1 Gymnastatins as anticancer agents

1.1 Marine-Derived fungi as a source of bioactive natural products

Marine derived fungi are an ecological group divided into two subgroups, indigenous and non-indigenous species. Indigenous species can be further divided into obligate (exclusively grow and sporulate in the marine environment) and facultative fungi (retain their ability to grow and/or sporulate in the marine environment). Non-indigenous species stay dormant and are unable to grow and multiply in the marine environment.[1]

The investigation of marine-derived fungi as sources of natural products has been a promising and growing field since the discovery of unusual nucleoside derivatives in the sponge *Tethya crypta* in the 1950s by Bergmann and Feeney. The nucleosides provided the basis for antiviral and anticancer drugs, most notably Ara-C (cytarabine), an anticancer agent, and Ara-A (vidarabine), the first antiviral drug (Figure 1.1). [2-3]

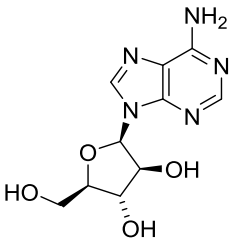

1

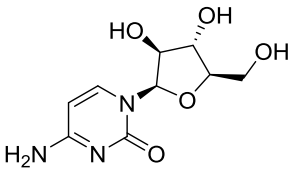

2

*Figure 1.1: Structures of Vidarabine **(1)** and Cytarabine **(2)***

Vidarabine **1** inhibits viral DNA polymerase and DNA synthesis of herpes, vaccinica and varicella zoster viruses. Cytarabine **2** is one of the most effective drugs for the treatment of acute myeloid leukemia.[4-5]

There have been several reports on the use of natural products derived from fungi as anti-viral, anti-microbial, anti-tumour, anti-inflammatory, anti-protozoal,

immunosuppressive, anti-fouling agents, and they also display a range of other bioactivities. [6-8]

1.1.1 Marine Sponges (Porifera)

Among all marine organisms investigated, sponges are the richest sources of new marine natural products, with over 4000 compounds to date, contributing to nearly 30% of all marine natural products discovered so far. Sponges are aquatic animals that dominate in benthic habitats. They produce secondary metabolites which protect them from microbial infections, biofouling and overgrowth by other organisms. This property makes them attractive as natural products.

Gymnascella dankaliensis OUPS- N134 is derived from one such sponge, *Halichondria Japonica*. Several strains have been isolated from *Halichondria Japonica* e.g. Phoma sp. Q60596 which gave rise to the antibiotic YM-202204 which exhibits potential antifungal activity (Fig 1.2). Other products with antibacterial, antileukemic, antimalarial and anticancer activity have also been reported. [7-9]

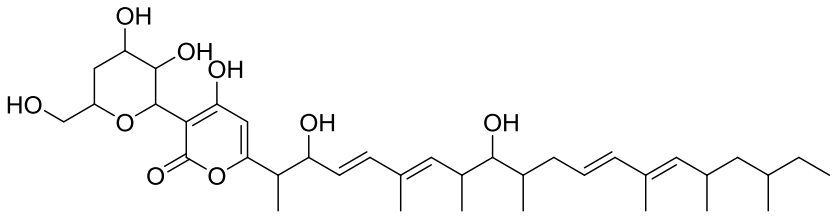

3

Figure 1.2: Chemical structure of antibiotic YM-202204 ***(3)***

Gymnastatins are produced by a strain of *Gymnascella dankaliensis* OUPS-N134 which was initially isolated from the sponge *Halichondria japonica (Figure 1.3)*, collected from Osaka bay in Japan in April 1994.

Figure 1.3: Image of H. Japonica

Several gymnastatins have shown potent cytotoxicity and growth inhibition against cultured human cancer cell lines.[10] Gymnastatins and their derivatives studied to date are discussed below.

1.2 Gymnastatins A-E

Gymnastatins were first isolated and their stereostructures established by Numata and co-workers in 1998.[10] They reported the isolation and establishment of stereostructures of gymnastatins A-E (Figure 1.4) which exhibited significant cytotoxicity against tumour cells.

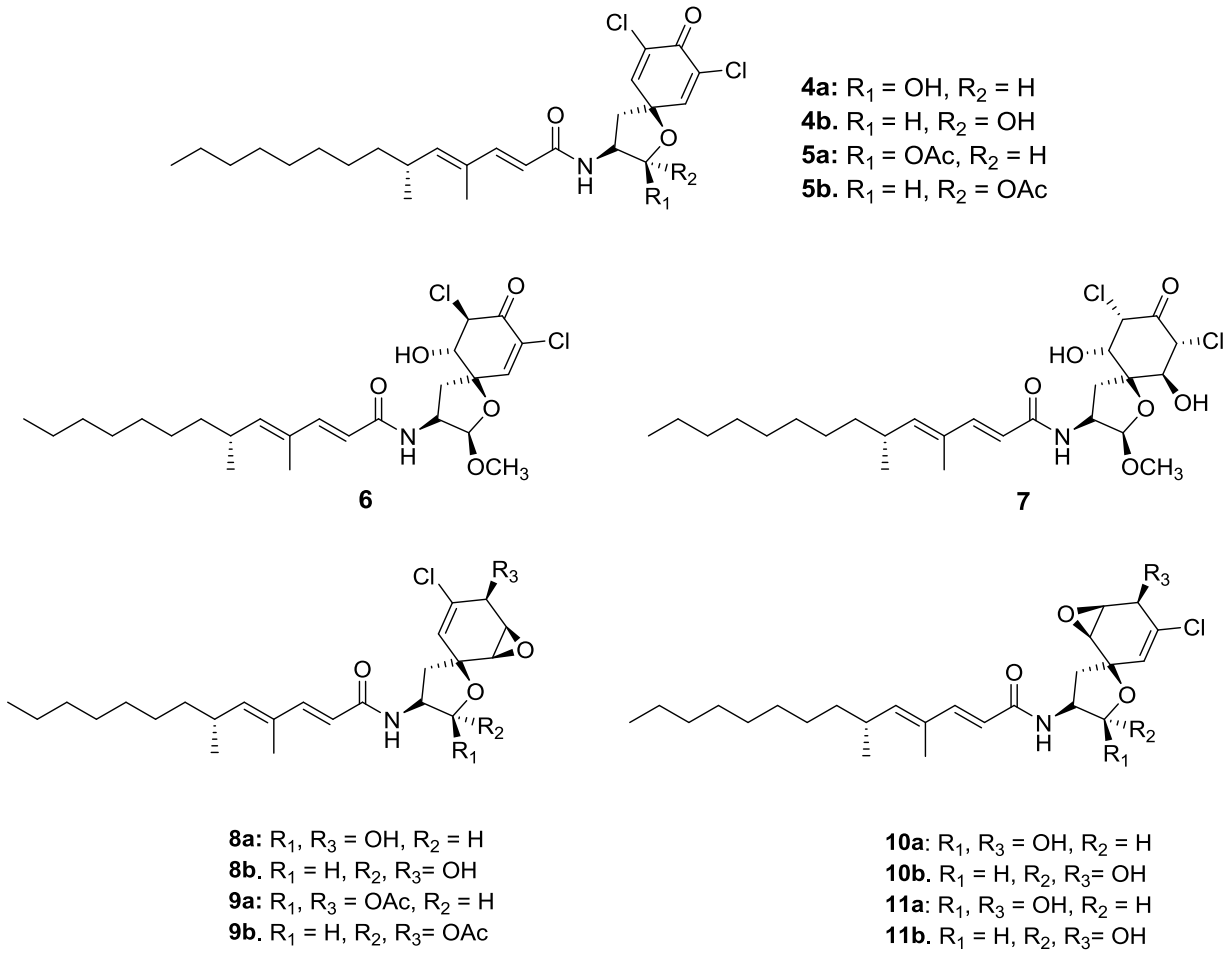

*Figure 1.4: Structures of Gymnastatin A (**4, 5**), Gymnastatin B (**6**), Gymnastatin C (**7**), Gymnastatin D **(8-9)**, Gymnastatin E **(10-11)***

Upon evaluation, NMR data suggested that gymnastatin A existed in a 2:1 mixture of stereoisomers (**4a** and **4b**) which could not be separated by column chromatography; however, acetylation afforded two separable acetates (**5a** and **5b**). Gymnastatins B-C existed as single isomers. Gymnastatins D-E both contain epoxy rings and are isomeric with each other. Like gymnastatin A they also exist in a 2:1 mixture of stereoisomers (**8a** and **8b; 10a** and **10b**). Acetylation of the two stereoisomers gave diacetates which could be separated by column chromatography (**9a** and **9b; 11a** and **11b**).

Cytotoxicity activities of compounds A-C were examined in the P388 lymphocytic leukemia test system according to a method reported by Numata *et al*.[11] This study showed that all three compounds exhibited significant potency against the cancer cell line. Gymnastatin A was the most potent with an ED_{50} of 0.018 $\mu g.cm^{-3}$ compared to gymnastatins B and C (0.108 and 0.106 $\mu g.cm^{-3}$). The strong cytotoxicity in gymnastatin A was attributed to the conjugated ketone. [10,11]

Ogamino *et al* reported the synthesis of Gymnastatin A with oxidative cyclisation, amide coupling and Evans asymmetric alkylation as key steps.[12] (Scheme 1.1).

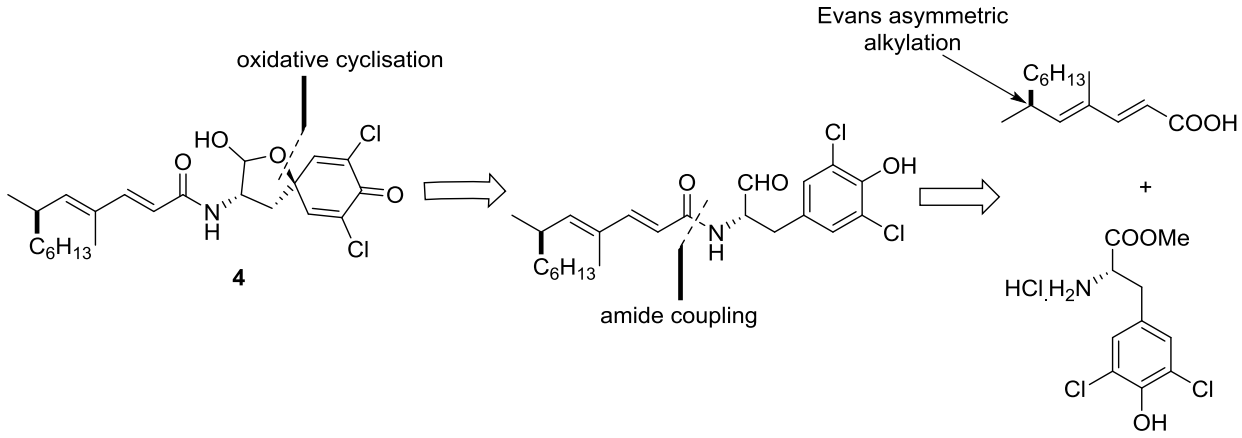

*Scheme 1.1: Retrosynthetic analysis of Gymnastatin A **(4)** reported by Ogamino et al.*

1.3 Gymnastatin F, G, H and gymnamide

Amagata reported the isolation and structure elucidation of gymnastatins F-H and gymnamide. (Fig 1.5).[13] All compounds featured the same side chain as the gymnastatins previously reported. However, gymnastatins F, G and H possessed different ring systems. Gymnastatin F and G feature a unique bicyclo[3.3.1]nonane ring system whereas gymnastatin H has a tyrosine methyl ester moiety.

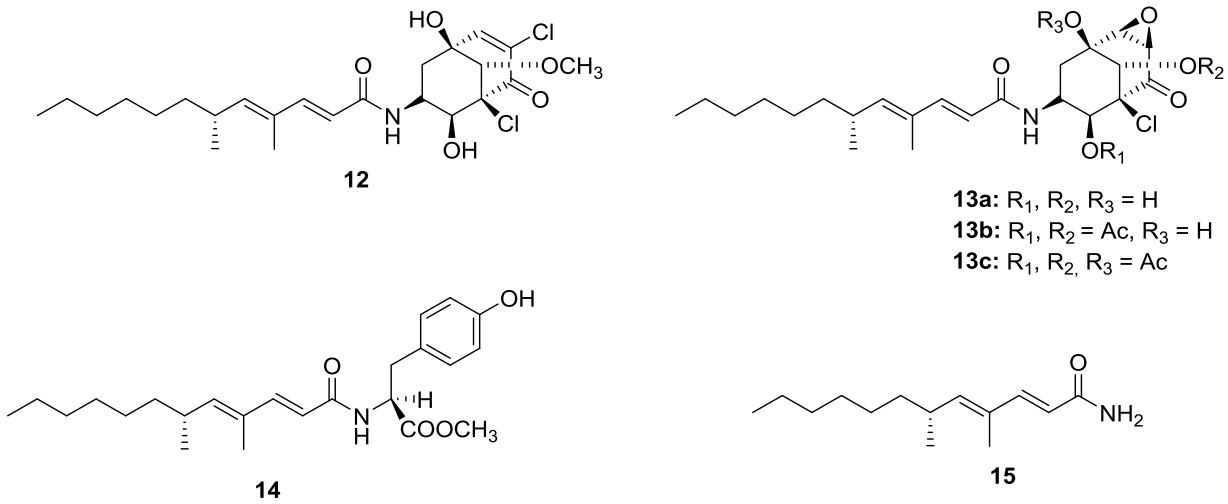

*Figure 1.5: Structures of Gymnastatin F (**12**), Gymnastatin G (**13**), Gymnastatin H (**14**) and Gymnamide (**15**)*

The structure elucidation as well as the relative stereochemistry were determined by 1D and 2D NMR. Gymnastatin G **13** was acetylated due to instability during NMR measurements. It has the molecular formula $C_{24}H_{35}NO_4$ established by HREIMS (High-Resolution Electron Ionisation Mass Spectrometry). The total synthesis of gymnastatin H allowed for its stereoconfiguration to be determined. (Scheme 1.2)

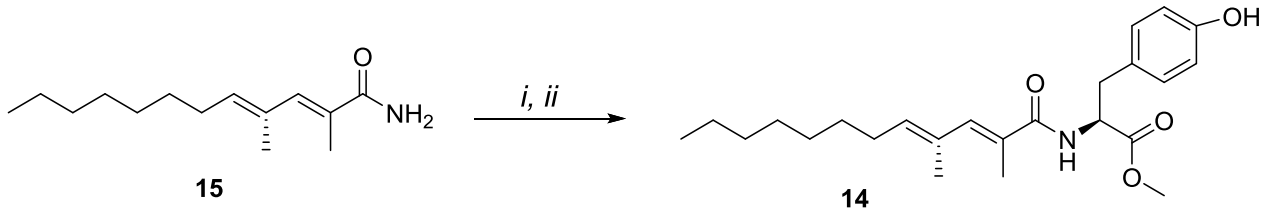

*Scheme 1.2: Synthesis of Gymnastatin H **(14)** from Gymnamide **(15)** - (i) KOH, (ii) L-tyrosine methyl ester, WSC.*

Gymnamide **(15)** which was also isolated from Halichondria sponge derived from *Gymnascella dankaliensis* was hydrolysed to give an acid which was subsequently treated

with *L*-tyrosine methyl ester in the presence of water soluble carbodiimide to furnish the desired molecule **14**.[11]

Gymnastatins F-H and gymnamide were evaluated for cancer cell growth inhibition against the P388 lymphocytic leukemia cell line. Upon evaluation, gymnastatins F and G showed significant growth inhibition (ED_{50} 0.13, 0.03 $\mu g.cm^{-3}$, respectively). Gymnastatin H and gymnamide were inactive.[13,14]

Raffier *et al* used diastereoselective photodeconjugation of an α, β-unsaturated ester to synthesise gymnastatin H starting with aldehydes. (Scheme 1.3)[15] The synthesis was achieved in 14 synthetic steps.

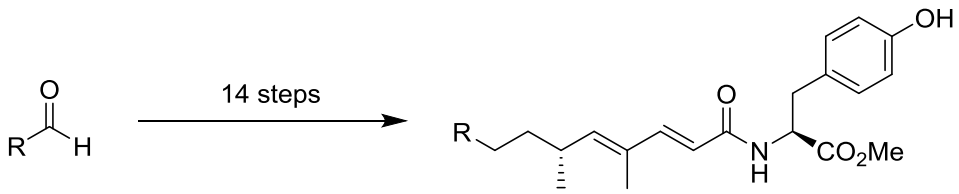

Scheme 1.3: Gymnastatin H synthesis reported by Raffier et al.

1.4 Gymnastatins Q and R

Gymnastatins Q and R were isolated in 2008 and their structures elucidated (Fig 1.6).[11]

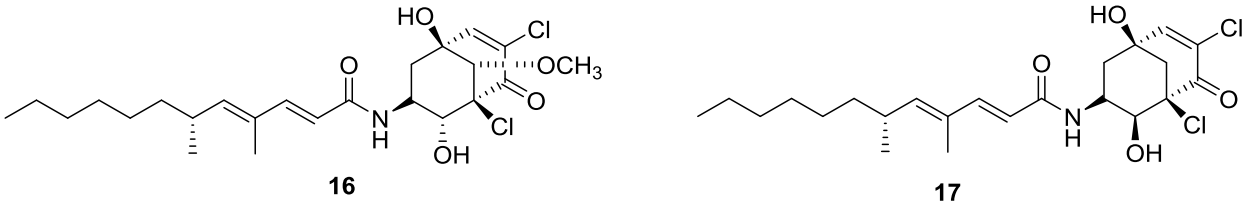

*Figure 1.6: Structures of Gymnastatin Q **(16)** and Gymnastatin R **(17)***

The cancer cell growth inhibition properties of gymnastatin Q and R were examined against P388 lymphocytic leukemia cell line (ED_{50} 1.7, 2.8 $\mu g.cm^{-3}$, respectively).

Furthermore, gymnastatin Q showed growth inhibition against BSY-1 (breast) and MKN7 (stomach) cell lines (IC_{50} = 0.7, 0.71 µg.cm^{-3}, respectively) [14]

1.5 Gymnastatins I-K, S-Y and 11'-carboxygymnastatin N

More recently, gymnastatins I-K and T-Y (Figure 1.7) were isolated from a soil fungus collected near the Giza pyramids in Egypt and assessed for biological activity. [16-18]

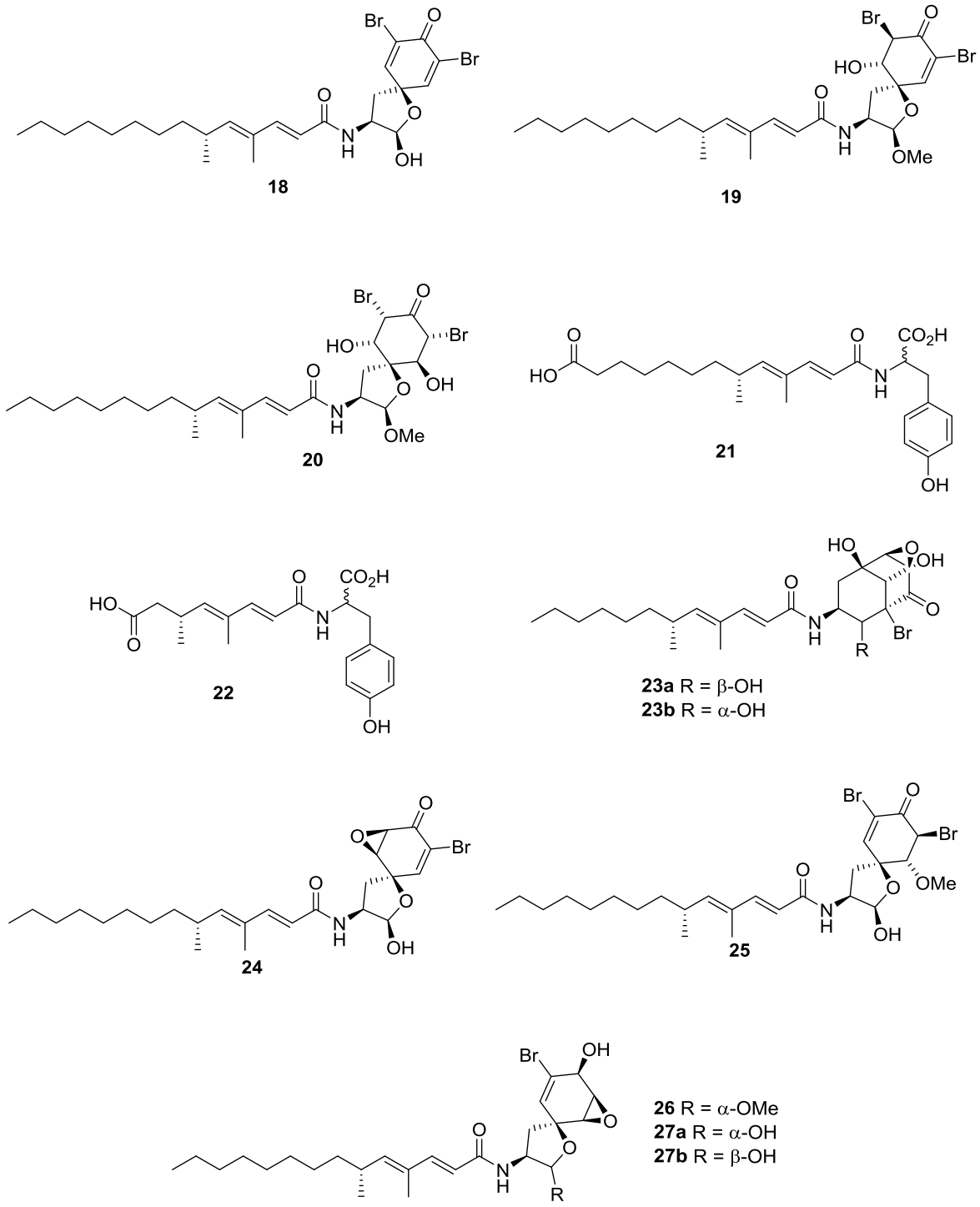

Figure 1.7: Structures of Gymnastatins I-K ***(18-20),*** *11'-carboxygymnastatin N* ***(21),*** *Gymnastatin S-Y* ***(22-27)***

Gymnastatins I-K, T-Y are brominated tyrosine derived alkaloids. Gymnastatins T, V, Y, I, J and K can be considered derivatives of gymnastatins G, D, A, B and C whose chlorines

have been replaced by bromine. *Halichondria* is known to produce mainly chlorinated alkaloids. Halogenating enzymes including halogenases and haloperoxidases have been discovered and are used to halogenate natural products. Hammerschmidt and Wang *et al.* fermented fungal cultures isolated from *Halichondria* in the presence of NaCl or KBr to produce chlorinated or brominated metabolites respectively. The fungal controls were not chlorinated or brominated as indicated by LCMS. [17]

Gymnastatins I-K, T-Y **(18-27b)** were evaluated for their cytotoxicity against murine lymphoma L5178Y cell line.[18] They showed moderate to significant activity against the cancer cell line (IC_{50} 0.078 to 14.1 μM). Gymnastatin K was the most potent (0.078 μM). A comparison between **25** *vs* **27** and **19** *vs* **20** suggested the conjugated ketone system to be important for the cytotoxic activity (Table 1.1). Gymnastatins I **(18)** and J **(19)** were compared to their chlorinated analogues, gymnastatins A **(1)** and B **(2)**. Gymnastatin I showed similar activity to gymnastatin A, whereas gymnastatin I exhibited much stronger activity than gymnastatin B[17,18]

Entry	Compound	IC_{50} (μM)
18	Gymnastatin I	0.55
19	Gymnastatin J	0.078
20	Gymnastatin K	9.6
23a	Gymnastatin T	1.3
23b	Gymnastatin U	3.0
24	Gymnastatin V	3.6
25	Gymnastatin W	0.99
26	Gymnastatin X	14.1
27a	Gymnastatin Y	6.2
27b	Gymnastatin Y	3.0
4	Gymnastatin A	0.64
6	Gymnastatin B	5.8

Table 1.1: Cytotoxicity of gymnastatins against L5178Y mouse lymphoma cells

1.6 Gymnastatin N

It has been suggested that gymnastatin N **28** (Figure 1.8) is an important intermediate in the biosynthetic pathway of tyrosine derived amides isolated from *Gymnascella* derived alkaloids.

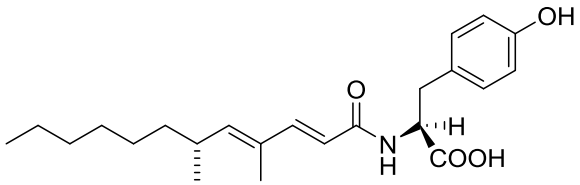

28

*Figure 1.8: Structure of Gymnastatin N **(28)***

Gymnastatin N has an intact tyrosine unit. Cytotoxic evaluation of gymnastatins has shown no cytotoxic activity of compounds with an intact tyrosine unit. However, an examination of the biological properties of gymnastatin N **28** and a range of analogues showed that gymnastatin N and its analogues inhibited the protein kinase POLO-like kinase (Plk 1).[17-19] It was proposed that the conjugated diene and free acid on the tyrosine unit functionalities were responsible for bioactivity against Plk1.[19]

1.6.1 Plk1 and protein kinases

Protein kinases are enzymes that phosphorylate specific amino acids in protein substrates. They are involved in a wide variety of growth hormones and growth factors which trigger cell growth and cell division. In most cancers, there is an overexpression or excess of a growth hormone. In other cases, there is an excess of a protein kinase receptor. Due to their role in processes that drive cell growth and division, there has been keen interest in developing and using protein kinase inhibitors as anti-cancer agents.[20]

Plk1 is a protein kinase belonging to a family of serine-threonine kinases. Plk1 plays a key role in regulating the cell cycle and ensuring proper cell cycle progression. Other proteins called cyclins, and enzymes, including cycline-dependent kinases (Cdk), also play various roles in different stages of the cell cycle. Cdk 1 functions as a serine-threonine kinase and is sequentially activated and deactivated during the cell cycle as required. Excessive and insufficient production of these enzymes has been associated

with imbalances and errors in the cell cycle which lead to tumourigenesis, birth defects and spontaneous abortions.[21-23]

1.6.2 The Cell Cycle

The cell cycle is divided into four phases, the G_1, S, G_2 and the M phase. During the S phase, the cell replicates its nuclear DNA. The M-phase is the most important part of the entire cell cycle and it consists of six stages followed by cytokinesis (Figure 1.9). It is accompanied by major reorganization of the entire cell. Events in the M-phase vary in different organisms; however, the fundamental and basic events are conserved in eukaryotic cells. These events include chromosome condensation, formation of the mitotic spindle, attachment of the chromosomes to the spindle microtubules and finally the formation of daughter nuclei. During the gap phases (G_1 and G_2) the cell monitors its environment to ensure the conditions are suitable before moving on to the S or M phases. The gap phases also give the cell time to grow. Plk1 as well as cycline-dependent kinases (Cdks) are prominent in the M-phase.[22, 24,25]

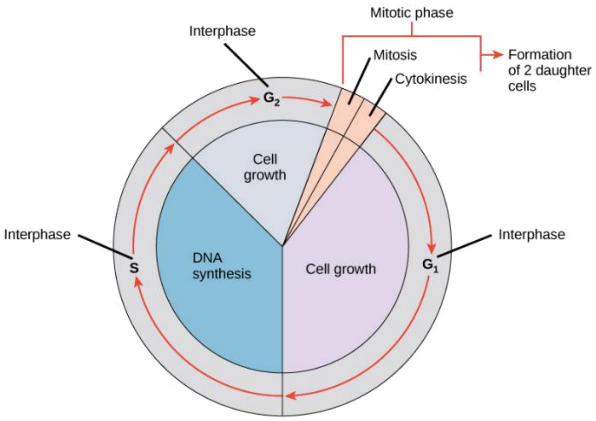

Figure 1.9: Schematic view of the cell cycle in eukaryotic cells.[26]

1.6.3 Plk1 and cancer

Excessive, insufficient and/or deregulation of Plk1 has been associated with imbalances and errors in the cell cycle which lead to tumourigenesis, birth defects and spontaneous

abortions. Several studies have linked overexpression of Plk1 with numerous types of cancer and their aggressiveness, e.g. lung, oesophageal, gastric, melanoma, and breast cancers. If Plk1 can enhance tumour formation, then selective inhibition of Plk1 can be used to achieve tumour regression. Hence Plk1 has been proposed as a prognostic marker for malignancies and as a potential target for cancer therapy.[27-30]

Efforts are ongoing to identify molecular inhibitors of Plk1. These inhibitors would deplete Plk1 activity at various stages of the cell cycle where Plk1 is prominent, thereby suppressing tumour growth. In several studies, inhibitors have induced apoptosis and caused mitotic spindle abnormalities thereby inhibiting tumour cell proliferation. One such molecule is ON01910 (Figure 1.10) which was found to be a potent inhibitor and exhibits very little or no toxicity[21, 27, 31]

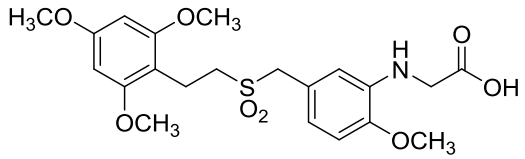

25

Figure 1.10: Structure of ON01910

ON01910, trade name Estybon inhibits Plk1 and is currently on Phase III clinical trials for the treatment of chronic myelomonocytic leukaemia.[32]

1.7 Conclusion

This chapter introduces gymnastatins beginning with their first discovery and details the gymnastatins that have been reported to date. The cytotoxicity of these compounds against various cell lines are also discussed. Moreover, an overview of protein kinases and Plk1, the role they play in the cell cycle, and their relevance to cancer is presented. Although gymnastatins have shown promising cytotoxic activity, their mode of action of gymnastatins is not fully understood. Literature reports to date focus primarily on the

natural product chemistry and there is little detail on the mechanism of action of these and other related compounds.

1.8 References

1. Kim, S; *Marine Pharmacognosy: Trends and Applications*. CRC Press, **2012.**
2. Bergmann, W.; Feeneyz, R. J. *J. Am. Chem. Soc.* **1950**, *72* (1), 2809–2810.
3. Bergmann, W.; Feeney, R. J. *J. Org. Chem.* **1951**, *16*, 981–987.
4. Sagar, S.; Kaur, M.; Minneman, K. P. *Mar. Drugs.* **2010**, *8* (10), 2619–2638.
5. Momparler, R. L. *Exp. Hematol. Oncol.* **2013**, *2*, 1-5.
6. Mehbub, M. F.; Lei, J.; Franco, C. and Zhang, W. *Mar. Drugs.* **2014**, 4539–4577.
7. Blunt, J. W.; Copp, B. R.; Hu, W.-P., Munro, M. H. G.; Northcote, P. T; and Prinsep, M. R. *Nat. Prod. Rep.* **2008,** *25*, 35–94.
8. Hoshino, S.; Takeda, M. and Watanabe,. *Boll. Mus. Ist. Biol. Univ. Genova.* **2003**, *68*, 373–379.
9. Nagai, K.; Kamigiri, K.; Matsumoto, H.; Kawano, Y.; Yamaoka, M.; SHIMOI, H.; Watanabe, M.; Suzuki, K. *J. Antibiot. (Tokyo).* **2002**, *55* (12), 1036–1041.
10. Amagata, T.; Doi, M.; Ohta, T.; Minoura, K. and Numata, A., *J. Chem. Soc., Perkin Trans. 1*. **1998**, 3585–3599.
11. Numata, A.; Amagata, T.; Minoura, K.; *Tetrahedron Lett.* **1997**, *38* (32), 5675–5678.
12. Ogamino, T.; Ohnishi, S.; Ishikawa, Y.; Sugai, T.; Obata, R.; Nishiyama, S. *Sci. Technol. Adv. Mater.* **2006**, *7* (2), 175–183.
13. Amagata T.; Minoura, K. and Numata, A. *J. of Nat. Prod.* **2006**, *69*, 1384–8
14. Amagata, T.; Tanaka, M.; Yamada, T.; Minoura, K., and Numata, A., *J.N. Prod.* **2008**, *71*, 340–345.

15. Raffier, L.; Piva, O. *Beilstein J. Org. Chem.* **2011**, *7*, 151–155.

16. Amagata, T.; Takigawa, K.; Minoura, K.; Numata, A. *Heterocycles*. **2010**, 81, 897–907

17. Hammerschmidt, L.; Aly, A. H.; Abdel-Aziz, M.; Müller, W. E. G.; Lin, W.; Daletos, G.; Proksch, P. *Bioorg. Med. Chem.* **2015**, *23* (4), 712–719.

18. Wang, H.; Dai, H.; Heering, C.; Janiak, C.; Lin, W.; Orfali, R. S.; Müller, W. E. G.; Liu, Z.; Proksch, P. *RSC Adv.* **2016**, *6* (85), 81685–81693.

19. Phoon, C. W.; Somanadhan, B.; Heng, S. C. H.; Ngo, A.; Ng, S. B.; Butler, M. S.; Buss, A. D.; Sim, M. M. *Tetrahedron.* **2004**, *60*, 11619–11628.

20. Patrick, G, L. *An Introduction to Medicinal Chemistry*. Oxford University Press. *5th Edition.* **2013**

21. Lu, L.-Y.; Yu, X. *Cell Division.* **2009**, *4*, 1-6.

22. Barr, F.; Silljé, H. H. W.; Nigg, E., *Nature Reviews Molecular Cell Biology.* **2004**, *5*, 429–440.

23. Knecht, R.; Elez, R.; Oechler, M.; Solbach, C.; von Ilberg, C.; Strebhardt, K. *Cancer Research.* **1999**, *59*, 2794–2797.

24. Alberts, B.; Bray, D.; Hopkin, K.; Johnson, A.; Lewis, J.; Raff, M.; Roberts, K.; Walter, P. *Essential Cell Biology.* Garland Science. *2nd Ed.* **2006**.

25. Cooper G. M., *Cell A Molecular Approach. 2nd Ed.* **2000**, 5–9.

26. http://cnx.org/contents/GFy_h8cu@9.87:1tJ55Ot6@7/The-Cell-Cycle (accessed 22/05/17)

27. Van De Weerdt, B. C. M.; Medema, R. H. *Cell Cycle.* **2006**, *5*, 853–864.

28. Reagan-Shaw, S.; Ahmad, N. *IUBMB Life.* **2005**, *57*, 677–682.

29. Takai, N.; Hamanaka, R.; Yoshimatsu, J.; Miyakawa, I. *Oncogene.* **2005**, *24*, 287–291.

30. Morgan, O., D. *The Cell Cycle: Principles of Control*. New Science Press, **2007.**

31. Gumireddy, K.; Reddy, M. V. R.; Cosenza, S. C.; Nathan, R. B.; Baker, S. J.; Papathi, N.; Jiang, J.; Holland, J.; Reddy, E. P. *Cancer Cell.* **2005**, *7*, 275–286.

32. https://clinicaltrials.gov/ct2/show/NCT01928537 (accessed 08/05/17

2. Magnetically tagged drugs for cancer treatment

2.1. Introduction

Cancer is a leading cause of death worldwide. There were an estimated 14.1 million cancer cases around the world in 2012, of these 7.4 million cases were in men and 6.7 million in women. Europe carries a significant load of the global burden, with one quarter of the global burden of cancer observed in Europe despite a total population that comprises one-ninth of the world's population. Cancer is the second most common cause of death in Ireland. According to the Irish cancer society, one in three people in Ireland will develop cancer during their lifetime. An average of 30,000 new cases of cancer are diagnosed each year. The number is expected to rise to over 40,000 per year by 2020. Table 2.1 shows cancer incidences and deaths in Europe.[1,2]

Region	Incidences in 2012	Deaths in 2012
Central and Eastern Europe	1,036,900	638,200
Northern Europe	525,900	245,100
Southern Europe	769,200	390,500
Western Europe	1,110,300	482,600
Ireland	20,515	8,544

Table 2.1: Cancer incidences in 2012

Chemotherapy, radiation therapy and surgery are the most common methods of treatment with the first accounting for 50% of all procedures. Chemotherapeutics suffer from several barriers that limit their delivery to specific targets. Only 0.1-1% of administered therapeutic agents reach the tumour and the rest enter healthy tissue resulting in undesirable side effects. Toxic effects are thus significant, and desired therapeutic effects

are suboptimal. Targeted drug delivery aims to increase the bioavailability of a drug at a specific part of the body for a defined duration of time. Current efforts are focused on developing drug delivery systems that are target specific, i.e., have the ability to target the tumour cells, thereby leaving healthy cells unharmed. The advantages of this approach are the reduction in quantity and frequency of dosage, reduced costs and fewer side effects. [3, 4,5,6,7]

Over the last two decades, nanotechnology has evolved into a multidisciplinary topic. It has revolutionized fields such as catalysis, robotics, design, imaging, data storage and medicine. Advances in nanotechnology are enabling the development of nanoparticles with specific functional properties to address current limitations in a range of chemical and biological applications. [8]

A number of nanomedicines have been approved for clinical use in cancer therapy. These include liposomal doxorubicin used to treat breast cancer;[9] polymer based PEG-L-Asparaginase (Oncaspar®) for leukemia; [10] micellar paclitaxel for breast, lung and ovarian cancer; albumin based nanoparticle containing paclitaxel for breast cancer.[11] There are several other drugs still undergoing clinical trials. (Table 2.2)

Nanocarrier	Nanodrug	Indication	Phase in clinical trials
Micelles	Paclitaxel (Genexol-PM)	Breast cancer	IV
	il	Ovarian	Approved
	Paclitaxel	Non-Small Cell Lung Cancer	III
	Docetaxel-PM	Head and Neck Squamous Cell Carcinoma	II
Polymer-drug conjugate	Pegylated Irinotecan	Small Cell Lung Carcinoma	II
	NC-6004	Head and Neck Cancer	I
	Docetaxel-PNP	Advanced Solid Malignancies	I
Liposome	Myocet (Non-pegylated liposomal doxorubicin)	Metastatic breast cancer	Approved
	LipoDox (liposomal doxorubicin)	Kaposi's sarcoma, breast and ovarian cancer	Approved
	Doxil (liposomal doxorubicin)	AIDS-related Kaposi's sarcoma, recurrent ovarian cancer, metastatic breast cancer and multiple myeloma	Approved

Table 2.2: Examples of tumour-targeted nano-carriers in cancer therapy. Extracted from https://clinicaltrials.gov/ct2/home 2016

In the first part of this review, the use of targeted drug delivery for cancer treatment will be discussed. In the second part the unique properties of superparamagnetic iron oxide nanoparticles (SPIONPs), their synthesis and subsequent protective coatings will be discussed. Finally, advances in magnetically tagged drugs for cancer treatment, limitations, tagging of SPIONPS to chemotherapeutics and their release *in vivo* will be presented.

2.1.1. Targeted Drug Delivery

Chemotherapy is the most common form of cancer treatment and has considerable impact on the patient. To overcome the drawbacks with chemotherapy, it is important to improve the pharmacokinetics and target site accumulation of drugs through sufficient bioavailability. Even intravenous drug delivery does not guarantee that the drug is freely available at the target site due to competing particles such as red blood cells, leukocytes and proteins such as albumin. Over the last number of years, several drug delivery systems have been designed to overcome this low efficiency. Liposomes, antibodies, micelles, polymers and nanoparticles have demonstrated clinical relevance for cancer therapy. The advantage of using these drug delivery systems includes improved selective delivery of chemotherapeutics to target sites and their guidance away from healthy tissue. [14, 15, 16]

Cancerous cells have different biological characteristics from healthy cells and targeted therapies take advantage of these differences. Cancerous cells replicate faster than tumour cells and therapies like doxorubicin capitalise on this by intercalating DNA and disrupting its replication. This is termed circumstantial targeting, but has limited efficacy due to sub optimal drug concentrations that must be used to avoid cytotoxic effects on healthy cells. Therefore, there is urgent need to develop more efficient systems for targeted delivery of cancer treatments. [14, 17]

2.1.2. Magnetic Drug Targeting

In 1960, Freeman *et al* established the concept of magnetic drug targeting (MDT) using iron oxide nanoparticles (IONPs). Subsequently there has been significant interest in using IONPs and other magnetic nanoparticles for targeted delivery in cancer treatment. (Figure 2.1) Biocompatible magnetic nanoparticles (MNPs), conjugated with drugs have

been injected into the bloodstream and accumulated at a tumour site with the help of an external magnetic field. [14, 16, 18]

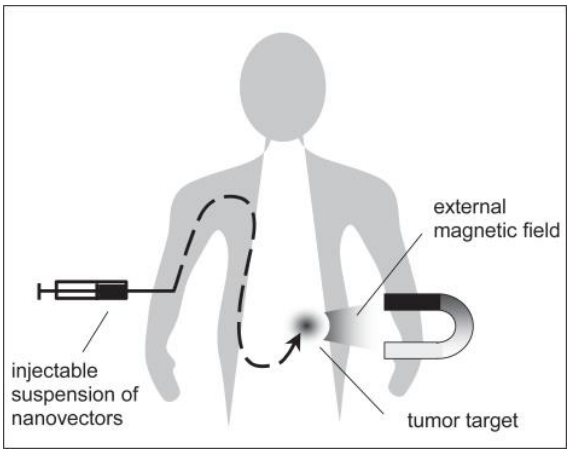

Figure 2.1: Principle of magnetic drug targeting [8]

IONPs typically have two structural configurations, namely magnetite and maghemite. Magnetite is the most commonly used IONP because of its biocompatibility. It possesses a cubic inverse spinel with oxygen forming a face centred cubic (fcc) close packing and Fe occupying the octahedral sites. (Figure 2.2) [6, 7]

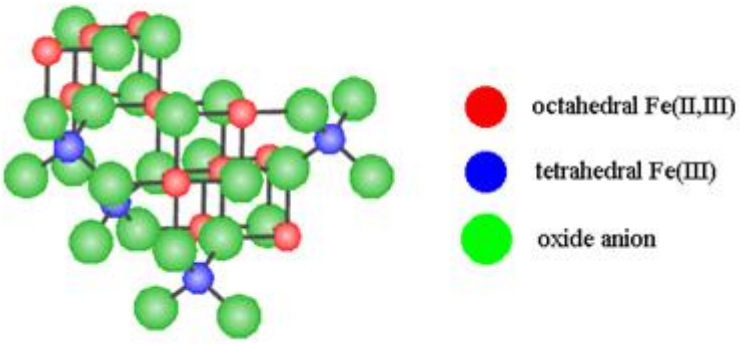

Figure 2.2: Structure of inverse spinel magnetite (Fe_3O_4)

For magnetisable nanoparticles to be introduced into a biological system, they should only display magnetic behaviour under the influence of an external magnetic field and lose the behaviour when the field is withdrawn. This can be achieved by restricting their size to be a specific range. Superparamagnetism arises when such nanoparticles have a

diameter in the region of 10-20 nm, and are at a temperature above the so-called "blocking temperature". To be used *in vivo,* the blocking temperature has to be below room temperature to guarantee disappearance of residual magnetism when the magnetic field is removed. In this review, such nanoparticles will be referred to as superparamagnetic nanoparticles (SPIONPs). [15, 16, 19]

Much research has focused on numerous innovative targeting strategies to increase selectivity of chemotherapeutics and minimize their accumulation in healthy tissues. Nanomedicines can be passively or actively targeted to the tumour tissue. Passive and active targeting have been used together with MDT to improve efficacy of chemotherapeutics.

2.1.3. Passive targeting

Passive targeting relies on the preferential delivery of nanomedicines to solid tumours due to the enhanced permeability and retention (EPR) effect.[20] Tumour tissues lack an effective lymphatic drainage and are leaky due to abnormality in form and architecture. Nanoparticles, due to their size, easily diffuse passively through the leaky vasculature to reach the tumour. This enables high local drug concentration at the tumour site instead of normal tissue. In order to achieve sufficient targeting at the tumour site, the circulation time of the therapeutic agent must be sufficiently long.[21] The size and surface chemistry of nanoparticles influence circulation time and therefore can be manipulated to avoid premature clearance. Surface modification of nanoparticles has been used to prolong the circulation time. Nanoparticles with a size range of 10-100 nm are big enough to avoid renal filtration but are small enough to slow down activation of the reticuloendothelial system (RES). RES is part of the immune system that is responsible for clearance of foreign material from the body.[22] Upon administration, nanoparticles are quickly recognised as foreign particles and are opsonized by blood opsonins (protein markers).

The opsonized nanoparticles interact with receptors on macrophages in the spleen and are rapidly eliminated *via* RES. Larger IONPs are more visible to RES and are cleared faster. RES is the main barrier in nanoparticle systemic circulation. In order to evade RES and opsonisation IONPs have to be modified and thereby increasing their circulation time.[23] Passive targeting also uses charges on nanoparticles to induce targeting towards the tumour. Myocet, Doxil and Abraxane are amongst passively targeted nanomedicines. [14]

2.1.4. Active Targeting

In active targeting, the delivery systems are designed to interact with specific biomolecules usually by the attachment of a ligand/linker on the outer surface of a nanocarrier. Active targeting relies on disease-selective molecular markers. The molecular recognition of a ligand coupled to a nanodrug surface promotes cellular entry *via* receptor-mediated endocytosis thereby enhancing cellular uptake of the nanomedicine. [24] In active targeting long circulation time is important to allow effective transport of nanoparticles to the tumour site; moreover, the targeting molecule enhances endocytosis. [11]

Active targeting can also be used to target cell proliferation receptors that are expressed in certain tumour cells. Most of the research regarding actively targeting nanoparticle systems have been directly associated with a type of cancer.[11]

2.1.5. Tumour cell targeting

Tumour cell targeting is specific to a type of cancer. The most established cell proliferation targets used by actively targeting nanoparticles include human endothelial transferrin, HER-2 and folate receptors. (See section 2.2.)

Prostate, breast, lung and bowel are the most common non-melanoma cancers in Ireland. These four account for 53% of new cancer cases per year (2008-2010). [25] Current

treatment methods include surgery, radiation therapy, chemotherapy and hormone therapy. Table 2.3 shows the most common types of cancer in Ireland, their prevalence and receptors that are usually targeted in treatment methods.

Cancer	% of all cancer deaths Ireland (2008-2010)	Receptor targets	Clinically approved drugs targeting receptor	References
Prostate	12.2	PSMA	Prostascint	26, 27
		sigma	--	28, 29
		folate	--	30, 31
Breast	7.9	HER-2	Trastuzumab lapatinib	32, 33
		LHRH	--	34
		sigma	--	35
Bowel/Colorectal	11	EGFR	Panitumab, Cetuximab	36
		VEGF	Avastin, ramucirumab	37
		guanylyl cyclase C	--	38, 39
Lung	20.4	aptamers	--	40
		VEGF	--	41

Table 2.3: Most common cancers in Ireland [2, 12]

The overexpression of certain receptors in cancer cells has provided important tools for exploitation in the active targeting of drugs to cancer cells. SPIONs can achieve specific targeting of tumours with high accuracy when conjugated with targeting ligands. Ligands

can be designed to be specific to receptors that are over- expressed on cancerous cells, but are normally expressed on healthy cells. In the next section, the most common receptor molecules and their mode of operation are evaluated.[2]

2.2. Tagging

2.2.1. Folate

Folate receptors stand out as one of the most promising and most investigated cell markers. Folate based targeting systems have shown great potential for therapeutic applications. [38] The folate receptor, also known as the high affinity membrane folate binding protein, is often overexpressed in many human carcinomas including malignancies of the ovary, brain, kidney, breast, colon, myeloid cells and lung. In normal tissue however, folate is either absent or inaccessible to circulating drugs. [42] Two general strategies are used for targeted delivery of drugs to folate receptor positive cells (a) coupling to a monoclonal antibody against folate receptor (b) coupling to a high affinity ligand of folate receptor- folic acid.

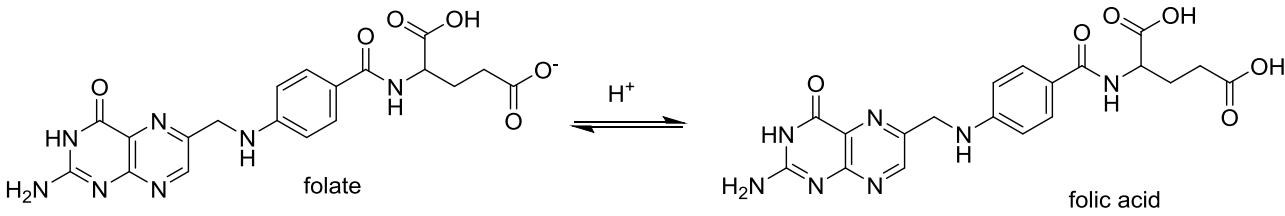

Scheme 2.1: Structures of folate and folic acid

Folic acid (FA), the conjugate acid of folate (Scheme 2.1), is required for essential cell function. It has a high binding affinity to the folate receptor that is overexpressed in tumours and therefore provides a distinguishable marker from normal cells. Moreover, FA is cheap, non-immunogenic, highly stable and gets internalized quickly through cell membranes. FA is usually conjugated to nanoparticles *via* the carboxylic acid or the

amine moiety. Socaci *et al.* developed folic acid di-ester functionalized MNPs and used 1° and 2° amine sites as the anchoring reaction sites instead of the carboxylic acid. [43]

Pourjavadi *et al* developed PEGylated dendritic nano-carriers functionalized with folic acid as tumour targeting agents. FA conjugated agents showed enhanced cytotoxicity against carcinoma cell line A431 and improved cellular uptake of cancerous cells compared to free nano-carriers.[44] Huang *et al* reported modified IONPs with poly (glycidyl methacrylate) (PGMA) followed by conjugation with different amounts of FA to form SPIONs–PGMA–FA. These folate modified nano-carriers achieved a significantly higher uptake by cancer cells than those by macrophages and 3T3 fibroblasts. [45]

Cis-platin is one of the most effective therapeutic agents for the treatment of head and neck cancer. However, it has many disadvantages including rapid clearance, binding to plasma proteins and toxicity.[46] Chen *et al* recently developed a pH sensitive therapeutic agent release system using folic acid modified *cis*-platin loaded MNPs to overcome problems associated with *cis*-platin and to improve its efficacy. The resulting moiety exhibited superparamagnetic properties andhigh stability and released *cis*-platin in a low pH environment which is ideal for targeted delivery to acidic tumour environment. [46]

Ma *et al* developed a magnetic polymer nano-carrier with folate receptor-targeting and pH sensitive functionalities loaded with doxorubicin (DOX) (F-PDOX) for the treatment of advanced gastric cancer. F-PDOX displayed FR-targeting specificity and pH sensitivity that were hoped to improve uptake. Encouragingly the cytotoxicity studies *in vitro* and *in vivo* showed tumour suppression and tumour accumulation, demonstrating that F−PDOX were indeed effective on gastric cancer treatment, importantly without significant side effects. [47]

Li *et al* developed nanosized folate-conjugated PEGylated PLGA nanoparticles co-encapsulated with anticancer drug (sorafenib). The folic acid-conjugated NP exhibited sustained drug release and enhanced cellular uptake in BEL7402, liver cancer cells**.** [48]

Maeng *et al* synthesized multifunctional polymeric IONPs, carrying the anticancer drug doxorubicin (DOX), for treatment of liver cancer. The formation of nanoparticles was mediated by poly (ethylene oxide)-trimellitic anhydride chloride-folate (PEOTMA-FA) (Figure 2.3) containing folate as the targeting moiety. [49]

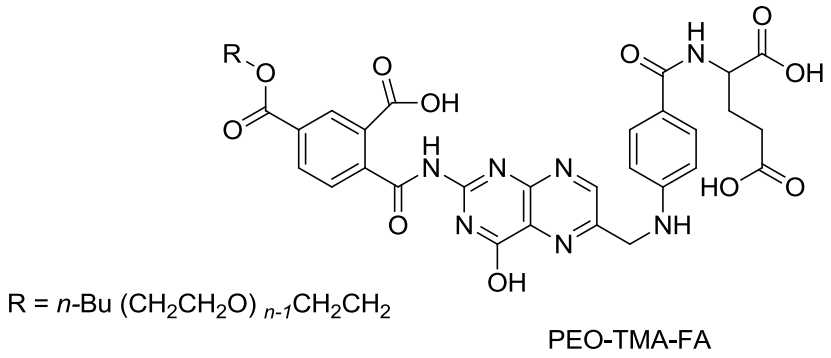

Figure 2.3: Structure of PEO-TMA-FA polymer

The presence of the folate significantly facilitated the specific delivery of DOX to folate receptor-positive liver tumour cells and inhibited tumour growth without causing any toxic effects such as body weight loss or cardiac toxicity that are usually associated with the use of DOX. [49]

2.2.2. Integrins

Linkage of the cell to the extracellular matrix requires adhesion proteins that act as matrix receptors. Integrins are the principal receptors used by animal cells to bind to the extracellular matrix. Integrins, unlike other cell surface receptors, bind their ligand with lower affinity to stop them being irreversibly glued to the cellular matrix.[50] In addition to this, integrins function as signal transducers, activating various intracellular signalling pathways when activated by cellular binding. Integrin receptors are highly

expressed in tumour cells but not in normal cells. They are heterodimers and there are at least 24 distinct integrin heterodimers formed by the combination of 18 α subunits and 8 β subunits. Studies have shown that integrins can influence tumour survival both positively or negatively by either enhancing cell survival or initiating apoptosis. Expression of integrins αvβ3, αvβ5, α5β1, α6β4, α4β1and αvβ6 has been associated with tumour progression in various tumour types and therefore these integrins are the most widely studied. [50, 51] Table 2.4 shows the most studied integrins and tumours associated with them. The advances in integrin facilitated drug delivery in cancer treatment are reviewed elsewhere. [52]

Tumour type	Integrins expressed	Associated phenotypes
Melanoma	αvb3 and α5b1	Vertical growth phase and lymph node metastasis
Breast	α6b4 and αvb3	Increased tumour size and grade, and decreased survival (α6b4). Increased bone metastasis (αvb3)
Prostate	αvb3	Increased bone metastasis
Pancreatic	αvb3	Lymph node metastasis
Ovarian	α4b1 and αvb3	Increased peritoneal metastasis (α4b1) and tumour proliferation (αvb3)
Cervical	αvb3 and αvb6	Decreased patient survival
Glioblastoma	αvb3 and αvb5	Both are expressed at the tumour–normal tissue margin and have a possible role in invasion
Non-small-cell lung carcinoma	α5b1	Decreased survival in patients with lymph node-negative tumours
Colon	αvb6	Reduced patient survival

Table 2.4: Integrins in cancer progression, adapted from Desgrosellier [53]

IONPs have been used in combination with integrin targeting receptors for enhanced drug delivery. Nazli *et al* developed DOX loaded nano-carriers designed for integrin receptor specific uptake. [54]

2.2.3. Prostate specific antigen (PSA)

There are several treatment methods for prostate cancer, however chemotherapy is the primary clinical treatment to prolong overall patient survival. Prostate specific antigen (PSA) is overexpressed in prostate cancer cells and is the most studied target for cancer treatment. PSA specific ligands are good candidates for prostate cancer targeting.

Yang *et al* developed a dual targeting nanomedicine, PTX-HMNC-EPEG-APSMA and combined it with magnetic targeting to increase local accumulation of paclitaxel. Paclitaxel (PTX) was conjugated to non-toxic high magnetization nano-carriers. The surface was functionalized with long, carboxylated EPEG linkers to prolong the circulation time. Antiprostate PSA (APSA) were then conjugated to the carrier to recognize PSA and bind to cancer cells using active targeting. The treatment was significantly more effective in low doses against cancer cells, compared to free paclitaxel. Moreover, functionalizing the surface increased the circulation time from 6 minutes to 120 minutes before being cleared by the RES. [42]

Docetaxel is one of the commonly used therapeutic options for prostate cancer. Nagesh *et al* developed PSA targeted IONPs loaded with Docataxel to improve its efficacy. The resulting moiety showed potent anti-cancer effect in prostate cancer cells and immunofluorescence data confirmed that only PSA positive cancer cells were targeted. [55]

2.3. IONPs Synthesis

To be used *in vivo,* nanoparticles must be biocompatible and studies have shown that this behaviour is highly dependent on their morphology and physical properties. The size and shape of IONPs affects their magnetic and biological properties, toxicity, stability, bio-distribution and elimination. The choice of synthetic route is important as it influences the size and morphological properties of IONPs. [56-57]

Several studies have linked high surface area on IONPs to toxicity *in vivo*. Changes in the shape and size of nanoparticles are accompanied by alterations on the surface that influences cytotoxicity. A study by Han-Lee *et al* revealed that rod shaped IONPs had a high surface area compared to spherical IONPs. The high surface area in the rod shaped IONPs resulted in increased cytotoxicity towards mouse macrophage cells. [58]

The size of IONPs also influences the circulation time of IONPs *in vivo.* Lin Yang *et al* studied the effect of size on the bio-distribution, toxicokinetics and toxicity of various size carboxyl coated IONPs ranging from 10-40 nm (Figure 2.4. The smallest IONPs showed highest uptake by the liver and were cleared fast from the liver and kidneys. [59]

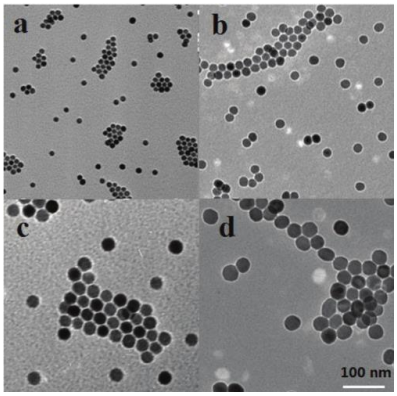

Figure 2.4: TEM and DLS images of carboxyl coated IONPs (a) 10 nm, (b) 20 nm (c) 30 nm (d) 40 nm [59]

The particles also entered the uterus more readily and penetrated the blood brain barrier. On the other hand, larger IONPs (over 40 nm) were mostly taken up and eliminated by the spleen. In a study by Gil *et al*, the large IONPs changed expression levels of genes associated with oxidative stress and metabolic processes in mice. [18, 59]

Roohi *et al* carried out a study on the effect of size of IONPs on blood half-life and systemic clearance. This study demonstrated a decrease in the blood half-life from 50 to

3 minutes when the hydrodynamic size of nanoparticles was increased from 19 to 86 nm. [60]

Ideally, IONPs should be in the range of 10-100 nm. At this range, they are small enough to delay the mononuclear phagocyte system but big enough to avoid renal filtration. Due to the importance of size and shape on IONPs, it is vital to use the appropriate synthetic method to obtain the desirable nanoparticles for use *in vivo*. Over the last number of years, different synthetic routes have been developed including co-precipitation, thermal decomposition, hydrothermal synthesis, wet grinding, micro emulsion and laser pyrolysis, amongst others. These routes allow the size range, shape and stability of the nanoparticles to be manipulated and tailored to enable interaction with specific biomolecules. [61, 62, 63]

2.3.1 Co-Precipitation

Co-precipitation is the most common, simplest and convenient way to synthesise IONPs. It involves the use of readily available starting materials under mild reaction conditions, resulting in naked magnetite in high concentrations. Massart *et al* first reported the synthesis of IONPs using the co-precipitation method in 1981.[64] In this synthesis, the particles were roughly spherical and had a diameter of 8 nm. Since then, a number of modified synthetic methods have been reported where parameters are varied to achieve certain properties suited for their application.

Addition of a base to an aqueous solution of Fe^{2+}/Fe^{3+} ions in a ratio of 1:2 produces a black precipitate of magnetite in uniform sizes under alkaline conditions and an oxygen free environment. The chemical reaction of dissolved iron salts to magnetite can be summarized according to the equation below.[64]

$$Fe^{2+} + 2Fe^{3+}\,8OH^{-} \rightarrow Fe_3O_4 \downarrow + 4H_2O$$

In co-precipitation, the chemical, physical, structural and magnetic properties of nanoparticles can be manipulated by varying certain reaction conditions. The size and shape of nanoparticles is dependent on the type of salt used, pH value and ionic strength of the aqueous media, reaction temperature and ratio of Fe^{3+} /Fe^{2+} ions. [65]

Berensmeier *et al* recently studied the effects of process parameters on particle size and saturation magnetization. Nanoparticles with diameters of 3 – 17 nm and saturation magnetization of 29 – 89 Am^2/kg were obtained by varying the following (1) iron salt concentration (2) reaction temperature (3) ratio of hydroxide ions to iron ions (4) ratio of Fe^{3+} /Fe^{2+} ions. High saturation magnetization was reported at high synthesis temperatures, high iron salt concentrations and lowest ratios of Fe^{3+} /$Fe^{2+.}$ Furthermore, the particle size of magnetite was increased by using a higher iron salt concentration and a higher ratio of hydroxide ions to iron ions. The particles also showed superparamagnetic behaviour. [66]

Despite being the most widely used method for the synthesis of IONPs, co-precipitation has several disadvantages. Naked NPs synthesised by this method need to be coated *in situ* or in a subsequent step to prevent oxidation and agglomeration at ambient temperature. The use of alkaline solution for the synthesis represents environmental issues, and as a subsequent treatment step is required before disposal of waste. [65]

2.3.2 Hydrothermal

Hydrothermal synthesis of nanoparticles involves the synthesis in water, of crystals at high temperature and high pressure using materials that would otherwise be insoluble at normal conditions. In this technique, nanoparticles are synthesised by other methods and then treated under hydrothermal conditions where the pressure can be higher than 2000 psi and the temperature can be above 200 °C. Techniques like microemulsion, co-

precipitation and microwave have been utilised in combination with hydrothermal methods to form SPIONPs.[66, 67, 68, 69] Kockar *et al and* Wang *et al* reported that increasing hydrothermal treatment temperatures, up to 200 °C, resulted in high crystallinity and increased saturation magnetization. [67, 70] It has also been reported that increasing reaction time results in an increase in nanoparticle size. More recently, Fester *et al* reported a detailed study on the influence of process parameters on nanoparticle characteristics using a continuous hydrothermal system (CHS) synthesis. This study revealed that an increase in temperature and flow rate of CHS resulted in a major increase in nanoparticle crystallinity. [71]Varying other process parameters like concentration, pressure, residence time etc. had minimal effect on nanoparticle crystallinity. [71, 72]

2.3.3. Thermal Decomposition

Thermal decomposition involves the decomposition of an organometallic precursor in a high boiling organic solvent in the presence of a surfactant. It is a recognised method for the synthesis of monodisperse SPIONPS with a narrow size distribution. The synthesis of monodisperse SPIONPs through the thermal decomposition method involves two stages. Firstly, tiny crystal nuclei are formed at around 200°C, and this is called nucleation. The second stage involves the growth of the nuclei at the boiling point of the organic solvent used. It is at this stage that the size, shape and magnetic properties of the nanoparticles can be manipulated by varying the reaction time and temperature. The use of high temperatures makes this process expensive and limited to small batch reactions because of difficulties in maintaining a uniform temperature in large scale reactions.[73] Continuous flow and microwave assisted thermal decomposition methods have been proposed to overcome this limitation. [74, 75, 76] The prepared nanoparticles are water insoluble due to their hydrophobic surfaces and thus cannot be used in a biological system. This can be

overcome by employing a ligand exchange strategy to substitute the hydrophobic layer with a hydrophilic one.

Other considerations for this method include long reaction times, use of organic solvents, and the safety issues associated with use of high temperatures. [66, 77, 78, 79]

2.3.4 Other methods

Other methods for the synthesis of IONPs include laser pyrolysis, sol gel synthesis and microemulsion. [80-87]

2.4. Surface modification of Iron Oxide Nanoparticles

Their application in biology and therapy require IONPs to be stable in water at neutral pH and at physiological salinity. Naked IONPs are very unstable and tend to aggregate at ambient conditions leading to rapid clearance from the system before their intended use. To address this, IONPs are coated with a surface layer during or after synthesis. This layer provides an interface between the surrounding environment and the core. The presence of a surface layer reduces opsonisation, inhibits corrosion/oxidation of the magnetic core, ensures colloidal stability under physiological conditions and enhances circulation time. Moreover, the coating layer can also be functionalized by attaching carboxyl groups, carbodiimide and other molecules that can be augmented to drug molecules by covalent attachment, adsorption or entrapment to the nanoparticles. [88, 89] Coating systems can also be made stimuli sensitive, e.g. to pH and temperature, to favour release at a specific site.

However, coatings affect the magnetic properties of IONPs. The extent to which magnetic properties are affected depends on the molecular weight, composition and thickness of coating. Conjugation to other molecules also deteriorates the magnetic properties. [7]

Several organic and inorganic coatings have been reported to date and include dextran, silica, lipids, polyethylene glycol (PEG), and chitosan (Figure 2.5) amongst others and these are discussed in more detail in this section.

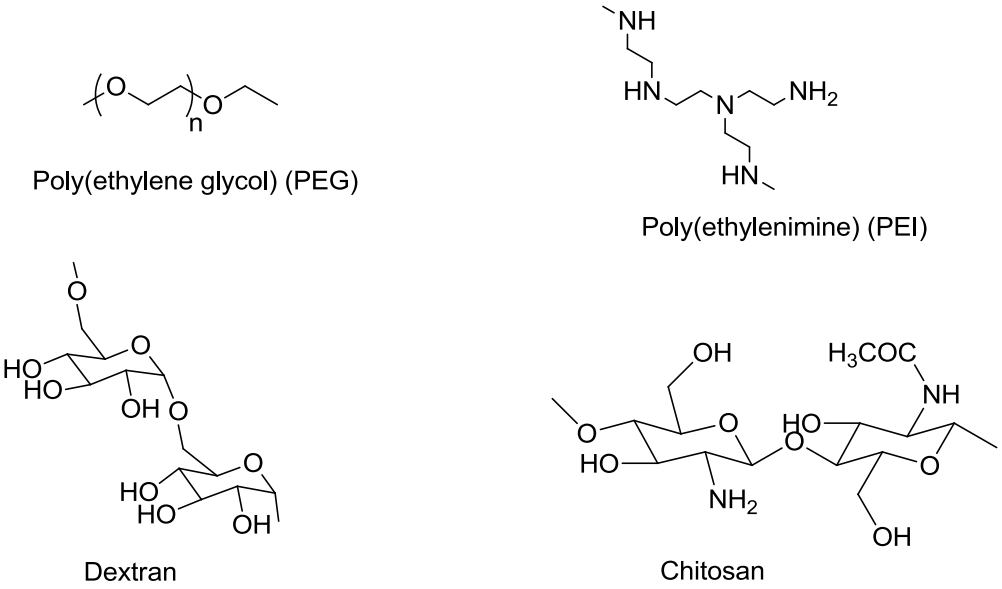

Figure 2.5: Chemical structures of selected coating materials

Like nanoparticles, the coatings should be biocompatible, nontoxic and hydrophilic. Their size should be less than 100 nm so they can avoid elimination *via* the RES. [90, 91]

2.4.1. Organic Coatings

2.4.1.1. Polyethylene glycol (PEG) and its derivatives

One way of increasing the circulation time and the blood half-life of nanoparticles *in vivo* is by using hydrophilic polymers. PEG can be integrated onto IONPs surface to form a hydrophilic, uncharged, biocompatible and non-immunogenic layer. IONPs are coated during synthesis *in situ* or post synthesis *via* adsorption or end grafting resulting in uniform encapsulation.[92] Studies have shown that PEG provides the nanoparticles with functionality, stability and compatibility in the biological environment and improves their hydrophilicity.[90, 91] At sizes below 100,000 dalton, PEG polymers are amphiphilic and soluble in water as well as many organic solvents. This property makes them compatible

with a range of chemistries in aqueous or organic phases. Bio distribution studies have also shown that PEGylated IONPs preferentially accumulate in the tumour region *via* enhanced permeability and the retention effect. [92, 94] Cytotoxicity studies by Pisciotti *et al* revealed that IONPs coated with PEG were nontoxic up to concentrations as high as 100 µg/mL. In the same study, an increased tumour uptake (160%) *in vivo* was observed when PEG coated SPIONPS were used in the presence of a magnetic field. [95]

Several reports have been published on the use of so-called PEGylated IONPs with a commercially available drug, Doxorubicin (DOX) (Figure 2.6), to increase its efficacy. [93]

DOX is an anti-cancer chemotherapy drug used for several cancers including breast, gastric, liver and ovarian cancer. Its clinical use is limited due to its adverse side effects, resistance developed by cancer cells to it, dose dependent cardiotoxicity and hematotoxicity.[94, 96]

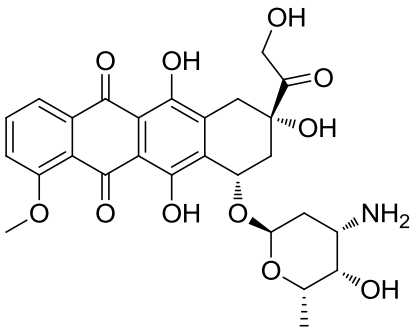

Figure 2.6: Structure of Doxorubicin (DOX)

As well as making nanoparticles stealth, PEGylation can also have an important influence on drug loading, drug release, use with other therapies and nanoparticle distribution into the cell.

Quinto *et al* synthesized PEG coated IONPs loaded with DOX for chemotherapy-hyperthermia combinatorial treatment.[97] It was also found that the presence of PEG not only gave protection to IONPs but also has the potential to concurrently deliver DOX and

generate heat for an enhanced multimodal cancer treatment. The synergy between chemotherapy and hyperthermia has a potential for a more effective treatment of cancer. [97]

Gautier *et al* developed DOX loaded IONPs and investigated the release of DOX *in vitro* in order to observe how PEGylation modifies the release.[89] The study showed a pH dependent release of DOX from the polymer coating. A sustained, gradual release with no burst effect was observed at pH 7.4. Release was accelerated when the pH was lowered to 4. [89]

There are also several reports on using PEG derivatives for surface modification to improve stealthiness of IONPs. Orlando *et al* reported the synthesis of IONPs coated with an amphiphilic polymer (PMA) followed by PEGylation in order to form PEG-IONP-PMA.[94, 98] The PMA polymer coating not only gives the IONP extra protection but also bears several carboxylate groups for further functionalization. IONP-PMA were synthesized according to a previously reported procedure[99] and PEGylated using PEG-NH_2 and an amide-coupling agent to form PEG-IONP-PMA. The nanoparticles did not exhibit cytotoxicity and were less internalized by macrophages or human endothelial cells (HUVEC). Moreover, these nanoparticles crossed the blood brain barrier, which makes them potentially useful as therapeutic agents for brain diseases. [98]

There has been several reports by Nagasaki *et al* on the use of PEG based hydrophilic block copolymers demonstrating their stability even in harsh conditions (e.g. high salt concentrations and broad range of pHs).[94] Block copolymers are commonly used for the encapsulation of SPIONs for direct use in cancer therapy and imaging. Block copolymers are prepared by controlled polymerization of one monomer (A), followed by chain extension with a different monomer (B) and in some case a third monomer (C) to form

AB or ABC block copolymers. In one of their reports, IONPs were synthesized by co-precipitation in the presence of PEG-poly (4-vinylbenzylphosphonate) (PEG-b-PVBP) (Figure 2.7) as a surface coating to form PEG-PION4 block co polymer.[64] The nanoparticles were strongly bound to the polymer through multi point anchoring *via* the phosphate group.

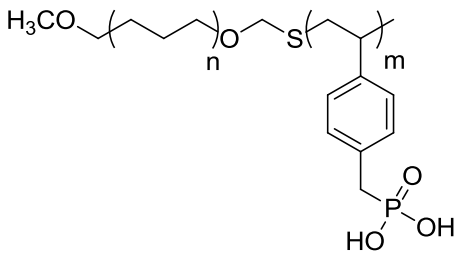

Figure 2.7: Structure of PEG-b-PVBP

Following *in vivo* administration to mice, these modified nanoparticles showed prolonged blood circulation time and significant EPR-mediated tumour accumulation. PEG-PION4 also showed excellent dispersion stability, remaining intact after one week in serum containing solution due to the strong phosphate anchoring. More recently, the same group synthesized DOX loaded IONPs coated with PVBP to study their encapsulation efficiency and stability in tumour bearing mice.[62] They showed high drug loading efficiency and excellent dispersion stability under physiological conditions. Furthermore, the IONPs had a crystalline structure, superparamagnetic properties and exhibited sufficient saturation magnetization to be used in MDT. [62, 94, 100]

Yang *et al* developed PEG modified, cross-linked starch coated magnetic nanoparticles using *N*-hydroxysuccinimide chemistry to produce nanoparticles with long circulation time.[20] Recently, Prabha *et al* developed β-cyclodextrin (Figure 2.8) (β-CD)-PEG–PEI coated iron oxide nanoparticles as drug delivery agents.[102] β-CD is an oligosacharride with a hydrophilic surface layer used to improve solubility, stability and bioavailability thereby enhancing drug delivery.

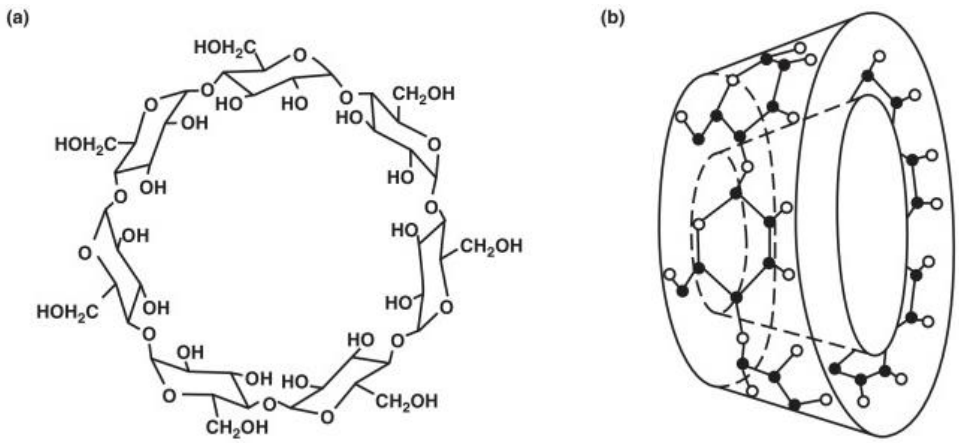

Figure 2.8: (a) chemical structure and (b) toroidal shape β-cyclodextrin molecule[101]

The resulting coated NPs exhibited superparamagnetic behaviour and were used as a carrier vehicle for the hydrophobic anti-cancer drug 5-fluorouracil.[102]

Schleich *et al* reported paclitaxel loaded PEGylated PLGA (poly (lactide-co-glycolide)-based IONPs with excellent magnetic properties for theranostic purposes. They had high cellular uptake and showed growth inhibition against colon carcinoma (CT26) tumour cells at a range of PTX concentrations (2–20 μg/ml). This concentration corresponds to plasma levels of the drug achievable in humans. [103]

Polyethylene oxide (PEO), like PEG, is a polymer of ethylene oxide. However, polymers of PEO have a molecular weight above 20000 g/mol compared to a molecular weight of lower 20000 g/mol in PEG.[104] PEO chains present a steric barrier against the adsorption of proteins on the nanoparticle surface. This reduces opsonisation and hence increase the blood circulation of NPs.[105]

Aqil *et al* prepared poly (acrylicacid)-b-poly (ethyleneoxide), PAA–PEO, and poly (acrylicacid)-b-poly (acrylate methoxy poly (ethyleneoxide)), PAA–PAMPEO, by reversible addition fragmentation chain transfer (RAFT) polymerization. RAFT is an organic process of controlled radical polymerization technique, applicable for a wide range of monomers under mild reaction conditions. The stealthiness of PAA–PAMPEO

and PAA–PEO (Scheme 2.2) was investigated *in vitro* by assessing the amount of proteins adsorbed to NP surface. The block copolymers demonstrated stealthiness and stability.[106]

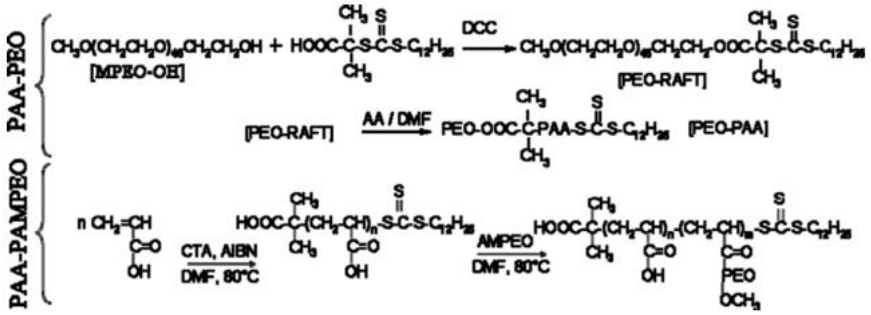

Scheme 2.2: Strategy for synthesis of PAA-PEO and PAA-PAMPEO by Aqil et al [107]

Hafeli *et al* investigated the toxic properties of polyethylene oxide (PEO) triblock copolymers and found that the PEO tail length was inversely correlated to toxicity. The study concluded that magnetite nanoparticles coated with triblock copolymers containing PEO tail lengths of above 2 kDa were biocompatible and appropriate for in vivo application. [108]

PEI is a polycation (highly positive polymer), also used as a capping agent to stabilize IONPs**.** It is a branched biopolymer with amine groups on it with potential to bind to other molecules. PEI has been used together with PEG to form hydrophilic, biocompatible SPIONPS, resulting in increased blood circulation. [102, 109]

The use of PEG and other organic coatings does not render sufficient protection of SPIONPS against physiological conditions. Drug loading efficiency and specific bio distribution *in vivo* remains a challenge. There is still need to improve the surface immobilization density of the PEG chains as well as their binding stability to the nanoparticle surface.

2.4.2. Inorganic Coatings

2.4.2.1. Silica

Silica is one of the most abundant minerals and the most widely used inorganic coating for IONPs in MDT for cancer therapy. (Figure 2.9) Philipse et al. [110] first reported the use of silica for coating magnetite. Since then, the stability and biocompatibility of silica coated IONPs have been studied extensively. The toxicity of silica nanoparticles has also received significant attention because of their use in food[111], food packaging[112], sunscreen[113], clothing[114] and detergents[115] to improve texture, kill microbes, or enhance shelf life, among other uses. Surface modifications using silica are easy due to the presence of silanol groups on the silica layer that are compatible with a variety of functional groups. The free silanol groups (Si-OH) can be used as scaffolds for attaching other molecules such as drugs and enzymes for use in biological applications. The hydroxyl groups present on the surface of silica coated NPs also gives them a hydrophilic character, which enhances their biocompatibility. More importantly, silica provides a chemically inert surface on IONPs giving them high stability against aggregation and oxidation.[116, 117]

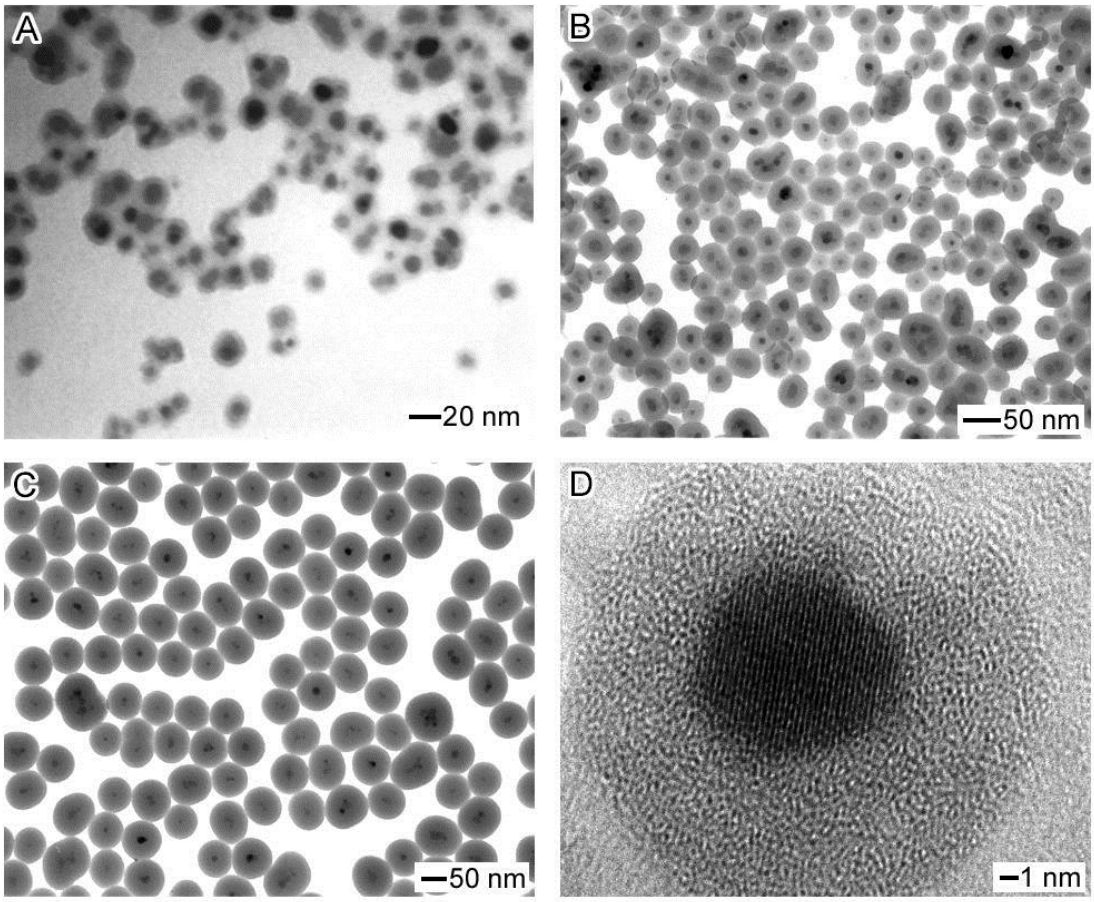

Figure 2.9: TEM images of IONPs whose surface has been coated with silica at various thicknesses, depending on the amount of precursor added to the solution. (A) 10 mg (B) 60 mg (C) 1000 mg of TEOS added to solution. (D) HRTEM image of the iron oxide nanoparticle uniformly coated with a 6 nm thin amorphous silica shell. Reproduced with kind permission from ref.173

Several methods have been reported for coating IONPs with silica; these include the sol-gel process, Stöber methods, non-transferred arc plasma and reverse micelle method.[118]

Since its discovery in 1968 by Werner Stöber and co-workers, the Stöber process has been researched extensively and various modifications of the method published. The Stöber process permits controlled growth of silica particles. The Stöber method involves hydrolysis followed by condensation of tetraethoxy silicates in alcohol under alkaline

conditions resulting in a coreshell structure. Naked NPs are mixed together with an aqueous solution and an alkoxysilane in alcohol. Ammonia was used as a morphological catalyst. Scheme 2.3 shows a summary of the reactions.

(a) Hydrolysis $Si\text{-}[OC_2H_5]_4 + 4\ H_2O \rightarrow Si\text{-}(OH)_4 + 4\ C_2H_5OH$

(b) Alcohol condensation $Si\text{-}(OH)_4 + Si\text{-}[OC_2H_5]_4 \rightarrow \equiv Si\text{-}O\text{-}Si \equiv + 4\ C_2H_5OH$

(c) Water condensation $Si\text{-}(OH)_4 + Si\text{-}(OH)_4 \rightarrow \equiv Si\text{-}O\text{-}Si \equiv + 4\ H_2O$

Scheme 2.3: Summary of reactions in Stöber process for the synthesis of silica nanoparticles

The coating thickness, which can be 5 – 200 nm, is controlled by varying the reaction conditions. The main disadvantage of this method is that it results in polydisperse particles that limit its use *in vivo.*[65, 118, 119, 120, 121]

The reverse micelle method (inverse microemulsion) represents a more convenient and versatile method to coat IONPs with silica. It allows for the control of coating thickness and roughness by manipulating process parameters.[122, 123]

Jang *et al* completed a study which compared the stability and toxicity of silica coated IONPs *vs* uncoated IONPs. The silica-coated nanoparticles were stable and demonstrated enhanced resistance to acidity compared to uncoated nanoparticles. A study on the cytotoxicity indicated that at concentrations of up to 250 µg/mL, both silica coated and uncoated nanoparticle IONPs did not significantly decrease cell viability. [124]

Magnetite can be stabilized prior to coating. Zare *et al.* reported the coating of NPs with polyvinylpyrrolidone (PVP) prior to silica coating.[125]

Arpanaeia *et al* studied the effect of using sodium citrate as a stabilizer on silica coated NPs. Sodium citrate-modified and non-modified magnetite nanoparticles synthesized at

pH 9 were coated with amorphous silica *via* the Stöber method. Results indicated that the stabilised silica coated NPs were more homogenous and had a narrower size distribution. This is because the presence of the citrate groups prevents the NPs from aggregating. On the other hand unmodified NPs showed stronger magnetic properties. This was attributed to the presence of the nonmagnetic layer on the surface of magnetite. [126]

2.4.3. Natural Coatings

2.4.3.1. Chitosan

Chitosan is a natural polymer available from various sea species. It is cationic, biocompatible, hydrophilic, biodegradable, non-immunogenic, non-toxic and non-antigenic. Chitosan has limited solubility under basic conditions; however, it contains several free amino groups that are protonated under acidic conditions, making it cationic; this increases solubility and is responsible for the biocompatibility of chitosan. Chitosan nanoparticles have been developed and several studies on their use for intracellular drug delivery reported.[127, 128] Chitosan-coated IONPs have demonstrated superparamagnetic properties and promising drug release profiles by the use of an external magnet, and therefore could be an effective coating for use in targeted therapy.[129] The limited solubility of chitosan at basic pH makes it difficult to coat IONPs *in situ* because of the basic conditions required to precipitate IONPs.[130]

Y. Ding *et al* recently reported the synthesis of chitosan polymerised IONPs loaded with the anticancer drug 5-fluorouracil *via* emulsion chemical cross-linking.[131] In this study, the chitosan swelling effect (degradation of the chitosan matrix) was investigated at different pH. The drug release rate was rapid in acidic buffer solution as opposed to neutral and basic buffer solution. The study also demonstrated how the thicker polymer diameters slowed down the release of the drug.[131]

2.4.3.2. Dextran

Dextran, a branched polysaccharide, comprising of glucose sub units up to 150 kDa has been used successfully for many applications *in vivo* and *in vitro*. It is non-toxic, biocompatible, biodegradable and inexpensive. Dextran-coated SPIONPs (DSPIONPs) are a well-established platform for the synthesis of imaging agents for applications in diagnostic imaging by MRI, positron emission tomography and photodynamic therapy. Superparamagnetic iron oxide ferumoxtran-10 (Combidex) is approved for clinical use as an MRI contrast agent.[132, 133, 134]

In a recent study, Peng *et al* developed DSPIONPs loaded with Dox (Dox-DSPIONPs) and evaluated cytotoxicity of free Dox, DSPIONPS and Dox-DSPIONPs. The DSPIONPS (up to 2000 µl/mL) showed no cytotoxicity. The IC_{50} values for free Dox and Dox-DSPIONPs were 1.36 µg/mL and 0.533 µg/mL respectively, indicating that Dox-DSPIONPs had reduced cytotoxicity compared to free Dox. In the same study, it was found that Dox was released from Dox-DSPIONPs conjugate after being taken up by cells, released in the cytoplasm, entered the nuclei and eventually intercalated DNA base pairs. Further evaluation *in vitro* showed pH dependency of release of DOX. [133]

Lima *et al* synthesized SPIONPs *via* thermal decomposition in the presence of oleic acid to yield crystalline, monodisperse NPs with a mean diameter of 18 nm. Functionalisation with Dextran or PEG resulted in particles with a hydrodynamic diameter of 170 ± 70 nm and 120 ± 40 nm respectively. Cytotoxicity studies revealed that SPIONPS coated with PEG were non-toxic up to 100 µg/mL, Dextran coated NPs presented low toxicity at concentrations as high as 400 µg/mL. *In vivo* experiments determined the amount of PEG coated and Dextran coated SPIONPS accumulating in the liver, lung, tumour and skin. The majority of nanoparticles accumulated in the lungs and liver. This suggests that when

adsorbed, IONP distribution takes place mainly *via* RES leading to high concentrations in the liver, lungs and the spleen.[135]

Several researchers have reported treating IONPs with epichlohydrin to promote Dextran to form cross-linked iron oxide nanoparticles (CLIOs). Dextran molecules have weak interactions with IONPS, which are prone to detachment after administration *in vivo.* The CLIOs prevent Dextran dissociation and reduce opsonisation thereby increasing the circulation time and blood half-life. Moreover, cross-linking introduces functional groups e.g. amine and acid groups these can be used for conjugation with targeting ligands or therapeutics.[20, 128, 136, 136]

2.4.3.3. Surfactants

SPIONPS may be coated with surfactants. Surfactants usually have a hydrophobic and hydrophilic segment. The hydrophilic segment is adsorbed onto the surface of the nanoparticles, while the hydrophobic segment faces outwards to the solvent to produce a steric effect, thus improving the dispersion state of nanoparticles. The hydrophilic end groups can be –OH, -COOH, -PO $(OH)_2$, -$S(=O)_2OH$.[7]

Various surfactants have been investigated to date and these include sodium oelate, modified polyacrylic acid, sodium hyaluronan, sodium citrate, Triton-X-100 etc. (Figure 2.10)**.** Some surfactants which have been used for IONPs are discussed in this section. [138-140]

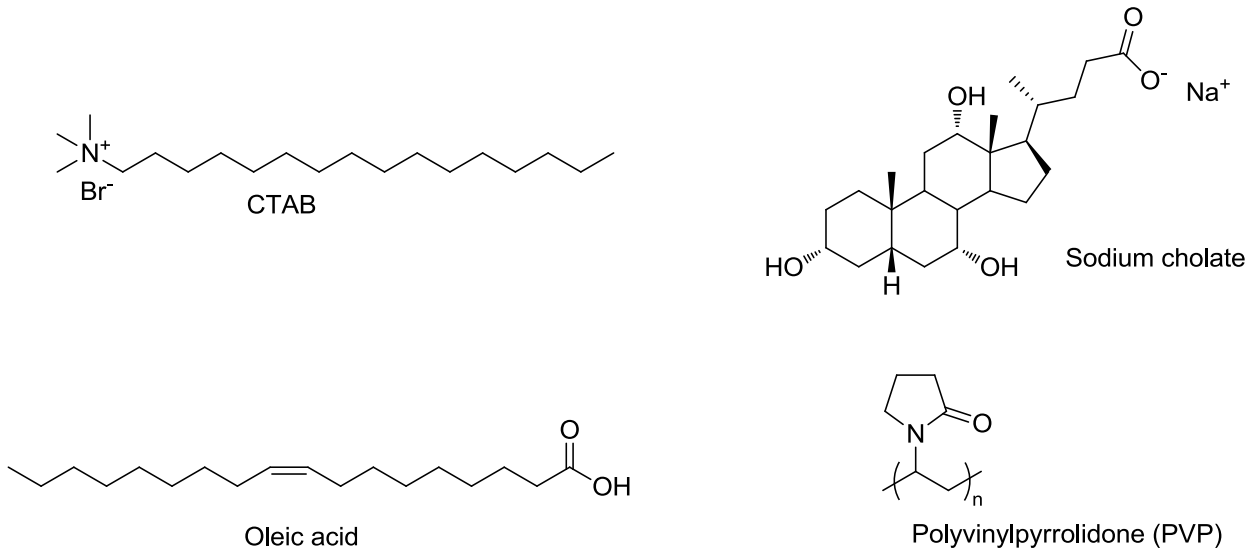

Figure 2.10: Selected surfactants used for INOP surface protection

Filippousi *et al* evaluated three different surfactants, cationic cetyltrimethylammonium bromide (CTAB) surfactant, the nonionic polyvinylpyrrolidone, K30 (PVP) surfactant, and the anionic sodium cholate (S.C.) surfactant. These surfactants vary in terms of molecular weight, as well as polar head group and charge. He found that these distinctions between the surfactants had an impact on morphological, structural and magnetic properties of the resulting coated adduct.[141] Li *et al* recently reported the synthesis of double-layered sodium alpha-olefin sulfonate SPIONPS. They were stable, maintained their original crystallinity and exhibited high water solubility and superparamagnetic properties.[142]

Tietze *et al developed* IONPs stabilised with lauric acid and loaded with anti-cancer drug mitoxantrane. The delivery system efficiently delivered chemotherapeutic drug mitoxantrane to the tumour tissue of rabbits.[143]

Oleic acid (OA) is a commonly used surfactant for modifying IONPs and consists of a non-polar hydrophobic tail and a polar carboxylic acid head group. It forms a very strong

bond between its carboxylic head group and the amorphous IONP surface. OA modified IONPs are biocompatible and OA has been reported to have anti-bacterial activity. Zhang *et al.* characterized OA modified NPs using Fourier transform infra-red and X-ray photoelectron spectroscopy and found that the OA molecules were adsorbed on the magnetic nanoparticles *via* chemisorption.[144-145]

Coating with OA makes IONPs dispersible only in organic solvents and incompatible with an aqueous environment thus their use in the biological system is limited. In a recent study by Pawar *et al,* OA coated IONPs were further coated with chitosan to make them suitable for biological applications. The OA-chitosan coated IONPs showed superparamagnetic behavior at room temperature, high magnetization values, high colloidal stability and low cytotoxicity.[146]

Ligand exchange of oleic acid with dopamine and tiron has been previously investigated. Ligand exchange is an approach based on the mixing of hydrophobic IONPs with a hydrophilic molecule. The hydrophilic ligand displaces the hydrophobic layer on the IONPs, due to its affinity towards IONPs surface resulting in aqueous-stable nanoparticles. Blum *et al* used ligand exchange of oleic acid for tiron (4,5-dihydroxy-1,3-benzenedisulfonic acid disodium salt) and dopamine. Tiron is a cheap, commercially available capping agent that forms strong complexes with iron. Dopamine is also commercially available and can be further functionalized with acids through amide bonds. The IONPs retained their shape, size and superparamagnetic properties after ligand exchange.[147] More recently, Blum *et al* used a single step mechanochemical approach to convert hydrophobic OA-coated SPIONPS to water compatible Tiron-capped.[148] A separate study by Lee *et al* using dopamine capped SPIONPS confirmed the presence of dopamine quinone, a highly reactive compound that is believed to be neurotoxic. (Scheme 2.4) [149, 150, 151]

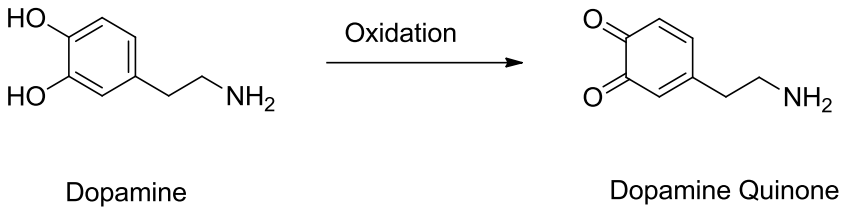

Scheme 2.4: Oxidation of dopamine to dopamine quinone

2.4.3.4. Sugars

There have also been reports on the use of sugars to stabilise IONPs, e.g. sucrose by Patsula *et al.*[152] Herea *et al* reported a modified hydrothermal, single step reaction under alkaline conditions for MNPs coated with glucose-derived polymerization products using glucose and iron salts as starting materials. [153]

Several other reports have been published on using mannose, maltose, lactose and galactose to stabilize IONPs. [7]

2.5. Conjugation

Iron oxide nanoparticles do not possess suitable surface properties for specific applications. Functionalisation with organic groups on their surface can allow them to be conjugated to other molecules. When conjugated with a drug payload, NPs can act as efficient, precise drug delivery systems. The conjugate should be able to carry a drug or multiple drugs without compromising its functionality once attached. Moreover, the drug loaded nanoparticles should release the drug at the target site at a desired rate.

Drugs are usually associated with IONPs *via* direct binding to the iron oxide surface or by encapsulation of both the drug and IONP within a biodegradable polymer matrix. Direct binding can be achieved by covalent or non-covalent linkage.[154]

2.5.1. Covalent Linkage

Covalent linkage involves linking the therapeutic agent to the nanoparticle *via* an amino or hydroxyl functional group already present on the surface of the nanoparticles. The covalent bond should be cleavable on demand, stable in the bloodstream and should not alter the drug's structure. Iodoacetyls, maleimides and pyridyl disulfides have also been used as linkers. Figure 2.11 shows examples of functional groups that have been used for targeted delivery with IONPs.

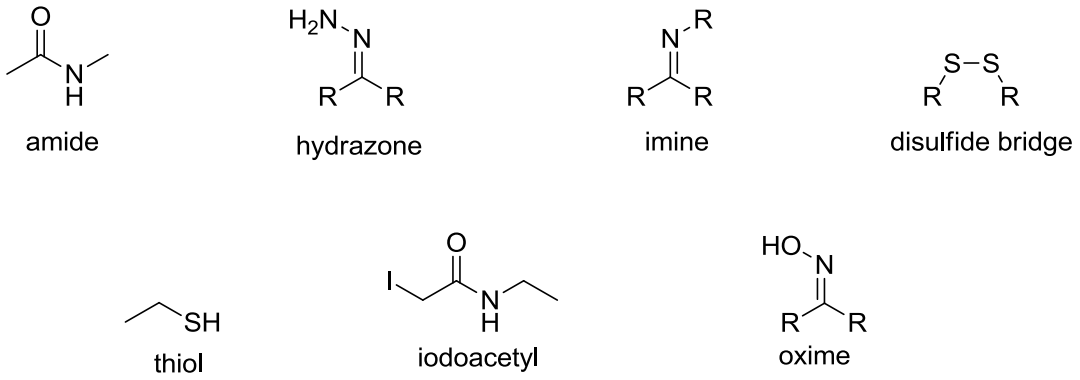

Figure 2.11: Functional groups used for covalent conjugation on targeted delivery[154]

Covalent drug loading involves many synthetic procedures. However, by selecting an appropriate linker, it is possible to ensure drug release only occurs in specifically targeted areas. Covalent bonds which are pH sensitive have been exploited for controlled release. (Table 2.5)

Bond	Notes	Drug Loaded and release trigger	Optimum Release	Ref
Amide	Very robust and can improve the thermal stability of anti-cancer drugs. Amide bond can be cleaved at low pH.	Methotrexate/Citric acid pH	70% (pH 4, 37 °C, 48 h)	155
Hydrazone	Most used pH sensitive bond.	DOX/PEI pH	33% (pH 4.5, 37 °C, 24 h)	156
Schiff's base (Imine)	Stable at physiological pH, low pH facilitates hydrolysis of bond and high temperature accelerates hydrolysis	DOX pH	57.8% (pH 5.7, 50 °C, 8 h)	157
Disulfide bridges	Can be cleaved in the presence of reducing agents such as glutathione which is over expressed in cancer cells.	O^6 – benzylguanine Reduction	100% (pH 5, 37 °C, 100 mM glutathione)	158

Table 2.5: Examples of covalent IONP-drug conjugates

2.5.2. Non-covalent

Non-covalent interactions include electrostatic, absorption, coordination, hydrophobic/hydrophilic and affinity interactions (Table 2.6).

Non-covalent	Notes	Drug matrix	Release kinetics	Ref
Hydrophobic	The hydrophobic zone created by coating acts as a reservoir and is destabilised in acidic environments	DOX/Oleic acid	70% (pH 6.5, 37 °C)	159
Electrostatic and hydrophobic	DOX absorbed through hydrophobic and electrostatic interactions.	DOX/PEG	75% (pH 5.5, RT, 25 h)	160
Coordination	pH sensitive metal to ligand coordination	DOX	67.2% (pH 4, 37 °C, 24 h)	161
Encapsulation		DOX/PEG/liposome		162

Table 2.6: Non covalent drug interactions

The choice of chemistry depends on the IONP surface and the ligand. Non-covalent binding has several synthetic advantages, i.e. no modification step required and therefore fewer synthetic steps, resulting in reduced potential for toxicity, and better cost effectiveness.

2.6. Release

The release mechanism of a magnetically tagged drug further enhances its selective destruction of tumours. It has been observed in several studies that the drug payload is quickly released *in vivo* following administration before it reaches its target. This is referred to as the "burst effect". Recently, stimuli responsive polymer coated SPIONs have become popular in the field of targeted delivery for cancer therapy. These polymers can undergo structural and physical transitions with change in the environmental conditions, e.g. pH, ionic strength, light, temperature, magnetic or electric properties.[162]

2.6.1. pH triggered

The slightly acidic pH in the tumour region and endosomes makes a pH responsive mechanism a good approach. Therefore, drug delivery systems that release the drug payload at low pH are preferred.

Several polymers undergo rapid dissolution when the pH of the medium is less than 6.5 and hence are expected to release their contents once within the acidic tumour microenvironment and endo/lysosome compartments of cells.[163] Fang *et al* evaluated the drug release rate of SPIONPs with a biodegradable, pH sensitive poly (beta-amino ester), copolymer loaded with DOX. The model showed higher release rates at lower pH compared to physiological pH.[164] Kievet *et al* conjugated DOX to PEI coated IONPs *via* the pH sensitive hydrazine bond. The highest Dox release was achieved at pH below 6.[165] Gautier *et al* studied the *in vitro* release of DOX from DOX loaded PEG-SPIONPs. The results demonstrated that the PEG layer delays drug release at physiological pH 7.4. However, lowering the pH to 4 accelerated the release of the drug by up to 85% in one hour.[89]

Recently Prabha *et al* developed β-cyclodextrin (β-CD) – polyethyleneglycol (PEG) – polyethyleneimine (PEI) coated IONPs with particle size range or 151-300 nm for drug delivery applications. The IONPs were loaded with 5-fluorouracil (5-FU), a low molecular weight antineoplastic used for solid tumours like stomach, colon, breast cancer etc. The loading capacity and in vitro release behaviour of 5-FU from the nanocomposites was evaluated in a phosphate buffer at pH 1.2 and 6.8 and at temperatures 37 °C and 45 °C. Drug release was faster at pH 6.8 than at pH 1.2. This was attributed to a high polymer swelling effect which is a consequence of high pH. Increasing the temperature also resulted in faster release rate. The amount of drug encapsulated in this study ranged from 10-50%. In this study, it was also noted that slowest release rate was observed where the least amount of drug was loaded onto the nanocomposites. This was attributed to the additional free void spaces that the drug molecules had to travel through.[102] Peng *et al* developed dextran coated SPIONPs conjugated to DOX (Dox-DIONP). DOX release *in vitro* assays were carried out at pH 5, 6 and 7 to simulate lysosomal, endosomal and extra cellular components of the tumour microenvironment respectively. A high release rate was observed at pH 5 and the lowest release rate observed at physiological pH 7. The optimum release was at acidic pH, this was attributed to degradation of dextran at acidic pH.[133]

Zhu *et al* reported the synthesis of IONPs attached to cystamine tert-acylhydrazine (CTA). The disulfide and acylhydrazine groups were attached onto the surface of SPIONPs through the coordination of CTA sulfur groups with Fe_3O_4 nanoparticles. DOX and PEG were conjugated onto the surface of IONPs nanoparticles via pH-sensitive acylhydrazone link. Accordingly, a multifunctional pH-sensitive SPIO nanocomposite system with long circulation, magnetic targeting and controlled release ability was successfully constructed. Under an acidic environment, the drug release of the nanocarrier

was accelerated greatly, attributed to the cleavage of pH-sensitive acylhydrazone linkages.[166]

The findings from these studies suggest that the release of DOX under neutral conditions i.e. in blood plasma and normal tissue would be minimal, thereby reducing the systemic distribution of DOX during drug delivery.

Nigam *et al.* developed citric acid functionalized (citrate-stabilized) IONPs (CA-IONPs) loaded with DOX (Figure 2.12) and evaluated the potential of the conjugate as a carrier system.[167]

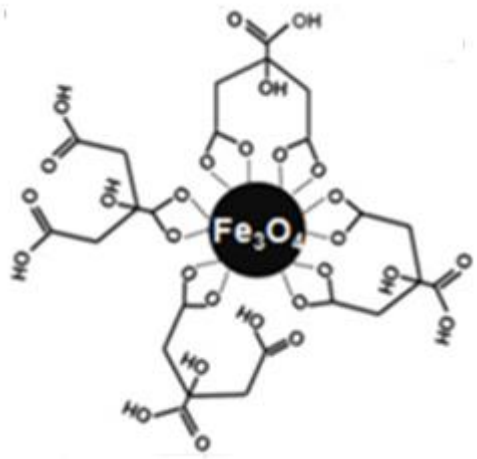

Figure 2.12: Structure of citrate stabilized IONP

The positively charged DOX was bound to the surface of the negatively charged CA-IONPs *via* electrostatic interactions. Drug release profiles were investigated at pH 5 and pH 7.3. The optimum release was obtained at pH 5. A sustained release of 60% of drug molecules was observed over 50 hours. At acidic pH, the carboxyl groups on the nanoparticle surface becomes partially neutralised due to the presence of protons. This leads to weakening of the electrostatic forces, resulting in the release of the drug. This is a slow process, which results in long, sustained release of the drug load.[167]

2.6.2. Hyperthermia

Cancer cells are susceptible to heat, a change in temperature from 37 °C to 43 °C is sufficient to kill cancer cells provided this temperature be maintained for a sufficient period. Moreover, when the temperature is above 46 °C, tissues undergo thermal necrosis, also known as thermoablation.

MNPs, in an alternating magnetic field, can be used to target a specific tumour location and deliver a toxic dose of heat. This heat has been proposed as a mechanism to trigger release of chemotherapeutic agents, a concept known as magnetic hyperthermia. By killing cancer cells and damaging proteins and structures within cells, hyperthermia may shrink tumours. To be efficient, magnetic hyperthermia requires that MNPs have a sufficiently high specific absorption rate (SAR), to deposit heat quickly onto cancer cells while minimizing damage on healthy tissue. SAR is dependent on physical properties such as size, saturation magnetization of the nanoparticles, particles structure and interparticle interactions.[168]

As the size of IONPs decreases, the saturation magnetization also tends to decrease, thereby reducing heating efficiency. To overcome this, the use of core/shell IONPs has been proposed by several researchers. It has been reported that core/shell IONPs provide high saturation magnetization and increases hysteresis losses, enhancing its use for hyperthermia.

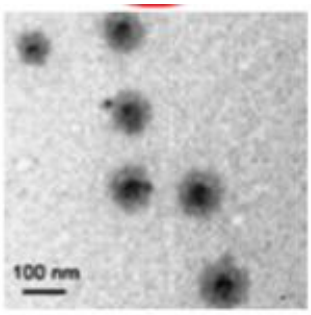

Figure 2.13: TEM Image of core-shell polymer-coated IONPs[169]

Nemati *et al* developed core/shell IONPs with average sizes of 8, 12, 14 nm and studied how size affected their heating properties for magnetic hyperthermia. Their results indicated that the bigger the core/shell IONPs had better heating efficiency and magnetic properties. Moreover, these IONPs retained their core/shell morphology for longer periods, making them more suited for biological applications.[170]

Temperature responsive polymers have become popular for controlled drug release. The drug release is dependent upon the change in temperature. Below what is known as a critical solution temperature (CST), thermoresponsive polymers are soluble in water and, after heating, they become insoluble and form an emulsion. Much work has focused on raising the lower critical solution temperature (LCST), i.e. the critical temperature below which the components of a mixture are miscible for all compositions. Polymers which become insoluble upon heating, have a so-called lower LCST. Below the LCST, the polymer is hydrophilic. However, above this temperature the polymer becomes hydrophobic and cloudy. (Figure 2.14).[162]

Figure 2.14: Image of poly-SPIONs below and above LCST [162]

The thermos-responsive nature of the polymer means that upon reaching LCST, the polymer becomes hydrophobic and shrinks, releasing its aqueous content and expelling DOX at the same time.

Kakwere *et al* developed thermo-responsive polymer-coated (N-isopropylacrylamide polymer), (Figure 2.15) cubic-IONPs loaded with DOX to obtain thermo-responsive, biocompatible nanohybrids.[171]

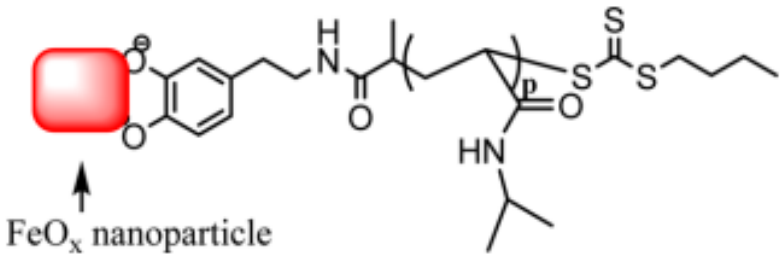

Figure 2.15: IONPs functionalized with thermoresponsive polymer (PNIPAAM)

In this study, the LCST was 47 °C. The drug release was assessed at 25, 37 and 50 ° C (above the LCST). The DOX loaded IONPs exhibited a negligible drug release below 37 °C. However, at higher temperatures (50 °C), they showed a consistent release of DOX by exploiting the capability of the IONPs to generate heat under an alternating magnetic field.[171] Rastogi *et al.* also studied the drug release profile of PNIPAAM-PEGMA IONPs loaded with DOX, with an LCST of 44 °C. The optimum release was observed at hyperthermia temperature (45 ° C) and a slightly acidic pH 5.5, with 72.42 ± 5.25 % of the drug released over 48 h.[172]

2.6.3. Dual Responsive Release:

Dual responsive release systems, where temperature and/or pH are used to trigger drug release have also been reported. They offer advanced features for the targeted delivery of drug molecules *via* the combination of magnetic targeting, and dual pH- and thermo-responsive behaviour, which offers spatial and temporal control over the release of a drug load.

Wadajkar *et al.* investigated the drug release of DOX loaded poly (*N*-isopropylacrylamide-chitosan) (PAC)-coated MNPs linked to DOX. The drug release was investigated by incubating the drug-loaded nanoparticles at different temperature (37 °C and 40 °C) and pH (6 and 7.4). Enhanced drug release was obtained at 40 °C and at pH 6. This shows that a combination of external heat and low pH would result in enhanced drug release. In this case, the presence of chitosan further enhanced the pH responsiveness.[169]

Hervault *et al.* developed magnetic, thermo sensitive nano-carriers conjugated to anti-cancer drug DOX *via* acid-cleavable imine linker. A PEG based polymer P (DEGMA-co-PEGMA-b-[TMSPMA-co-VBA]) consisting of two monomers di (ethylene glycol)

methyl ether methacrylate (DEGMA) and poly(ethylene glycol) methyl ether methacrylate (PEGMA) was used.

The use of two PEG chains of different length provides temperature-responsive behaviour to the polymer, with the possibility to tune the LCST by varying the molar ratio PEGMA: DEGMA.

DOX was conjugated to the nano-carriers through an imine bond, also called a Schiff base bond, between the primary amine group of DOX and the aldehyde group of P(DEGMA-co-PEGMA-b-[TMSPMA-co-VBA]). The drug release studies were performed at 25 °C, 37 °C (<LCST) and 50 °C (LCST). For each temperature, one sample was held at pH = 7.4 and another at pH = 5.7. The optimal release was found at pH 5.7 and temperature of 50 °C. At physiological pH and temperature, the release of DOX was low. The acidic pH facilitated the hydrolysis of the imine bond. In this case the accelerated temperature has two effects, facilitating the burst effect upon reaching LCST and temperature-accelerated hydrolysis of the imine bond.[157]

In this multi-stimulus system, the drug release could be triggered as a consequence of magnetic drug targeting, hyperthermia and tumour acidic pH.

2.7. Limitations of the use of IONPs

2.7.1. Toxicity

The increasing applications of IONPs are accompanied by concerns about their toxicological properties and long term effect on human health and aquatic life. Over the last number of years, efforts have been made to investigate the potential effects of IONPs and address the safety issues associated with their use. Many studies have demonstrated that at concentrations of 100 µg/mL or higher, IONPs may cause low toxicity or cytotoxicity. Several *in vitro* studies have demonstrated that silver and zinc based

nanoparticles are more toxic than IONPs. The toxicity of IONPs cannot be properly established yet since results from *in vitro* studies are often contradictory; *in vivo* and human epidemiological studies are scarce.

A study by Sundarraj *et al* on mice indicated that IONPs can cross the blood testes barrier causing testicular cytotoxicity due to oxidative stress and apoptosis.[174] A study by Zhu *et al* on zebrafish demonstrated that IONPs caused serious delays in embryonic hatching; causing malformation in some zebrafish embryos and larvae and eventual mortality.[175]

It has been suggested that most NP toxicity *in vivo* is a result of the production of reactive oxygen species (ROS) such as singlet oxygen, superoxide, hydrogen peroxide, and hydroxyl radicals. ROS are important in certain physiological processes such as respiration and cell signalling. However, an outburst of ROS results in what's known as oxidative stress. Oxidative stress causes oxidative damage of biomolecules and disruption of cell signalling mechanisms.[176-178]

Several studies have suggested that area and surface chemistry influence nanoparticle toxicity. Passivation of the IONPs by surface functionalization may enhance their resistance to lysosomal acidity, prevent agglomeration and also modulate dissolution kinetics, thereby reducing the overall toxicity. Dextran, silica, and PEG coated IONPS have shown reduced cytotoxicity in *in vitro* tests. There have been reports of NP size, and shape-related toxicity. Nanoparticle size and shape can be controlled during synthesis. (See Section 2.3.).[178]

Several techniques are used to assess the toxicity on nanoparticles *in vitro* and they are shown on Table 2.7.

Technique	Notes
In vitro assays	• For cell viability, proliferation and differentiation
Microscopy	• Electron and atomic force microscopy for intracellular localization
In vitro hemolysis assays	• Effects of nanoparticle exposure on red blood cells, • Evaluates hemoglobin release in the plasma as an indicator of red blood cell lysis
Genotoxicity assays	• Evaluates the ability of NPs to damage chromosomes and/or DNA

Table 2.7 : Currently used in vitro toxicity testing techniques [181]

These *in vitro* techniques are used for initial evaluation of NPs, to identify specific characteristics and as indicators of toxicity. They shed light on changes in membrane integrity, metabolic activity, and genetic material of cells upon reacting with IONPs. However, they have limitations such as their interaction with assay components and they cannot be used as a good prognostic indicator of long term physiological effects.[180] Even though some IONPs are approved for use as MRI agents, translation to use in other *in vivo* applications such as drug delivery is limited due to concentration dependent toxicity. Very little correlation has been made between *in vitro* and *in vivo* studies due to the inability of *in vitro* studies to mimic the complex environment *in vivo.* Researchers have found that some toxic responses found *in vitro* are not reproduced *in vivo.* This could be attributed to homeostasis which regulate the changes in pH, chemical composition and ionic strength in the blood.[181] Before registration of any drug for FDA approval on clinical trials, *in vivo* studies explaining absorption, distribution, metabolism and elimination should be completed, and this remains a challenge.

Analytical Tool	Advantages	Disadvantages
Inductively Coupled Plasma	Can determine nanoparticles composition, concentration, size, size distribution, and agglomeration	Acid digestion during sample preparation means sample cannot be used further
TEM	Good resolution for visualisation of individual particles.	Resolution is limited to two dimensions Extensive preparation is required which may alter cells
Confocal	Less invasive sample preparation	May require fluorescent tags which alter particle behavior
Coherent anti-Stokes Raman Speectroscopy	Three-dimensional visualisation of metal oxide nanoparticles in intact biological tissue Requires little sample preparation	Limited in its ability to resolve sub-cellular structure.

Table 2.8: Analytical tools currently used for analysis (adapted from Scown et al) [182]

The diverse potential applications of nanotechnology mean that it will inevitably yield considerable benefits to society. However, as the nano industry grows and the use of nanoparticles increase, so will the quantities released to the environment. The aquatic environment is particularly at risk because it acts as a sink for most environmental contaminants. Like in humans, NPs are likely to have different effects in aquatic life compared to their bulkier counterparts. Also, their small size means they can pass barriers that prohibit entry of bulkier particles.

One of the factors making it challenging to determine the toxicity in aquatic life and *in vivo* is the lack of techniques and equipment to trace, measure, visualise and quantify the nanoparticles. Table 2.8 shows equipment currently used and their limitations.

Overall, the toxicity of nanoparticles is not fully understood. Current literature suggests that nanoparticles have potential adverse effects. More detailed studies in their physicochemistry and their interaction with other systems is required. Standardized approaches are also required in order to classify nanoparticles according to their hazard. Testing every nanoparticle type with every given size and coating, in every aquatic test media would not be time or cost effective and current efforts are focused on developing standard test methods and analytical tools for effective tracing and quantification of nanomaterials.[182]

2.7.2. Other limitations

Another limitation for using IONPs as nano-carriers for *in vivo* targeting is creating suitable magnetic field gradient is required for effective targeting and localization. The magnetic force should be strong enough to overcome resistance of blood flow from veins and arteries. Also, the magnetic field diminishes rapidly as a function of distance from the target tissue. This limits the targeting ability *in vivo*, and means that only areas close to the surface of the skin can be targeted. Efforts are being made to engineer a magnetic field that penetrates to a greater depth.

Lack of appropriate surface engineering on nanoparticles results in premature release of the drug load before it reaches its target site, known as the "burst effect". The heterogeneous and complex structure of tumours make them very difficult to target. The EPR vary substantially between tumours and patients. Even parts of a tumour vary in terms of vascular permeability. This presents problems in specific targeting.

2.8. Conclusion

This review has discussed cancer, the current treatment methods and their limitations. Several drug delivery mechanisms for specific targeting of anti-cancer drugs have been discussed and their current developments. IONPs in targeted drug delivery have been discussed in detail; their synthesis, surface modification and conjugation to chemotherapeutics. Targeted release is important as it ensures that the drug payload is released at a specific site and therefore enhancing drug selectivity. Different release mechanisms that ensure the drug payload is released at a specific site have been discussed.

The use of IONPs for targeted delivery is a promising field, however there are still no FDA approved IONP drug delivery system on the market. Further research is required to understand how IONPs behave *in vivo,*and address toxicity *in vivo* and to aquatic life,

2.9. References

1. Lammers, T.; Kiessling, F.; Hennink, W. E.; Storm, G. *J. Control. Release* **2012**, *161*, 175–187.
2. https://www.cancer.ie/ (accessed 26/11/2016)
3. Lammers, T.; Rizzo, L. Y.; Storm, G.; Kiessling, F. *Clin. Cancer Res.* **2012**, *18*, 4889–4894.
4. Wahajuddin; Arora, S. *Int. J. Nanomedicine* **2012**, *7*, 3445–3471.
5. Hasany, S. F.; Ahmed, I.; J, R.; Rehman, A. *Nanosci. Nanotechnol.* **2012**, *2*, 148–158.
6. Kandasamy, G.; Maity, D. *Int. J. Pharm.* **2015**, *496*, 191–218.
7. Douziech-Eyrolles, L.; Marchais, H.; Herve, K.; Munnier, E.; Souce, M.; Linassier, C.; Dubois, P.; Chourpa, I. *Int J Nanomedicine.* **2007**, *2* (4), 541–550.
8. Tietze, R.; Zaloga, J.; Unterweger, H.; Lyer, S.; Friedrich, R. P.; Janko, C.; Pöttler, M.; Dürr, S.; Alexiou, C. *Biochem. Biophys. Res. Commun.* **2015**, 1–8.

9. Khan, D. R.; Webb, M. N.; Cadotte, T. H.; Gavette, M. N. *Breast Cancer (Auckl).* **2015**, *9* (Suppl 2), 1–5.

10. Dinndorf, P. A.; Gootenberg, J.; Cohen, M. H.; Keegan, P.; Pazdur, R. *Oncologist* **2007**, *12* (8), 991–998.

a. Morilla, M. J.; Romero, E. L. *Nanomedicine (Lond).* **2015**, *10* (3), 465–481.

11. Ferlay, J.; Steliarova-Foucher, E.; Lortet-Tieulent, J.; Rosso, S.; Coebergh, J. W. W.; Comber, H.; Forman, D.; Bray, F. *Eur. J. Cancer.* **2013**, *49* (6), 1374–1403.

12. health.gov.ie (accessed 27/17/2016)

13. http://www.who.int/mediacentre/factsheets/fs297/en/ (accessed 27/17/2016)

14. Lammers, T.; Kiessling, F.; Hennink, W. E.; Storm, G. *J. Control. Release.* **2012**, *161*, 175–187.

15. Van de Waterbeemd, H.; Gifford, E. *Nat. Rev. Drug Discov.* **2003**, *2*, 192–204.

16. Prokop, A.; Davidson, M., J. *J. Pharm. Sci.* **2008**, *97*, 3518–3590.

17. Juillerat-Jeanneret, L.; Schmitt, F. *Med. Res. Rev.* **2007**, *27*, 574–590.

18. Gil, P. R.; Parak, W. J. *ACS Nano.* **2008**, *2*, 2200–2205.

19. Rumpf, K.; Granitzer, P.; Morales, P. M.; Poelt, P.; Reissner, M. *Nanoscale Res. Lett.* **2012**, *7*, 445–449.

20. Cole, A. J.; David, a E.; Wang, J.; Galban, C. J.; Hill, H. L.; Yang, V. C. *Biomaterials.* **2011**, *32*, 2183–2193.

21. Wahajuddin; Arora, S. *Int. J. Nanomedicine.* **2012**, *7*, 3445–3471.

22. Borny, R.; Lechleitner, T.; Schmiedinger, T.; Hermann, M.; Tessadri, R.; Redhammer, G.; Neumüller, J.; Kerjaschki, D.; Berzaczy, G.; Erman, G.; Popovic, M.; Lammer, J.; Funovics, M. *Contrast Media Mol. Imaging.* **2015**, *10* (1), 18–27.

23. Bazak, R.; Houri, M.; Achy, S. El; Hussein, W.; Refaat, T. *Mol. Clin. Oncol.* **2014**, *2* (6), 904–908.

24. Dilnawaz, F.; Singh, A.; Mewar, S.; Sharma, U.; Jagannathan, N. R.; Sahoo, S. K. *Biomaterials.* **2012**, *33* (10), 2936–2951.

25. http://www.ncri.ie/data (accessed 30/5/2017)

26. Zhang, H.; Liu, X.; Wu, F.; Qin, F.; Feng, P.; Xu, T.; Li, X.; Yang, L. *Int. J. Mol. Sci.* **2016**, *17* (5), 676-680.

27. Nagesh, P. K. B.; Johnson, N. R.; Boya, V. K. N.; Chowdhury, P.; Othman, S. F.; Khalilzad-Sharghi, V.; Hafeez, B. B.; Ganju, A.; Khan, S.; Behrman, S. W.; Zafar, N.; Chauhan, S. C.; Jaggi, M.; Yallapu, M. M. *Colloids Surf. B. Biointerfaces.* **2016**, *144*, 8–20.

28. Puri, R.; Kaur Bhatia, R.; Shankar Pandey, R.; Kumar Jain, U.; Katare, O. P.; Madan, J. *Drug Dev. Ind. Pharm.* **2016**, *9045* (June), 1–11.

29. Kim, F. J.; Schrock, J. M.; Spino, C. M.; Marino, J. C.; Pasternak, G. W. *Biochem. Biophys. Res. Commun.* **2012**, *426* (2), 177–182.

30. Bahrami, B.; Mohammadnia-Afrouzi, M.; Bakhshaei, P.; Yazdani, Y.; Ghalamfarsa, G.; Yousefi, M.; Sadreddini, S.; Jadidi-Niaragh, F.; Hojjat-Farsangi, M. *Tumour Biol.* **2015**, *36* (8), 5727–5742.

31. Cancer in Ireland 2013: Annual report of the National Cancer Registry

32. Recondo, G.; de la Vega, M.; Galanternik, F.; Díaz-Cantón, E.; Leone, B. A.; Leone, J. P. *Cancer Manag. Res.* **2016**, *8*, 57–65.

a. Slamon, D. J.; Clark, G. M.; Wong, S. G.; Levin, W. J.; Ullrich, A.; McGuire, W. L. *Science*. **1987**, *235* (4785), 177-182.

33. Slamon, D. J.; Clark, G. M.; Wong, S. G.; Levin, W. J.; Ullrich, A.; Mcguire, W. L. *Science* .**1987**, *235* (21), 177–182.

a. Leone, J. P.; Bhargava, R.; Theisen, B. K.; Hamilton, R. L.; Lee, A. V; Brufsky, A. M. *Oncotarget.* **2015**, *6* (30), 1–7.

34. Leuschner, C.; Kumar, C. S. S. R.; Hansel, W.; Soboyejo, W.; Zhou, J.; Hormes, J. *Breast Cancer Res. Treat.* **2006**, *99* (2), 163–176.

35. Aydar, E.; Onganer, P.; Perrett, R.; Djamgoz, M. B.; Palmer, C. P. *Cancer Lett.* **2006**, *242* (2), 245–257.

a. Schweiger, T.; Hegedüs, B.; Nikolowsky, C.; Hegedüs, Z.; Szirtes, I.; Mair, R.; Birner, P.; Döme, B.; Lang, G.; Klepetko, W.; Ankersmit, H. J.; Hoetzenecker, K. *Ann. Surg. Oncol.* **2014**, *21* (3), 946–954.

36. Schweiger, T.; Hegedüs, B.; Nikolowsky, C.; Hegedüs, Z.; Szirtes, I.; Mair, R.; Birner, P.; Döme, B.; Lang, G.; Klepetko, W.; Ankersmit, H. J.; Hoetzenecker, K. *Ann. Surg. Oncol.* **2014**, *21* (3), 946–954.

37. Zong, S.; Li, H.; Shi, Q.; Liu, S.; Li, W.; Hou, F. *Clin. Chim. Acta.* **2016**, *458*, 106–114.

38. Byrne, J. D.; Betancourt, T.; Brannon-Peppas, L. *Adv. Drug Deliv. Rev.* **2008**, *60* (15), 1615–1626.

39. Fortina, P.; Kricka, L. J.; Graves, D. J.; Park, J.; Hyslop, T.; Tam, F.; Halas, N.; Surrey, S.; Waldman, S. A. *Trends Biotechnol.* **2007**, *25* (4), 145–152.

40. Chen, H. W.; Medley, C. D.; Smith, J. E.; Sefah, K.; Shangguan, D. *Chem. Med Chem.* **2013**, *3* (6), 991–1001.

41. Zhan, P.; Wang, J.; Lv, X.; Wang, Q.; Qiu, L.; Lin, X.; Yu, L.; Song, Y. *J. Thorac. Oncol.* **2009**, *4* (9), 1094–1103.

42. Yang, H.-W.; Hua, M.-Y.; Liu, H.-L.; Tsai, R.-Y.; Chuang, C.-K.; Chu, P.-C.; Wu, P.-Y.; Chang, Y.-H.; Chuang, H.-C.; Yu, K.-J.; Pang, S.-T. *ACS Nano.* **2012**, *6* (2), 1795–1805.

43. Socaci, C.; Magerusan, L.; Turcu, R.; Liebscher, J. *Mater. Chem. Phys.* **2015**, *162*, 131–139.

44. Pourjavadi A,; Tehrani Z,; Moghanaki A. *Pharm. Res.* **2016,** *33*, 417-432.

45. Huang, C.; Neoh, K. G.; Kang, E. T. *Langmuir*. **2012**, *28* (1), 563–571.

46. Chen, S.; Zhang, H.; Wan, L.; Jiang, S.; Xu, Y.; Liu, F.; Zhang, T.; Ma, D.; Xie, M. *Mol. Med. Rep.* **2016**, 5059–5067.

47. Ma, H.; Liu, Y.; Shi, M.; Shao, X.; Zhong, W.; Liao, W.; Xing, M. M. Q. *Biomacromolecules.* **2015**, *16* (12), 4022–4031.

48. Li, Y.-J.; Dong, M.; Kong, F.-M.; Zhou, J.-P. *Int. J. Pharm.* **2015**, *489* (1), 83–90.

49. Maeng, J. H.; Lee, D.-H.; Jung, K. H.; Bae, Y.-H.; Park, I.-S.; Jeong, S.; Jeon, Y.-S.; Shim, C.-K.; Kim, W.; Kim, J.; Lee, J.; Lee, Y.-M.; Kim, J.-H.; Kim, W.-H.; Hong, S.-S. *Biomaterials* **2010**, *31* (18), 4995–5006.

50. Akhtar, M. J.; Ahamed, M.; Alhadlaq, H. A.; Alrokayan, S. A.; Kumar, S. *Clin. Chim. Acta* **2014**, *436*, 78–92.

51. Alberts, B.; Johnson, A.; Lewis, J. *Molecular Biology of the Cell*. 4th Edition. Garland Science; **2002**.

52. Arosio, D.; Casagrande, C. *Adv. Drug Deliv. Rev.* **2016**, *97*, 111–143.

53. Desgrosellier, J. S.; Cheresh, D. A. *Nat. Rev. Cancer.* **2010**, *10* (1), 9–22.

54. Nazli, C.; Demirer, G. S.; Yar, Y.; Acar, H. Y.; Kizilel, S. *Colloids Surfaces B Biointerfaces.* **2014**, *122*, 674–683.

55. Nagesh, P. K. B.; Johnson, N. R.; Boya, V. K. N.; Chowdhury, P.; Othman, S. F.; Khalilzad-Sharghi, V.; Hafeez, B. B.; Ganju, A.; Khan, S.; Behrman, S. W.; Zafar, N.; Chauhan, S. C.; Jaggi, M.; Yallapu, M. M. *Colloids Surf. B. Biointerfaces.* **2016**, *144*, 8–20.

56. Schwertmann, U.; Cornell, R. *The Iron Oxides: Structure, Properties, Reactions, Occurences and Uses*, Wiley-VCH, **2003**.

57. Krishnan, K. M. *IEEE Trans. Magn.* **2010**, *46*, 2523–2558.

58. Lee, J. H.; Ju, J. E.; Kim, B. Il; Pak, P. J.; Choi, E. K.; Lee, H. S.; Chung, N. *Environ. Toxicol. Chem.* **2014**, *33* (12), 2759–2766.

59. Yang, L.; Kuang, H.; Zhang, W.; Aguilar, Z. P.; Xiong, Y.; Lai, W.; Xu, H.; Wei, H. *Nanoscale*. **2015**, *7* (2), 625–636.

60. Roohi, F.; Lohrke, J.; Ide, A.; Schutz, G.; Dassler, K. *Int. J. Nanomedicine.* **2012**, *7*, 4447–4458.

61. Krishnan, K. M. *IEEE Trans. Magn.* **2010**, *46*, 2523–2558.

62. Ujiie, K.; Kanayama, N.; Asai, K.; Kishimoto, M.; Ohara, Y.; Akashi, Y.; Yamada, K.; Hashimoto, S.; Oda, T.; Ohkohchi, N.; Yanagihara, H.; Kita, E.; Yamaguchi, M.; Fujii, H.; Nagasaki, Y. *Colloids Surfaces B Biointerfaces.* **2011**, *88*, 771–778

63. Roth, H.-C.; Schwaminger, S. P.; Schindler, M.; Wagner, F. E.; Berensmeier, S. *J. Magn. Magn. Mater.* **2015**, *377*, 81–89.

64. Massart, R. *IEEE Trans. Magn.* **1981**. *17*, 1247–1248.

65. Wu, W.; He, Q.; Jiang, C. *Nanoscale Res. Lett.* **2008**, *3* (11), 397–415.

66. Wang, J.; Zhang, B.; Wang, L.; Wang, M.; Gao, F. *Mater. Sci. Eng. C. Mater. Biol. Appl.* **2015**, *48*, 416–423.

67. Ozel, F.; Kockar, H. *J. Magn. Magn. Mater.* **2015**, *373*, 213–216.

68. Daou, T. J.; Pourroy, G.; Bégin-Colin, S.; Grenèche, J. M.; Ulhaq-Bouillet, C.; Legaré, P.; Bernhardt, P.; Leuvrey, C.; Rogez, G. *Chem. Mater.* **2006**, *18*, 4399–4404.

69. Wang, J.; Sun, J.; Sun, Q.; Chen, Q. *Mater. Res. Bull.* **2003**, *38*, 1113–1118.

70. Wang, F.; Qin, X.F.; Meng, Y.F.; Guo, Z.L.; Yang, L.X.; Ming, Y.F. *Mater. Sci. Semicon. Process*. **2015**, *16*, 802–806

71. Kriedemann, B.; Fester, V. *Chem. Eng. J.* **2015**, *281*, 312–321.

72. Wu, M.; Long, J.; Huang, A.; Luo, Y.; Feng, S.; Xu, R. *Langmuir*. **1999**, *15*, 8822–8825.

73. Xu, Y.; Xu, R. *Modern Inorganic Synthetic Chemistry*, Elsevier, **2010.**

74. Glasgow, W.; Fellows, B.; Qi, B.; Darroudi, T.; Kitchens, C.; Ye, L.; Crawford, T. M.; Mefford, O. T. *Particuology*. **2016**.

75. Chang, C.-H.; Paul, B. K.; Remcho, V. T.; Atre, S.; Hutchison, J. E. *J. Nanoparticle Res.* **2008**, *10*, 965–980.

76. Gonzalez-Moragas, L.; Yu, S.-M.; Murillo-Cremaes, N.; Laromaine, A.; Roig, A. *Chem. Eng. J.* **2015**, *281*, 87–95.

77. Jiang, F.; Li, X.; Zhu, Y.; Tang, Z. *Phys. B Condens. Matter*. **2014**, *443*, 1–5.

78. Chen, Z. *Synth. React. Inorganic, Met. Nano-Metal Chem.* **2012**, *42*, 1040–1046.

79. Taboada, E.; Rodríguez, E.; Roig, A.; Oró, J.; Roch, A.; Muller, R. N. *Langmuir*. **2007**, *23*, 4583–4588.

80. Ujiie, K.; Kanayama, N.; Asai, K.; Kishimoto, M.; Ohara, Y.; Akashi, Y.; Yamada, K.; Hashimoto, S.; Oda, T.; Ohkohchi, N.; Yanagihara, H.; Kita, E.; Yamaguchi, M.; Fujii, H.; Nagasaki, Y. *Colloids Surfaces B Biointerfaces.* **2011**, *88*, 771–778.

81. Okoli, C.; Boutonnet, M.; Mariey, L.; Järås, S.; Rajarao, G. *J. Chem. Technol. Biotechnol.* **2011**, *86* (11), 1386–1393.

82. Bashir, M.; Riaz, S.; Naseem, S. *Mater. Today Proc.* **2015**, *2* (10), 5664–5668.

83. Owens, G.; Singh, R. K.; Foroutan, F.; Alqaysi, M.; Han, C.-M.; Mahapatra, C.; Kim, H.-W.; Knowles, J. C. *Prog. Mater. Sci.* **2016**, *77*, 1–79.

84. Du, Y.; Li, L.; Leung, C. W.; Lai, P. T.; Pong, P. W. T. *IEEE Trans. Magn.* **2014**, *50* (1), 1–4.

85. Eastoe, J. *Surfactant Chem.* **2003**, 59–95.

86. García, M. A.; Bouzas, V.; Costo, R.; Veintemillas, S.; Morales, P.; Madrid, C. *AIP Conf. Proc.* **2010**, 26–29.

87. Marcu, A.; Pop, S.; Dumitrache, F.; Mocanu, M.; Niculite, C. M.; Gherghiceanu, M.; Lungu, C. P.; Fleaca, C.; Ianchis, R.; Barbut, A.; Grigoriu, C.; Morjan, I. *Appl. Surf. Sci.* **2013**, *281*, 60–65.

88. Wang, M.; Thanou, M. *Pharmacol. Res.* **2010**, *62*, 90–99.

89. Gautier, J.; Munnier, E.; Paillard, a.; Hervé, K.; Douziech-Eyrolles, L.; Soucé, M.; Dubois, P.; Chourpa, I. *Int. J. Pharm.* **2012**, *423*, 16–25.

90. Mahmoudi, M.; Sant, S.; Wang, B.; Laurent, S.; Sen, T. *Adv. Drug Deliv. Rev.* **2011**, *63* (1–2), 24–46.

91. Tartaj, P.; Serna, C. J. *J. Am. Chem. Soc.* **2003**, *125* (51), 15754–15755.

92. Veiseh, O.; Gunn, J. W.; Zhang, M. *Adv. Drug Deliv. Rev.* **2010**, *62*, 284–304.

93. Allard-Vannier, E.; Cohen-Jonathan, S.; Gautier, J.; Hervé-Aubert, K.; Munnier, E.; Soucé, M.; Legras, P.; Passirani, C.; Chourpa, I. *Eur. J. Pharm. Biopharm.* **2012**, *81*, 498–505.

94. Hałupka-Bryl, M.; Asai, K.; Thangavel, S.; Bednarowicz, M.; Krzyminiewski, R.; Nagasaki, Y. *Colloids Surfaces B Biointerfaces.* **2014**, *118*, 140–147.

95. Mojica Pisciotti, M. L.; Lima, E.; Vasquez Mansilla, M.; Tognoli, V. E.; Troiani, H. E.; Pasa, A. A.; Creczynski-Pasa, T. B.; Silva, A. H.; Gurman, P.; Colombo, L.; Goya, G. F.; Lamagna, A.; Zysler, R. D. *J. Biomed. Mater. Res. Part B Appl. Biomater.* **2014**, *102*, 860–868.

96. Leonard, R. C. F.; Williams, S.; Tulpule, A; Levine, M.; Oliveros, S. *Breast.* **2009**, *18*, 218–24.

97. Quinto, C. A.; Mohindra, P.; Tong, S.; Bao, G. *Nanoscale* **2015**, *7* (29), 12728–12736.

98. Orlando, A.; Colombo, M.; Prosperi, D.; Gregori, M.; Panariti, A.; Rivolta, I.; Masserini, M.; Cazzaniga, E. *J. Nanoparticle Res.* **2015**, *17*, 351-375.

99. Mazzucchelli, S.; Colombo, M.; Verderio, P.; Rozek, E.; Andreata, F.; Galbiati, E.; Tortora, P.; Corsi, F.; Prosperi, D. *Angew. Chemie - Int. Ed.* **2013**, *52*, 3121–3125.

100. Hałupka-Bryl, M.; Bednarowicz, M.; Dobosz, B.; Krzyminiewski, R.; Zalewski, T.; Wereszczyńska, B.; Nowaczyk, G.; Jarek, M.; Nagasaki, Y. *J. Magn. Magn. Mater.* **2015**, *384*, 320–327.

101. Jambhekar, S. S.; Breen, P. *Drug Discov. Today.* **2015**, *21* (2), 356–362.

102. Prabha, G.; Raj, V. *Biomed. Pharmacother.* **2016**, *80*, 173–182.

103. Schleich, N.; Sibret, P.; Danhier, P.; Ucakar, B.; Laurent, S.; Muller, R. N.; Jérôme, C.; Gallez, B.; Préat, V.; Danhier, F. *Int. J. Pharm.* **2013**, *447* (1-2), 94–101.

104. Yamaguchi, Y.; Li, Z.; Zhu, X.; Liu, C.; Zhang, D.; Dou, X. *PLoS One* **2015**, *10* (5), 1–12.

105. Zhang, F.; Kang, E. T.; Neoh, K. G.; Wang, P.; Tan, K. L. *J. Biomater. Sci. Polymer Edn*, **2001**, *22* (2), 1541–1548.

106. Aqil, A.; Vasseur, S.; Duguet, E.; Passirani, C.; Benoît, J. P.; Roch, A.; Müller, R.; Jérôme, R.; Jérôme, C. *Eur. Polym. J.* **2008**, *44* (10), 3191–3199.

107. Aqil, A.; Vasseur, S.; Duguet, E.; Passirani, C.; Benoît, J. P.; Roch, A.; Müller, R.; Jérôme, R.; Jérôme, C. *Eur. Polym. J.* **2008**, *44* (10), 3191–3199.

108. Häfeli, U. O.; Riffle, J. S.; Harris-Shekhawat, L.; Carmichael-Baranauskas, A.; Mark, F.; Dailey, J. P.; Bardenstein, D. *Mol. Pharm.* **2009**, *6* (5), 1417–1428.

109. Benjaminsen, R. V; Mattebjerg, M. A.; Henriksen, J. R.; Moghimi, S. M.; Andresen, T. L. *Mol. Ther.* **2013**, *21* (1), 149–157.

110. Philipse, A.P.; Vanbruggen, M.P.B.; Pathmamanoharan, C. *Langmuir*. **1994,** *10* (1), 92-99

111. Yang, Y. X.; Song, Z. M.; Cheng, B.; Xiang, K.; Chen, X. X.; Liu, J. H.; Cao, A.; Wang, Y.; Liu, Y.; Wang, H. *J. Appl. Toxicol.* **2014**, *34* (4), 424–435.

112. Becaro, A. A., Puti, F. C., Correa, D. S., Paris, E. C., Marconcini, J. M., & Ferreira, M. D. *J. Nanosci. Nanotechnol*. **2015**, *15*(3), 2148-2156.

113. Tolbert, S. H.; McFadden, P. D.; Loy, D. A. *ACS Appl. Mater. Interfaces.* **2016**, *8* (5), 3160–3174.

114. Chinta, S. K.; Landage, S. M.; Swapnal, J. *Int. J. Innov. Res. Sci. Eng. Technol.* **2013**, *2* (7), 2882–2891.

115. Soleimani, M.; Khani, A.; Najafzadeh, K. *J. Mol. Catal. B Enzym.* **2012**, *74* (1-2), 1–5.

116. Wu, W.; He, Q.; Jiang, C. *Nanoscale Res. Lett.* **2008**, *3* (11), 397–415.

117. Vogt, C.; Toprak, M. S.; Muhammed, M.; Laurent, S.; Bridot, J. L.; Müller, R. N. *J. Nanoparticle Res.* **2010**, *12* (4), 1137–1147.

118. Kim, D. W.; Kim, T. H.; Choi, S.; Kim, K. S.; Park, D. W. *Adv. Powder Technol.* **2012**, *23* (6), 701–707.

119. Narita, A.; Naka, K.; Chujo, Y. *Colloids Surfaces A Physicochem. Eng. Asp*. **2009**, *336* (1-3), 46–56.

120. Ahmad, T.; Bae, H.; Rhee, I.; Chang, Y.; Lee, J.; Hong, S. *Curr. Appl. Phys.* **2012**, *12* (3), 969–974.

121. Chinta, S. K.; Landage, S. M.; Swapnal, J. *Int. J. Innov. Res. Sci. Eng. Technol.* **2013**, *2* (7), 2882–2891.

122. Qi, L. *Encycl. Surf. Colloid Sci.* **2006**, *2*, 6183–6207.

123. Avnir, D.; Braun, S.; Lev, O.; Ottolenghi, M. *Chem. Mater.* **1994**, *6* (12), 1605–1614.

124. Baber, O.; Jang, M.; Barber, D.; Powers, K. *Inhal. Toxicol.* **2011**, *23* (9), 532–543.

125. Sadjadi, M. S.; Fathi, F.; Farhadyar, N.; Zare, K. *Nano Research*. **2012**. *16*, 43-48.

126. Mohammad-Beigi, H.; Yaghmaei, S.; Roostaazad, R.; Bardania, H.; Arpanaei, A. *Phys. E Low-Dimensional Syst. Nanostructures.* **2011**, *44* (3), 618–627.

127. Souto, G. D.; Farhane, Z.; Casey, A.; Efeoglu, E.; McIntyre, J.; Byrne, H. J. *Anal. Bioanal. Chem.* **2016**, *408* (20), 5443–5455.

128. Muthiah, M.; Park, I.-K.; Cho, C.-S. *Biotechnol. Adv.* **2013**, *31*, 1224–1236.

129. Qin, H.; Wang, C. M.; Dong, Q. Q.; Zhang, L.; Zhang, X.; Ma, Z. Y.; Han, Q. R. *J. Magn. Magn. Mater.* **2015**, *381*, 120–126.

130. Kumar, R. M. N. V; Muzzarelli, R. A. A.; Sashiwa, H.; Domb, A. J. *Chem. Rev.* **2004**, *104*, 6017–6084.

131. Ding, Y.; Shen, S. Z.; Sun, H.; Sun, K.; Liu, F.; Qi, Y.; Yan, J. *Mater. Sci. Eng. C.* **2015**, *48*, 487–498.

132. Easo, S. L.; Mohanan, P. V. *Carbohydr. Polym.* **2013**, *92* (1), 726–732.

133. Peng, M.; Li, H.; Luo, Z.; Kong, J.; Wan, Y.; Zheng, L.; Zhang, Q.; Niu, H.; Vermorken, A.; Van de Ven, W.; Chen, C.; Zhang, X.; Li, F.; Guo, L.; Cui, Y. *Nanoscale* **2015**, *7* (25), 11155–11162.

134. Sharma, R.; Saini, S.; Ros, P. R.; Hahn, P. F.; Small, W. C.; de Lange, E. E.; Stillman, a E.; Edelman, R. R.; Runge, V. M.; Outwater, E. K.; Morris, M.; Lucas, M. *J. Magn. Reson. Imaging.* **1999**, *9* (2), 291–294.

135. Mojica Pisciotti, M. L.; Lima, E.; Vasquez Mansilla, M.; Tognoli, V. E.; Troiani, H. E.; Pasa, A. A.; Creczynski-Pasa, T. B.; Silva, A. H.; Gurman, P.; Colombo, L.; Goya, G. F.; Lamagna, A.; Zysler, R. D. *J. Biomed. Mater. Res. Part B Appl. Biomater.* **2014**, *102*, 860–868.

136. Tassa, C.; Shaw, S. Y.; Weissleder, R. *Acc. Chem. Res.* **2011**, *44* (10), 842–852.

137. Arami, H.; Khandhar, A.; Liggitt, D.; Krishnan, K. M. *Chem. Soc. Rev.* **2015**, *42* (12), 4906.

138. Kim, D. K.; Zhang, Y.; Voit, W.; Rao, K. V.; Muhammed, M. *J. Magn. Magn. Mater.* **2001**, *225* (1-2), 30–36.

139. Haracz, S.; Hilgendorff, M.; Rybka, J. D.; Giersig, M. *Nucl. Instruments Methods Phys. Res. Sect. B Beam Interact. Mater. Atoms* **2015**, *364*, 120–126.

140. Soares, P. I. P.; Alves, A. M. R.; Pereira, L. C. J.; Coutinho, J. T.; Ferreira, I. M. M.; Novo, C. M. M.; Borges, J. P. M. R. *J. Colloid Interface Sci.* **2014**, *419*, 46–51.

141. Filippousi, M.; Angelakeris, M.; Katsikini, M.; Paloura, E.; Efthimiopoulos, I.; Wang, Y.; Zamboulis, D.; Van Tendeloo, G. *J. Phys. Chem. C* **2014**, *118* (29), 16209–16217.

142. Li, H.; Qin, L.; Feng, Y.; Hu, L.; Zhou, C. *J. Magn. Magn. Mater.* **2015**, *384*, 213–218.

143. Tietze, R.; Lyer, S.; Dürr, S.; Struffert, T.; Engelhorn, T.; Schwarz, M.; Eckert, E.; Göen, T.; Vasylyev, S.; Peukert, W.; Wiekhorst, F.; Trahms, L.; Dörfler, A.; Alexiou, C. *Nanomedicine* **2013**, *9* (7), 961–971.

144. Velusamy, P.; Chia-Hung, S.; Shritama, a.; Kumar, G. V.; Jeyanthi, V.; Pandian, K. *J. Taiwan Inst. Chem. Eng.* **2015**, 1–7.

145. Zhang, L.; He, R.; Gu, H. C. *Appl. Surf. Sci.* **2006**, *253* (5), 2611–2617.

146. Shete, P. B.; Patil, R. M.; Tiwale, B. M.; Pawar, S. H. *J. Magn. Magn. Mater.* **2015**, *377*, 406–410.

147. Korpany, K. V.; Habib, F.; Murugesu, M.; Blum, A. S. *Mater. Chem. Phys.* **2013**, *138* (1), 29–37.

148. Korpany, K. V.; Mottillo, C.; Bachelder, J.; Cross, S. N.; Dong, P.; Trudel, S.; Friščić, T.; Blum, A. S. *Chem. Commun.* **2016**, *52* (14), 3054–3057.

149. Lee, C. M.; Jeong, H. J.; Kim, E. M.; Kim, D. W.; Lim, S. T.; Kim, H. T.; Park, I. K.; Jeong, Y. Y.; Kim, J. W.; Sohn, M. H. *Magn. Reson. Med.* **2009**, *62* (6), 1440–1446.

150. Shultz, M. D.; Ulises Reveles, J.; Khanna, S. N.; Carpenter, E. E. *J. Am. Chem. Soc.* **2007**, *129* (9), 2482–2487.

151. Ma, W.; Liu, H.-T.; Long, Y.-T. *ACS Appl. Mater. Interfaces.* **2015**, *7* (26), 14352–14358.

152. Patsula, V.; Moskvin, M.; Dutz, S.; Horák, D. *J. Phys. Chem. Solids.* **2016**, *88*, 24–30.

153. Herea, D. D.; Chiriac, H.; Lupu, N.; Grigoras, M.; Stoian, G.; Stoica, B.; Petreus, T. *Appl. Surf. Sci.* **2015**, *352*, 117–125.

154. Ulbrich, K.; Holá, K.; Šubr, V.; Bakandritsos, A.; Tuček, J.; Zbořil, R. *Chem. Rev.* **2016**, *11*, 5338-5431.

155. Gupta, J.; Bhargava, P.; Bahadur, D. *J. Appl. Phys.* **2014**, *115* (17).

156. Kievit, F. M.; Wang, F. Y.; Fang, C.; Mok, H.; Wang, K.; Silber, J. R.; Ellenbogen, R. G.; Zhang, M. *J. Control. Release.* **2011**, *152* (1), 76–83.

157. Hervault, A.; Dunn, A. E.; Lim, M.; Boyer, C.; Mott, D.; Maenosono, S.; Thanh, N. T. K. *Nanoscale.* **2016**, *8*, 21–24.

158. Stephen, Z. R.; Kievit, F. M.; Veiseh, O.; Chiarelli, P. A.; Fang, C.; Wang, K.; Hatzinger, S. J.; Ellenbogen, R. G.; Silber, J. R.; Zhang, M. *ACS Nano.* **2014**, *8* (10), 10383–10395.

159. Ma, H.; Liu, Y.; Shi, M.; Shao, X.; Zhong, W.; Liao, W.; Xing, M. M. Q. *Biomacromolecules.* **2015**, *16* (12), 4022–4031.

160. Semkina, A.; Abakumov, M.; Grinenko, N.; Abakumov, A.; Skorikov, A.; Mironova, E.; Davydova, G.; Majouga, A. G.; Nukolova, N.; Kabanov, A.; Chekhonin, V. *Colloids Surfaces B Biointerfaces.* **2015**, *136*, 1073–1080.

161. Wu, M.; Meng, Q.; Chen, Y.; Xu, P.; Zhang, S.; Li, Y.; Zhang, L.; Wang, M.; Yao, H.; Shi, J. *Adv. Funct. Mater.* **2014**, *24* (27), 4273–4283.

162. Patra, S.; Roy, E.; Karfa, P.; Kumar, S.; Madhuri, R.; Sharma, P. K. *ACS Appl. Mater. Interfaces.* **2015**, *7* (17), 9235–9246.

163. Shenoy, D.; Little, S.; Langer, R.; Amiji, M. *Mol. Pharm.* **2005**, *2* (5), 357–366.

164. Fang, C.; Kievit, F. M.; Veiseh, O.; Stephen, Z. R.; Wang, T.; Lee, D.; Ellenbogen, R. G.; Zhang, M. *J. Control. Release.* **2012**, *162* (1), 233–241.

165. Kievit, F. M.; Wang, F. Y.; Fang, C.; Mok, H.; Wang, K.; Silber, J. R.; Ellenbogen, R. G.; Zhang, M. *J. Control. Release.* **2011**, *152* (1), 76–83.

166. Zhu, L.; Wang, D.; Wei, X.; Zhu, X.; Li, J.; Tu, C.; Su, Y.; Wu, J.; Zhu, B.; Yan, D. *J. Control. Release.* **2013**, *169* (3), 228–238.

167. Nigam, S.; Barick, K. C.; Bahadur, D. *J. Magn. Magn. Mater.* **2011**, *323* (2), 237–243.

168. Dennis, C. L.; Jackson, A. J.; Borchers, J. A.; Ivkov, R.; Foreman, A. R.; Lau, J. W.; Goernitz, E.; Gruettner, C. *J. Appl. Phys.* **2008**, *103* (7).

169. Wadajkar, A. S.; Menon, J. U.; Tsai, Y. S.; Gore, C.; Dobin, T.; Gandee, L.; Kangasniemi, K.; Takahashi, M.; Manandhar, B.; Ahn, J. M.; Hsieh, J. T.; Nguyen, K. T. *Biomaterials.* **2013**, *34* (14), 3618–3625.

170. Nemati, Z.; Alonso, J.; Khurshid, H.; Phan, M. H.; Srikanth, H. *RSC Adv.* **2016**, *6* (45), 38697–38702.

171. Kakwere, H.; Leal, M. P.; Materia, M. E.; Curcio, A.; Guardia, P.; Niculaes, D.; Marotta, R.; Falqui, A.; Pellegrino, T. *ACS Appl. Mater. Interfaces.* **2015**, *7* (19), 10132–10145.

172. Rastogi, R.; Gulati, N.; Kotnala, R. K.; Sharma, U.; Jayasundar, R.; Koul, V. *Colloids Surfaces B Biointerfaces.* **2011**, *82* (1), 160–167.

173. Lu, Y.; Yin, Y.; Mayers, B. T.; Xia, Y. *Nano Lett.* **2002**, *2* (3), 183–186.

174. Sundarraj, K.; Manickam, V.; Raghunath, A.; Periyasamy, M.; Viswanathan, M. P.; Perumal, E. *Environ. Toxicol.* **2017**, *2*, 594-608.

175. Zhu, X.; Tian, S.; Cai, Z. *PLoS One*. **2012**, 1–7.

176. Remya, N. S.; Syama, S.; Sabareeswaran, A.; Mohanan, P. V. *Int. J. Pharm.* **2016**, *511* (1), 586–598.

177. Wu, H.; Yin, J. J.; Wamer, W. G.; Zeng, M.; Lo, Y. M. *J. Food Drug Anal.* **2014**, *22* (1), 86–94.

178. Malvindi, M. A.; De Matteis, V.; Galeone, A.; Brunetti, V.; Anyfantis, G. C.; Athanassiou, A.; Cingolani, R.; Pompa, P. P. *PLoS One.* **2014**, *9* (1), 1–12.

179. Patil, U. S.; Adireddy, S.; Jaiswal, A.; Mandava, S.; Lee, B. R.; Chrisey, D. B. *Int.l J. Mol. Sci.*; **2015**, *16*, 24417-24450.

180. Liu, G.; Gao, J.; Ai, H.; Chen, X. *Small*, **2013**, *9*, 1533–1545.

181. Li, L.; Jiang, L.-L.; Zeng, Y.; Liu, G. *Chinese Phys. B.* **2013**, *22* (12), 127503.

182. Scown, T. M.; van Aerle, R.; Tyler, C. R. *Crit. Rev. Toxicol.* **2010**, *40*, 653–670.

3 Synthesis of analogues of gymnastatins as potential anticancer agents

To date, there has been little research in the literature reporting the synthesis and anti-cancer activity of gymnastatins. This chapter describes synthetic work carried out towards the preparation of analogues of gymnastatin N. Two synthetic strategies were utilised and they are discussed in detail.

3.1 Synthetic Strategy 1

Two analogues of gymnastatins were prepared from octanal **1a** using the methodology presented in Scheme 3.1.

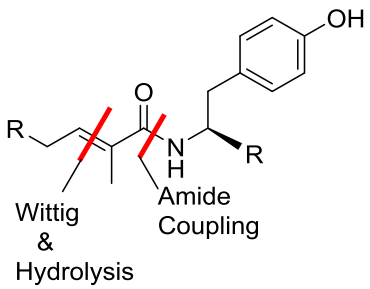

Figure 3.1: Retrosynthetic analysis of gymnastatin N analogue

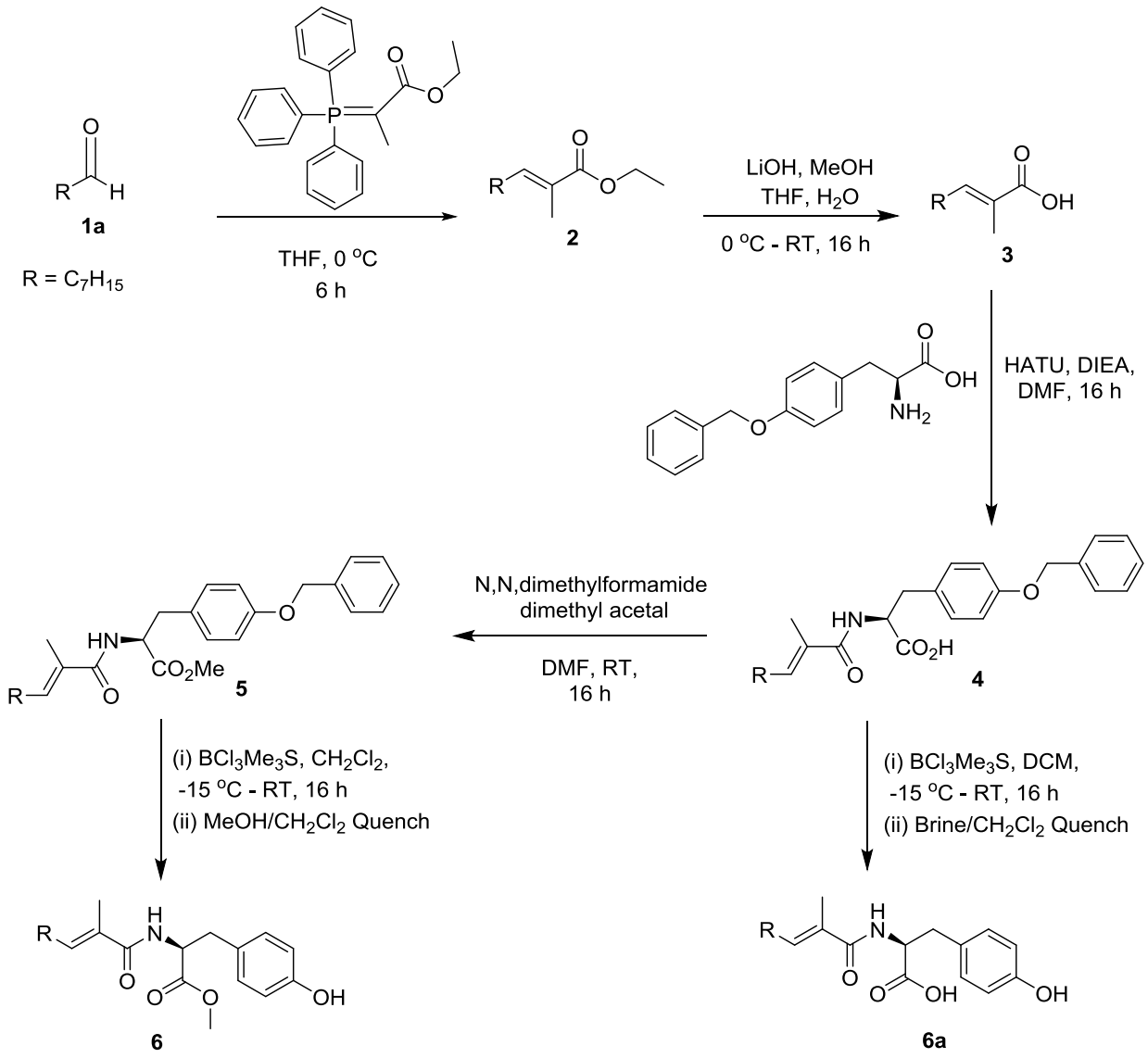

*Scheme 3.1: Overview of synthesis of synthesis of **6** and **6a***

The starting material is commercially available octanal **1a**. The first step is a Wittig reaction which installs an alkene and extends the chain length. This is followed by a base catalysed hydrolysis to yield the corresponding acid **3**. Coupling between the resulting acid and commercially available *O*-benzyl-L-tyrosine using HATU and DIEA to yield amide **4** is the key step. A reaction between the amide with *N*,*N*,dimethylformamide dimethyl acetal converts the acid moiety in the tyrosine unit to a methyl ester **5**. The final step is the removal of the benzyl protecting group using boron trichloride dimethyl sulfide complex to yield the target compounds **6** and **6a**.

3.1.1 The preparation of esters

The first step in this synthetic strategy was a Wittig reaction using (carbethoxyethylidene)triphenylphosphorane (Scheme 3.2). Commercially available octanal **1a** was used as a starting material.

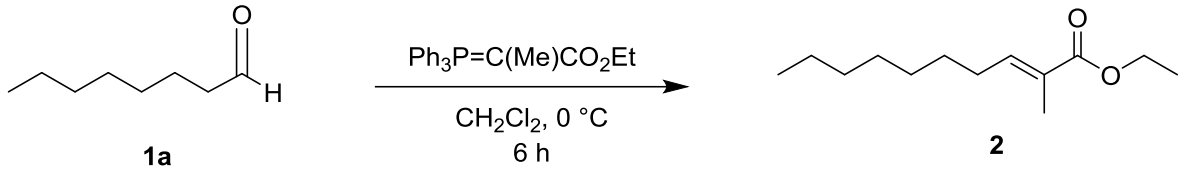

Scheme 3.2: Wittig reaction

(Carbethoxyethylidene)triphenylphosphorane was added to a solution of octanal **1a** in THF and the mixture was left stirring for 6 hours under argon. The reaction was monitored by TLC and upon completion was quenched and the product was purified using column chromatography.

The success of the Wittig reaction was confirmed by ^{1}H NMR. The disappearance of the aldehyde proton at 9.50 ppm and an additional signal in the alkene region of the ^{1}H NMR spectrum confirmed the installation of an alkene. The quartet at 4.10 ppm confirmed the presence of R-CH_2 corresponding to the ethyl group of the ester. Furthermore, the presence of the methyl group α to the carbonyl was confirmed by the observed singlet at 1.85 ppm in the ^{1}H NMR.

The mechanism for this reaction is illustrated in Scheme 3.3. The phosphorane attacks the carbonyl group of the octanal generating a negatively charged oxygen which attacks the positively charged phosphorus forming a very unstable 4-membered ring called an oxaphosphetane. The ring fragments to form an alkene as well as triphenylphosphine oxide (P=O) whose formation is the driving force of this reaction.[1-2]

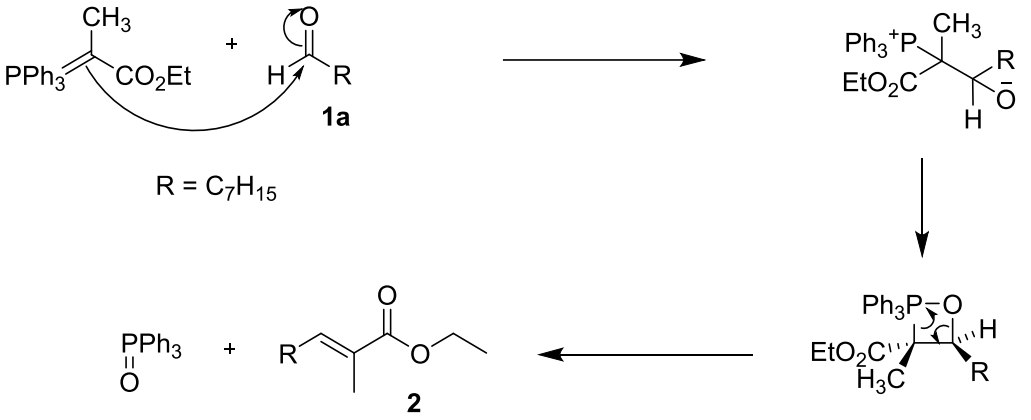

*Scheme 3.3: Wittig reaction mechanism involving octanal **1a***

3.1.2 Base catalysed hydrolysis

The next step involved a base catalysed hydrolysis of **2** to form an acid. This reaction was initially attempted using KOH in methanol under reflux for 2 hours (Scheme 3.4)

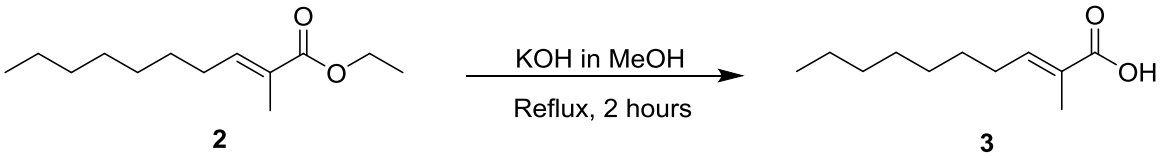

Scheme 3.4: Base catalysed hydrolysis using KOH in methanol

This method afforded the product, however the high temperatures promoted isomerisation and formation of other side products which were difficult to remove and resulted in a low yield. LiOH in THF/methanol/water at room temperature represented a milder route to the target compounds (Scheme 3.5). However, this reaction typically involves longer reaction times of up to 24 hours.

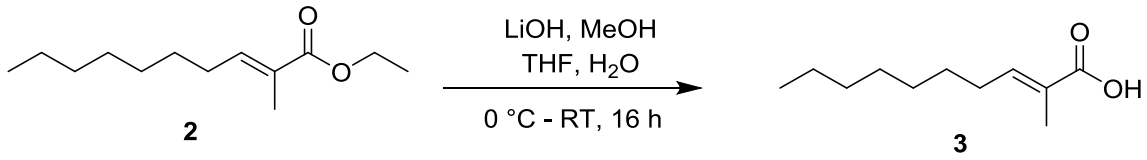

*Scheme 3.5: Base catalysed hydrolysis of ester **2***

The formation of the acid was confirmed by ^{1}H NMR disappearance of the quartet at 4.16 ppm corresponding to the R-CH_2 group of the ethyl group of the ester. Furthermore, the identity of the product was confirmed by the broad peak at 12.05 ppm representing the OH of the carboxylic acid. The presence of the OH was further confirmed by a D_2O shake and HSQC.

The mechanism for the base-catalysed hydrolysis is presented in Scheme 3.6. The lithium hydroxide provides a nucleophilic hydroxide which attacks the carbonyl on the ester creating a tetrahedral intermediate. The intermediate collapses, reforming the carbonyl and the ethoxide leaves resulting in a carboxylic acid.[1]

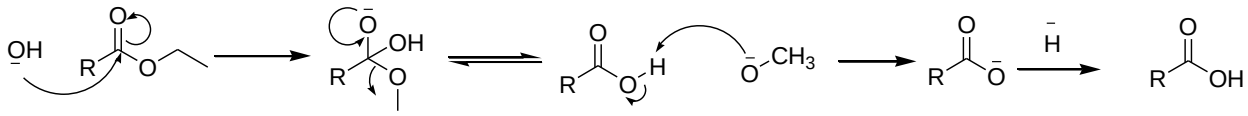

Scheme 3.6: Base catalysed hydrolysis reaction mechanism

3.1.3 Amide coupling

Coupling between acid **3** and commercially available protected tyrosine thereby installing an amide bond was the key step. The amide functionality is a common feature in natural products. It is found in proteins which play a crucial role in most biological processes such as enzyme catalysis, transport (haemoglobin), immune protection (antibodies) and support (collagen). Amide bond formation presents difficulties such as low yields,

racemisation, degradation and purification issues. This is overcome by using different coupling reagents which not only activate the acid but also reduce racemisation, optimise the reaction and reduce the formation of by-products.[1, 3-4]

In this work, several procedures were attempted to form an amide link between the acid side chain and the tyrosine. Initially, cheap Boc protected *O*-benzyl-L-tyrosine was used as the reagent (Scheme 3.7).

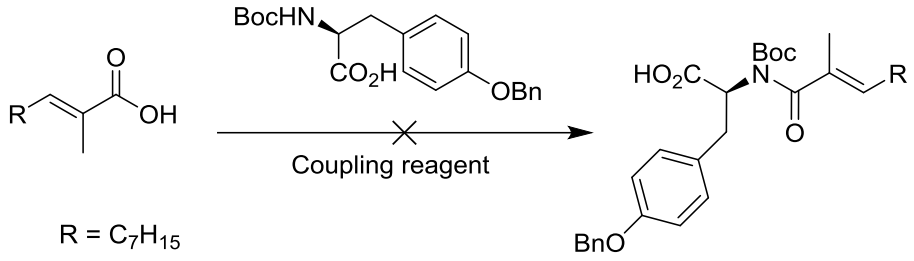

Scheme 3.7: Attempted amide coupling using N-Boc- O-benzyl-L-tyrosine

Several coupling reagents, e.g. diphenylphosphinic acid, EDC and oxalyl chloride, in different reaction conditions were used to form an amide link but no product was formed or in the case of oxalyl chloride, (entries 1a-1c), a very low yield was achieved. (Table 3.1)

Entry	Coupling reagent	Additive	Base	Reaction time/ hours	Temp/ ° C	Yield/%
1a	Oxalyl chloride	--	Et_3N	6 – 24	RT 50	< 10%
1b	Oxalyl chloride	DMF,	Et_3N	6 – 24	50	< 10%
1c	Oxalyl chloride	DMF	Et_3N	6 – 24	70	< 10%
2a	EDC	--	DMAP	12 – 24	RT	0
2b	EDC	--	DIEA	12 – 24	RT	0
2c	EDC	HOBt,	DMAP	12 – 24	RT	0

Table 3.1: Attempted amide coupling reaction conditions

It was postulated that NH was not sufficiently reactive. The next attempt involved the use of *O*-benzyl-L-tyrosine (Figure 3.2). This approach involves a primary amine which is more reactive. In addition, the need for a Boc deprotection will be avoided.

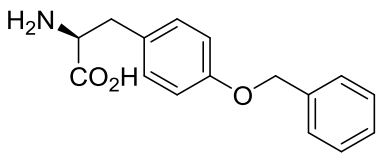

Figure 3.2: O-benzyl-L-tyrosine

The first approach towards amide formation using *O*-benzyl-L-tyrosine was using an acid chloride. There were two options for this, the use of thionyl chloride or oxalyl chloride.

Oxalyl chloride was used as it is milder, more selective and requires lower temperatures. Triethylamine was used as a base to maintain basic pH conditions during the reaction, CH_2Cl_2 was used as the solvent. The reaction (Scheme 3.8) was monitored by ^1H NMR.

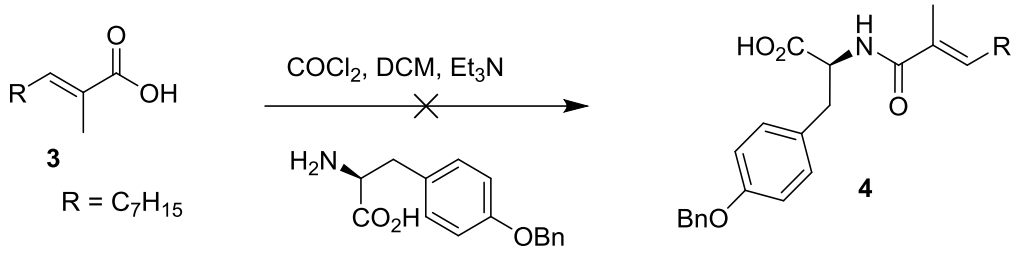

Scheme 3.8: Attempted amide coupling using oxalyl chloride

The reaction shown in Scheme 3.8 using oxalyl chloride resulted in a poor yield (< 10%). Increasing the temperature to 50 °C resulted in isomerisation of the alkenes, and formation of side products and did not improve the yield. Adding catalytic DMF to accelerate the reaction did not improve yield. We decided to explore other coupling reagents to improve yields and reduce isomerisation.

The next approach was using 1-ethyl-3-(3-dimethylaminopropyl)carbodiimide (EDC) (Scheme 3.9.)

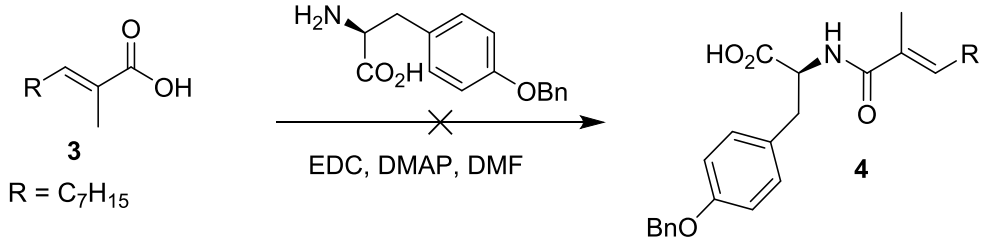

Scheme 3.9: Attempted amide coupling using EDC

In this reaction, the carbodiimide reacts with the carboxylic acid to form the *O*-acylisourea anhydride, which reacts with the amine to yield the desired amide. A urea by-product which is water soluble and can be eliminated by aqueous work up is also formed.

4-Dimethylaminopyridine (DMAP) was used as a nucleophile to enhance selectivity. The reaction did not go to completion even after 48 hours.

3.1.4 Coupling with HATU

The failure of EDC and oxalyl chloride meant considering alternative routes. HATU was the obvious choice. HATU is one of the most efficient coupling reagents and was first reported by Carpino *et al* in 1993.[5] It has proven to be efficient in difficult sterically hindered couplings and gives minimal racemisation. The first test reaction with HATU gave 82% yield, with no side products or racemisation and the crude mixture was purified by column chromatography.[4-6] (Scheme 3.10)

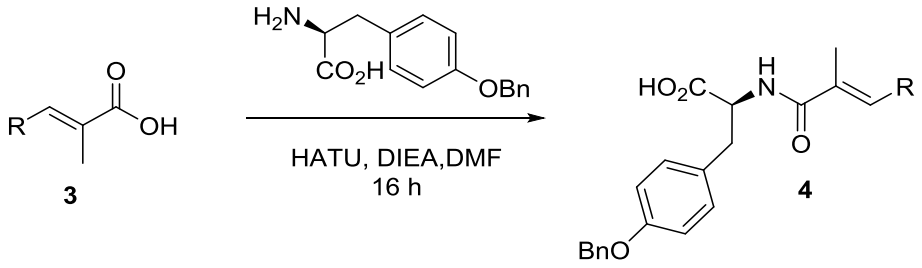

Scheme 3.10: Amide coupling using HATU

This reaction was carried out using DMF as a solvent and DIEA was used as a base. The product was purified using column chromatography. The identity of the product was confirmed by ^{1}H NMR. A signal was present at 171 ppm in the ^{13}C NMR assigned to the carbonyl of the amide group. A multiplet at 7.20 ppm and a singlet at 4.80 ppm corresponding to the benzyl protecting group were present. An NH stretch and an amide band were also present, at 1511 and 1611 cm^{-1}, respectively in the IR spectrum. Furthermore, LRMS showed a signal at *m/z = 438.2,* calculated for $C_{27}H_{35}NO_4$ $[M+H]^+$: 438.3 corresponding to the parent ion.

The mechanism for the amide bond formation using HATU is outlined below. The reaction is initiated by the removal of the proton of the acid to form a carboxylate anion (Scheme 3.11).

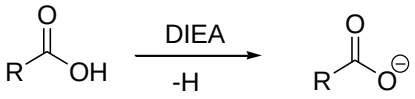

Scheme 3.11: Deprotonation of acid

The carboxylate anion attacks the HATU forming an unstable isouronium salt. The OAt anion attacks the isouronium salt affording an active OAt active ester. Addition of an amine (nucleophile) to the OAt ester results in acylation.[4]

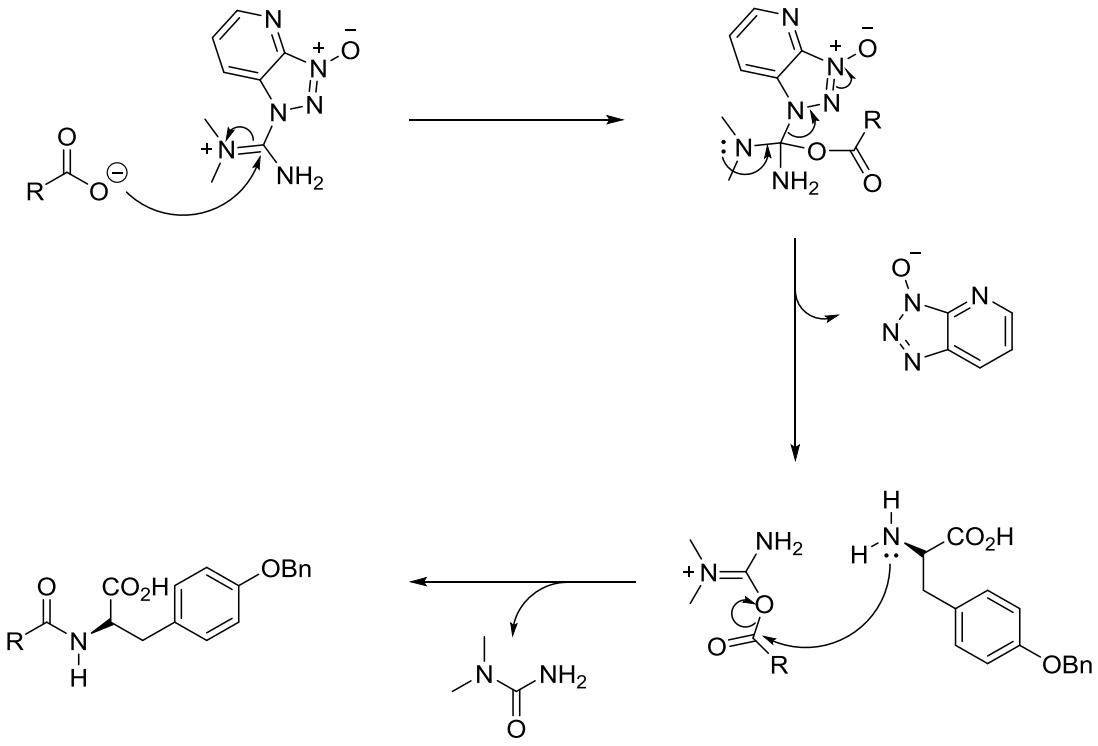

Scheme 3.12: Proposed reaction mechanism for amide formation using HATU

3.1.5 Methylation of acid side group

In this step the acid group on the tyrosine unit was converted to a methyl ester using *N,N,*dimethylformamide dimethyl acetal. The effect of the presence of a methyl ester rather than acid side group on the anti-cancer activity of the gymnastatin analogues was of interest. To this end, a reaction was set up as shown in Scheme 3.13 to convert the acid side group on the tyrosine unit to a methyl ester.

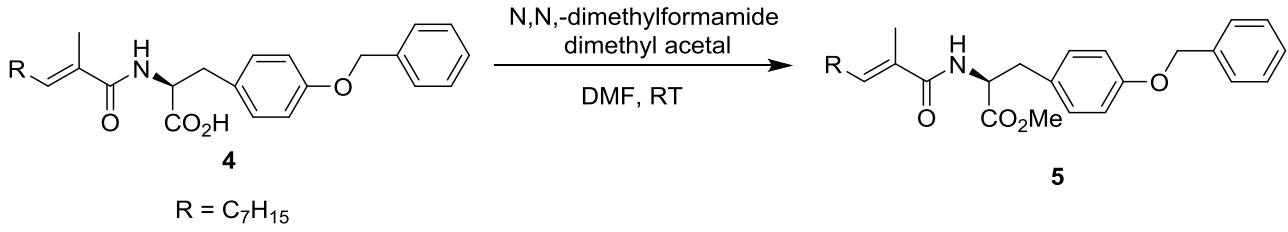

Scheme 3.13: Methylation of acid moiety in tyrosine unit

Amide **4** was dissolved in DMF and to the solution was added *N,N*-dimethylformamide dimethyl acetal and the reaction stirred at room temperature for 16 hours. The identity of the product was confirmed by a ^{1}H NMR CH_3 signal at 3.1 ppm and a ^{13}C NMR signal at 52.3 ppm. Furthermore, removal of the acid side group results in significant change in the polarity of the molecule. Therefore, TLC was also used to confirm that the acid group had been removed. Furthermore, LRMS showed a signal at *m/z* = 452.2 calculated for $C_{28}H_{37}NO_4$ $[M+H]^+$: 452.3.

3.1.6 Benzyl deprotection

3.1.6.1 Debenzylation using Pd/C H_2

The final step in this synthetic route was the removal of the benzyl ether protecting group. Benzyl ethers are usually removed by hydrogenation over a palladium catalyst which cleaves the benzylic C-O bond. The presence of easily reducible functional groups makes hydrogenation difficult. Caine and Bindra *et al* however reported the selective removal

of a benzyl ether protecting group in the presence of alkenes.[9-10] To this end, this reaction was attempted on a small scale (Scheme 3.14). This did not yield the desired product as the alkenes were also reduced during the reaction.

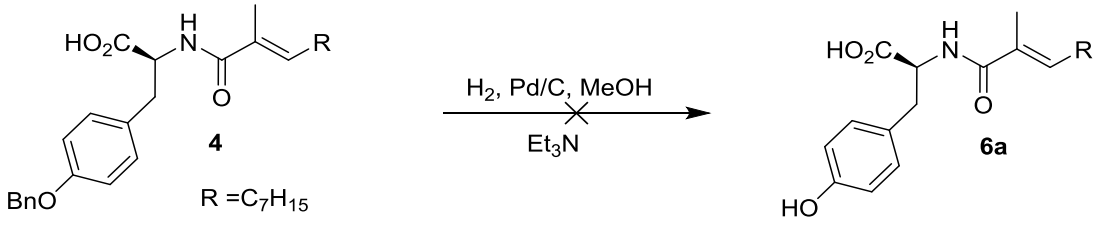

Scheme 3.14: Attempted O-Benzyl deprotection using H_2, Pd/C

3.1.6.2 Pd $(OAc)_2$ / Et_3SiH

When hydrogenation using Pd/C and H_2 did not yield the desired compound, other methods for selectively removing the benzyl protecting group while leaving the alkene intact were explored.

Coleman *et al.* reported the selective cleavage of benzyl protecting group in the presence of acyl chlorides, bromides, cyclopropanes and alkenes using triethyl silane catalysed with $Pd(OAc)_2$.[11]

This reaction was attempted as illustrated in Scheme 3.15 below.

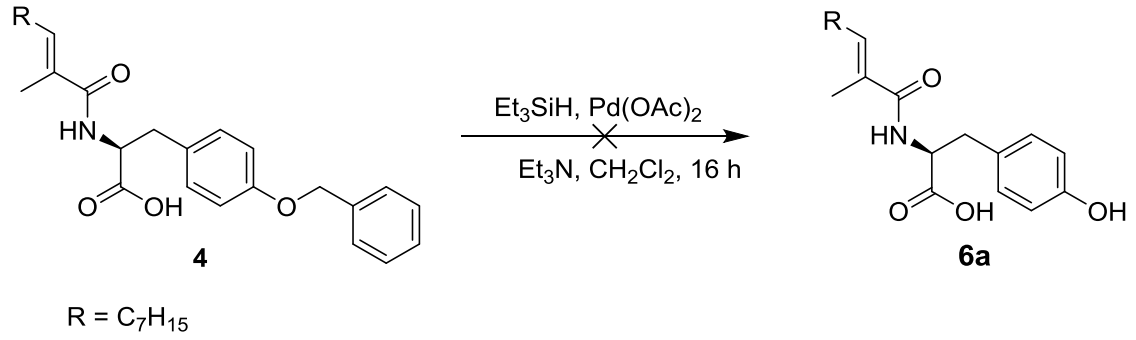

Scheme 3.15: Attempted O-benzyl deprotection

However, this procedure did not result in debenzylation or reduction of the alkene, only the starting material was recovered.

3.1.6.3 Debenzylation using BCl_3

Boron trichloride is a Lewis acid that can be used to cleave ethers, acetals, and in some cases, esters. Boron trichloride is toxic and difficult to handle. Its complex with dimethyl sulfide ($BCl_3.S(CH_3)_2$), also used to cleave ethers, is solid, stable in air, and easier to handle.

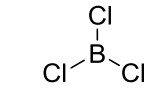

boron trichloride

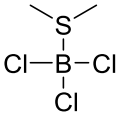

boron trichloride dimethyl sulphide complex

In this work, the deprotection of the benzyl ether was attempted using boron trichloride dimethyl sulfide (2 M in CH_2Cl_2). There have been several reports on the selective removal of benzyl ethers using ($BCl_3.S(CH_3)_2$) in the presence of other functional groups, e.g. olefins, at temperatures as low as -83 °C in dry CH_2Cl_2.[18] This reaction was attempted with a view to selectively remove the benzyl protecting group illustrated in Scheme 3.16.

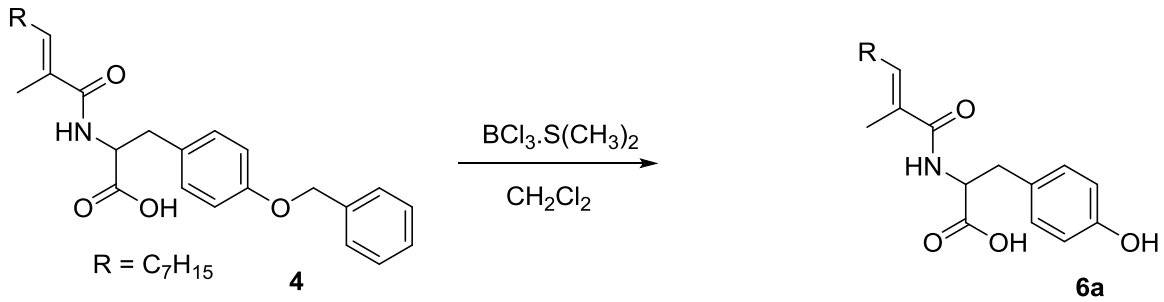

Scheme 3.16: Benzyl deprotection using boron trichloride dimethyl sulfide complex

Initially the reaction was attempted using a procedure reported in the literature. $BCl_3.S(CH_3)_2$ was added to a solution of amide **4** in dry CH_2Cl_2 under argon at -78 °C. The reaction was maintained at this temperature for 3 hours. After three hours, the reaction was not complete. The unreacted starting material was recovered and the reaction attempted using several reaction conditions. (Table 3.2). The reaction only went to

completion when 8 equivalents of $BCl_3.S(CH_3)_2$ were used. The reaction mixture was initially left stirring at -15 °C for 1 hour and warmed to room temperature and left stirring overnight (entry 6).

Entry	Conditions			Comments
	Temperature	Duration/h	Eq. of $BCl_3.S(CH_3)_2$	*Yields
1	-78 °C	3	5	<10%
2	-78 °C for 1 h to RT	3	5	< 20%
3	-78 °C for 1 hour to RT	16	5	< 40%
4	-15 °C	3	5	< 40%
5	-15 °C for 1 hour to room temperature	16	5	< 70%
6	-15 °C for 1 hour to room temperature	16	8	Complete

Table 3.2: Debenzylation reaction conditions using $BCl_3.S(CH_3)_2$. Yields reported are estimates calculated from NMR integration

It was concluded that 8 eq. $BCl_3.S(CH_3)_2$ was required for the complete debenzylation of amide **6a.**

When NMR indicated that the reaction had gone to completion, the reaction was quenched with ice cold methanol and CH_2Cl_2. The crude product was purified using column chromatography. NMR analysis revealed an unexpected singlet at 3.6 ppm integrating to 3 protons. This suggested the presence of a methyl group within the

structure. LCMS analysis was used to determine the mass of the parent ion. The *m/z* confirmed that the compound had a molecular weight 15 g/mol greater than expected. There were two possibilities: methylation of the acid side group on the tyrosine unit or the methylation of the OH on the phenol (Scheme 3.17).

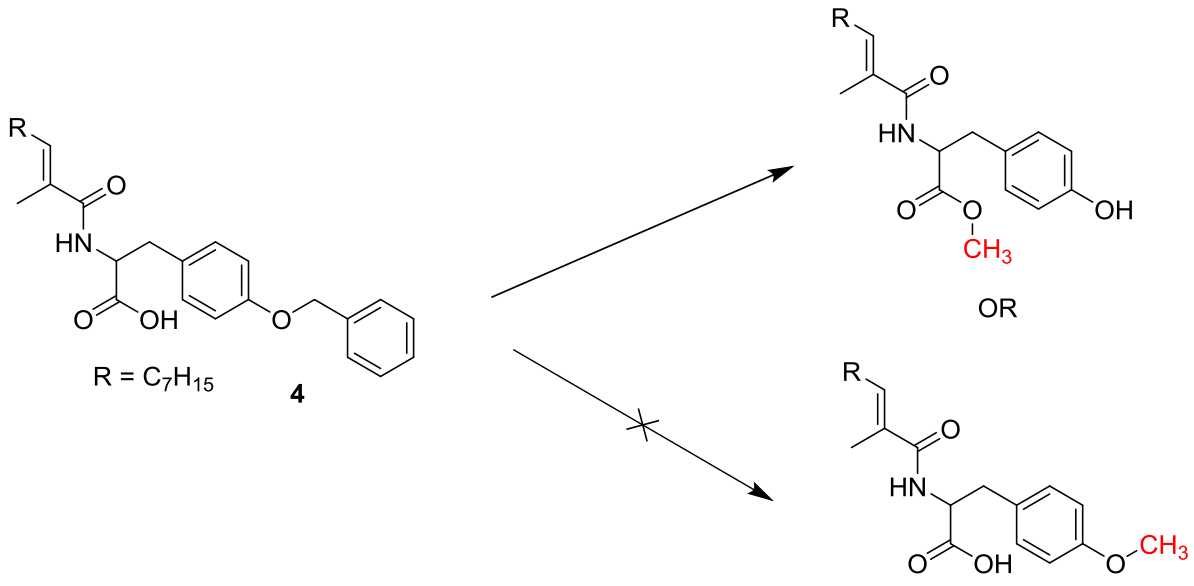

Scheme 3.17: Possible sites of methylation highlighted in red

After analysis using HMBC, it was confirmed that methylation at the acid group rather than the hydroxyl group at the phenol took place. A singlet was observed at 8.20 ppm and this was attributed to the phenolic OH. The OH was further confirmed by D_2O shake and HSQC.

When it was confirmed that the methylation occurred on the acid side group, we set out to determine if quenching the reaction with methanol was responsible for methylation. To this end, the reaction was repeated and quenched with ethanol rather than methanol. It was confirmed by NMR that ethylation had occurred at the acid side group. The singlet that was associated with the methyl group during methylation was absent. NMR analysis showed signals at 4.04 ppm and 1.10 ppm corresponding the ethyl group of the ethyl ester.

Further analysis using HMBC confirmed the ethylation of the acid to form **6b**. (Figure 3.3)

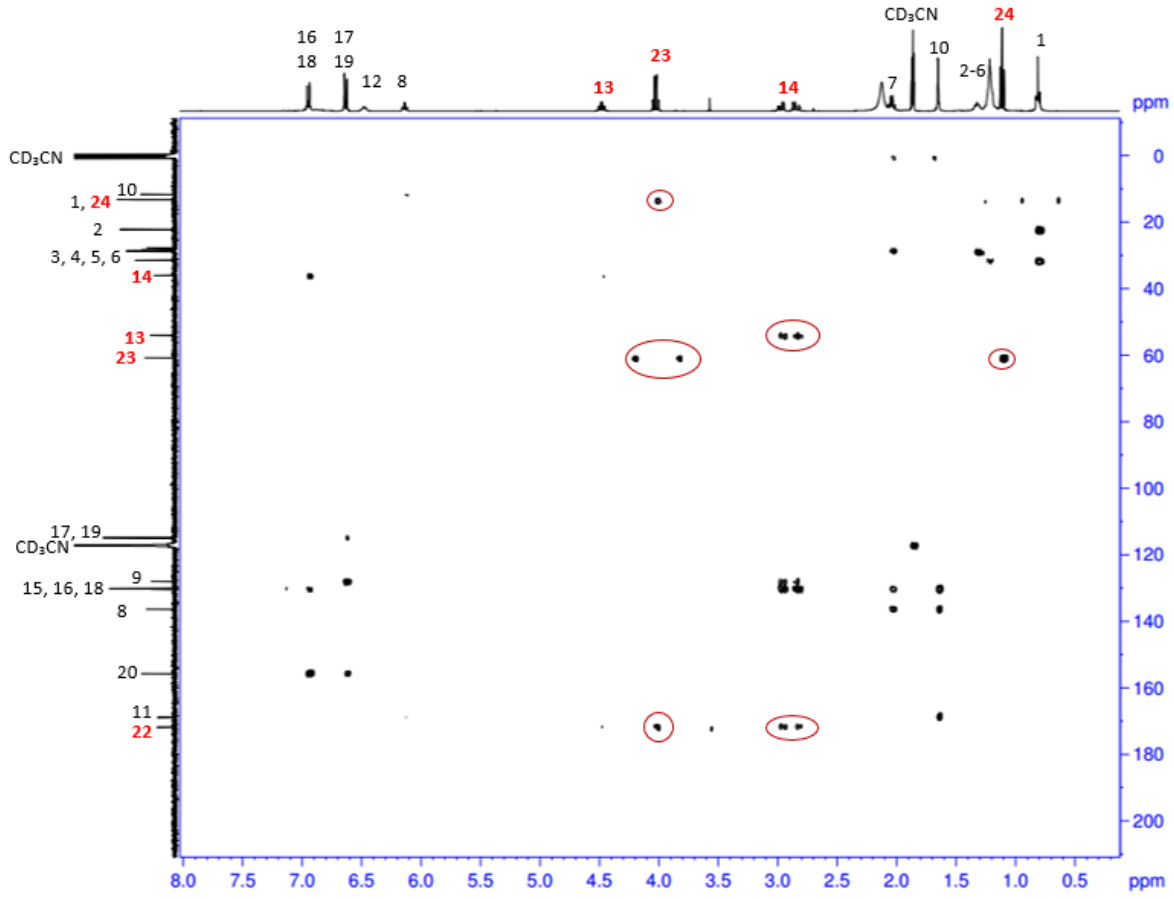

*Figure 3.3: Assigned HMBC spectrum of **6b***

These findings suggested that an acid chloride intermediate is formed, by conversion of the acid side group to an acid chloride. Quenching the reaction with methanol and ethanol results in methylation and ethylation respectively. (Scheme 3.18)

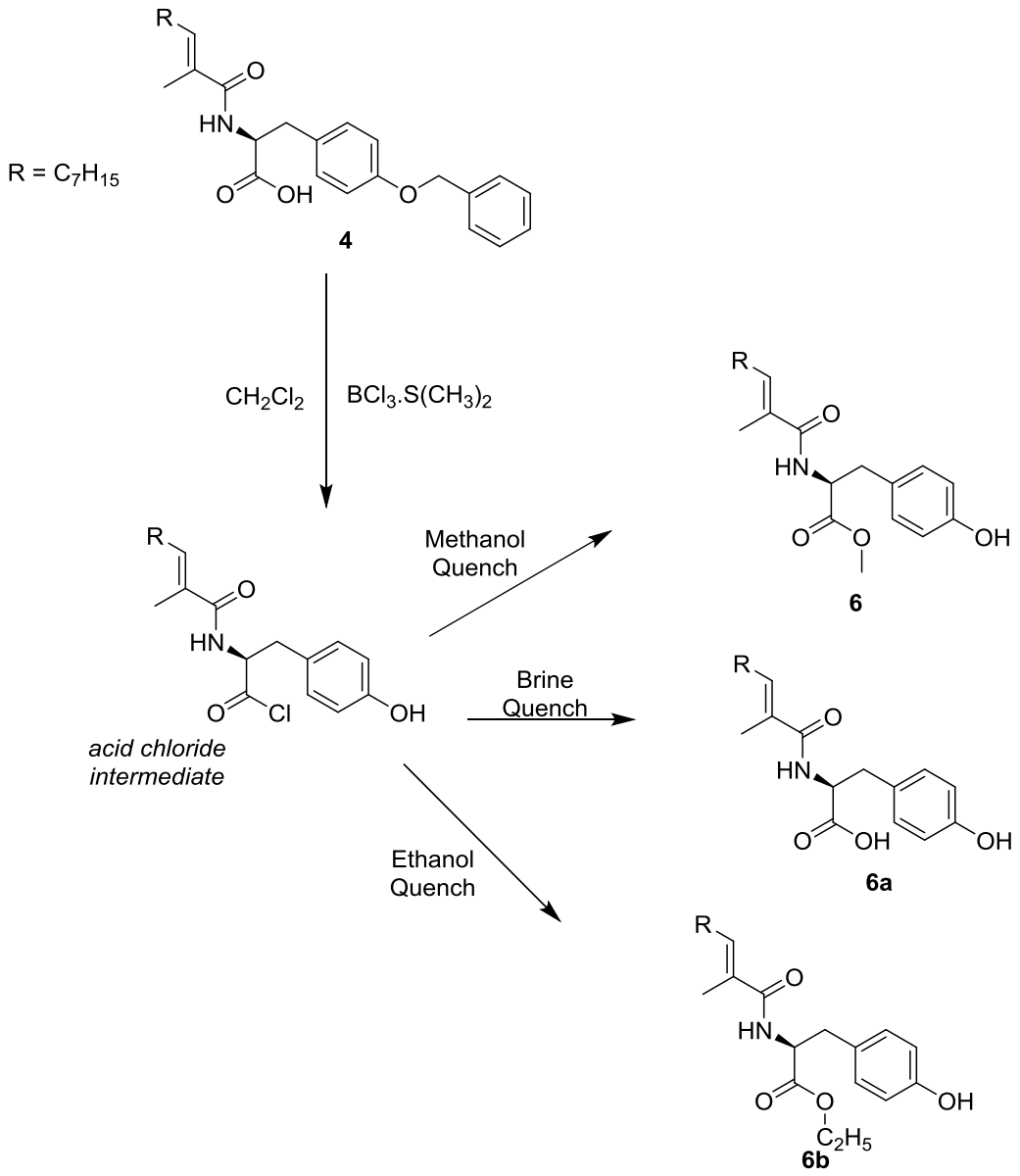

Scheme 3.18: Debenzylation reactions using $BCl_3.S(CH_3)_2$

To preserve the acid side-group the reaction was quenched using brine to yield **6a.** The successful synthesis of **6a** was confirmed by ^{1}H NMR analysis by the absence of a singlet around 3.5 ppm. The signal corresponding to the acid did not appear on the ^{1}H NMR spectrum. HRMS was used to further confirm the structure of **6a.**

Further analysis of the compounds **6, 6a** and **6b** using HRMS confirmed this reaction pathway.

Entry	Reaction quenched with	Chemical formula	Calculated mass	Found mass
6	Methanol	($C_{21}H_{31}NO_4$)	$[M+H]^+$: 362.2331,	Found: 362.2345.
6a	Brine	($C_{20}H_{29}NO_4$)	$[M+Na]^+$: 370.1994,	Found: 370.2001
6b	Ethanol	($C_{22}H_{33}NO_4$)	$[M+H]^+$: 376.2488,	Found: 376.2475

*Table 3.3: HRMS analysis of **6, 6a** and **6b** (samples ran by Jimmy Muldoon in UCD Dublin)*

The general mechanism for the reaction between an acid chloride and an alcohol (ROH) is illustrated in Scheme 3.19. It involves a straightforward nucleophilic substitution at the carbonyl.

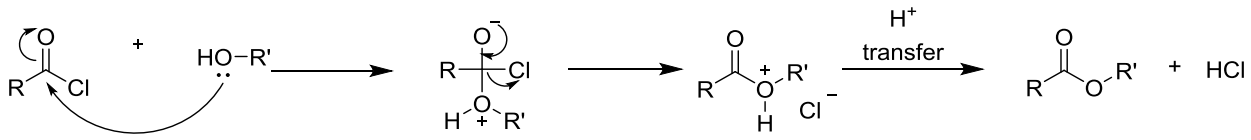

Scheme 3.19: General mechanism of the reaction between an acid chloride and an alcohol

The methylation of the acid group during this step meant that the methylation of the acid group step (section 3.1.5) could be eliminated.

3.2 Synthetic Strategy 2

Scheme 3.20 shows an overview of the synthesis of gymnastatin analogues with varying chain lengths, and an additional alkene.

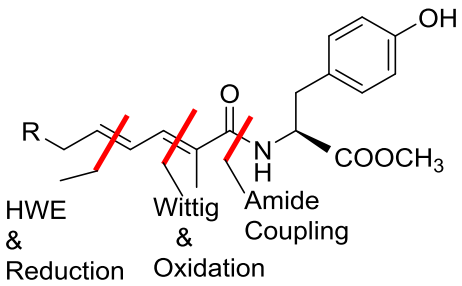

Figure 3.4: Retrosynthetic analysis of gymnastatin analogues

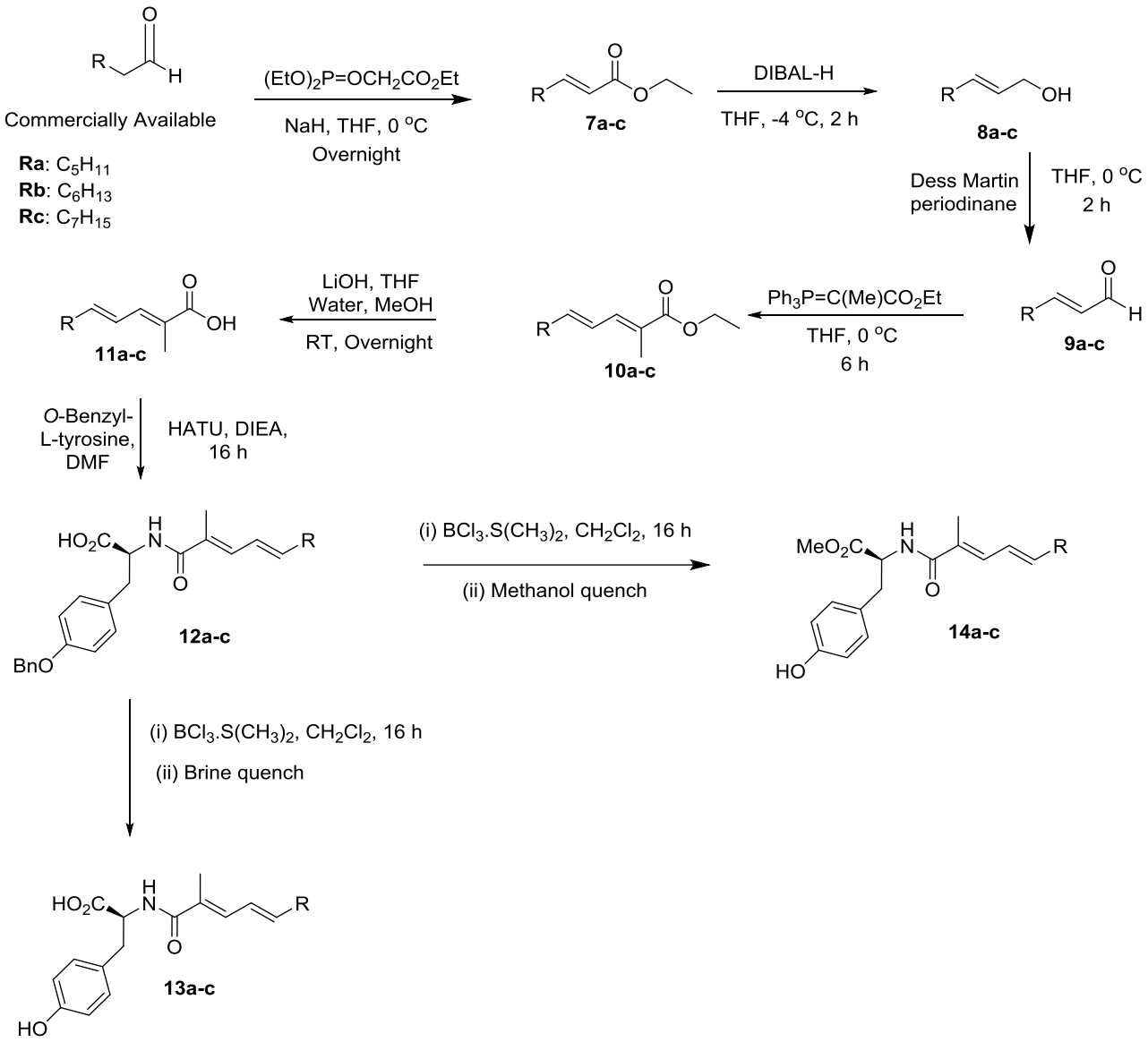

Scheme 3.20: Overview of synthesis

Herein, an eight step procedure towards the synthesis of analogues of gymnastatin N is discussed. The starting materials and the reagents are commercially available and cheap. The first step is a Horner-Wadsworth-Emmons (HWE) reaction which extends the chain length by two carbons and installs an alkene. This is followed by a reduction to the corresponding alcohols using di*iso*butyl aluminium hydride. Oxidation of the alcohols using Dess-Martin periodinane yields the corresponding aldehydes. A Wittig reaction further extends the chain and installs a methyl alkene. This is followed by a base catalysed hydrolysis to yield the corresponding acids. Coupling between the resulting acids and

commercially available *O*-benzyl-L-tyrosine using HATU and DIEA installing an amide bond is the key step. The final step is the deprotection of the benzyl ether to form the target compounds. The details of each of the procedures are discussed below.

3.2.1 The preparation of esters

The first step was a Horner-Wadsworth-Emmons (HWE) reaction, which involved a reaction between aldehydes and a phosphonate to obtain an alkene.[7] The aldehydes used were cheap and commercially available heptanal, octanal and nonanal. The aldehydes used in this step defined the R-group for each reaction. Triethyl phosphonoacetate was the reagent of choice as it afforded the desired product with regioselectivity resulting in the formation of *E*- isomer (Scheme 3.21).

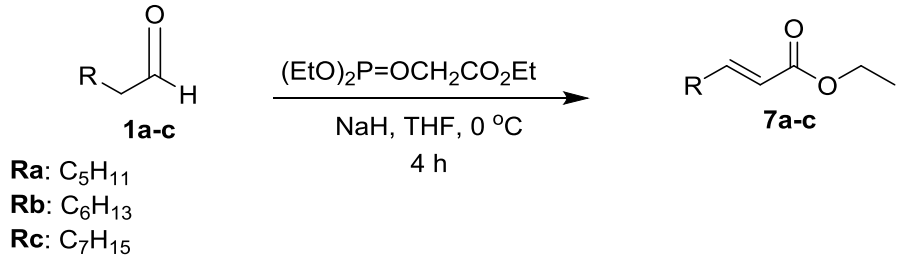

Scheme 3.21: The synthesis of alkenes

Triethyl phosphonoacetate was added to a solution of sodium hydride in THF and the mixture stirred under argon at 0 °C for 10 minutes. The appropriate aldehyde **1a-1c** was added dropwise and the resulting mixture stirred for 4 hours. TLC and the disappearance of the aldehyde proton in ^{1}H NMR analysis were used to monitor the reaction. The mixture was quenched with ammonium chloride solution and extracted with ether. The phosphorus containing side product is water soluble and therefore was easily removed in the quenching step. The product was then purified by column chromatography.

Entry	R	% Yield
7a	C_5H_{11}	92
7b	C_6H_{13}	89
7c	C_7H_{15}	88

The formation of the ester was confirmed by ^{1}H NMR by the disappearance of the doublet at 9.00 ppm corresponding to the aldehyde functional group of the starting material. The presence of 2 signals in the alkene region of ^{1}H NMR confirmed the installation of an alkene. Furthermore, the quartet at 4.20 ppm confirmed the presence of R-CH_2 corresponding to the ethyl group of the ester. The formation of the *E* alkene was confirmed by measuring the coupling constants of the alkenyl protons. (*J = 15-16 Hz*).

The reaction mechanism is outlined below. The reaction begins with deprotonation of triethyl phosphonoacetate using NaH (Scheme 3.22) to give a carbanion.

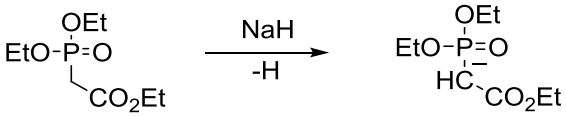

Scheme 3.22: Deprotonation of triethyl phosphonoacetate

Nucleophilic attack of the carbanion on to the carbonyl group generates a negatively charged oxygen which attacks the positively charged phosphorus forming a very unstable 4-membered ring, an oxaphosphetane. The ring fragments to form an alkene and P=O. (Scheme 3.23) The P=O bond has a bond energy of 575 kJmol^{-1} and is one of the strongest bonds in chemistry. Its formation is the driving force of this reaction.[1]

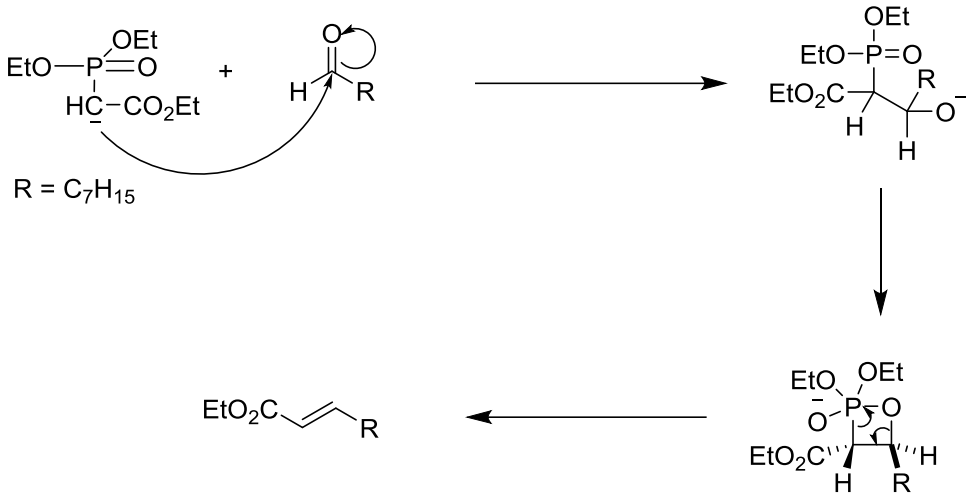

Scheme 3.23: Proposed mechanism for Horner-Wadsworth-Emmons reaction

3.2.2 The preparation of the alcohols

There were two options for the reduction of the ester to an alcohol; lithium aluminium hydride ($LiAlH_4$) and di*iso*butylaluminium hydride (DIBAL-H). $LiAlH_4$ is a powerful reducing agent, however, it is difficult to handle. Lithium borohydride has been used as a milder alternative, however it reduces esters to alcohols very slowly. DIBAL-H was used for the preparation of alcohols **8a-8c** as it is easy to handle and involves quicker reaction times (< 2 h). DIBAL-H reduces esters to aldehydes at low temperatures, however at higher temperatures the ester is further reduced to an alcohol.[1,8]

The ester reduction was initially attempted using 1.2 equivalents of DIBAL-H in CH_2Cl_2 at 0 °C and at room temperature. No product was formed and the starting material was recovered. Increasing the temperature and reaction times resulted in isomerisation. Using excess DIBAL-H resulted in partial reduction and an emulsion was formed which was very difficult to separate resulting in low yields. The reaction went to completion with good yields when the temperature was maintained at -4 °C and 2 equivalents DIBAL-H used (Scheme 3.24).

The successful reduction of the ester to the alcohol was confirmed by ^{1}H NMR by the disappearance of the quartet at 4.16 ppm and the triplet at 1.45 ppm corresponding to the ethyl group of the ester. The loss of ^{1}H NMR signal at 166.8 ppm and of the IR peak at 1720 cm^{-1} corresponding to the carbonyl of the ester also confirmed the successful reduction. Furthermore, the presence of the hydroxyl group was confirmed by the broad peak at 3321 cm^{-1} on the IR spectrum.

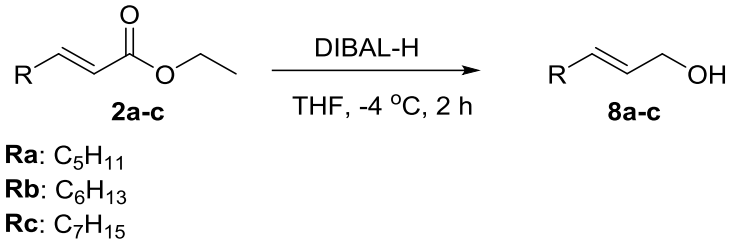

Scheme 3.24: The synthesis of alcohols

The appropriate ester **7a-7c** in CH_2Cl_2 was cooled to -4 °C and stirred under argon after which DIBAL-H in $CH_2Cl_2$was added and the resulting mixture stirred for 2 hours. The reaction mixture was quenched using 1M HCl and extracted using ethyl acetate.

Although the reaction went to completion, the initial yields were very low. DIBAL-H is an aluminium hydride which when used in excess, results in the formation of an aluminium salt emulsion between the aqueous and organic layer. This makes the work-up very difficult and results in very low yields. To overcome this, a saturated aqueous solution of Rochelle's salt was prepared. This was added to the completed reaction mixture and the solution vigorously stirred in an ice bath for 5 minutes. This broke up the emulsion and the crude mixture was purified using flash chromatography.

Entry	R	% Yield
8a	C_5H_{11}	84
8b	C_6H_{13}	85
8c	C_7H_{15}	91

The mechanism for DIBAL-H reduction is shown in Scheme 3.25. The reduction of the ester is initiated by the attack of the nucleophilic hydrogen on the carbonyl to give a tetrahedral intermediate. The tetrahedral intermediate collapses and loses an alkoxide to form an aldehyde. The aldehyde is further reduced to form another tetrahedral intermediate with negatively charged oxygen which is protonated during the work up to form the alcohol product.

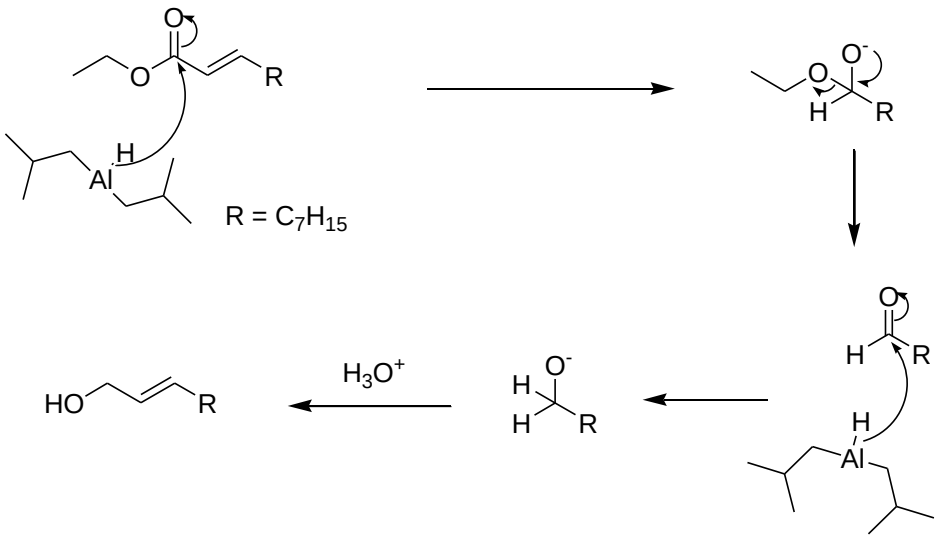

Scheme 3.25: Reaction mechanism for DIBAL-H reduction

3.2.3 The preparation of aldehydes

Dess-Martin periodinane (DMP) was used to oxidise the alcohols to aldehydes **9a-9c**. The use of DMP as an oxidising agent was first reported in 1983 by Martin *et al.* It oxidises

primary alcohols to aldehydes and secondary alcohols to ketones. Despite its cost, DMP is an efficient oxidising agent compared to 2-iodoxybenzoic-acid (IBX), DMSO and chromium based oxidising agents (pyridinium chlorochromate or pyridinium dichromate).[12] Its advantages include short reaction times of between 0.5 – 2 hours, mild reaction conditions, good solubility in most organic solvents and high yields. The iodo by-product is easily separated from the product *via* work up. DMP is commercially available, however it can be prepared from IBX. Dess *et al* reported the first synthesis of DMP in 1983. In 1993, Ireland and Liu reported an improved procedure for the preparation of DMP illustrated in Scheme 3.26. Due to the risks associated with its synthesis, commercially available DMP was used.[13-14]

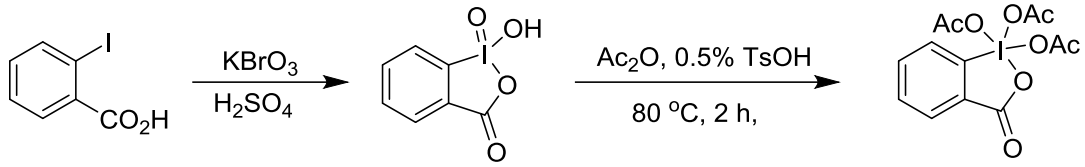

Scheme 3.26: Improved procedure for preparation of Dess-Martin Periodinane using iodobenzoic acid as reported by Ireland.[14]

The oxidation of alcohols **8a-8c** is outlined in Scheme 3.27. The reactions went to completion in less than 90 minutes in good yield. The aldehydes had to be used straight away or stored at -20 °C. When stored at higher temperatures for a few hours or purification attempted, the aldehydes degraded or hydrolysed to corresponding acids.

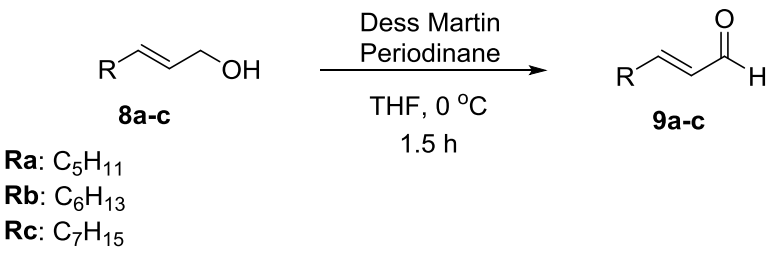

Scheme 3.27: The synthesis of aldehydes

The appropriate alcohol **8a-8c** in CH_2Cl_2 was cooled to 0 °C. Dess-Martin periodinane in CH_2Cl_2, also at 0 °C, was added and the reaction mixture stirred for 1.5 hours under argon. The reaction mixture was quenched using 1M NaOH and extracted using ether. The product was used immediately without further purification or stored at -20 °C under argon.

The successful oxidation of the alcohol to the aldehyde was confirmed by ^{1}H NMR by the loss of the doublet of doublets at 4.10 ppm corresponding to the CH_2 α to the hydroxyl group. Furthermore, the presence of a doublet at 9.50 ppm in the ^{1}H NMR confirmed the presence of an aldehyde.

Entry	R	Yield
9a	C_5H_{11}	94
9b	C_6H_{13}	90
9c	C_7H_{15}	91

The proposed mechanism is illustrated in Scheme 3.28.

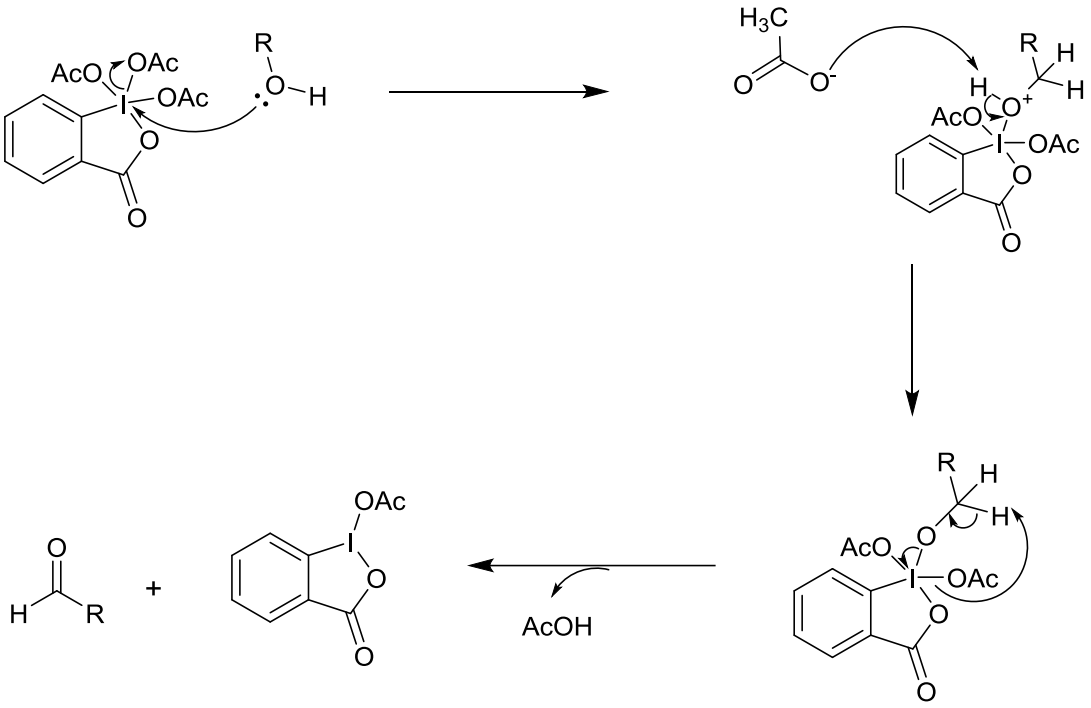

Scheme 3.28: Proposed reaction mechanism for oxidation of alcohol to aldehyde using Dess-Martin periodinane

The lone pair of electrons on the alcohol attacks the iodine on the periodinane resulting in a positively charged oxygen. The acetoxy group deprotonates the alcohol to form AcOH. Another molecule of AcOH is lost. The I-O bond breaks resulting in a neutral iodine species and an aldehyde is formed. The reaction is quenched using NaOH which hydrolyses the side product acetoxyiodinane into 2-iodosobenzoate which together with acetic acid are removed during the work-up.[15]

3.2.4 The preparation of esters

A Wittig reaction in the presence of (carbethoxyethylidene) triphenylphosphorane increased the chain length by addition of another alkene according to Scheme 3.29.

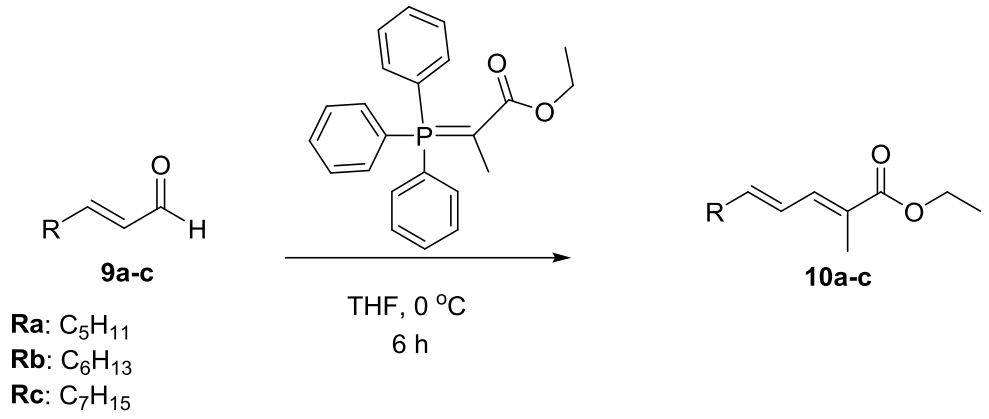

Scheme 3.29: The synthesis of alkenes

The appropriate aldehyde **9a-c** in CH_2Cl_2 and (carbethoxyethylidene) triphenylphosphorane were stirred under argon for 6 h before being quenched with ammonium chloride and extracted with diethyl ether and the volatiles removed *in vacuo*. The crude product was purified using column chromatography.

Entry	R	Yield
10a	C_5H_{11}	81
10b	C_6H_{13}	75
10c	C_7H_{15}	72

The success of the Wittig reaction was confirmed by disappearance of the doublet at 9.50 ppm in the ^{1}H NMR corresponding to the proton of the aldehyde. The presence of an additional signal in the alkene region of ^{1}H NMR confirmed the installation of an additional alkene. The quartet at 4.10 ppm confirmed the presence of R-CH_2 corresponding to the ethyl group of the ester. Furthermore, the presence of the methyl group α to the carbonyl was confirmed by the ^{1}H NMR singlet at 1.85 ppm.

The proposed mechanism for this reaction is similar to that presented in section 3.1.1.

3.2.5 The preparation of acids

The next step involved a base catalysed hydrolysis of the esters to form an acid using LiOH in THF/methanol/water at room temperature.

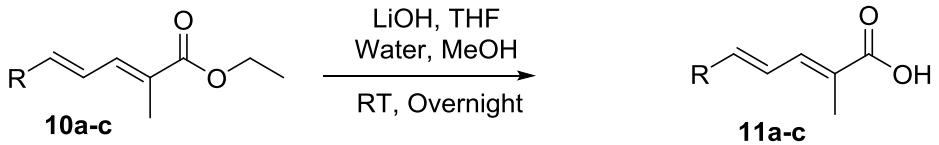

Ra: C_5H_{11}
Rb: C_6H_{13}
Rc: C_7H_{15}

Scheme 3.30: The synthesis of acids

The procedure in Scheme 3.30 was employed for the synthesis of acids. After 24 hours, 1M HCl was added to the reaction mixture followed by extraction using ether. This reaction was difficult to reproduce as a salt was formed in most cases. The acid was instead obtained by flushing the salt through silica gel several times. This lowered the yield but gave a clean acid product. The formation of the acid was confirmed by ^{1}H NMR. The quartet at 4.16 ppm corresponding to the R-CH_2 of the ethyl group of the ester was no longer present. Furthermore, the identity of the product was confirmed by the broad peak at 12 ppm representing the OH proton. This was further confirmed by a D_2O shake.

The proposed mechanism for this reaction is similar to the one presented in section 3.1.2.

Entry	R	% Yield
11a	C_5H_{11}	80
11b	C_6H_{13}	89
11c	C_7H_{15}	70

3.2.6 Amide coupling

Coupling of acids **11a-11c** with *O*-benzyl protected tyrosine was carried out as previously described in section 4.1.4 *via* amide coupling using HATU, DIEA and DMF. (Scheme 3.31)

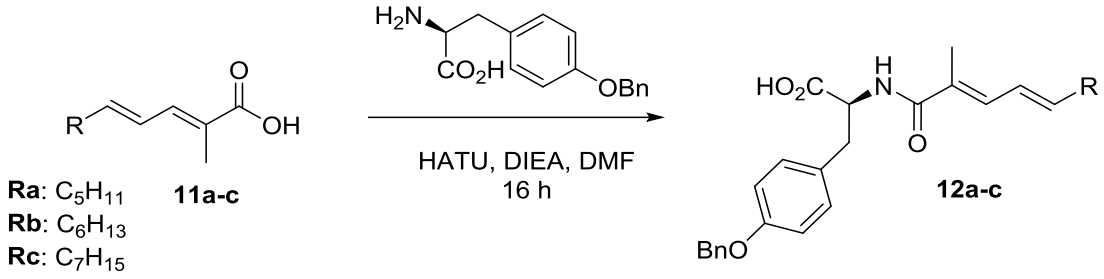

Scheme 3.31: Amide coupling using HATU

The reaction was monitored by NMR and was complete in 16 h. The identity of the product was confirmed by NMR. An NH signal (doublet) was observed at 6.8 ppm and confirmed by a D_2O shake. LRMS was also used to confirm the identity of the product. (Table 3.4)

Entry	R	% Yield	Calc $(M+H)^+$	Found *m/z*
12a	C_5H_{11}	80	450.3	450.2
12b	C_6H_{13}	85	464.6	464.2
12c	C_7H_{15}	72	478.3	478.2

Table 3.4: Yields and LRMS results for amide products.

The mechanism for this reaction is discussed in section 3.1.4.

3.2.7 Benzyl deprotection

The final step was the removal of the benzyl protecting group. This was carried out as previously described in section 3.1.6.2 using boron trichloride methyl sulfide complex in

CH_2Cl_2. The reaction was quenched using brine or methanol, to preserve the acid side group, or install a methyl ester side group, respectively.

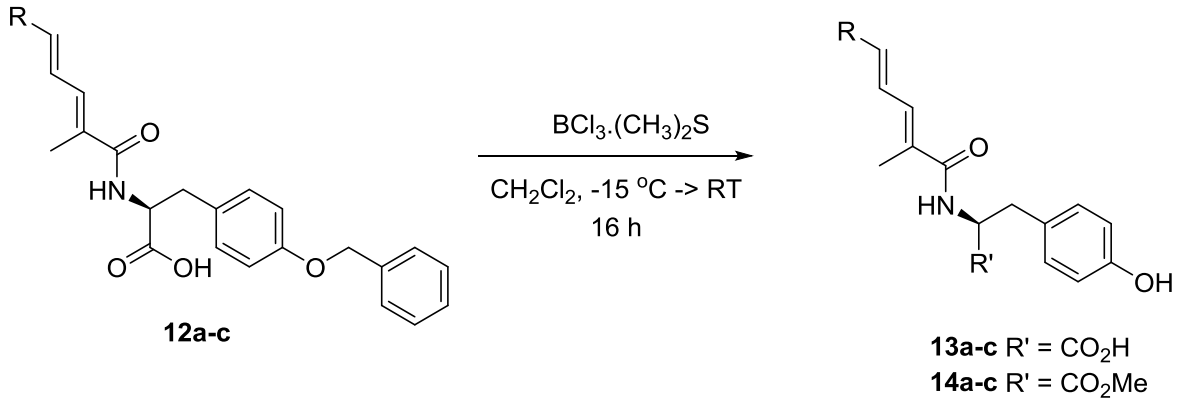

Scheme 3.32: O-benzyl deprotection using boron trichloride dimethyl sulfide complex

Entry	R	R'	% Yield
13a	C_5H_{11}	$-CO_2H$	95*
13b	C_6H_{13}	$-CO_2H$	85*
13c	C_7H_{15}	$-CO_2H$	73*
14a	C_5H_{11}	$-CO_2Me$	80
14b	C_6H_{13}	$-CO_2Me$	79
14c	C_7H_{15}	$-CO_2Me$	72

*Table 3.5: Yields of final compounds. * not purified*

Difficulties were encountered in the purification of the target compounds containing the acid side group **13a–13c**. The compounds degraded during purification. The yields and characterisation reported are of the crude product.

3.2.8 Methyl ester derivative compound characterisation

The yields of the reactions are illustrated in Table 3.5. The spectrum of **14a** is used in this section to characterise the final compound. The ^{1}H NMR and COSY spectra of **14a** are shown in Figure 3.5.

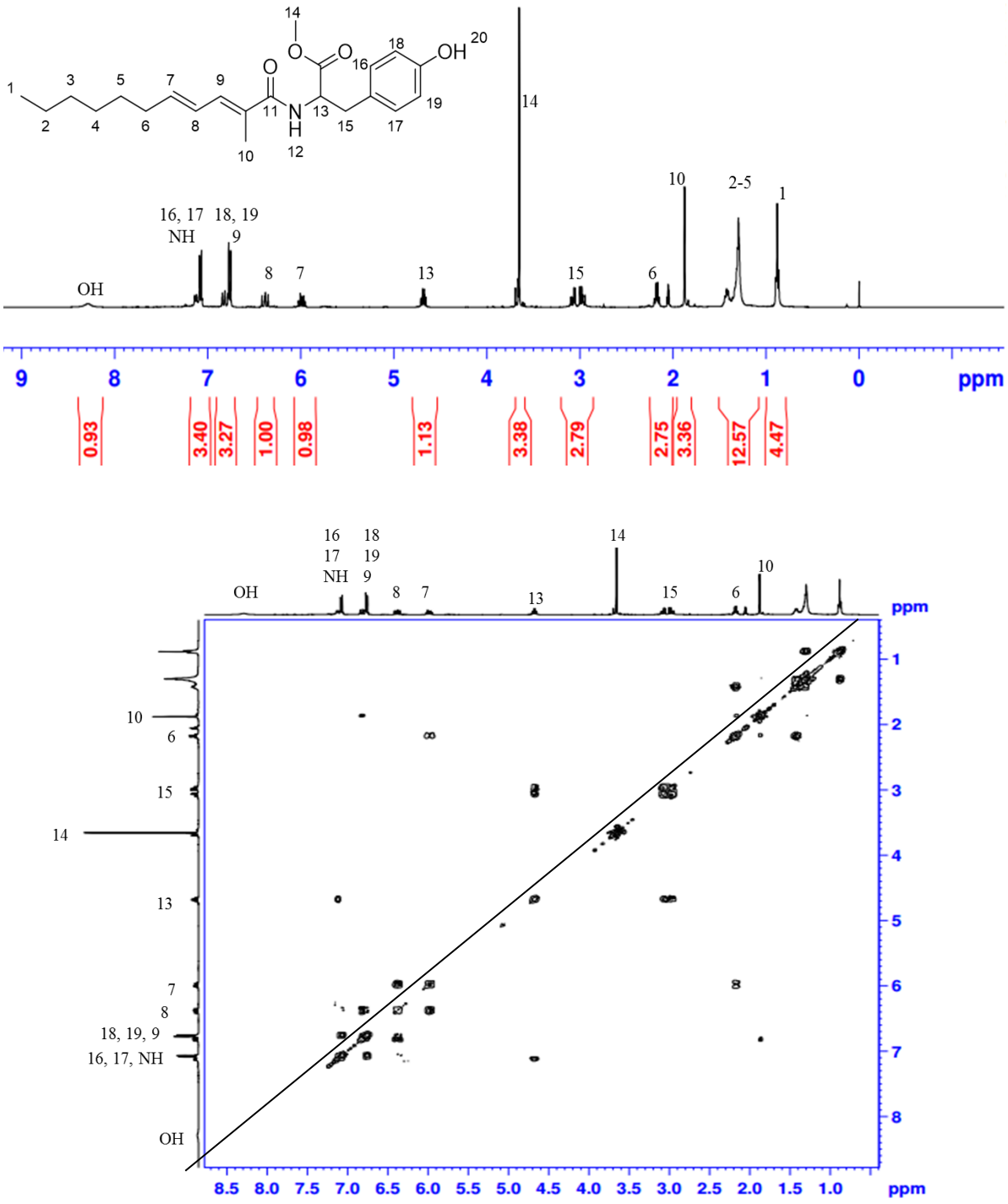

*Figure 3.5: Assigned ^{1}H NMR and COSY of **14a** in CD_3CN*

The successful debenzylation was confirmed by ^{1}H NMR. The characteristic protons of the benzyl protecting group at 7.30 and 4.90 ppm were no longer present. The distinctive splitting pattern of the *para*- disubstituted benzene ring is observed in the aromatic region. A doublet corresponding to the secondary amide was observed at 7.20 ppm. The NH was confirmed by disappearance on D_2O shake, and by HSQC. Furthermore, the NH signal

coupled with the proton at position 13 was evident in the COSY (Figure 3.5.). The alkenyl protons were observed in the alkenyl region. The proton at position 13 was observed at 4.60 ppm as a quartet. Furthermore, the presence of the OH resulting from debenzylation was confirmed by a broad peak observed at 8.2 ppm. HSQC and a D_2O shake confirmed that this was an OH signal. A diastereotopic splitting pattern was observed at 3.0 ppm corresponding to the $–CH_2$ at position 15. The singlet at 3.70 ppm represents a methyl group corresponding to the methyl ester on the tyrosine unit.

3.3 Conclusion

A library of eight novel gymnastatin analogues were prepared with various chain lengths. The compounds consisted of an unsaturated side chain linked to a tyrosine unit using an amide bond. The side chain was prepared by a HWE, reduction, oxidation, Wittig and hydrolysis reactions. The resulting acid was coupled to a benzyl protected tyrosine using HATU. Additional functionality was added to the tyrosine unit by methylation of the acid side group to prepare methyl ester derivatives. The final compounds were obtained by removal of the benzyl protecting group. The resulting final compounds were characterised using NMR, IR and HRMS.

Prior to this work, there are few reports in the literature on the synthesis of compounds of this nature. While three compounds with an acid side group were isolated, they were very difficult to purify. Future work within the group will involve purification of these compounds using preparative HPLC.

3.4 References

1. Clayden, J.; Greeves, N.; Warren, S. *Organic Chemistry,* Oxford, **2001,** *2nd Edition.*

2. Wadsworth, W. S.; Emmons, W. D. *J. Am. Chem. Soc.* **1961**, *83* (7), 1733–1738.

3. Montalbetti, C. a. G. N.; Falque, V. *Tetrahedron.* **2005**, *61*, 10827–10852.

4. Valeur, E.; Bradley, M. *Chem Soc Rev.* **2009**, *38*, 606–631.

5. Carpino, L. *J. Am. Chem. Soc.* **1993**, *115*, 4397–4398.

6. Carpino, L. A.; Imazumi, H.; El-Faham, A.; Ferrer, F. J.; Zhang, C.; Lee, Y.; Foxman, B. M.; Henklein, P.; Hanay, C.; Mügge, C.; Wenschuh, H.; Klose, J.; Beyermann, M.; Bienert, M. *Angew. Chemie - Int. Ed.* **2002**, *41*, 441–445.

7. Caine, D.; Smith, T. L. J. *J. Am. Chem. Soc.* **1980**, *102*, 7569–7570.

8. Bindra, J.; Grodski, A. *J. Org. Chem.* **1978**, *43*, 3240–3241.

9. Wadsworth, W. S.; Emmons, W. D. *J. Am. Chem. Soc.* **1961**, *83*, 1733–1738.

10. Garner, P.; Park, J. M. *Org. Synth.* **1992**, *70*, 18-22.

11. Coleman, R. S. *Synthesis (Stuttg).* **1999**, (S1), 1399–1400.

12. Corey, E. J.; Suggs, J. W. *Tetrahedron Lett.* **1975**, *16*, 2647–2650.

13. Dess, D. B.; Martin, J. C. *J. Org. Chem.* **1983**, *48*, 4155–4156.

14. Ireland, R. E.; Liu, L. *J. Org. Chem.* **1993**, *58*, 2899–2899.

15. Dess, D. B.; Martin, J. C. *J. Am. Chem. Soc.* **1991**, *113*, 7277–7287.

16. Harwood, L. M.; Moody, C. J.; Percy, J. M., *Experimental Organic Chemistry*, Blackwell Science, **1999**, 2nd Edition.

17. Albericio, F.; Chinchilla, R.; Dodsworth, D. J.; Najera, C., *Org. Prep. Proc. Int.* **2001**, *33*, 203-313.

18. Xie, J.; Ménand, M.; Valéry, J. M. *Carbohydr. Res.* **2005**, *340* (3), 481–487.

4. Biological evaluation of gymnastatin analogues

4.1. Introduction

This chapter documents the biological evaluation of the library of synthesised gymnastatins. This includes cytotoxic evaluation in the A549 cancer cell line. It begins with the background of the cell line used and the techniques used for measuring cytotoxicity. This is followed by the results and discussion of the biological evaluation using two assays, the MTT and the alamar blue assay.

The last section of this chapter details preliminary work carried out on the evaluation of some compounds as potential Plk1 inhibitors. This is followed by a discussion of the preliminary results obtained from an ELISA assay targeting Plk1.

4.1.1. Cell lines

The compounds prepared were evaluated in the A549 cancer cell line. The A549 cell line is a continuous cell line derived from a human pulmonary adenocarcinoma. It was isolated in 1973 from cancerous lung tissue in the tumour of a 58-year-old caucasian male. It was later characterised as a representative of the alveolar type II pneumocytes of the lung cell. The alveolar epithelium comprises two cell types: the alveolar type I (ATI) and alveolar type II (ATII) cell. ATI cells are squamous cells that cover around 95% of the alveolar surface. ATII cells cover the remaining 5%. ATII cells play an important role within the lung and have been described as defenders of the alveolus. The A549 cell line is a useful model for the isolated ATII pneumocyte. It was selected for this work because of its facile manipulation. A549 cells are also a robust cell line providing a good starting point for an inexperienced researcher in this area.[1-3]

4.1.2. Cytotoxicity assays

As an initial screen for potential drug candidates it is common to establish whether the drug candidates exhibit a cytotoxic effect. Cell based assays are often used to screen compounds to determine if test molecules show direct cytotoxic effects that will lead to cell death. There are a variety of assays used to estimate the number of viable cells at the end of an experiment. Most cytotoxicity assays are based on colorimetric assays involving the use of an organic dye. Many assays employed are based on the metabolic activity of healthy cells. The results are determined using UV-vis or fluorescence spectroscopy. The absorbance or fluorescence intensity corresponds to the metabolic activity of the cells. Damaged or dead cells have lower metabolic activity and thus generate a lower signal compared to healthy, undamaged cells.[4-7]

To evaluate the response of A549 cells to the synthesised analogues of gymnastatins, the alamarBlue ® (AB) and MTT assays were used. The AB and MTT assays were conducted on separate plates. Briefly, cells were seeded into 96 well plates and incubated for 24 hours. The cells were exposed to varying drug concentrations at different time points from 24 to 72 hours. The details of each of the assays are discussed below.

4.1.3. MTT assay

3-[4,5-Dimethylthiazol-2-yl]-2,5-diphenyltetrazolium bromide (MTT), **1** is a yellow water soluble tetrazolium salt which is actively absorbed into cells. It is reduced to a purple formazan dye **2** in the mitochondria of viable cells by the cleavage of the tetrazolium ring by dehydrogenase enzymes. [1,2] The reaction is illustrated in Scheme 4.1.

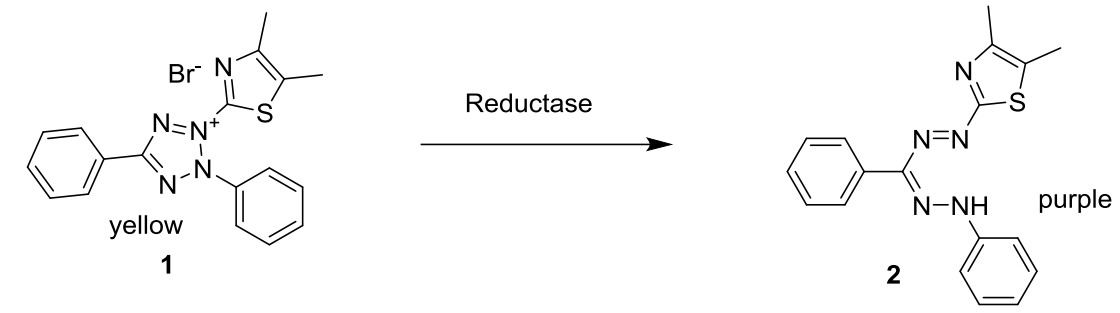

*Scheme 4.1: Reduction of MTT **1** by mitochondrial enzymes to give the formazan dye **2.***

Cells lose their ability to reduce tetrazolium compounds shortly after death. Therefore, the ability of cells to reduce MTT is used as an indicator of mitochondrial activity which is interpreted as a measure of cell viability. The absorbance of the treated sample at 570 nm is proportional to the quantity of viable cells in the sample.[8]

4.1.4. AlamarBlue®

AB monitors the reducing environment of a living cell. Its active ingredient, resazurin (7-hydroxy-10-oxidophenoxazin-10-ium-3-one) is a redox indicator. It is non-toxic, water soluble and stable in culture media. Viable cells with active metabolism reduce the blue, non-fluorescent, resazurin **3** into the resofurin product which is pink and fluorescent.[9] (Scheme 4.2)

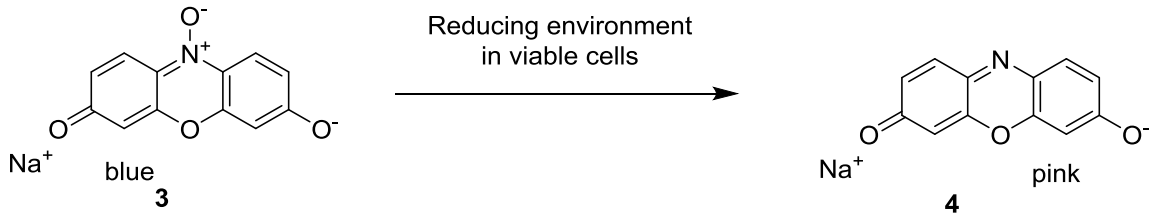

*Scheme 4.2: Reduction of resozurin sodium salt **(3)** to strongly fluorescent resofurin sodium salt **(4)** in the presence of viable cells*

The quantity of resofurin produced is proportional to the number of viable cells which can be quantified using a microplate reader at 560 nm excitation and 590 nm emission.[10-12]

4.1.5. Methodology

The A549 cell line was maintained in Dulbecco's modified Eagle's medium (DMEM) supplement, with 10% fetal bovine serum (FBS) and 5 mM *L*-glutamine in appropriate asceptic conditions, at 37 °C in 5% CO_2 humidified incubator.

Fig 4.1 shows the characteristic growth pattern of cells. The plot shows cell density *versus* the time spent in each phase by the cell in culture.

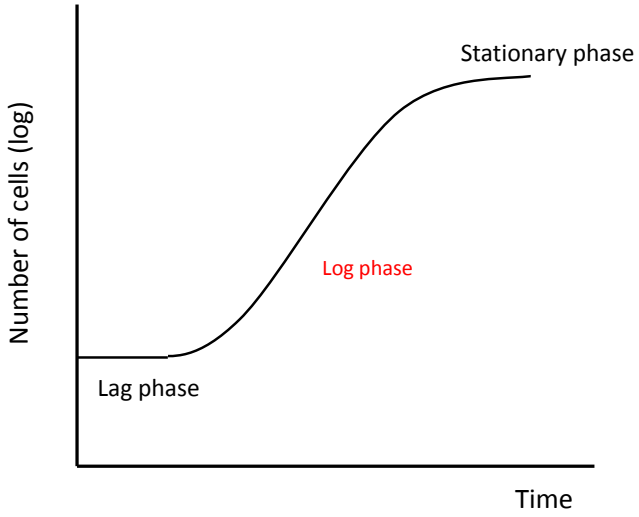

Figure 4.1: Characteristic growth curve of cells

The lag phase is the period just after the cells have been seeded. It is characterised by slow growth as the cells adapt to the media and the new environment. This is followed by the log phase. During the log phase, also called the logarithmic phase, the cells have adapted and proliferate exponentially. The cells enter stationary phase when all the media has been used up, or growing cells have occupied all of the available substrate. At this stage, proliferation is greatly reduced and eventually stops entirely. Cells have to be subcultured/seeded/passaged before they reach the stationary phase.

A standard procedure available in the laboratory was used for cytotoxic evaluation. Cells were harvested for experiments when they were in the "log" phase of growth. The cells were then seeded into 96 well plates at densities ranging from $3*10^4$ to $1.2*10^5$ depending on the duration of exposure (24, 48 and 72 h). The cells were incubated for 24 hours to allow for attachment. Drug solutions were prepared in DMSO (up to 1% v/v). Final test solutions were prepared by serial dilution of a 700 μM working stock solution. Following attachment, the cells were exposed to five different drug concentrations in eight replica wells. The final concentration was achieved by addition of the drug solution to the medium containing cell suspensions in the wells. Three replica plates were used for each experiment.

Following exposure, the cells were incubated in appropriate asceptic conditions at 37 °C in 5% CO_2 humidified incubator for 24, 48 and 72 hours. At the appropriate times, the assays were terminated by discarding the test solutions from plates and rinsing each plate using PBS. This was followed by the addition of fresh unsupplemented media and MTT solution. The cells were further incubated for 3 hours, during which time, the mitochondria in viable cells absorbed and metabolised MTT. The supernatant was then removed and each well was washed with PBS to remove any unmetabolised MTT. The water-insoluble formazan salt was solubilised using DMSO and shaken for 10 minutes. The well plate was subsequently placed in a Genios plate reader and absorbance 570 nm was recorded. Figure 4.2 summarises the steps involved in the MTT assay.

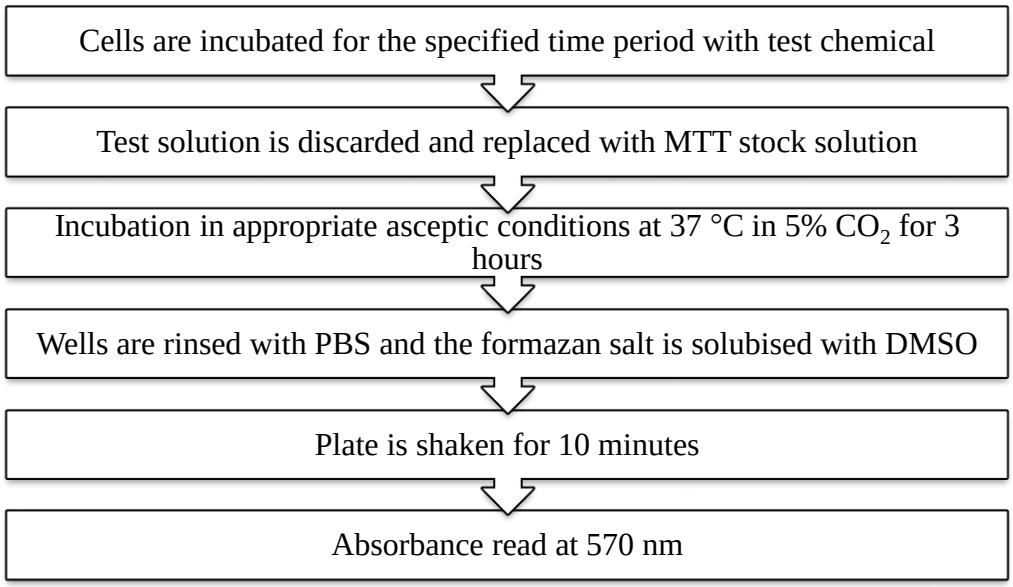

Figure 4.2: Summary of MTT assay procedure

For the alamar blue® assay, a slight variation of this procedure was used. Following exposure for the appropriate time, the test chemical was removed and replaced with AB dye stock solution. The plates were incubated for three hours after which time the plates were placed in a microplate reader and read at 560 nm excitation and 590 nm emission.

This experimental procedure was performed in triplicate for each drug at each time point. The percentage viability was calculated using the following equation:

$$\%\ viability = \frac{absorbance\ of\ treated\ cells}{absorbance\ of\ untreated\ control\ cells} \times 100$$

The cell viability was used to generate a concentration-response curve which was used to calculate the EC_{50} at each time point. The EC_{50} is defined as the concentration at which 50% of the cell population exhibited the desired response from the drugs, in this case, cell death. The % cell viability *versus* concentration plot and the dose response curve for **3b** at 72 hours are outlined in Figure 4.3 below as a representative example.

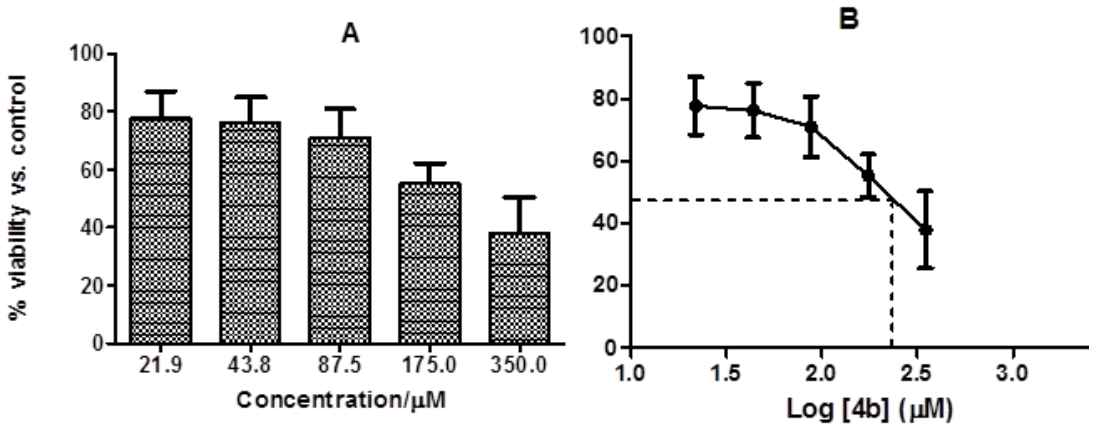

*Figure 4.3: **A** % viability of treated A549 cells versus the concentration of **3b.** % Viability values are calculated from three independent experiments and are shown +/- the standard deviation. **B** Dose response curve for **3b** in A549 cells at 72 hour exposure.*

Fig 4.3 shows the viability of A549 cells treated with **3b** over a range of concentrations. It can be seen that the drug reduces cell viability in a dose-dependent manner. The sigmoidal dose-response curve is the average response over three independent experiments.

All drug solutions were prepared in DMSO. DMSO is a widely used organic solvent due to its ampiphilic properties, high polarity and liquid state over a large temperature range. In cell culture, DMSO is widely used as a vehicle. It has been used as a solvent vector in many studies including the study of paclitaxel anticancer properties by Fujimoto.[13] Most literature procedures recommend maintaining DMSO concentration below 1% v/v.

To assess the cytotoxicity of DMSO, an MTT assay was performed for various concentrations of DMSO (0.5 to 10%) at two timepoints, 24 h and 72 h. The study demonstrated that at a concentration of 1% or lower, DMSO was non-toxic to A549 cells. (Figure 4.4).

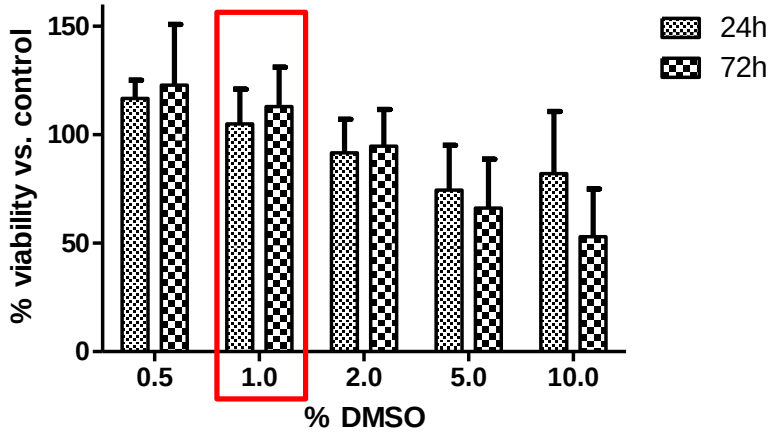

Figure 4.4: % viability of A549 cells treated with increasing concentration of DMSO versus untreated cells

4.1.6. Results of cytotoxic evaluation Gymnastatin analogues in A549 cells

The analogues of gymnastatin **1a-4b (**Figure 4.5) were assessed for cytotoxicity in A549 cells at concentrations 21.9 µM to 350 µM. A negative and positive control were included in each plate. All compounds assessed had good solubility in DMSO.

4.1.6.1. Statistics

Cytotoxicity data are the average of at least three experiments expressed as a mean percentage viability relative to the control (100 % media) ± standard deviation (SD). The results have been statistically analysed using one-way analysis of variance (ANOVA) followed by a post-ANOVA Dunnett's test using GraphPad Prism software ®. Test results are considered relevant when $P < 0.05$ (denoted with *) and very significant when $P < 0.01$ (denoted with #) for the Dunnets analysis (see Appendix). Statistical data was calculated using Microsoft excel. EC_{50} values were calculated using GraphPad Prism software ®.

4.1.6.2. MTT Assay

Initially all compounds were evaluated for potential anticancer activity using the MTT assay. The results of the evaluation are reported as EC_{50} values calculated as described in

section 5.1.5. The results for the cytotoxic assessment of analogues synthesised are summarised in Table 4.1 followed by the discussion of the results. Figure 4.5 shows a legend of the compounds evaluated using MTT assay at three different time points.

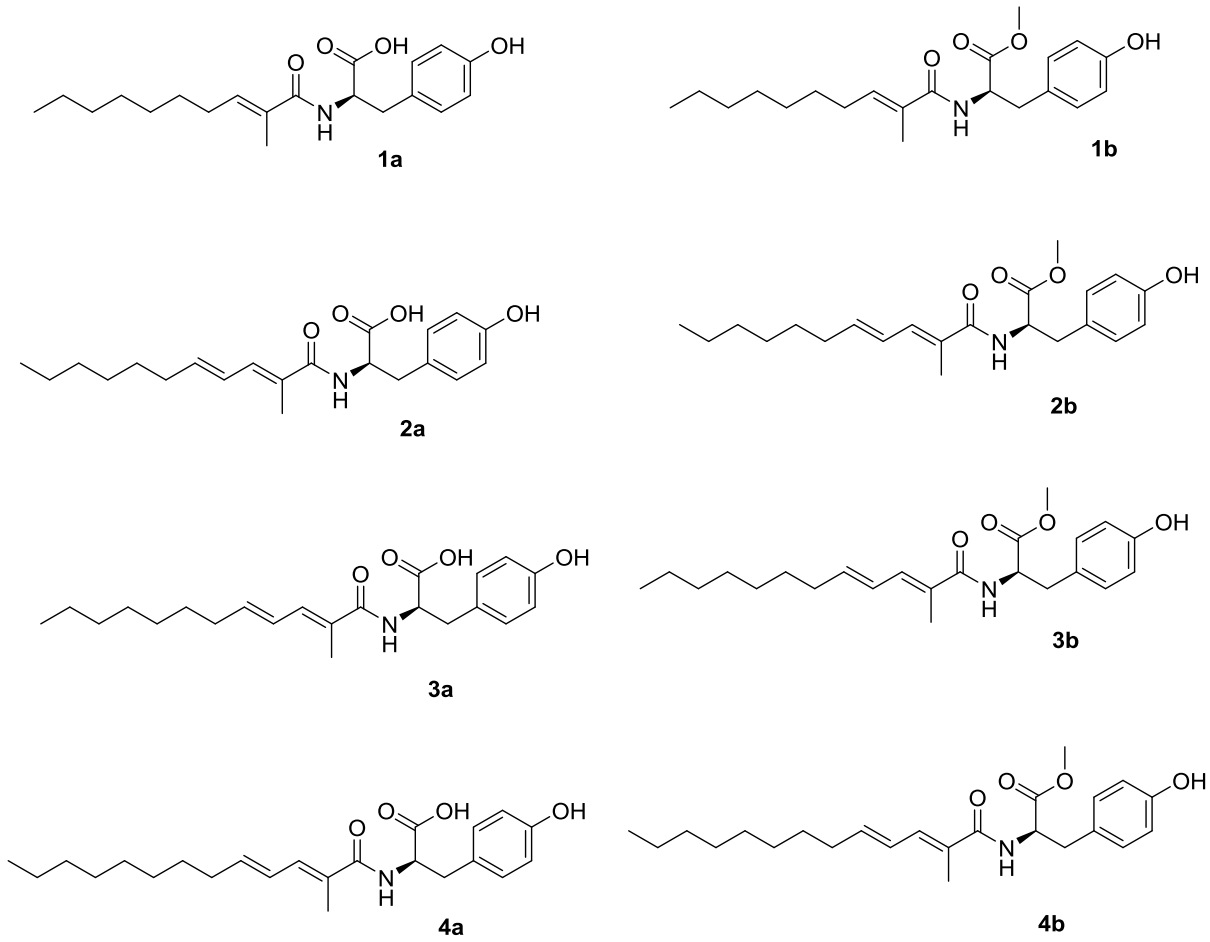

Figure 4.5: Legend for Table 4.2

Compound	$\underline{EC_{50}}$ μM (+/- s. d.)		
	24 h	**48h**	**72h**
1a	> 350 [a]	> 350 [a]	> 350 [a]
1b	> 350 [a]	> 350 [a]	227.5 (1.2)
2a	> 350 [a]	> 350 [a]	> 350 [a]
2b	> 350 [a]	> 350 [a]	216.7 (1.3)
3a	> 350 [a]	> 350 [a]	> 350 [a]
3b	> 350 [a]	218 (1.1)	123 (1.2)
4a	> 350 [a]	> 350 [a]	>350 [a]
4b	> 350 [a]	126.2(1.4)	91.4(1.3)

[a] EC_{50} could not be determined due to little or no activity at the concentrations used

Table 4.1: (MTT Assay) EC_{50} (μM) of compounds against A549 at three time points: 24, 48 and 72 hours post exposure. EC_{50} values are expressed as mean +/- standard deviation (s.d.) of at least three experiments.

It can be seen from the EC_{50} values presented in Table 4.1 that the compounds containing the methyl ester side group in the tyrosine moiety showed time and dose dependent activity against A549 cells. For all methyl ester containing compounds, the best activity was observed after 72 hours of exposure. It is interesting to note that increasing the chain length resulted in increased activity. Analogue **4b** which exhibited the longest chain length showed the best activity (91.4 μM) after 72 hours of exposure. The compound with

the shortest chain length showed the least activity (227 μM) against the A549 cell line. Fig 4.6 compares the dose response of compounds containing a methyl ester on the tyrosine unit.

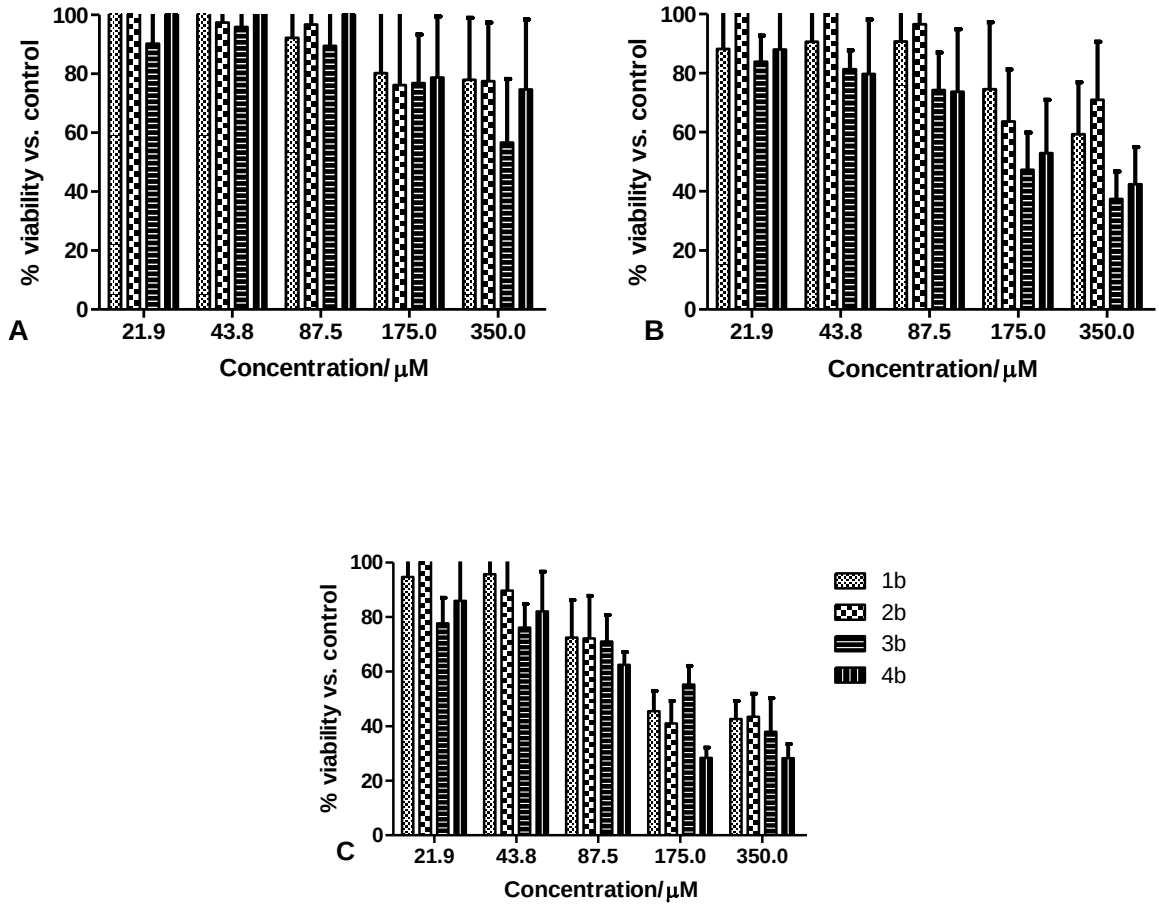

*Figure 4.6: Comparison of the dose-response of compounds containing methyl ester side group **(1b-4b)** at three timepoints 24, 48 and 72 hours (**A**, **B**, **C** respectively)*

At 24 hours there was no significant activity for any of the compounds evaluated. After 48 hours there was some activity at concentrations above 87.5 μM, most notably **3b** and **4b** which showed a viability of less than 60%. After 72 hours of exposure, all compounds showed activity at 175 and 350 μM. Compound **4b,** possessing the longest chain length

clearly showed the most activity (< 30% viability). This initial data seems to suggest that the activity is dependent on the chain length.

To assess the importance of the additional alkene, a comparison between compounds **1b** and **2b** is shown below.

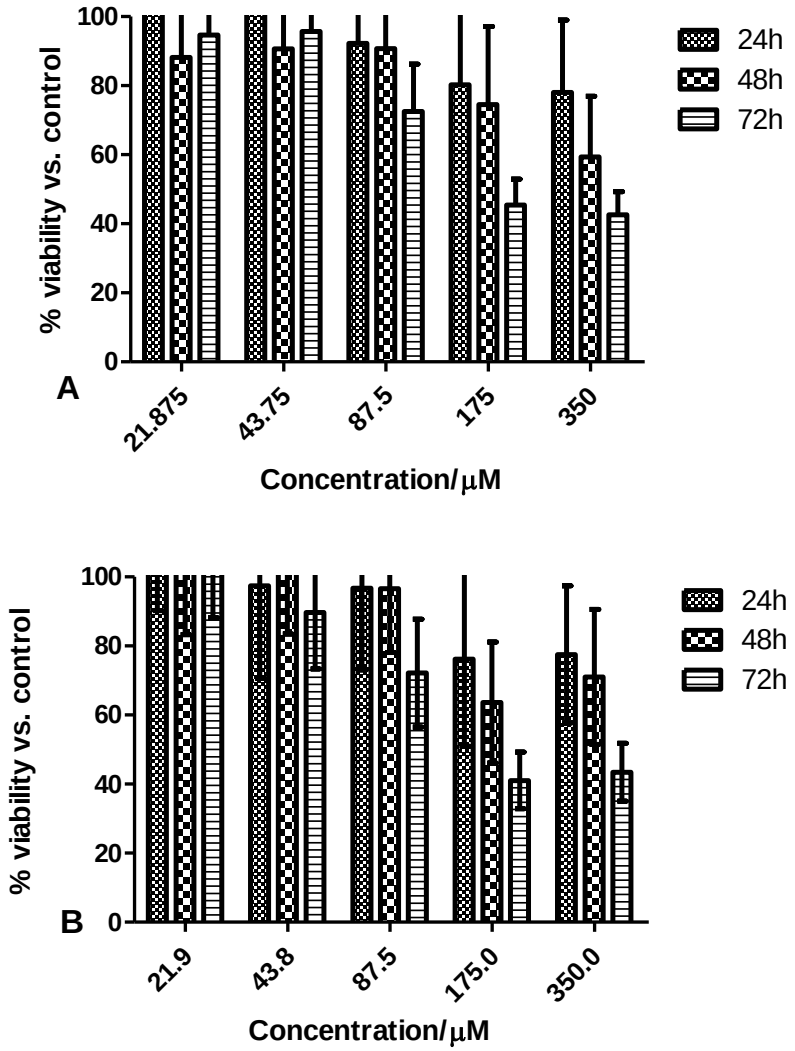

*Figure 4.7: Comparison of the dose-response of compounds **1b** and **2b** (**A** and **B** respectively) at three time points 24, 48 and 72 hours.*

There was no significant difference in activity between the two compounds assessed. Compound **2b** had a slightly lower EC_{50} (216.7 μM) compared to **1b** (EC_{50} = 227.5 μM).

Both compounds only showed significant activity after 72 hours at a concentration of 175 μM or above. While the activity of these compounds was disappointing, it did suggest that the additional alkene did not offer significant benefit to the activity in this assay.

Figure 5.8 shows a comparison of compounds containing the acid side group in the tyrosine unit. These compounds were also evaluated at three different timepoints.

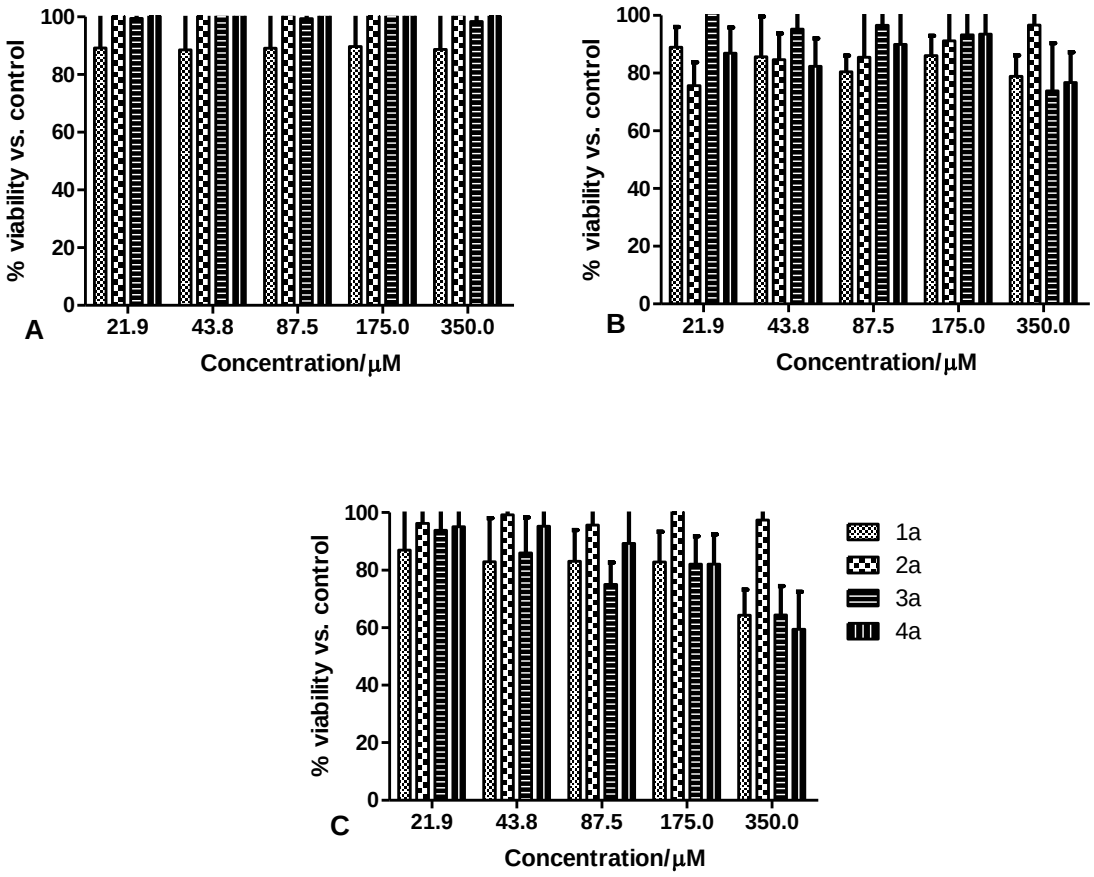

Figure 4.8: Comparison of the dose-response of compounds containing acid side group ***(1a-4a)*** *at three timepoints 24, 48 and 72 hours (**A**, **B**, **C** respectively)*

It was disappointing to note that compounds **1a-4a** did not show significant activity at concentrations tested (350 μM), even after 72 hours of exposure. While these results were

disappointing, they suggested that the presence of an acid side group did not impact the cytotoxicity in this assay.

Overall the results for the activity of synthetic gymnastatin analogues using the MTT assay were disappointing, with the exception of **4b**. At this stage, it was decided to use a different assay to determine if the drugs targeted a different part of the cell.

4.1.6.3. Alamar Blue® Assay

The compound showing the best activity for MTT **4b** as well as **1b** and **4a** were assessed using alamar blue. **4a** was chosen to evaluate the potential effect of the acid group on activity. **1b** was chosen in order to assess the effect of the chain length and presence of an additional alkene.

AB does not necessarily specifically indicate a mitochondrial dysfunction like the MTT assay. There have been reports which have suggested that cytosolic and microsomal enzymes also contribute towards the reduction. AB remains a suitable indicator of the cellular health and viability.[11-14] AB was used to examine if some of the compounds assessed using the MTT assay targeted other parts of the cell other than the mitochondria.

A legend for the compounds evaluated using the AB assay is presented in Figure 4.9.

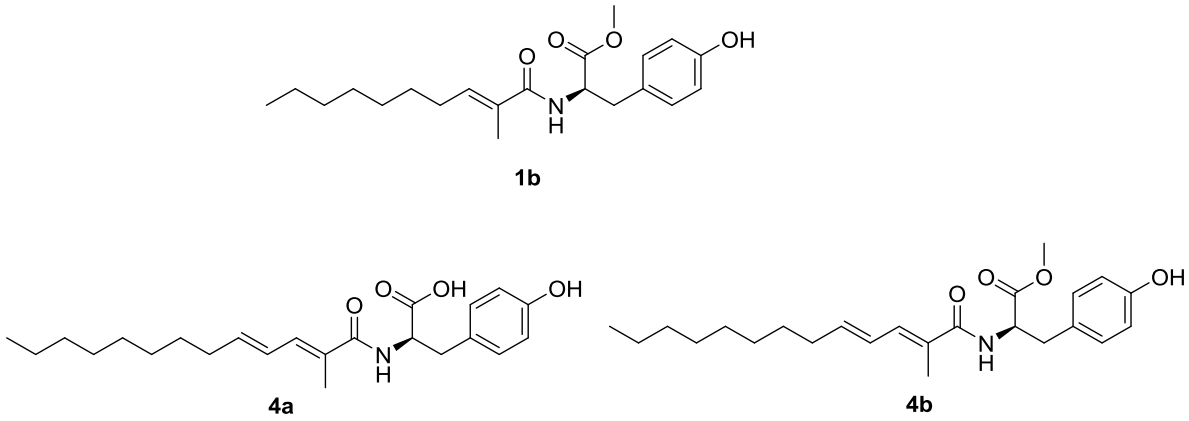

Figure 4.9: Legend for compounds assessed using alamar blue assay

Evaluation of compounds **1b, 4a** and **4b** gave a different outcome. A significant difference in activity between compounds assessed using MTT *versus* AB was observed. All compounds assessed performed better in the AB assay compared to the MTT assay. (Figure 4.10).

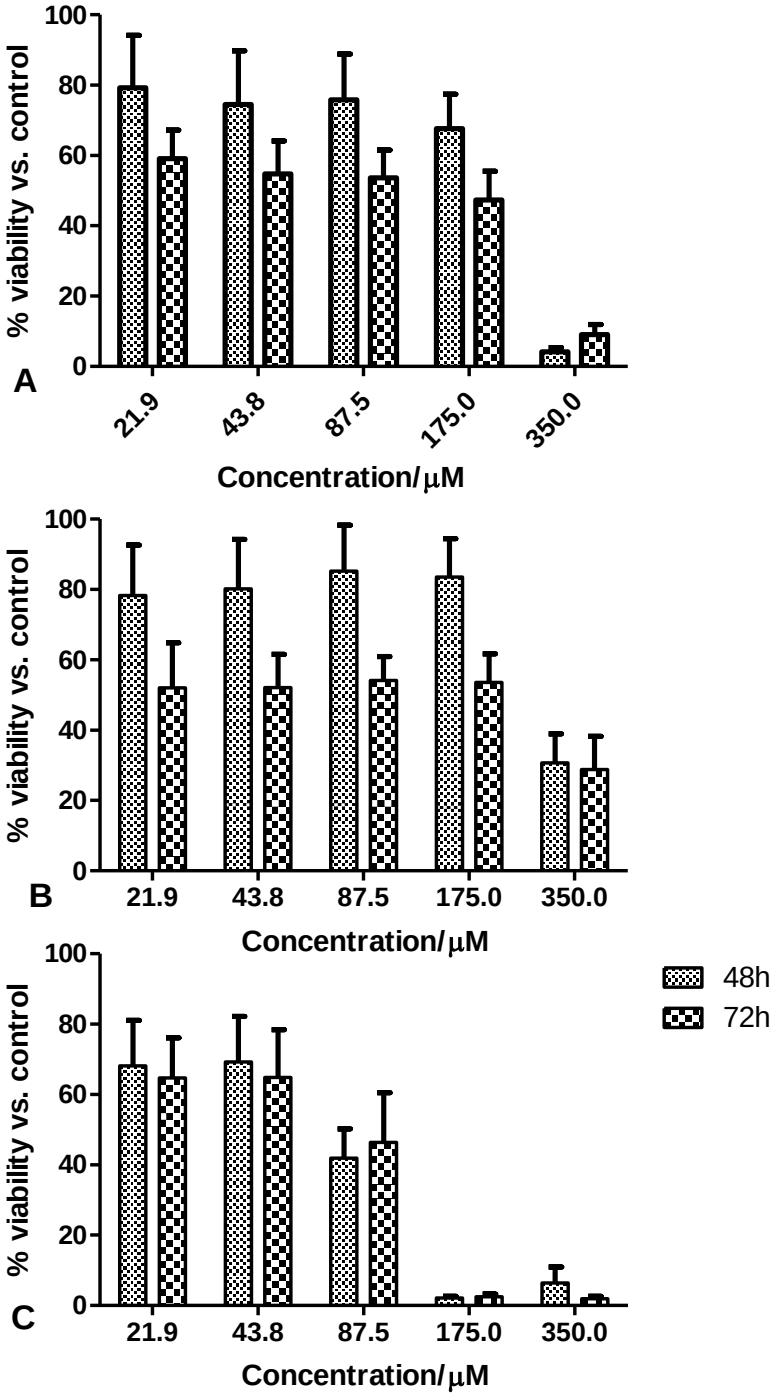

*Figure 4.10: Comparison of the dose-response of compounds **1b, 4a,** and **4b** (**A**, **B** and **C** respectively) assessed using AB assay at two timepoints, 48 and 72 hours.*

As can be seen in Figure 4.10, the compounds assessed showed significant cytotoxicity at high concentrations. The compounds were evaluated at 48 and 72 hours. Compound **1b** showed significant activity at 350 μM, however at lower concentrations, lower activity

was observed. However, the activity was still higher than the activity observed when the MTT assay was used. Interestingly, compound **4a,** which contains an acid side group showed a vast improvement in cytotoxicity in the AB assay. **4a** showed moderate activity at lower concentrations and 48 hours exposure time. However, at 350 μM good activity was observed at 48 hours and at 72 hours. Compound **4b** showed the best activity of the compounds evaluated using the AB assay. Compound **4b** exhibited significant cytotoxicity after 24 hours of exposure. The cytotoxicity observed was almost 50% better than that observed in the MTT assay. Table 4.2 shows a comparison of the EC_{50} values from AB and MTT assays for compounds **1b, 4a** and **4b.**

Compound	**EC_{50} μM (+/- s. d.)**			
	AlamarBlue®		**MTT**	
	48 h	**72 h**	**48 h**	**72 h**
1b	160.5 (1.5)	71.4 (1.4)	>350	227.5 (1.2)
4a	309.5 (1.5)	83.2 (1.6)	>350	>350
4b	51.8 (1.3)	49.1 (1.4)	126.2 (1.4)	91.4 (1.3)

Table 4.2: (Alamar Blue Assay) EC_{50} (μM) of compounds against A549 at three time points: 48 and 72 hours post exposure. EC_{50} values are expressed as mean +/- standard error of at least three experiments.

Overall, all three compounds performed better in the AB assay. The compounds containing the methyl ester were still more active than those containing the acid side group. From these results, it can be suggested that the methyl ester is responsible for the activity of these compounds. Increasing the chain length also resulted in increased activity.

This structure activity relationship could be because of the hydrophilic/hydrophobic nature of the compounds. It is well known that in order to be transcellularly absorbed, a drug must possess a degree of lipophilicity. This is a requirement in order for a drug to pass through the lipophilic environment of the cell membrane. There are several examples

where polar, ionisable groups of molecules have been masked with an ester to increase lipophilicity and promote membrane permeability. The more hydrophobic a molecule is, the faster it crosses the cell membrane. The methyl ester containing compounds are hydrophobic and acid containing compounds hydrophilic. An increase in the chain length also adds to the hydrophobicity of the compounds.[15-16]

4.2. ELISA Assay

4.2.1. Gymnastatins and Plk1

Gymnastatin N and a range of analogues were screened against Plk1 by Phoon *et al*. and their IC_{50} values measured. The same compounds were also tested against Cdk 2, another serine/threonine kinase to eliminate common inhibitors. Only the samples which had 5 times more potency against Plk1 *versus* Cdk 2 were selected for further assessment. Table 4.4 shows a selection of the IC_{50} values of the compounds assessed. The assays were performed in well plates using heparin as a sample.[17]

Entry	Structure	Plk1 IC_{50} (μM)
1	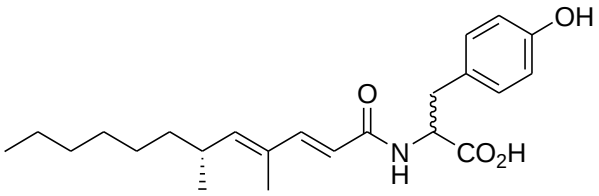	13
2	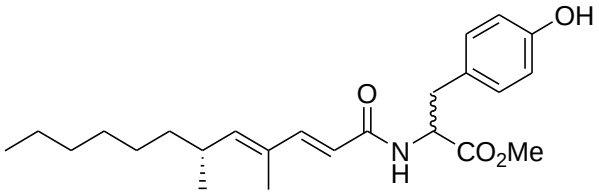	>208
3	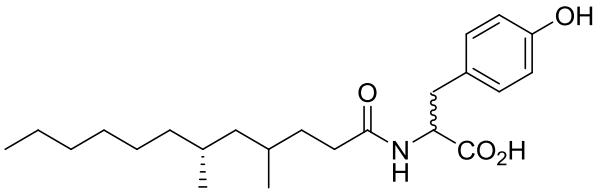	82
4	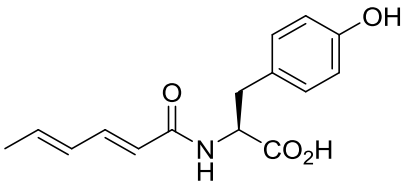	2.2
5	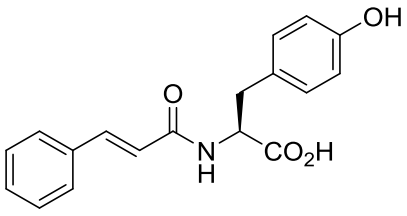	> 268

*Table 4.3: Plk1 study of Gymnastatin N **(24)** and its analogues*

The natural product Gymnastatin N (entry 1) was identified as a Plk1 inhibitor. The methyl ester (entry 2) and fully saturated (entry 3) analogues showed a decrease in the

bioactivity compared to Gymnastatin N (entry 1). This structure activity relationship suggested the importance of the carboxylic acid group and conjugated diene functionalities in the bioactivity against Plk1. A shorter chain length analogue (Entry 4) which contained a tyrosine unit and a conjugated diene exhibited the highest potency. [17]

We set out to determine if the compounds prepared inhibited Plk1. Of particular interest were the compounds containing the acid side group which did not show significant activity in cytotoxicity assays.

4.2.2. Methodology

The details of sample preparation are detailed in Chapter 6. In summary, A549 cells were exposed to drug solutions at EC_{50} values calculated from the MTT assay. The cells were exposed to the drug concentration at 5 time points, 1, 2, 4, 6 and 18 hours, in 6 well plates. A control well was included for each experiment. Following trypsinisation, the cell suspension was centrifuged and the resulting pellet washed with PBS three times. The pellet was lysed using a sonicator and the resulting suspension centrifuged further to pellet any debris. The supernatant was transferred to a micro centrifuge tube and stored at – 80 °C until required for use.

The Plk1 ELISA assay used in this work employs the quantitative sandwich enzyme immunoassay technique. The plates were pre-coated with an antibody specific for Plk1. Samples, controls and blanks were introduced into respective wells. The plate was incubated at 37 °C for 90 minutes. The samples were discarded and biotin-detection antibody was added followed by further incubation for 1 hour. A biotinylated detection antibody specific for Plk1 and Streptavidin horseradish peroxide (SABC) were added successively to each microplate well and incubated. The plate was then washed to remove any non-specific binding that may have occurred. A substrate solution was then added. Only wells containing Plk1 exhibit a colour change. The assay was terminated by adding

a sulfuric acid solution and the change in optical density measured in a plate reader at a wavelength of 450 nm. The optical density value is proportional to the concentration of Plk1 in the sample. The percentage Plk1 inhibition of cells exposed to the drugs was calculated using the following equation:

$$\%\ Plk1\ inhibition = \frac{optical\ density\ of\ treated\ cells}{optical\ density\ of\ untreated\ cells\ (control)} \times 100$$

4.2.3. Results

To assess the activity of compounds prepared against Plk1, the compounds outlined in Table 4.4 were used. A549 cells were treated with drug concentrations equal to the calculated EC_{50} from Section 4.16 and assessed at different time points.

Compound	EC_{50} calculated from MTT/μM
1a	350
1b	227.5
2a	350
2b	216.7
4a	350
4b	91.4

Table 4.4: Compounds and their EC_{50} values for Plk1 inhibition study.

The experiments were done at time points shown in Table 4.5 to give an indication as to how long it took for the inhibition to occur. The different time points used could also be used to estimate the stages of the cell cycle where Plk1 inhibition is prominent.

Time/hours	Stage of the cell cycle
1	M Phase
2	G_2 – M phase
4	G_2
6	S phase
16	G_1

Table 4.5: Time spent in each phase of a 24 hour cell cycle.[28]

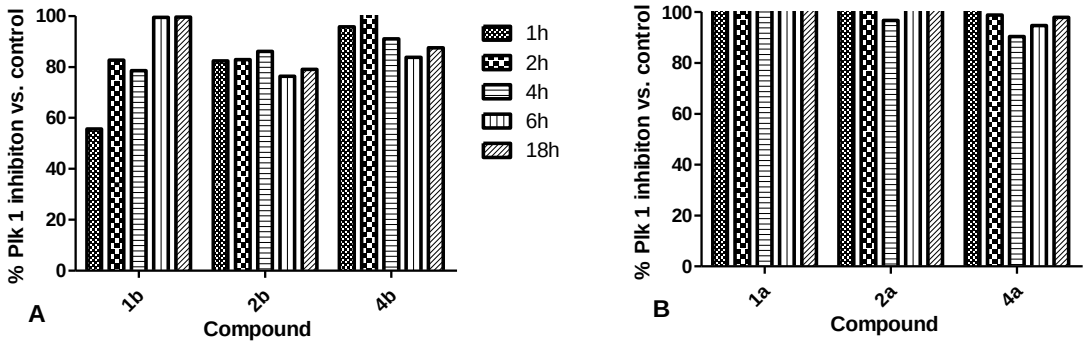

Figure 4.11: % Plk11 inhibition of A549 cell exposed to compounds (A): containing methyl ester side group (B): containing acid side group.

As can be seen in Figure 4.14 (A), compounds containing the methyl ester inhibited Plk1 at concentrations tested, with two exceptions (**4b** at 2 hours, **1b** at 6 and 18 hours). Care should be taken when comparing the inhibition between samples as they were tested at different concentrations. It is interesting to note that compound **4b** did not perform as well as it did in the MTT and AB assays.

It was disappointing to note that the compounds containing the acid side group did not perform as expected. According to a study by Phoon *et al.,* discussed in Section 4.2.4, the conjugated diene and the free acid were responsible for the activity against Plk1. However in our study, compounds containing the free acid did not show significant inhibition against Plk1. Also, there was no significant difference in inhibition between compounds with a single alkene (**1a** and **2a)** and compounds with a conjugated diene **(4a**, **4b).**

In this assay, the drugs permeating the cell membrane should not have been an issue as the cells have been lysed and therefore the cell membrane removed.

In summary, the results on the Plk1 inhibition were not illuminating. They did not show a clear pattern of inhibition at different time points. The results do however show that the compounds containing the acid side group do not inhibit Plk1, and compounds with the methyl ester side group inhibit Plk1.

4.3. Conclusion

A library of compounds was assessed for toxicity against the A549 lung cancer cell line. All compounds were assessed using the MTT assay. Compounds containing the methyl ester side group showed the best activity, while compounds containing the acid side group did not show any activity at concentrations and time points tested. Compounds **1b, 4a** and **4b** were further evaluated using the AB assay. There was an improvement in cytotoxicity observed in all the three compounds. Of all compounds assessed, **4b** showed the best activity. It was observed that compounds containing a methyl ester on the tyrosine side unit and longer chain compounds performed the best.

Several compounds were screened against Plk1 at concentrations equal to their respective EC_{50} values calculated from the MTT assay (Section 4.1.6). The best activity was observed in compounds containing the methyl ester side group. Future work should

involve cell imaging using organelle specific dyes to identify the subcellular localisation of the compounds prepared. This, as well as flow cytometry will be carried out within the group as future work.

The level of activity observed would suggest that the compounds and their analogues are worthy of further investigation. It is well known that cellular response may vary between cell lines. It would be interesting to evaluate these compounds against various cell lines e.g. Caco-2, HeLa and BEAS-2B. The different responses between different cell lines and different assays would increase the understanding of the mechanism of action of these compounds.

4.4. References

1. Cooper, J. R.; Abdullatif, M. B.; Burnett, E. C.; Kempsell, K. E.; Conforti, F.; Tolley, H.; Collins, J. E.; Davies, D. E. *PLoS One.* **2016**, *11*.
2. Nardone, L. L.; Andrews, S. B. *Biochim. Biophys. Acta - Lipids Lipid Metab.* **1979**, *573* (2), 276–295.
3. https://www.pheculturecollections.org.uk/products/celllines/generalcell/detail.jsp?refId=95102433&collection=ecacc_gc (accessed 16/05/2017)
4. Fadeel, B.; Pietroiusti, A.; Shvedova, A. *Adverse Effects of Engineered* Nanomaterials*Exposure, Toxicology, and Impact on Human Health,* Academic Press, *1st Edition,* **2012.**
5. Celic J, E.; Carter, N. *Cell Biology - A laboratory handbook,* Academic Press, *3rd Edition,* **2005**.
6. Barile, F. A. *Introduction to in-vitro cytotoxicity, mechanisms and methods*. CRC Press, **1994**.
7. Hughes, D.; Mehmet, H. *Cell proliferation and apoptosis,* Garland Science, **2003**.
8. Supino, R. *Methods in Molecular Biology.* Humana Press, **1995.**

9. Rampersad, S. N. *Sensors* **2012**, *12*, 12347–12360.
10. White, M. J.; Dicaprio, M. J.; Greenberg, D. A. *J. Neurosci. Methods* **1996**, *70* (2), 195–200.
11. Bonnier, F.; Keating, M. E.; Wróbel, T. P.; Majzner, K.; Baranska, M.; Garcia-Munoz, A.; Blanco, A.; Byrne, H. J. *Toxicol. Vitr.* **2015**, *29* (1), 124–131.
12. Souto, G. D.; Farhane, Z.; Casey, A.; Efeoglu, E.; McIntyre, J.; Byrne, H. J. *Anal. Bioanal. Chem.* **2016**, *408* (20), 5443–5455.
13. Fujimoto, S.; *Jpn. J. Cancer. Chemother.* **1994**, *21*, 671-677.
14. Hamid, R.; Rotshteyn, Y.; Rabadi, L.; Parikh, R.; Bullock, P. *Toxicol. Vitr.* **2004**, *18*, 703–710.
15. Weaver, F. R. *Molecular Biology.* McGraw-Hill Education*; 5th Edition,* **2011**.
16. Beaumont, K.; Webster, R.; Gardner, I.; Dack, K. *Curr. Drug Metab.* **2003**, *4* (6), 461–485.

5. Conclusion and Future Work

This chapter summarises the outcomes of this research and details suggestions for future work.

The aim of this work was to prepare analogues of gymnastatin N and assess them for biological activity. Eight analogues of gymnastatin N were successfully prepared starting with commercially available aldehydes. The aldehyde used in the first step defined the chain length of the final product. To begin with, a side chain was prepared using a series of HWE, reduction, oxidation, Wittig and hydrolysis reactions. For the short chain analogues, the side chain was prepared by a Wittig followed by a hydrolysis reaction. The resulting acid was coupled with a commercially available benzyl protected tyrosine. Several difficulties were encountered during the amide coupling, however, successful coupling was achieved using HATU and DIEA.

The selective removal of the benzyl protecting group presented difficulties, however, boron trichloride methyl sulfide complex successfully removed the benzyl protecting group while leaving the alkenes intact. Also, quenching the reaction with methanol resulted in methylation of the acid side group. This meant that the methylation step could be eliminated.

Several difficulties were encountered in the purification of target compounds containing the acid side group. However, the compounds had 95% purity which was deemed sufficient for biological evaluation. Future work should be aimed at purification of the acid side group using preparative HPLC.

The prepared gymnastatin analogues were evaluated for anti-cancer activity using MTT assay. A selection of the prepared compounds were further assessed using the AB assay. The compounds containing a methyl ester side group showed more activity than

compounds containing the acid side group. It was also observed that increasing the chain length also resulted in increased activity against the cancer cells. The presence of an additional alkene did not result in significant improvement of activity. Furthermore, preliminary results of the activity of compounds using an ELISA assay showed that the compounds containing the methyl ester side group inhibited Plk1, where the compounds with the acid side group showed no inhibition. A more thorough biological evaluation of these compounds is required in order to evaluate their activity against other cell lines e.g. Caco-2 and HeLa cells which can be readily obtained in our laboratory.

An investigation to assess the selectivity of these compounds should also be carried out. For example, evaluation against BEAS-2B, a healthy cell line isolated from normal human bronchial epithelium obtained from autopsy of non-cancerous individuals.

To understand the subcellular localisation and drug distribution of these compounds, cell imaging experiments should be done. These should be done at times and concentrations when the drugs are known to display cytotoxicity. The mechanism of cell death induced by the prepared analogues can also be determined by flow cytometry.

In this thesis, iron oxide nanoparticles and their use in targeted drug delivery for cancer treatment have been reviewed. Future work will include conjugation of the synthesised gymnastatin analogues to iron oxide nanoparticles at the phenol functionality. Work on conjugating iron oxide nanoparticles to organic compounds is already ongoing within the group.

6 Experimental Procedures

6.1 Part A: Synthetic Procedures

6.1.1 General Experimental

All reagents and dry solvents were purchased from Sigma-Aldrich and Apollo Scientific and were used without further purification. Argon and hydrogen were obtained from BOC gases and were used without further purification.

^{1}H NMR and ^{13}C NMR spectra were recorded on a Bruker Avance 400 MHz spectrometer at room temperature in deuterated solvents. Chemical shifts (σ) are given in parts per million (ppm) and coupling constants (*J)* are expressed in Hertz (Hz). An arbitrary numbering system is employed to aid assignment of NMR signals. High resolution mass spectrometry was carried out in University College Dublin by Dr Jimmy Muldoon on a Waters/Micromass LCT Mass Spectrometer with 40 % water (with ~1 % formic acid) and 60 % methanol. All samples were prepared in MeOH. Infrared (IR) spectra were recorded on a Perkin Elmer Spotlight 400N FT-IR spectrometer with UATR accessory.

Thin layer chromatography (TLC) was carried out on aluminium sheets pre-coated with silica gel 60 and visualised under a 254 nm UV lamp and stained with anisaldehyde solution (1.7 mL anisaldehyde, 0.7 mL glacial acetic acid, 2.3 mL concentrated sulfuric acid in 62.5 mL ethanol). Column chromatography separations were performed using Davisil silica gel LC60A (35-70 μm).

6.1.2 Synthesis of short chain gymnastatin analogues

6.1.2.1 Wittig reaction

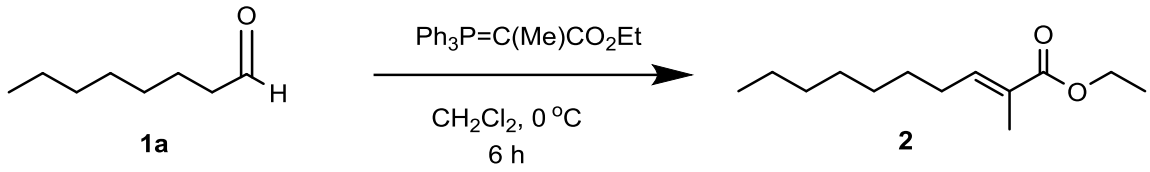

(Ethyl- (*E*)-2-methyldec-2-enoate (2) To a solution of octanal **1a** (7.8mmol, 1 g, 1 eq.) in CH_2Cl_2 (30 mL) at 0 °C was added a solution of (carbethoxyethylidene)triphenylphosphorane (8.6 mmol, 3.1 g, 1.1 eq.) in CH_2Cl_2 (20 mL), also at 0 °C. The reaction mixture was left stirring at room temperature under argon for 6 hours before being quenched with ammonium chloride. The reaction mixture was transferred to a separating funnel and diluted with diethyl ether (40 mL). The organic layer was collected and the aqueous layer was extracted two more times with ether. The organic layers were combined and dried over anhydrous magnesium sulfate. The volatiles were evaporated under vacuum using a rotary evaporator. The crude mixture was purified by flash chromatography using as the eluent, petroleum ether 9:1 ethyl acetate and the target compound **2** was isolated as a yellow oil.

Ethyl *(E)* 2-methyldec-2-enoate (2)

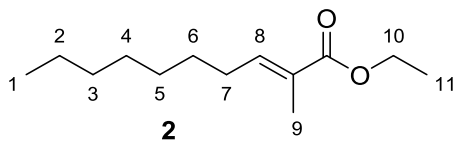

Yield = 79.8%, $\mathbf{R_f}$ = 0.5 (petroleum ether 9:1 ethyl acetate)

δ_H /ppm (400 MHz; $CDCl_3$) 6.764 (1H, m, H_8), 4.19 (2H, q, *J = 7.2 Hz*, H_{10}), 2.15 (2H, q, *J = 7.2 Hz*, H_7) , 1.75(3H, s, H_9), 1.35 (13H, m, $H_{2,3,4,5,6,11}$), 0.88 (3H, t, *J = 7.2 Hz*, H_1).

δ_C /ppm (100 MHz; $CDCl_3$) 168.3 (*C*=O), 143.1 (*C*=C), 127.6 (*C*=CO), 60.3 (*C*-O), 31.8 (CH_2), 29.5(CH_2), 29.3 (CH_2), 29.1 (CH_2), 28.7 (CH_2), 28.6 (CH_2), 22.6 (CH_2), 14.3 (CH_2), 14.1 (CH), 12.3 (CH_3).

υ_{max}/ cm^{-1} (neat) 2956, 2925, 2856, 1710, 1650, 1464, 1367, 1266, 1140, 1098

6.1.2.2 Hydrolysis

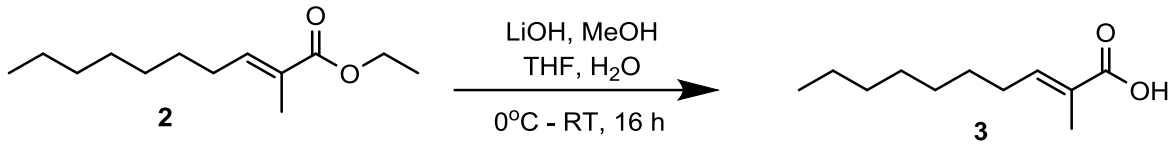

2-Methyl-(*E*)-dec-2-enoic acid (3) To a stirring solution of LiOH (24.5 mmol, 587 mg, 15 eq.) in ice-cold water (8 mL) was added a solution of **2** (1.63 mmol, 301 mg, 1 eq) in MeOH (4 mL) and THF (4 mL), also at 0 °C. The reaction mixture was warmed to RT and stirred for 16 hours. The reaction was then cooled to 0 °C and ice cold HCl (1M) added slowly to the rapidly stirring solution until pH 1. The reaction mixture was transferred to a separating funnel and diluted with diethyl ether (20 mL). The organic layer was collected and the aqueous layer extracted two more times with ether. The organic layers were combined and dried over anhydrous magnesium sulfate. The volatiles were evaporated under vacuum using a rotary evaporator. The target compound **3** was isolated as yellow solid and used without further purification.

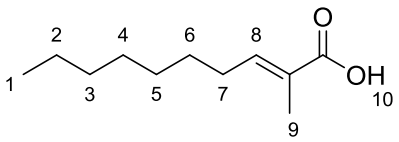

3

Yield 94% yield.

δ_H /ppm (400 MHz; $CDCl_3$) 11.92 (1H, s, H_{10}), 6.92 (1H, m, , H_8), 2.19 (2H, q, *J = 7.2 Hz*, H_7), 1.83 (3H, s, H_9), 1.37 (10H, m, $H_{2\text{-}6}$), 0.89 (3H, t, *J = 7.2 Hz,* H_1).

δ_C /ppm (100 MHz; $CDCl_3$) 169.2 (*C*=O), 142.7 (*C*=C), 126.0 (*C*-CO), 32.6 (CH_2), 31.2 (CH_2), 28.6 (CH_2), 28.4 (CH_2), 22.1 (CH_2), 17.6 (CH_3), 12.4 (CH_3).

6.1.2.3 Amide Coupling

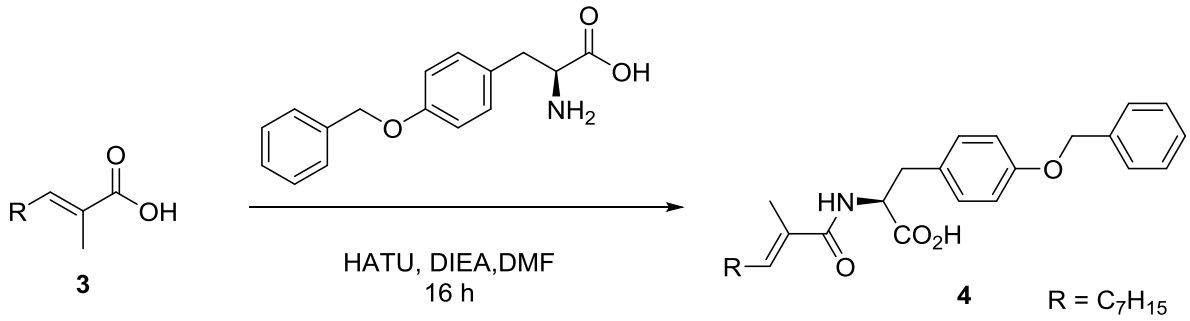

[2-Methyl-(*E*)-dec-2-enamido]-3-[4-(benzyloxy) phenyl] propanoic acid (4) To a solution of acid **3** (2.35 mmol, 432 mg, 1 eq.) in dry DMF (10 mL) was added HATU (2.35 mmol, 823 mg, 1 eq.) and the resulting solution was stirred for 10 minutes at room temperature under argon. DIEA (7.10 mmol, 1.7 mL, 3 eq.) was added and the resulting solution was stirred for 20 minutes before *O*-benzyl-L-tyrosine (2.82 mmol, 874 g, 1.2 eq.) was added. The reaction mixture was stirred at room temperature for 16 hours. The solvent was removed *in vacuo* and the crude mixture was purified by flash column chromatography using as the eluent petroleum ether 8.5:1.5 ethyl acetate. The product was isolated as a sticky, yellow oil in 86% yield.

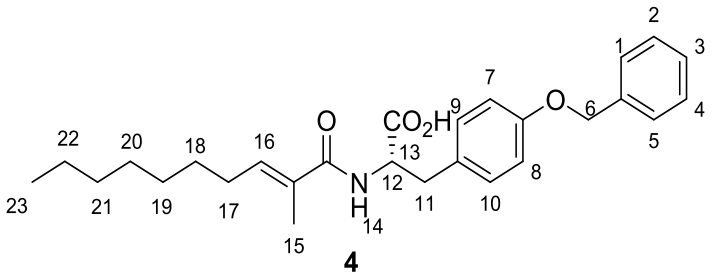

δ_H /ppm (400 MHz; MeOD) 7.68 (5H, m, H_{1-5}), 7.08 (2H, d, *J = 8.4 Hz*, H_{7-8}) , 6.90 (2H, d, *J = 8.4 Hz*, H_{9-10}), 6.33(1H, m, H_{16}), 6.19 (1H,d , *J = 7.2 Hz*, H_{14}) , 5.02 (2H, s, H_6), 4.84 (1H, m, H_{12}), 3.19 (2H, m, H_{11}), 2.10 (2H, q, *J = 7.2 Hz*, H_{17}), 1.77 (3H, s, H_{15}), 1.34 (10H, m, H_{18-22}), 0.88 (3H, t, *J = 6.8 Hz*, H_{23}).

δ_C /ppm (100 MHz; MeOD) 174.0 (*C*=OOH), 171.4 (*C*=O), 158.0 (*C*-Ar), 138.4 (*C*=C), 136.9 (*C*-Ar), 130.5 (*C*-Ar), 129.6 (*C*-Ar), 128.6(*C*-Ar), 128.1(*C*-Ar), 127.9 (*C*-Ar), 127.4 (*C*-Ar), 115.0 (*C*=C), 70.1 (CH_2), 53.5(*C*H), 36.3 (CH_2), 32.5 (CH_2), 31.8 (CH_2), 29.3 (CH_2), 28.4 (CH_2), 14.1 (CH_3), 12.4 (CH_3).

υ_{max}/cm^{-1} ($CHCl_3$ film) 3427, 2926, 2856, 1884, 1723, 1660, 1612, 1511, 1455, 1384, 1240, 1218, 1177, 1025.

LRMS (ES$^+$) calculated for $C_{27}H_{35}NO_4$ $[M+H]^+$: 438.3, found: 438.2.

6.1.2.4 Methylation of acid side group

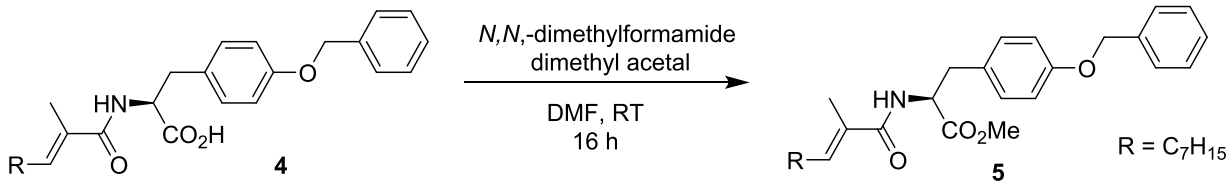

To a stirring solution of **4** (0.27 mmol, 119 mg, 1 eq.) in dry DMF (5 mL) was added *N,N,*-dimethylformamide dimethyl acetal (1.36 mmol, 0.2 mL, 5 eq.) under argon. The reaction mixture was stirred at room temperature for 16 h. The solvent was removed *in*

vacuo and the crude mixture purified by flash chromatography using as the eluent petroleum ether 6: 4 ethyl acetate. The product was isolated as a yellow oil in 72% yield.

[2-methyl-(*E*)-dec-2-enamido]-3-[4-(benzyloxy)phenyl]propanoate (5)

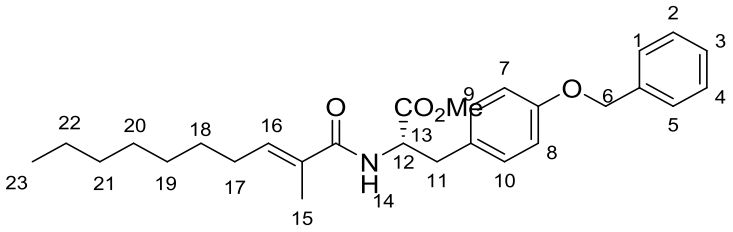

5

δH /ppm (400 MHz; $CDCl_3$) 7.33 (5H, m, H_{1-5}), 6.94 (2H, d, *J=8.8 Hz*, H_{7-8}), 6.82 (2H, d, *J=8.8 Hz*, H_{9-10}), 6.26 (1H, td, *J = 13.6, 6, 1.6 Hz*, H_{16}), 6.06 (1H, d, *J=7.6 Hz* , H_{14}), 4.96 (2H, s, H_6), 4.82 (1H, m, H_{12}), 3.66 (3H, s, H_{13}), 3.03 (2H, m, H_{11}), 2.06 (2H, q, *J = 6.8 Hz*, H_{17}), 1.73 (3H, s, H_{15}), 1.24 (10H, m, H_{18-22}), 0.81 (3H, t, *J=7.2 Hz*, H_{23}).

δC /ppm (400 MHz; $CDCl_3$) 172.4 (*C*=OCH_3), 168.7 (*C*=O), 158.0 (*C*-Ar), 137.4 (*C*=C), 136.9 (*C*=Ar), 130.3 (*C*=Ar), 130.3 (*C*=Ar), 130.1 (*C*=Ar), 128.6 (*C*=Ar), 128.2 (*C*-CO), 128.0 (*C*=Ar), 127.9 (*C*=Ar), 127.5 (*C*=Ar), 114.9 (*C*=Ar), 70.0 (*C*H_2-O), 53.4 (*C*H-NH), 52.3 (O-*C*H_3), 37.0 (*C*H_2), 31.8(*C*H_2), 29.3(*C*H_2), 29.1(*C*H_2), 28.7(*C*H_2), 28.4(*C*H_2), 22.7(*C*H_2), 14.1(*C*H_3), 12.5(*C*H_3).

LRMS (ES$^+$) calculated for $C_{28}H_{37}NO_4$ $[M+H]^+$: 452.3, found: 452.2.

6.1.2.5 Debenzylation General procedure 1

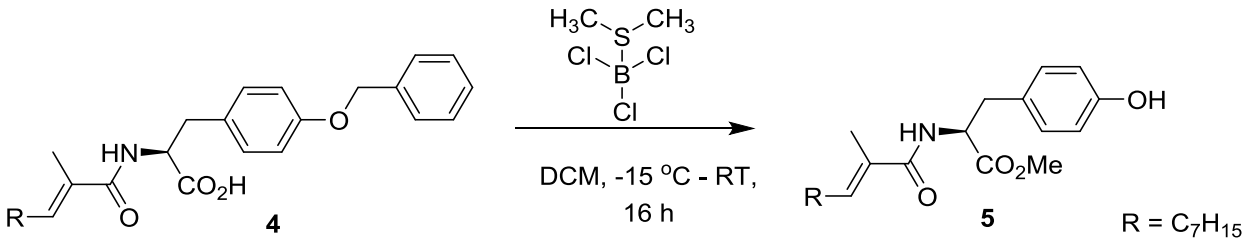

To a solution of **4** (1 eq.) in dry CH_2Cl_2 at -15 °C, under argon, was added boron trichloride methyl sulfide complex (2 M in CH_2Cl_2, 8 eq.), dropwise. The reaction was warmed to room temperature and left stirring overnight. The reaction mixture was quenched with the appropriate solvent and the solvent evaporated *in vacuo*. The product was purified by flash chromatography.

6.1.2.5.1 Methanol Quench

Methyl-(*N*-methyl *(E)*-dec-2-enoyl)tyrosinate (6)

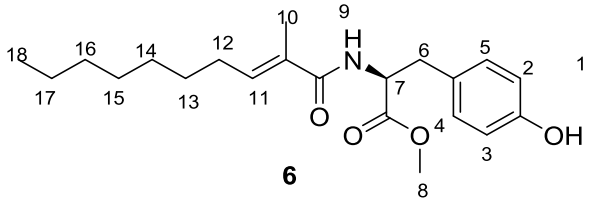

6

Methyl (*N*-methyl-*(E)*-dec-2-enoyl)tyrosinate (6) was prepared using general procedure 1 using **4** (0.09 mmol, 40 mg, 1 eq.) in dry CH_2Cl_2(5 mL), boron trichloride methyl sulfide complex (2 M in CH_2Cl_2, 0.73 mmol, 0.37 mL, 8 eq.) under argon. The crude mixture was quenched using methanol (10 mL) and the volatiles removed *in vacuo.* The product was purified using petroleum ether 3: 7 ethyl acetate and the target compound **6** was isolated as a yellow oil in 80% yield. R_f = 0.39 (petroleum ether 6: 4 ethyl acetate).

δ_H /ppm (400 MHz; $(CD_3)_2CO$) 8.234 (1H, s, H_1), 7.07 (3H, m, $H_{4,5,9}$), 6.76 (2H, d, H_{2-3}), 6.31 (1H, m, , H_{11}), 4.65 (1H, m, H_7), 3.66 (3H, s, H_8), 3.10 (2H, m, H_6), 2.14 (2H, q, H_{12}), 1.77 (3H, s, H_{10}), 1.34 (10H, m, H_{13-17}), 0.88 (3H, t, H_{18}).

δ_C /ppm (100 MHz; $(CD_3)_2CO$)) 173.2 (*C*-OOMe), 169.3 (*C*=O), 157.2 (*C*-Ar), 136.5 (*C*=C), 131.7 (*C*-Ar), 131.1(*C*-Ar), 128.8 (*C*-CO), 116.0 (*C*-Ar), 55.0(*C*-NH), 52.2 (O-

*C*H$_3$), 37.3 (*C*H$_2$-Ar), 32.6 (*C*H$_2$), 30.4 (*C*H$_2$), 30.3 (*C*H$_2$), 29.5 (*C*H$_2$), 29.3 (*C*H$_2$), 28.8 (*C*H$_2$), 23.3 (*C*H$_2$), 14.4 (*C*H$_3$), 12.7 (*C*H$_3$).

$\upsilon_{max/}$ cm^{-1} (CHCl$_3$ film) 3313, 3020, 2953, 2925, 2855, 1736, 1659, 1614, 1595, 1500, 1438, 1363, 1267, 1216, 1173, 1124, 1105.

HRMS (ES$^+$) calculated for $C_{21}H_{31}NO_4$ $[M+H]^+$: 362.2331, found: 362.2345.

6.1.2.5.2 BCl$_3$ reaction quenched with Ethanol

Ethyl--(*N*-methyl-*(E)*-dec-2-enoyl)tyrosinate (6b)

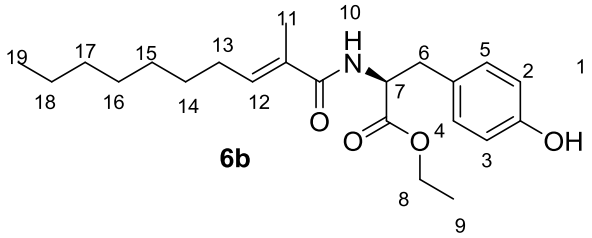

6b

Ethyl-(*N*-methyl-*(E)*-dec-2-enoyl)tyrosinate (6b) was prepared using general procedure 1 using **4** (0.10 mmol, 45 mg, 1eq.) and boron trichloride methyl sulfide complex (2 M in CH_2Cl_2, 0.82 mmol, 0.41 mL, 8 eq.) under argon. The reaction mixture was quenched using ethanol (10 mL) and the solvent removed *in vacuo*. The product was purified using petroleum ether 6: 4 ethyl acetate and the target compound **8a** was isolated as a yellow oil in 75% yield. R_f = 0.44 (petroleum ether 6: 4 ethyl acetate).

δ_H /ppm (400 MHz; CD_3CN) 6.95 (2H, d, *J = 8.8 Hz*, $H_{4,5,}$), 6.64 (2H, d, *J = 8.8 Hz*, H_{2-3}), *(*6.47 (2H, d, *J = 7.6 Hz*, H_{10}), 6.12-6.16 (1H, m, H_{12}), 4.45-4.50 (1H, m, H_7), 4.03 (2H, q, *J = 7.2 Hz*, H_8), 2.94 (2H, m, H_6), 2.04 (2H, m, *J = 7.2 Hz*, H_{13}), 1.65 (3H, s, H_{11}), 1.20 (10H, m, H_{14-18}), 1.11 (3H, t, *J = 7.2 Hz*, H_9), 0.89 (3H, t, *J = 6.8 Hz*, H_{19}).

δ_C /ppm (100 MHz; CD_3CN) 171.7 (*C*-OOEt), 168.7 (*C*=O), 155.6 (*C*-Ar), 136.3 (*C*=C), 130.4 (*C*-Ar), 130.2 (*C*-Ar), 128.0 (*C*-CO), 114.9(*C*-Ar), 60.8 (CH_2O-*C*H_3), 54.0 (O-

*C*H$_3$), 36.0(*C*H$_2$-Ar), 31.4 (*C*H$_2$), 28.8 (*C*H$_2$), 28.7 (*C*H$_2$), 28.3 (*C*H$_2$), 27.7 (*C*H$_2$), 22.3 (*C*H$_2$), 13.3 (*C*H$_2$), 13.2 (*C*H$_3$), 11.7 (*C*H$_3$).

υ_{max}/cm^{-1} ($CHCl_3$ film) 3323, 2926, 2856, 1734, 1660, 1615, 1595, 1509, 1447, 1376, 1349, 1269, 1215, 1126, 1028, 827, 756.

HRMS (ES$^+$) calculated for $C_{22}H_{33}NO_4$ [M+H]$^{+:}$ 376.2488, found: 376.2475

6.1.2.5.1 BCl_3 reaction quenched with water

***N*-methyl-(*E*)-dec-2-enoyl tyrosine (6a)**

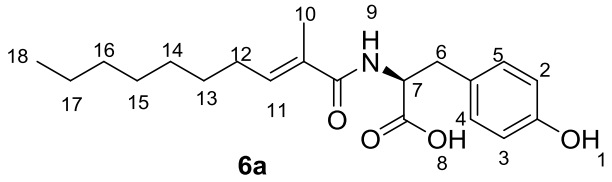

6a

***N*-methyl-(*E*)-dec-2-enoyl tyrosine (6a)** was prepared using general procedure 1 using **4** (0.14 mmol, 62 mg, 1 eq.) and boron trichloride methyl sulfide complex (2 M in CH_2Cl_2, 1.13 mmol, 0.57 mL, 8 eq.), dropwise, under argon. The reaction was quenched using water (10 mL) and the resulting mixture transferred to a separating funnel and diluted with dichloromethane (15 mL). The organic layer was collected and the aqueous layer extracted two more times with ether. The organic layers were combined and dried over anhydrous magnesium sulfate. The volatiles were evaporated under vacuum using a rotary evaporator. The crude mixture was purified by flash chromatography using 10% methanol in CH_2Cl_2. The product **11b** was isolated as a yellow oil in 65% yield.

δ_H /ppm (400 MHz; MeOD) 6.90 (2H, d, *J = 8.4 Hz*, $H_{4\text{-}5}$), 6.55 (2H, d, *J = 8.8 Hz*, $H_{2\text{-}3}$), 6.13 (1H, t, *J = 7 Hz*, H_{11}), 4.38 (1H, m, H_7), 2.96 (2H, m, H_6), 2.02 (2H, q, *J = 7.2 Hz*, H_{12}), 1.66 (3H, s, H_{10}), 1.24 (10H, m, $H_{13\text{-}17}$), 0.81 (3H, t, *J = 6.8 Hz*, H_{18}).

δ_C /ppm (100 MHz; MeOD) 175.3 (*C*-OOH), 172.2 (*C*=O), 157.3 (*C*=O), 138.2 (*C*-CO), 131.3 (*C*-Ar), 129.9 (*C*-Ar), 129.2 (*C*-Ar), 124.8 (*C*-Ar), 116.2 (*C*-Ar), 57.9 (*C*H-NH), 37.3 (CH_2-NH), 33.0 (CH_2), 29.6 (CH_2), 30.7 (CH_2), 31.8 (CH_2), 23.8 (CH_2), 14.5 (CH_3), 12.5 (CH_3).

υ_{max}/cm^{-1} ($CHCl_3$ film) 3373, 2926, 2856, 1590, 1509, 1412, 1245.

HRMS (ES$^+$) calculated for $C_{20}H_{29}NO_4$ $[M+Na]^+$: 370.1994, found: 370.2001.

6.1.3 Synthetic Strategy 2

6.1.3.1 General procedure 2: HWE

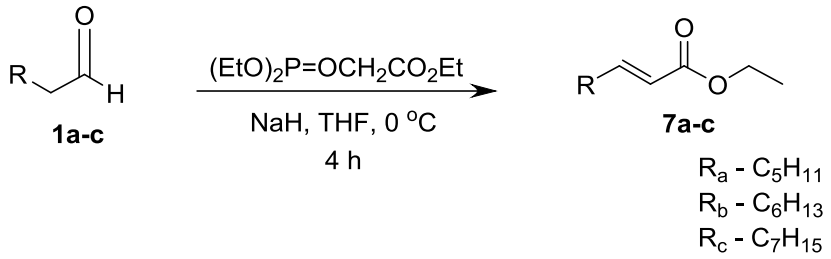

To a suspension of NaH (60% in mineral oil) (1.2 eq.) in dry THF at 0 °C was added triethyl phosphonoacetate (1.2 eq.) dropwise under argon and the mixture left stirring for 0.5 hours. The reaction temperature was brought to room temperature. The appropriate aldehyde **1a-c** (1 eq.) was added slowly and the reaction mixture was left stirring for 4 hours. The reaction mixture was quenched using ammonium chloride (30 mL), transferred to a separating funnel and diluted with diethyl ether (30 mL). The organic layer was collected and the aqueous layer extracted two more times with ether. The organic layers were combined and dried over anhydrous magnesium sulfate. The volatiles were evaporated under vacuum using a rotary evaporator. The crude mixture was purified by flash column chromatography using as the eluent, petroleum ether 9.5:0.5 ethyl acetate.

Ethyl (*E*)-non-2-enoate (7a)

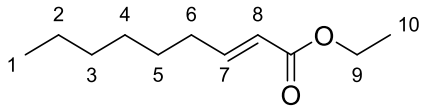

7a

Ethyl (*E*)-non-2-enoate (7a) was prepared using general procedure 2 using NaH (60% in mineral oil) (21 mmol, 0.84 g, 1.2 eq.) in dry THF (60 mL), triethyl phosphonoacetate (26.3 mmol, 5.6 mL, 1.5 eq.) and heptanal **1a** (17.5 mmol, 2.5 mL, 1 eq.). The target

compound **7a** was isolated as yellow oil (1.46 g) in 88% yield. R_f = 0.48 (petroleum ether 9:1 ethyl acetate).

δ_H /ppm (400 MHz; $CDCl_3$) 6.96 (1H, dt, *J = 15.0, 6.8 Hz.* H_7), 5.81 (1H, dt, *J = 15.6, 1.6 Hz,* H_8), 4.18 (2H, q, *J = 6.8 Hz*, H_9), 2.16-2.22 (2H, m, H_6), 1.37 (11H, m, $H_{2\text{-}5}$, H_{10}) 0.88 (3H, t, *J = 6.8 Hz,* H_1).

δ_C /ppm (100 MHz; $CDCl_3$) 166.8 (*C*=O), 149.5 (*C*=C), 121.2 (*C*=C), 60.1 (*C*H_2-O), 32.2 (*C*H_2), 31.6 (*C*H_2), 29.7 (*C*H_2), 29.0 (*C*H_2), 28.0 (*C*H_2), 22.5 (*C*H_2), 14.2 (*C*H_3), 14.0 (*C*H_3).

$\upsilon_{max/}$ cm^{-1} (neat) 2957, 1720, 1654, 1465, 1367, 1263, 1123, 1096, 1028, 973, 845, 724.

Ethyl *(E)* dec-2-enoate (7b)

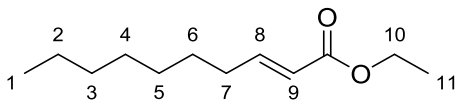

7b

Ethyl *(E)* dec-2-enoate (7b) was prepared using general procedure 2 using NaH (60% in mineral oil) (10 mmol, 1 g, 1.2 eq.) in dry THF (40 mL), triethyl phosphonoacetate (10 mmol, 1.95 mL, 1.2 eq.) and octanal **1b** (8.3 mmol, 0.8 mL, 1 eq.). The target compound **7b** was isolated as yellow oil in 92% yield. R_f = 0.5 (petroleum ether 9:1 ethyl acetate).

δ_H /ppm (400 MHz, $CDCl_3$) 6.89 (1H, m, , H_8), 5.74 (1H, m, H_9), 4.11 (2H, m, , H_{10}), 2.12 (2H, q, *J = 6.8, 1.6 Hz*, H_7),1.31 (13H, m, $H_{2\text{-}6}$, H_{11}) 0.81 (3H, t, *J = 7.2 Hz,* H_1).

δ_C /ppm (100 MHz, $CDCl_3$) 165.8 (*C*=O), 148.5 (*C*=C), 120.16 (*C*=C), 59.1 (*C*H_2-O), 31.2 (*C*H_2), 30.7 (*C*H_2), 28.1 (*C*H_2), 28.1 (*C*H_2), 27.0 (*C*H_2), 21.6 (*C*H_2), 13.2 (*C*H_3),13.3 (*C*H_3).

$\upsilon_{max/}$ cm^{-1} (neat) 1721, 1654, 1463, 1367, 1264, 1166, 1126, 1095, 1042, 979, 855, 723.

ethyl *(E)*-undec-2-enoate (7c)

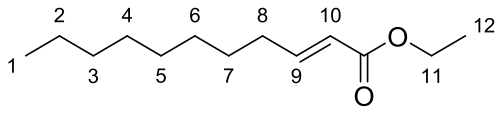

7c

ethyl *(E)*-undec-2-enoate (7c) was prepared using general procedure 2 using NaH (60% in mineral oil) (16.8 mmol, 0.67 g, 1.2 eq.) in dry THF (60 mL), triethyl phosphonoacetate (21 mmol, 4.4 mL, 1.5 eq.) and nonanal **1c** (14 mmol, 2.4 mL, 1 eq.). The target compound **7c** was isolated as a yellow oil in 89% yield. R_f = 0.58 (petroleum ether 9:1 ethyl acetate).

δ_H /ppm (400 MHz; $CDCl_3$) 6.96 (1H, m, H_9), 5.82 (1H, m, H_{10}), 4.19(2H, q, *J = 7.2 Hz*, H_{11}), 2.18 (2H, *m*, , H_8), 1.38 (2H, m, H_7) 1.13 (13H, m, $H_{2\text{-}6}$, H_{12}) 0.88 (3H, t, *J = 7.2 Hz*, H_1).

δ_C /ppm (100 MHz; $CDCl_3$) 166.8 (*C*=O), 149.5 (*C*=C), 121.2 (*C*=C), 60.1 (*C*H_2-O), 32.2 (*C*H_2), 31.8 (*C*H_2), 29.4 (*C*H_2), 29.2 (*C*H_2), 29.2 (*C*H_2), 28.0 (*C*H_2), 22.7 (*C*H_2), 14.3 (*C*H_3), 14.1 (*C*H_3).

υ_{max}/ cm^{-1} (neat) 2925, 2855, 1721, 1655, 1465, 1367, 1264, 1179, 1126, 1042, 979, 722.

6.1.3.2 General procedure 3: Reduction

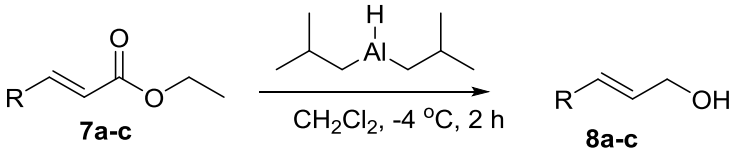

R_a - C_5H_{11}
R_b - C_6H_{13}
R_c - C_7H_{15}

To a solution of the appropriate ester **7a-c** (1 eq.) in dry THF at -4 °C, under argon, was added dropwise DIBAL-H (1M in CH_2Cl_2) (2 eq.). The mixture was maintained at this temperature and left stirring for 2 hours before being quenched by HCl (1M) until pH 1

at 0 °C. The reaction mixture was transferred to a separating funnel and diluted with diethyl ether (30 mL). The organic layer was collected and the aqueous layer extracted two more times with ether. The organic layers were combined and dried over anhydrous magnesium sulfate. The volatiles were evaporated under vacuum using a rotary evaporator. The crude mixture was purified by flash column chromatography using as the eluent petroleum ether 9: 1 ethyl acetate.

(*E*)-Non-2-en-1-ol (8a)

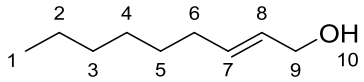

8a

(*E*)-Non-2-en-1-ol (8a) was prepared using general procedure 3 using **7a** (11 mmol, 2 g, 1 eq.) in dry THF (60 mL) and DIBAL-H (1M in CH_2Cl_2) 13.2 mmol, 13.2 mL, 1.2 eq.). The target compound **8a** was isolated as yellow oil in 91% yield. R_f = 0.32 (petroleum ether 9:1 ethyl acetate).

δ_H /ppm (400 MHz; $CDCl_3$) 5.67 (2H, m, $H_{7\text{-}8}$), 4.10 (2H, d, *J = 6 Hz*, H_9), 2.04 (2H, q, *J =6.7 Hz*, H_6), 1.34 (8H, m, $H_{2\text{-}5}$), 0.89 (3H, t, *J = 6.8 Hz*, H_1).

δ_C /ppm (100 MHz; $CDCl_3$) 133.6 (*C*=C), 128.7 (*C*=C), 63.8 (*C*H_2-O), 32.2 (*C*H_2), 30.8 (*C*H_2), 29.1 (*C*H_2), 29.0 (*C*H_2), 22.6 (*C*H_3), 14.2 (*C*H_3).

υ_{max}/cm^{-1} (neat) 3321, 2956, 2924, 2855, 1671, 1458, 1378, 1089, 1003, 723.

(*E*)-Dec-2-en-1-ol (8b)

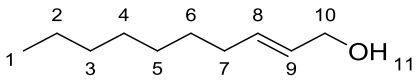

8b

(*E*)-Dec-2-en-1-ol (8b) was prepared using general procedure 3 using **7b** (12.5 mmol, 2.491 g, 1 eq.) in dry THF (60 mL) at -4 °C, under argon and DIBAL-H (15 mmol, 15

mL, 1.2 eq.). The target compound **8b** was isolated as a yellow oil in 84% yield. R_f = 0.3 (petroleum ether 9.5:0.5 ethyl acetate).

δ_H /ppm (400 MHz; $CDCl_3$) 5.66 (2H, m, H_{8-9}), 4.08 (2H, d, *J = 6.8 Hz,* H_{10}), 2.04 (2H, q, *J = 6.8 Hz,* H_7), 1.26 (10H, m, H_{2-6}), 0.88 (3H, t, *J = 6.8 Hz,* H_1).

δ_C /ppm (100 MHz; $CDCl_3$) 133.5 (*C*=C), 128.8 (*C*=C), 63.8 (*C*H_2-O), 32.2 (*C*H_2), 31.8 (*C*H_2), 29.2 (*C*H_2), 29.1 (*C*H_2), 27.4 (*C*H_2), 22.6 (*C*H_3), 14.1 (*C*H_3).

υ_{max}/cm^{-1} (neat) 1738, 1457, 1377, 1217, 1089, 1001, 968, 722.

(*E*)-Undec-2-en-1-ol (8c)

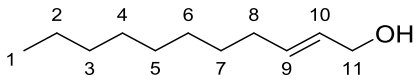

8c

***(E)*-undec-2-en-1-ol (8c)** was prepared using general procedure 3 using **7c** (9.5 mmol, 2 g, 1 eq.) in dry THF (60 mL) and DIBAL-H (11.4 mmol, 11.4 mL, 1.2 eq.) at -4 °C. The target compound **8c** was isolated as a yellow oil in 85% yield. R_f = 0.34 (petroleum ether 9:1 ethyl acetate).

δ_H /ppm (400 MHz; $CDCl_3$) δ ppm: 566 (2H, m, H_{9-10}), 4.12 (2H, d, *J = 6 Hz,* H_{11}), 2.03 (2H, q, *J = 6.4 Hz,* H_8), 1.43 (12H, m, H_{2-7}), 0.88 (3H, t, *J = 6.8 Hz,* H_1).

δ_C /ppm (100 MHz; $CDCl_3$) δ ppm: 133.6 (*C*=C), 128.8 (*C*=C), 63.9 8 (*C*H_2-O), 32.2 (*C*H_2), 31.9 (*C*H_2), 29.5 (*C*H_2), 29.3 (*C*H_2), 29.2 (*C*H_2), 29.1 (*C*H_2), 22.7 (*C*H_3), 14.1 (*C*H_3).

υ_{max}/cm^{-1} (neat) 3500, 2924, 2854, 1654, 1463, 1368, 1266, 969, 722.

6.1.3.3 General procedure 4: Oxidation

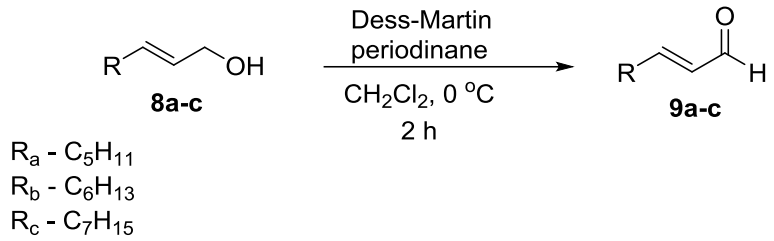

To a solution of appropriate alcohol **8a-c** (1 eq.) in dry CH_2Cl_2 at 0 °C under argon was added a solution of Dess-Martin periodinane (1.1 eq.) in CH_2Cl_2 also at 0 °C. The reaction was warmed to RT and left stirring for 2 hours before being quenched using 1M NaOH solution. The reaction mixture was transferred to a separating funnel and diluted with diethyl ether (30 mL). The organic layer was collected and the aqueous layer extracted two more times. The organic layers were combined and dried over anhydrous magnesium sulfate. The volatiles were evaporated under vacuum using a rotary evaporator. The product was used without further purification.

(E)-Non-2-enal (9a)

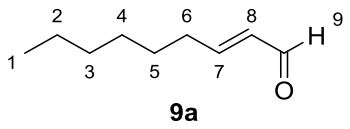

9a

(E)-Non-2-enal (9a) was prepared using general procedure 4 using **8a** (4.93 mmol, 0.7 g, 1 eq.) in dry CH_2Cl_2 (15 mL) and Dess-Martin periodinane (5.92 mmol, 2.5 g, 1.2 eq.) in CH_2Cl_2 (15 mL). The target compound **9a** was isolated as a yellow oil and was used without further purification in 91 % yield R_f = 0.47 (petroleum ether 9.5:0.5 ethyl acetate).

δ_H /ppm ^{1}H NMR (400 MHz; $CDCl_3$) 9.50 (1H, d, *J = 8 Hz,* H_9), 6.86 (1H, dt, *J = 15.6, 6.8 Hz,* H_7), 6.09-6.15 (1H, m, H_8), 2.35 (2H, m, H_6), 1.39 (8H, m, $H_{2\text{-}5}$), 0.89 (3H, t, *J = 6.8 Hz,* H_1).

(*E*)-Dec-2-enal (9b)

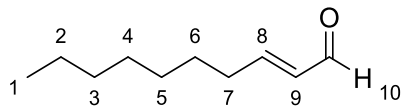

9b

(*E*)-Dec-2-enal (9b) was prepared using general procedure 4 using **8b** (10 mmol, 1.65 g, 1 eq.) in dry CH_2Cl_2 (20 mL) and Dess-Martin periodinane (11.6 mmol, 5 g, 1.1 eq.) in CH_2Cl_2 (20 mL). The target compound **9b** was isolated as a yellow oil and was used without further purification in 94 % yield R_f = 0.5 (petroleum ether 9.5:0.5 ethyl acetate).

δ_H /ppm (400 MHz; $CDCl_3$) 9.4 (1H, d, *J = 8 Hz,* H_{10}), 6.79 (1H, dt, *J = 15.6, 6.8 Hz,* H_8), 6.02-6.08 (1 H, m, H_9), 2.10-2.28 (2H, m, H_7), 1.21 (10H, m, $H_{2\text{-}6}$), 0.81 (3H, t, *J = 7.2 Hz,* H_1).

(*E*)-Undec-2-enal (9c)

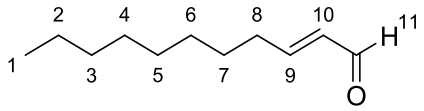

9c

(*E*)-Undec-2-enal (9c) was prepared using general procedure 4 using **8c** (5.9 mmol, 1 g, 1 eq.) in dry CH_2Cl_2 (25 mL) and Dess-Martin periodinane (7.14 mmol, 3.1 g, 1.2 eq.) in CH_2Cl_2 (20 mL). The target compound **9c** was isolated as a yellow oil and was used without further purification in 90 % yield R_f = 0.55 (petroleum ether 9.5:0.5 ethyl acetate).

δ_H /ppm (400 MHz; $CDCl_3$) 9.51 (1H, d, *J = 7.6 Hz,* H_{11}), 6.86 (1H, dt, *J = 15.6, 6.8 Hz,* H_{10}), 6.09-6.15 (1 H, m, H_9), 2.31-2.37 (2H, m, H_7), 1.36 (8H, m, $H_{2\text{-}7}$), 0.89 (3H, t, *J = 6.4 Hz,* H_1).

6.1.3.4 General procedure 5: Wittig

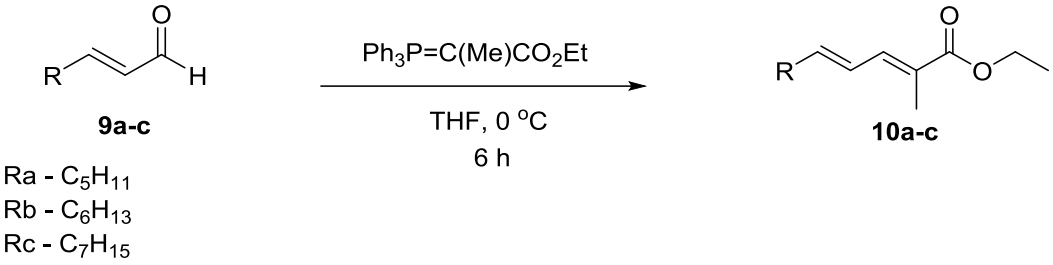

To a solution of appropriate aldehydes **9a-c** (1 eq.) in CH_2Cl_2 at 0 °C under argon was added a solution of (arbethoxyethylidene)triphenylphosphorane (1.2 eq.) in CH_2Cl_2also at 0 °C. The reaction mixture was left stirring at room temperature for 6 hours before being quenched with ammonium chloride (20 mL). The reaction mixture was transferred to a separating funnel and diluted with diethyl ether (25 mL). The organic layer was collected and the aqueous layer extracted two more times. The organic layers were combined and dried over anhydrous magnesium sulfate. The volatiles were evaporated under vacuum using a rotary evaporator. The crude mixture was purified by flash chromatography using petroleum ether 9:1 ethyl acetate.

Ethyl *(2E,4E)*- 2-methylundeca-2,4-dienoate (10a)

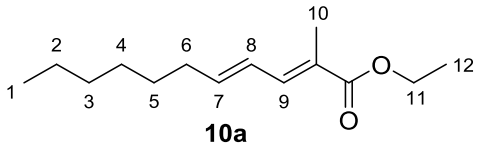

10a

Ethyl *(2E, 4E)*-2-methylundeca-2,4-dienoate (10a) was prepared using general procedure 5 using **9a** (4.23 mmol, 0.6 g, 1 eq.) in CH_2Cl_2 (15 mL) and (carbethoxyethylidene)triphenylphosphorane (5.07 mmol, 1.8 g, 1.2 eq.) in CH_2Cl_2 (10 mL). The target compound **10a** was isolated as a yellow oil 72% yield, R_f = 0.6 (petroleum ether 9:1 ethyl acetate).

δ_H /ppm (400 MHz; $CDCl_3$) 7.09 (1H, d, *J = 11.6 Hz,* H_9), 6.26 (1H, m, H_8), 6.02 (1H, quin, *J = 7.3 Hz,* H_7), 4.13 (2H, q, *J = 7.2 Hz,* H_{11}), 2.12 (2H, q, *J = 7.2 Hz,* H_6), 1.86 (3H, s, H_{10}), 1.28 (11H, m, $H_{2\text{-}5,\ 12}$), 0.81 (3H, t, *J = 7.2 Hz,* H_1).

δ_C /ppm (100 MHz; $CDCl_3$) 167.8 (*C*=O), 143.3 (*C*=C), 138.6 (*C*=C), 125.9 (*C*=C), 122.0 (*C*-CO), 60.4 (*C*H_2-O), 33.3 (*C*H_2), 31.9 (*C*H_2), 29.7 (*C*H_2), 29.4 (*C*H_2), 22.7 (*C*H_2), 14.3 (*C*H_2), 14.1 (*C*H_3), 12.6 (*C*H_3).

υ_{max}/cm^{-1} (neat) 2957, 2927, 2857, 1703, 1640, 1464, 1367, 1287, 1163, 1101, 970.

Ethyl *(2E,4E)*-2-methyldodeca-2,4-dienoate (10b)

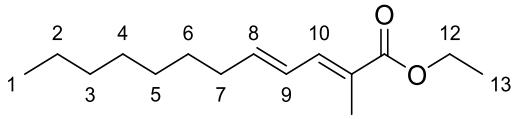

10b

Ethyl *(2E,4E)*-2-methyldodeca-2,4-dienoate (10b) was prepared using general procedure 5 using **9b** (2.88 mmol, 450 mg, 1 eq.) in CH_2Cl_2 (30 mL) and (carbethoxyethylidene)triphenylphosphorane (5.75 mmol, 2 g, 2 eq.) in CH_2Cl_2 (20 mL). The target compound **14b** was isolated as a yellow oil in 81% yield, R_f = 0.68 (petroleum ether 9:1 ethyl acetate).

δ_H /ppm (400 MHz; $CDCl_3$) 7.08 (1H, d, *J = 11.6 Hz,* H_{10}), 6.34 (1H, m, H_9), 6.06 (1H, quin, *J = 7.2 Hz,* H_8), 4.12 (2H, q, *J = 7.2 Hz,* H_{12}), 2.11 (2H, q, *J = 7.2 Hz,* H_7), 1.9 (3H, s, H_{11}), 1.22 (13H, m, $H_{2\text{-}6,\ 13}$), 0.85 (3H, t, *J = 6.8 Hz,* H_1).

δ_C /ppm (100 MHz; $CDCl_3$): 166.3 (*C*=O), 144.1 (*C*=C), 143.8 (*C*=C), 127.3 (*C*=C), 124.9 (*C*-CO), 59.1 (*C*H_2-O), 31.9 (*C*H_2), 30.8 (*C*H_2), 28.7 (*C*H_2), 28.1 (*C*H_2), 28.0 (*C*H_2), 27.7 (*C*H_2), 21.6 (*C*H_2), 13.3 (*C*H_3), 13.1 (*C*H_3).

υ_{max}/cm^{-1} (neat) 2956, 2926, 2855, 1704, 1639, 1464, 1367, 1229, 1176, 1101, 748.

ethyl *(2E,4E)*-2-methyltrideca-2,4-dienoate (10c)

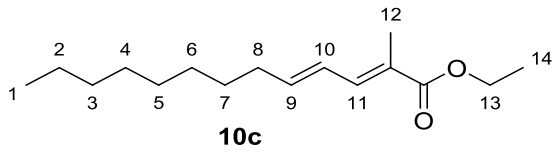

10c

ethyl (*2E,4E*)-2-methyltrideca-2,4-dienoate(10c) was prepared using general procedure 5 using **9c** (4.3 mmol, 0.72 g, 1 eq.) in CH_2Cl_2 (10 mL) and (carbethoxyethylidene)triphenylphosphorane (5.14 mmol, 1.86 g, 1.2 eq.) in CH_2Cl_2 (15 mL). The target compound **10c** was isolated as a yellow oil in 75% yield, R_f = 0.71 (petroleum ether 9:1 ethyl acetate).

δ_H /ppm (400 MHz; $CDCl_3$) 7.01 (1H, d, *J = 11.2 Hz*, H_{11}), 6.32 (1H, m, H_{10}), 6.01 (1H, quin, *J = 7.2 Hz*, H_9), 4.03 (2H, q, *J = 7.2 Hz*, H_{13}), 2.68 (2H, q, *J = 7.2 Hz*, H_8), 1.77 (3H, s, H_{12}), 1.24 (15H, m, $H_{2\text{-}7,}$ H_{14}), 0.74 (3H, t, *J = 7.2 Hz*, H_1).

δ_C /ppm (100 MHz; $CDCl_3$) 165.3 (*C*=O), 143.9 (*C*=C), 139.1 (*C*=C), 128.7 (*C*=C), 126.9 (*C*-CO), 60.8 (*C*H_2-O), 33.8 (*C*H_2), 33.5 (*C*H_2), 30.5 (*C*H_2), 30.1 (*C*H_2), 30.0 (*C*H_2), 29.9 (*C*H_2), 29.7 (*C*H_2), 23.3 (*C*H_2), 14.4 (*C*H_3), 12.7 (*C*H_3).

υ_{max}/cm^{-1} (neat) 2924, 2854, 1705, 1640, 1463, 1367, 1232, 1174, 1103, 1032, 970, 748.

6.1.3.5 General procedure 6 Hydrolysis

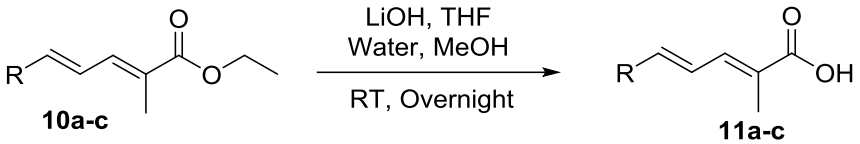

10a-c **11a-c**

R_a - C_5H_{11}
R_b - C_6H_{13}
R_c - C_7H_{15}

To a stirring solution of LiOH cooled in ice-cold water was added a solution of the appropriate ester **10a-c** in MeOH and THF, also at 0 °C. The reaction mixture was warmed to RT and stirred for 16 hours. The reaction was then cooled to 0 °C and ice cold HCl (1M) added slowly to the rapidly stirring solution until pH 1. The reaction mixture was transferred to a separating funnel and diluted with diethyl ether (20 mL). The organic layer was collected and the aqueous layer extracted two more times. The organic layers were combined and dried over anhydrous magnesium sulfate. The volatiles were evaporated under vacuum using a rotary evaporator.

(*2E,4E*)-2-Methylundeca-2,4-dienoic acid (11a)

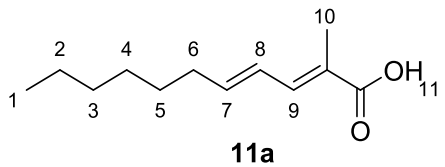

11a

(*2E,4E)*-2-Methylundeca-2,4-dienoic acid (11a) was prepared using general procedure 6 using **10a** (14.4 mmol, 345 mg, 1 eq.) in MeOH (2 mL) and THF (2 mL), LiOH (14.4 mmol, 345 mg, 15 eq.) in ice-cold water (5 mL). The target compound **11a** was isolated as white crystals and used without further purification in 70% yield.

δ_H /ppm (400 MHz; $CDCl_3$) 11.03 (1H, s, H_{11}), 7.22 (1H, d, *J = 12.4 Hz,* H_9), 6.28 (1H, m, H_8), 6.05 (1H, quin, *J = 7.2 Hz,* H_7), 2.13 (2H, q, *J = 7.2 Hz*, H_6), 1.85 (3H, s, H_{10}), 1.26 (8H, m, $H_{2\text{-}5}$), 0.80 (3H, t, *J = 7.2 Hz*, H_1).

(*2E,4E*)-2-Methyldodeca-2,4-dienoic acid (11b)

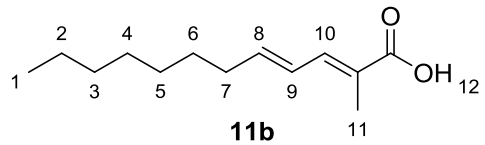

11b

(*2E,4E*)-2-methyldodeca-2,4-dienoic acid (11b) was prepared using general procedure 6 using **10b** (4.18 mmol, 1 g, 1 eq.) in MeOH (5 mL) and THF (5 mL), LiOH (63 mmol, 1.5 g, 15 eq.) in ice-cold water (3 mL) The target compound **11b** was isolated as a yellow solid and was used without further purification in 80% yield.

δ_H /ppm (400 MHz; $CDCl_3$) 12.32 (1H, s, H_{12}), 7.07 (1H, d, *J = 11.2 Hz*, H_{10}), 6.39 (1H, q, *J = 7.2 Hz*, H_9), 6.12 (1H, q, *J = 7.2 Hz*, H_8), 2.17(2H, q, *J = 7.2 Hz*, H_7), 1.83 (3H, s, H_{11}), 1.22 (10H, m, $H_{2\text{-}6}$), 0.86 (3H, t, *J = 7.2 Hz*, H_1).

(*2E,4E*)-2-Methyltrideca-2,4-dienoic acid (11c)

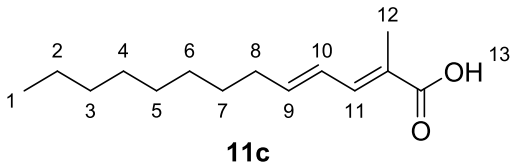

11c

(*2E,4E*)-2-Methyltrideca-2,4-dienoic acid (11c) was prepared using general procedure 6 using **10c** (0.95 mmol, 225 mg, 1 eq.) in MeOH (2 mL) and THF (2 mL), LiOH (14.2 mmol, 342 mg, 15 eq.) in ice-cold water (4 mL). The target compound **11c** was isolated as a yellow solid and was used without further purification in 89% yield.

δ_H /ppm (400 MHz; $CDCl_3$) 11.83 (1H, s, H_{13}), 7.19 (1H, d, *J = 13.6 Hz*, H_{11}), 6.28 (1H, m, H_{10}), 6.06 (1H, q, *J = 7.2 Hz*, H_9), 2.12 (2H, q, *J = 7.4 Hz*, H_8), 1.76 (3H, s, H_{12}), 1.28 (12H, m, $H_{2\text{-}7}$), 0.81 (3H, t, *J = 7.2 Hz*, H_1).

6.1.3.6 General procedure 7: Amide Coupling

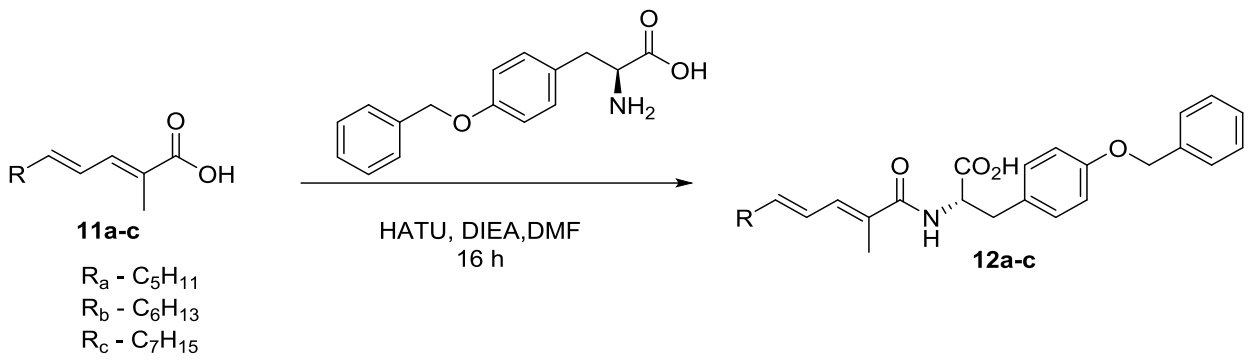

To a solution of the appropriate acid **11a-c,** in dry DMF, was added HATU and the resulting solution was stirred for 10 minutes at room temperature under argon. *O*-Benzyl-L-tyrosine was added and the resulting solution was stirred for 20 minutes before DIEA was added. The reaction mixture was stirred at room temperature for 16 hours. The solvent was removed *in vacuo* and the crude mixture was purified by flash column chromatography using as the eluent petroleum ether 8.5:1.5 ethyl acetate.

3-[4-(benzyloxy)phenyl]-2-[(*2E,4E*)-2-methylundeca-2,4-dienamido]propanoic acid (12a)

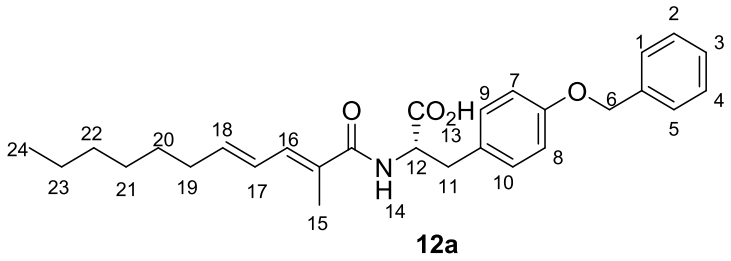

3-[4-(benzyloxy)phenyl]-2-[(*2E,4E*)-2-methylundeca-2,4-dienamido]propanoic acid (12a) was prepared using general procedure 7 using **11a** (1.12 mmol, 220 mg, 1 eq.), HATU (1.2 mmol, 420 mg, 1.1 eq.), DIEA (3.36 mmol, 1 mL, 3 eq.) and *O*-Benzyl-L-Tyrosine (1.34 mmol, 498 mg, 1.2 eq.). The target compound **12a** was isolated as a sticky, yellow oil in 80% yield.

δ_C /ppm (400 MHz; MeOD) 7.23 (5H, m, $H_{1\text{-}5,\ 14}$), 7.01 (2H, d, *J = 8.8 Hz,* $H_{7\text{-}8}$), 6.76 (2H, d, *J = 8.8 Hz,* $H_{9\text{-}10}$), 6.64 (1H, d, *J = 10.8 Hz,* H_{16}), 6.23 (1H, m, H_{17}), 5.87 (1H, m, H_{18}), 4.89 (2H, s, H_6), 4.48 (1H, m, H_{12}), 3.00 (2H, m, H_{11}), 2.05 (2H, q, *J = 7.2 Hz,* H_{19}), 1.73 (3H, s, H_{15}), 1.21 (8H, m, $H_{20\text{-}23}$), 0.79 (3H, t, *J = 7.2 Hz,* H_{24}).

δ_C /ppm (100 MHz; MeOD) 171.4 (*C*-OOH), 159.0 (*C*-Ar), 142.8 (*C*=C), 138.9 (*C*-Ar), 135.6(*C*=C), 131.6 (*C*-Ar), 131.5(*C*-Ar), 129.5 (*C*-Ar), 129.0(*C*-Ar), 128.8 (*C*-Ar), 128.6 (*C*-Ar), 127.0 (*C*=*C*), 115.7 (*C*-Ar), 71.0 (O*C*H_2-Ar), 57.0 (*C*H-NH), 37.8 (CH*C*H_2-Ar), 34.2 (*C*H_2), 32.9 (*C*H_2), 30.2 (*C*H_2), 30.0 (*C*H_2), 23.7 (*C*H_2), 14.5 (*C*H_3), 12.9 (*C*H_3).

υ_{max}/cm^{-1} (neat) 3424, 2929, 2858, 1660, 1510, 1439, 1386, 1255, 1092, 1063, 841.

LRMS (ES$^+$) calculated for $C_{28}H_{35}NO_4$ $[M+H]^+$: 450.3, found: 450.2.

3-[4-(benzyloxy)phenyl]-2-[(*2E,4E*)-2-methyldodeca-2,4-dienamido]propanoic acid (12b)

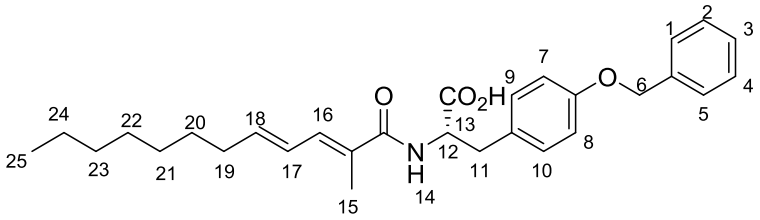

12b

3-[4-(benzyloxy)phenyl]-2-[(*2E,4E*)-2-methyldodeca-2,4-dienamido]propanoic acid (12b) was prepared using general procedure 7 using **11b** (0.63 mmol, 132 mg ,1 eq.), HATU (0.69 mmol, 242 mg, 1.1 eq.), DIEA (1.89 mmol, 0.6 mL, 3 eq.), *O*-Benzyl-L-Tyrosine (0.76 mmol, 283 mg, 1.2 eq.) and dry DMF (5 mL). The target compound **12b** was isolated as a sticky, yellow oil in 85% yield.

δ_H /ppm (400 MHz; CD_3CN) 7.31 (5H, m, $H_{1\text{-}5}$), 7.07 (2H, d, *J = 8.4 Hz,* $H_{7\text{-}8}$), 6.83 (2H, d, *J = 8.4 Hz,* $H_{9\text{-}10}$), 6.65 (1H, d, *J = 11.2 Hz,* H_{16}), 6.55 (1H, d, *J = 7.6 Hz,* H_{14}), 6.29

(1H, m, H_{17}), 5.95 (1H, m, H_{18}), 4.97 (2H, s, H_6), 4.50 (1H, m, H_{12}), 3.00 (2H, m, H_{11}), 2.08 (2H, q, *J = 7.6 Hz,* H_{19}), 1.73 (3H, s, H_{15}), 1.25 (10H, m, $H_{20\text{-}24}$), 0.79 (3H, t, *J = 7.2 Hz,* H_{25}).

δ_C /ppm (100 MHz; CD_3CN); CD_3CN 172.0 (*C*-OOH), 168.9 (*C*=O), 157.3 (*C*-Ar), 141.6 (*C*-Ar), 137.1 (*C*-Ar), 134.0 (*C*=C), 130.0 (*C*-Ar), 129.2 (*C*-Ar), 128.1 (*C*-Ar), 127.5 (*C*-Ar), 127.3 (*C*-Ar), 127.2 (*C*-Ar), 125.3(*C*=C), 117.0 (*C*-Ar), 114.3 (*C*-Ar), 69.2 (O*C*H_2-Ar) , 53.9 O (*C*H-NH), 35.3 (*C*H_2), 32.4 (*C*H_2), 31.2 (*C*H_2), 29.0 (*C*H_2), 28.5 (*C*H_2), 28.5 (*C*H_2), 22.0 (*C*H_2), 3.1(*C*H_3), 11.6 (*C*H_3).

υ_{max}/cm^{-1} (neat) 3484, 2929, 2859, 1657, 1505, 1386, 1256, 1091, 1063, 843.

LRMS (ES$^+$) calculated for $C_{29}H_{37}NO_4$ $[M+H]^+$: 463.6, found: 464.2.

3-[4-(benzyloxy)phenyl]-2-[(*2E,4E*)-2-methyltrideca-2,4-dienamido]propanoic acid (12c)

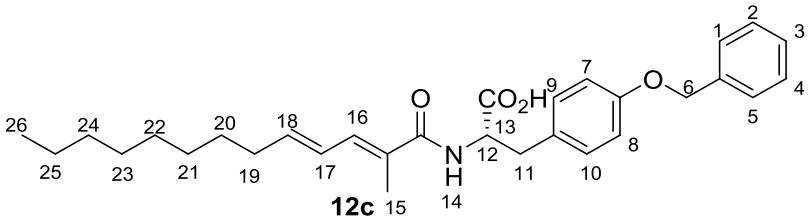

3-[4-(benzyloxy)phenyl]-2-[(*2E,4E*)-2-methyltrideca-2,4-dienamido]propanoic acid (12c) was prepared using general procedure 7 using **11c** (0.7 mmol, 147 mg, 1 eq.), HATU (0.72 mmol, 252 mg, 1.1 eq.), DIEA (2.1 mmol, 0.6 mL, 3 eq.), *O*-Benzyl-*L*-Tyrosine (0.84 mmol, 313 mg, 1.2 eq.) and dry DMF (5 mL) . The target compound **12c** was isolated as a sticky, yellow oil in 72% yield.

δ_H /ppm (400 MHz;) MeOD) 7.25(5H, m, $H_{1\text{-}5}$), 7.00 (2H, d, *J = 8.8 Hz,* $H_{7\text{-}8}$), 6.76 (2H, d, *J = 8.8 Hz,* $H_{9\text{-}10}$), 6.64 (1H, d, *J = 10.8 Hz,* H_{16}), 6.22 (1H, m, H_{17}), 5.86 (1H, m, H_{18}),

4.91 (2H, s, H_6), 4.41 (1H, m, H_{12}), 3.07 (2H, m, H_{11}), 2.07 (2H, q, *J = 6.8 Hz*, H_{19}), 1.74 (3H, s, H_{15}), 1.16 (12H, m, $H_{20\text{-}25}$), 0.79 (3H, t, *J = 6.8 Hz*, H_{26}).

υ_{max}/cm^{-1} (neat) 3329, 2925, 2855, 2487, 1609, 1512, 1381, 1240, 1177, 1026, 975.

LRMS (ES$^+$) calculated for $C_{30}H_{39}NO_4$ $[M+H]^+$: 478.3, found: 478.2.

6.1.3.7 General procedure 8: Debenzylation using boron trichloride

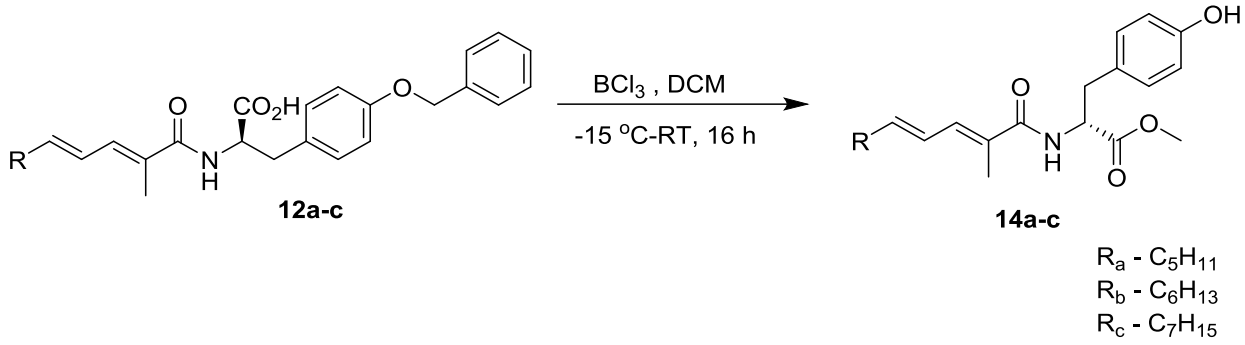

To a solution of (*E*)-3-(4-(benzyloxy) phenyl)-2-(2-methylundec-3-enamido) propanoic acid **(12a)** (1 eq.) in dry CH_2Cl_2 at -15 °C was added boron trichloride methyl sulfide complex (2 M in CH_2Cl_2, 8 eq.), dropwise. The reaction was warmed to room temperature and left stirring overnight. The reaction mixture was quenched with CH_2Cl_2/MeOH mixture and the solvent evaporated *in vacuo*.

methyl [(*2E,4E*)-2-methylundeca-2,4-dienoyl]tyrosinate (14a)

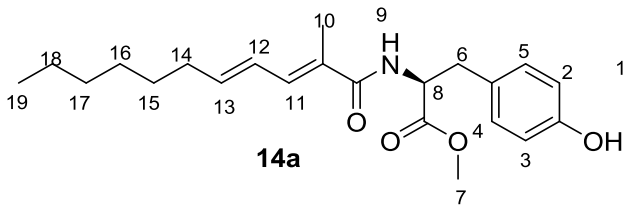

methyl [(*2E,4E*)-2-methylundeca-2,4-dienoyl]tyrosinate (14a) was synthesised according to general procedure 8 using **12a** (0.222 mmol, 100 mg, 1 eq.), boron trichloride methyl sulfide complex (1.776 mmol, 0.888 mL, 8 eq.). The product was purified using

purified using petroleum ether 4: 6 ethyl acetate and the target compound **14a** was isolated as a yellow oil in 80% yield. R_f = 0.54 (petroleum ether 4:6 ethyl acetate).

δ_H /ppm (400 MHz; $(CD_3)_2CO$) 7.13 (1H, d, *J = 8.8 Hz*, H_9), 7.08 (2H, d, *J* = 8.8 *Hz*, H_{4-5}), 6.83 (1H, d, *J* = 11.2 *Hz*, H_{11}), *(*6.76 (2H, d, *J = 8.8 Hz*, H_{2-3}), 6.39 (1H, m, H_{12}) 5.99 (1H, quin, *J = 7.2 Hz*, H_{13}), 4.68 (1H, m, H_8), 3.68 (3H, s, H_7), 3.02 (2H, m, H_6), 2.09 (2H, m , H_{14}), 1.86 (3H, s, H_{10}), 1.36 (12H, m, H_{15-18}), 0.88 (3H, t, *J = 6.8 Hz*, H_{19}).

δ_C /ppm (100 MHz; CD_3CN) 173.1 (*C*-OOMe), 169.3 (*C*=O), 157.2 (*C*-Ar), 141.2 (*C*=C), 134.5 (*C*=C), 131.1 (*C*-Ar), 129.1 (*C*-Ar), 128.8 (*C*-Ar), 126.8 (*C*=C), 116.1 (*C*-Ar), 53.9 (*C*H-NH), 51.4 (O-*C*H_3), 35.8 (CH*C*H_2-Ar), 32.4 (*C*H_2), 31.1 (*C*H_2), 28.4 (*C*H_2), 28.3 (*C*H_2), 23.3 (*C*H_2), 14.4 (*C*H_3), 12.9 (*C*H_3).

υ_{max}/cm^{-1} 3324, 2956, 2925, 2855, 1740, 1651, 1615, 1595, 1515, 1445, 1364, 1260, 1216, 1173, 1087, 1087, 1020, 971, 801, 751.

HRMS (ES$^+$) calculated for $C_{22}H_{31}NO_4$ $[M+H]^{+:}$ 374.2331, found: 374.2340.

methyl [(*2E,4E*)-2-methyldodeca-2,4-dienoyl]-L-tyrosinate (14b)

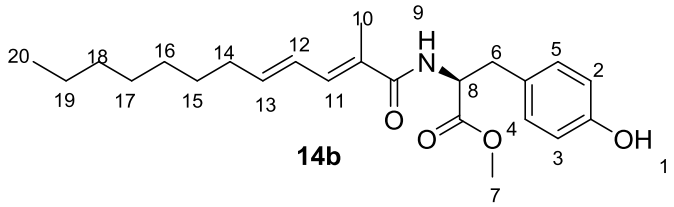

14b

methyl [(*2E,4E*)-2-methyldodeca-2,4-dienoyl]-L-tyrosinate (14b) was synthesised according to general procedure 8 using **12b** (0.323 mmol, 150 mg, 1 eq.), boron trichloride methyl sulfide complex (2.584mmol, 1.292 mL, 8 eq.). The product was purified using petroleum ether 3:7 ethyl acetate and the target compound **14b** was isolated as a yellow oil in 79% yield. R_f = 0.46 (petroleum ether 4: 6 ethyl acetate).

δ_H /ppm (400 MHz; $CDCl_3$) 6.94 (2H, d, *J = 8.4 Hz*, $H_{4\text{-}5}$), 6.63 (3H, m, $H_{2\text{-}3,\,11}$), 6.28(2H, m, H_{12}), 5.93 (1H,quin, *J = 7.6 Hz*, H_{13}), 4.54 (1H, m, H_8), 3.62 (3H, s, H_7), 2.91 (2H, m, H_6), 2.09 (2H, q, *J = 7.2 Hz*, H_{14}), 1.85 (3H, s, H_{10}), 1.30 (10H, m, $H_{15\text{-}19}$), 0.90 (3H, t, *J = 7.2 Hz*, H_{20}).

δ_C /ppm (100 MHz; $CDCl_3$) 174.9 (*C*-OOMe), 172.2 (*C*=O), 157.4 (*C*-Ar), 143.0 (*C*=C), 135.9 (*C*=C), 131.2 (*C*-Ar), 129 (*C*-Ar), 129.0 (*C*-Ar), 128.7 (*C*-Ar), 126.9 (*C*=C), 116.3 (*C*-Ar), 55.9 (*C*H-NH), 52.7 (O-*C*H_3), 37.3 (CH*C*H_2-Ar), 33.0 (*C*H_2), 30.3 (*C*H_2), 30.3 (*C*H_2), 30.2 (*C*H_2), 23.7 (*C*H_2), 14.5 (*C*H_3), 12.7 (*C*H_3).

$\upsilon_{max/}$ cm^{-1} (CH_3Cl film) 3302, 3028, 2954, 2925, 2855, 1740, 1647, 1615, 1514, 1445, 1365, 1222, 1106, 1085, 971.

HRMS (ES$^+$) calculated for $C_{23}H_{33}NO_4$ $[M+H]^{+\cdot}$388.2488, found: 388.2499.

Methyl [(*2E,4E*)-2-methyltrideca-2,4-dienoyl] tyrosinate (14c)

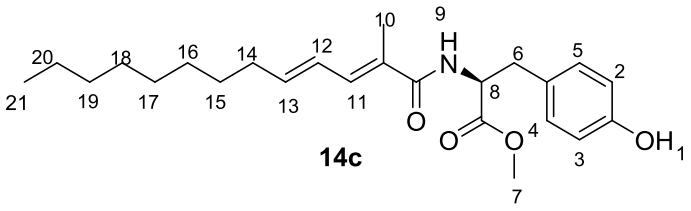

14c

Methyl [(*2E,4E*)-2-methyltrideca-2,4-dienoyl] tyrosinate (14c) was synthesised according to general procedure 8 using **12c** (0.167 mmol, 80 mg, 1 eq.), boron trichloride methyl sulfide complex (1.336 mmol, 0.668 mL, 8 eq.). The product was purified using petroleum ether 3: 7 ethyl acetate. The target compound **14c** was isolated as a yellow oil in 72% yield. R_f = 0.35 (petroleum ether 6: 4 ethyl acetate).

δ_H /ppm (400 MHz; CD_3CN) 7.18 (1H, s, H_1), 7.05 (2H, d, *J =7.6 Hz*, $H_{4\text{-}5}$), 6.76 (3H, m, $H_{2\text{-}3,\,11}$), 6.68 (1H, d, *J = 7.6 Hz*, H_9), 6.38 (2H, m, H_{12}), 6.06 (1H, quin, *J = 7.6 Hz*,

H_{13}), 4.64 (1H, m, H_8), 3.68 (3H, s, H_7), 3.02 (2H, m, H_6), 2.13 (2H, q, *J = 7.2 Hz*, H_{14}), 1.86 (3H, s, H_{10}), 1.37 (12H, m, $H_{15\text{-}20}$), 0.91 (3H, t, *J = 7.2 Hz*, H_{21}).

δ_C /ppm (100 MHz; CD_3CN) 171.9 (*C*-OOMe), 168.4 (*C*=O), 155.5 (*C*-Ar), 141.4 (*C*=C), 133.7 (*C*=C), 129.9 (*C*-Ar), 127.7 (*C*-Ar), 127.3 (*C*=C), 125.3 (*C*-Ar), 114.8 (*C*-Ar), 53.9 (*C*H-NH), 51.4 (O-*C*H_3), 35.9 (CH*C*H_2-Ar), 32.4 (*C*H_2), 31.3 (*C*H_2), 28.8 (*C*H_2), 28.7 (*C*H_2), 28.6 (*C*H_2), 28.4 (*C*H_2), 22.1 (*C*H_2), 13.1 (*C*H_3), 11.7 (*C*H_3).

υ_{max}/cm^{-1} (CH_3Cl film) 3306, 2955, 2926, 2856, 1740, 1648, 1615, 1595, 1515, 1445, 1366, 1261, 1216, 1086, 1023, 803, 750.

HRMS (ES$^+$) calculated for $C_{24}H_{35}NO_4$ $[M+H]^{+:}$ 402.2644, found: 402.2631.

6.1.3.8 General procedure 9: Debenzylation using boron trichloride

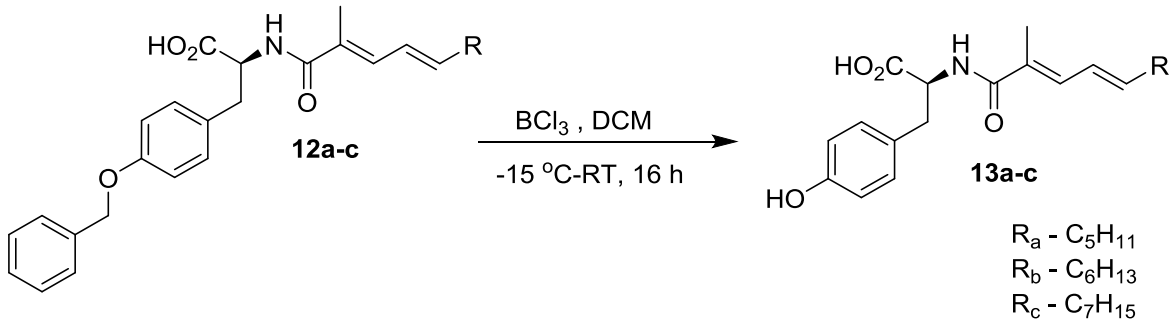

To a solution of (E)-3-(4-(benzyloxy) phenyl)-2-(2-methylundec-3-enamido) propanoic acid **(12a)** (1 eq.) in dry CH_2Cl_2 at -15 °C was added boron trichloride methyl sulfide complex (2 M in CH_2Cl_2, 8 eq.), dropwise. The reaction was warmed to room temperature and left stirring overnight. The reaction mixture was quenched with water. The mixture was transferred to a separating funnel and diluted with dichloromethane. The organic layer was collected and the aqueous layer extracted three times using dichloromethane. The organic layers were combined and dried over magnesium sulfate. The volatiles were evaporated under vacuum using a rotary evaporator.

Methyl [(*2E,4E*)-2-methylundeca-2,4-dienoyl]tyrosinate (13a)

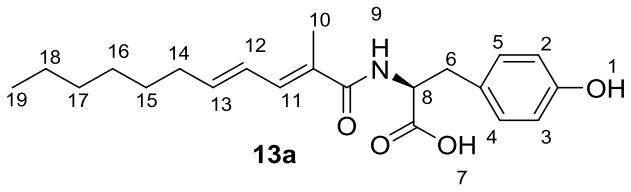

13a

Methyl [(*2E,4E*)-2-methylundeca-2,4-dienoyl]tyrosinate (13a) was synthesised according to general procedure 9 using **12a** (0.222 mmol, 100 mg, 1 eq.), boron trichloride methyl sulfide complex (1.776 mmol, 0.888 mL, 8 eq.). The product was purified using 10% MeOH in CH_2Cl_2 and the target compound **13a** was isolated as a yellow oil.

δ_H /ppm (400 MHz; MeOD) 6.91 (2H, d, *J =8 Hz*, $H_{4\text{-}5}$), 6.67 (2H, d, *J =11.2 Hz*, H_{11}), 6.56 (1H, d, *J =8 Hz*, $H_{2\text{-}3}$), 6.24 (1H, m, H_{12}), 5.90 (1H, m, H_{13}), 4.39 (1H, s, H_8), 2.87 (2H, m, H_6), 2.09 (2H, q, *J = 7.2 Hz*, H_{14}), 1.76 (3H, s, H_{10}), 1.27 (8H, m, $H_{15\text{-}18}$), 0.79 (3H, t, H_{19}).

υ_{max}/cm^{-1} 3290, 3015, 2956, 2925, 2854, 1707, 1614, 1591, 1514, 1446, 1386, 1234, 1106, 969, 806, 753.

HRMS (ES$^+$) calculated for $C_{21}H_{29}NO_4$ $[M+H]^+$: 360.2175, found: 360.2186.

[(*2E,4E*)-2-methyldodeca-2,4-dienoyl]tyrosine (13b)

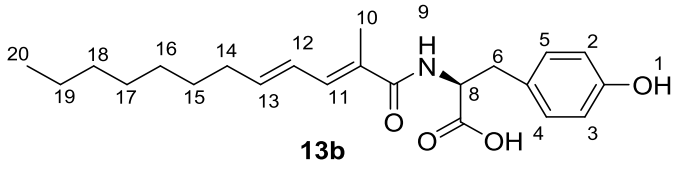

13b

[(*2E,4E*)-2-methyldodeca-2,4-dienoyl]tyrosine (13b) was synthesised according to general procedure 9 using **12b** (0.323 mmol, 150 mg, 1 eq.), boron trichloride methyl sulfide complex (2.584 mmol, 1.292 mL, 8 eq.). The product was purified using purified using 10% MeOH in CH_2Cl_2 and the target compound **13b** was isolated as a yellow oil.

δ_H /ppm (400 MHz; MeOD) 6.94 (2H, m, H_{4-5}), 6.61 (2H, m, $H_{11, 2-3}$), 6.26 (1H, m, H_{12}), 5.92 (1H, m, H_{13}), 4.54 (1H, m, H_8), 2.98 (2H, m, H_6), 2.10 (2H, m H_{14}), 1.76 (3H, s, H_{10}), 1.20 (H_{15-19}), 0.80 (3H, t, H_{20}).

υ_{max}/cm^{-1} 3336, 2970, 2927, 2858, 1595, 1516, 1466, 1380, 1303, 1261, 1161, 1128, 1106, 1026, 816.

HRMS (ES$^+$) calculated for $C_{22}H_{31}NO_4$ $[M+H]^{+:}$ 374.2331, found: 374.2338.

[(*2E,4E*)-2-methyltrideca-2,4-dienoyl]tyrosine (13c)

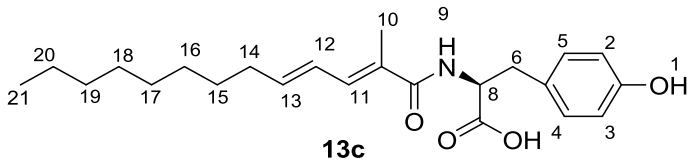

13c

[(*2E, 4E*)-2-methyltrideca-2, 4-dienoyl]tyrosine (13c) was synthesised according to general procedure 9 using **12c** (0.167 mmol, 80 mg, 1 eq.), boron trichloride methyl sulfide complex (1.336 mmol, 0.668 mL, 8 eq.). The product was purified using 10% MeOH in CH_2Cl_2 and the target compound **13c** was isolated as a yellow oil.

δ_H /ppm (400 MHz; MeOD) 6.90 (2H, d, *J =12 Hz*, H_{4-5}), 6.67 (2H, d, *J =12 Hz*, H_{11}), 6.55 (2H, d, *J =8.4 Hz*, H_{2-3}), 6.26 (1H, m, H_{12}), 5.89 (1H, m, H_{13}), 4.41 (1H, s-broad, H_8), 2.97 (2H, m, H_6), 2.09 (2H, q, *J = 7.2 Hz*, H_{14}), 1.76 (3H, s, H_{10}), 1.27 (broad), 0.77-0.82 (3H, t, H_{21}).

υ_{max}/cm^{-1} 3336, 2970, 2929, 1595, 1466, 1379, 1305, 1161, 1128, 1107, 817.

HRMS (ES$^+$) calculated for $C_{23}H_{33}NO_4$ $[M+H]^{+:}$ 388.2488, found: 388.2491.

6.1.4 Attempted amide coupling

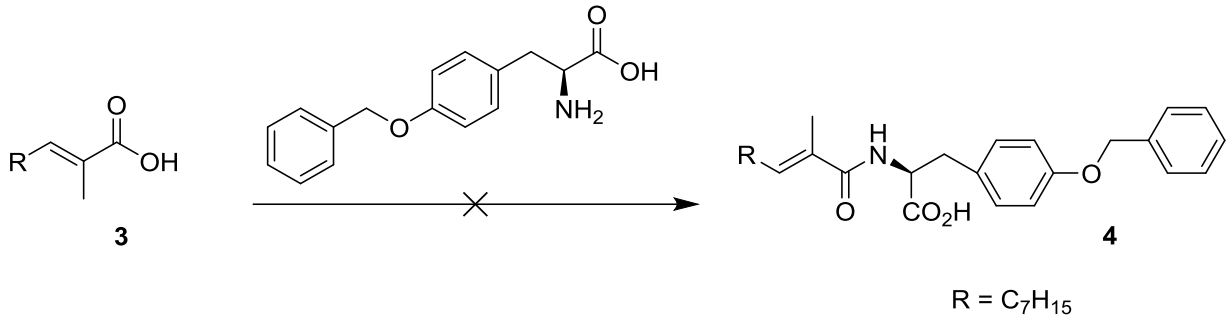

Amide coupling was attempted using the following procedures.

Entry	Coupling reagent	Additive	Base	Reaction time	Temp
1	Oxalyl chloride	DMF No DMF	Et_3N	6 – 24 h	RT, 50 ° C, 70 ° C
2	EDC	HOBt No HOBt	DMAP DIEA	12 – 24 h	RT

6.1.5 Attempted Debenzylation

6.1.5.1 Debenzylation using H_2

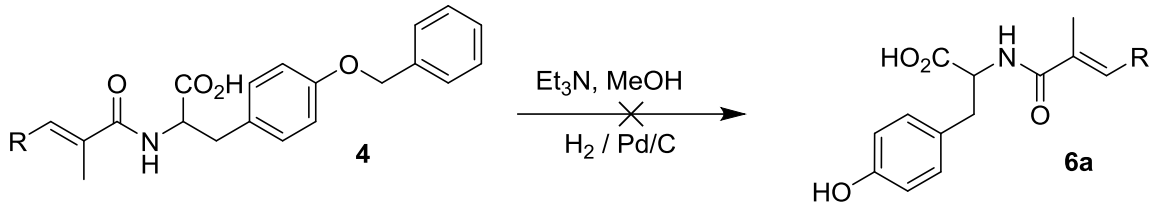

A mixture of methyl 2-((E)-2-methyldec-2-enamido)-3-(4-(benzyloxy) phenyl) propanoate **(4)** (0.45 mmol, 200 mg, 1 eq.), triethylamine, Pd/C (20 mg) and methanol (3 mL) was stirred under hydrogen atmosphere (balloon) at room temperature. The desired product was not formed.

6.1.5.2 Debenzylation using Et_3SiH

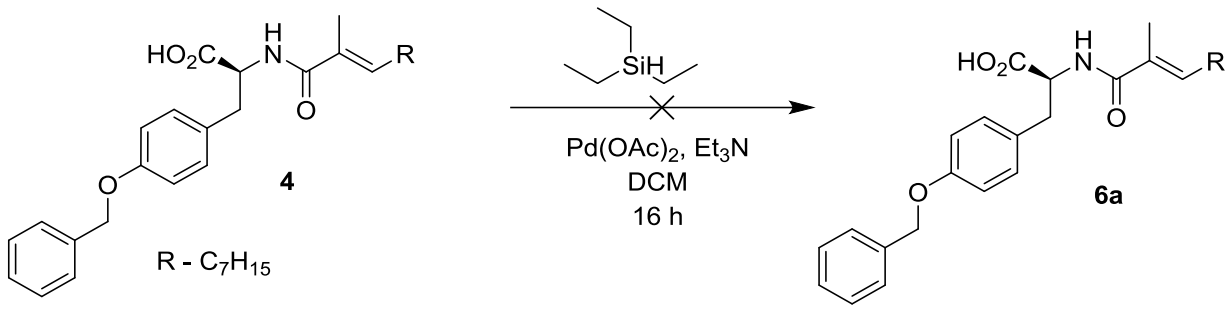

A solution of Pd $(OAc)_2$ (0.048 mmol, 1.07 mg, 0.04 eq.), Et_3SiH (0.16 mmol, 0.03 mL, 1.4 eq.) and Et_3N (0.02 mmol, 0.02 mL, 0.14 eq.) in anhydrous CH_2Cl_2 (4 mL) was stirred at room temperature under argon for 15 minutes. A solution of **4** (0.12 mmol, 50 mg, 1 eq.) in CH_2Cl_2 (2 mL) also under argon was added dropwise. The resulting mixture was stirred at room temperature under argon overnight before quenching using ammonium chloride (15 mL). The aqueous layer was extracted with CH_2Cl_22 (2 x 10 mL) and the

combined organic extracts were washed with brine (15 mL), dried under magnesium sulfate and the volatiles removed *in vacuo*. No product was formed.

6.2 Part B: Cytotoxicity assays using MTT and Alamar blue

6.2.1 Materials and instrumentation

The A549 cell line was obtained from the lab stock. Dulbecco's modified Eagles medium, foetal bovine serum (FBS), 3-(4, 5-dimethylthiazol-2-yl)-2, 5-diphenyltetrazolium bromide (MTT), resazurin sodium salt (Alamar Blue® (AB)) were purchased from Sigma Aldrich. All consumables were purchased from VWR. Cell counting was performed using a Beckmann Counter. Absorbance was measured using TECAN GENios multi plate reader.

6.2.1.1 Preparation of PBS solution

PBS solution was prepared by dissolving potassium phosphate monobasic (1.065 g, 7.5 mmol), sodium phosphate monobasic dihydrate (0.389 g, 2.5 mmol) and sodium chloride (8.498 g, 145 mmol) in ultra-pure water. The solution was made up to the mark using ultra-pure water and autoclaved for 20 minutes @ 121.5 °C and 15 psi.

6.2.1.2 Preparation of PBS-EDTA solution

PBS-EDTA solution was prepared by adding ethylenediaminetetraacetic acid (0.1 g, 0.34 mmol) to 500 mL of PBS solution prepared in section 7.1.6.1. The solution was autoclaved for 20 minutes @ 121.5 °C and 15 psi.

6.2.2 Procedures

Cells were maintained in Dulbecco's modified Eagles' media supplemented with FBS (10% v/v). Cells were sub cultured every 3-4 days. All cells were incubated at 37 °C in a

humidified atmosphere with 5% CO_2. Cells were harvested when they were in exponential or log phase. The cells were evaluated to ensure health and correct confluence by visualisation using a light microscope. The cells were then trypsinised and suspended in fresh media. Working solutions were prepared before use by preparing a stock solution in DMSO and dilution of the stock using medium (maximum concentration of DMSO used was 1%). Control assays were carried out on all experiments with 100% media (positive control) and 10% v/v DMSO (negative control). Stock solutions of MTT and AB were prepared up to 6 hours in advance and stored in darkness for up to three days. Trypsin was prepared in advance and stored for up to two weeks at 4 °C. Working solutions for MTT and AB were made immediately before use by diluting the stock solution with appropriate medium.

6.2.3 Procedure for trypsinising (splitting) cells

The cells were visually assessed under a light microscope. Old media was decanted from the flask into a waste beaker. The flask was rinsed with PBS to remove any dead cells. To the flask was added trypsin-EDTA solution (3 mL) and the cells were incubated at 37 °C for 5 -10 minutes. Trypsin-EDTA solution was prepared by asceptically adding 10 mL Vercene (EDTA) to an aliquot of trypsin (10 mL). The cells were returned to the laminar hood and sterile media (15 mL) added to neutralise the trypsin. The cell suspension was asceptically decanted into sterilin (25 mL). To a new flask, was added fresh media (15 mL). Cell suspension (500 μL) was added to the flask containing fresh media and the flask sealed. The cells were then incubated at 37 ° C in a humidified atmosphere with 5% CO_2. The health of the cells was assessed every 24 hours and trypsinisation carried out every 3 – 4 days. Only cells showing normal health were used for experiments.

6.2.4 Cytotoxicity Assays

6.2.4.1 Procedure for MTT assay

Part A: All experiments were carried out in triplicate. Cell count was performed using a haemocytometer. Stock solutions of cell suspensions were prepared depending on the length of exposure as shown in Table 6.1 below.

Exposure duration	Cell suspension concentration
24 h	1.2×10^5
48 h	5×10^4
72 h	3×10^4

Table 6.1: Cell suspension concentrations for various exposure duration.

The desired cells were seeded into 96-well microtitre plates with 100 µL of the appropriate cell concentration. The cells were incubated for 24 h in order to attach to the plate. Drug stock solutions were prepared in DMSO (1%). Final test concentrations were prepared by diluting the stock solution with medium. The cells were exposed to 5 drug concentrations, including a positive and negative control in 8 replicate wells per plate. Following exposure, the plates were incubated for the desired time; 24, 48 or 72 hours.

Part B: The assay was terminated by discarding supernatant media and rinsing with sterile PBS. MTT stock solution was prepared by adding MTT (20 mg) to sterile PBS (10 mL) followed by filter sterilisation. To each well, was added MTT (100 µL) (10% in unsupplemented fresh media) and the plates further incubated for 3 hours. During this time, viable cells absorbed and metabolised the MTT. After the three hours, the supernatant was removed and the cells washed with PBS to remove unmetabolised MTT. The remaining formazan was solubilised in DMSO (100 µL) and the plates shaken at 240

RPM for 10 minutes. The plates were placed in a plate reader and the absorbance of each solution read and recorded at 570nm. The percentage viability was calculated using corrected absorbance readings as follows:

$$\%\ viability = \frac{average\ absorbance\ of\ treated\ cells}{average\ absorbance\ of\ control} \times 100$$

6.2.4.2 Procedure for AB assay

Following part A from procedure for MTT assay, the assay was terminated by discarding supernatant media and rinsing with sterile PBS. AB stock solution was prepared by adding 0.5 mL sterile AB dye to 10 mL unsupplemented media. To each well, was added 100 µL of the AB solution and the plates further incubated for 3 hours. The plates were placed in a plate reader and each solution read and recorded using 540 nm excitation and 650 nm emission. The percentage viability was calculated using corrected absorbance readings as follows:

$$\%\ viability = \frac{average\ absorbance\ of\ treated\ cells}{average\ absorbance\ of\ control} \times 100$$

6.2.5 Preparation of cell suspensions and control and drug solutions

6.2.5.1 Working cell suspensions

Each cell suspension was diluted in supplemented media to give the appropriate cell density, dependent on period of exposure. The cell densities used were 1.2 x 10^5 cells/well for 24 h timepoint, 5 x 10^4 for 48 h timepoint and 3 x 10^4 for 72 h timepoint.

6.2.5.2 Preparation of drug solutions (700 µM)

Drug stock solutions were prepared in DMSO. All final drug solutions contained DMSO at a concentration no greater than 1%. The range of solutions were created by serial dilutions within the plates.

6.2.6 Plate seeding procedure

a) 100 µL of the appropriate cell suspension was added to **lanes 1 to 12** of each plate, with 8 replicates per lane.

b) The plates were incubated at 37 °C in a humidified 5% CO_2 atmosphere for 24 hours to allow for attachment.

c) After 24 h, the media was discarded and each well rinsed with 100 µL sterile PBS

d) To **lanes 1 - 11** of the plate was added 100 µL supplemented media

e) To **lane 12** was added 100 µL of 1% DMSO in supplemented media.

f) To **lane 11** was added 100µL of 350 µM drug solution, followed by serial dilutions to **lanes 10 – 7**.

g) To **lane 6** was added 100µL of 700 µM of a different drug solution, followed by serial dilutions to **lanes 5 – 2**.

h) Contents of each well were mixed by carefully pipetting up and down gently up to three times.

i) The plates were incubated at 37 °C in a humidified 5% CO_2 atmosphere for the desired times (24, 48 or 72 hours).

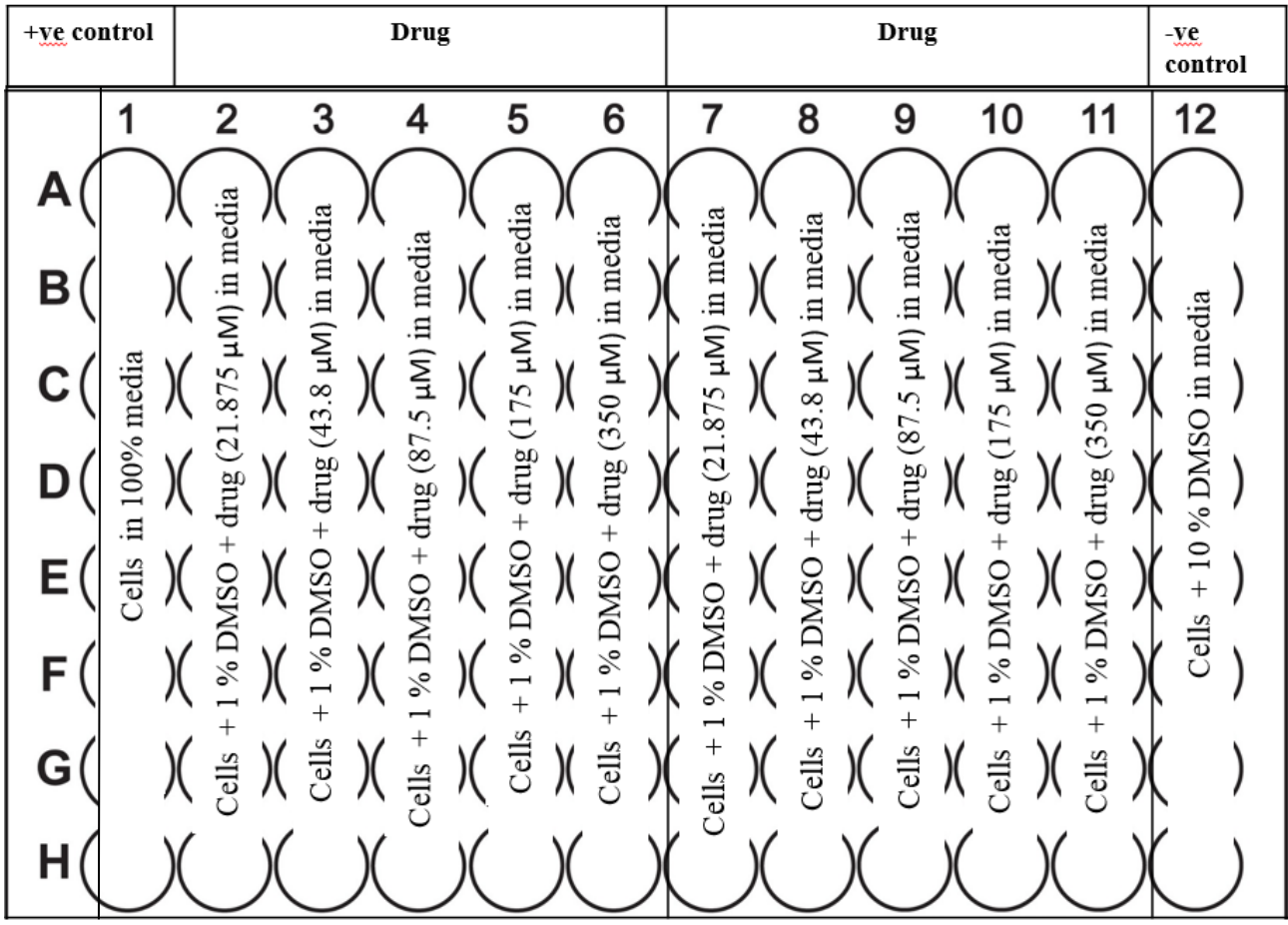

Figure 6.1: 96-Well plate set up for MTT assay with suspension cells, A549. 2 compounds at 5 drug concentrations were assessed per plate

6.2.7 MTT Exposure and absorbance reading

A stock solution of MTT in sterile PBS (10 mg/5 mL) was prepared and filter sterilised. MTT stock solution was diluted in unsupplemented media (10% v/v). Following exposure for the appropriate time, the test solutions were discarded from plates and each plate was rinsed with 100 µL sterile PBS. 100 µL of the MTT solution was added to each well and the plates were incubated at 37 ° C for 3 hours. The supernatant was carefully discarded and the plates rinsed with PBS. 100 µL DMSO was carefully added to each well and the plates shaken at 240 RPM for 10 minutes. The plates were placed in a plate reader and the absorbance of each solution read and recorded at 570 nm.

6.2.8 AB Exposure and absorbance reading

A stock solution of AB in sterile unsupplemented medium (0.5 mL/10 mL) was prepared. Following exposure for the appropriate time, the test solutions were discarded from plates and each plate rinsed with 100 μL sterile PBS. 100 μL of the AB solution was added to each well and the plates were incubated at 37 ° C for 3 hours. The plates were placed in a plate reader and each solution read and recorded using 540 nm excitation and 650 nm emission.

6.3 Part C: ELISA Assay

6.3.1 Materials and instrumentation

A FIRELISA Human PLK-1 ELISA Kit Assay purchased from Medical Supply Co. Ltd was used. The A549 cell line used was obtained from the lab stock. Dulbecco's modified Eagles medium, foetal bovine serum (FBS) were purchased from Sigma Aldrich. All consumables were purchased from VWR. Cell counting was performed using a Beckmann Counter. Absorbance was measured using TECAN GENios multi plate reader.

6.3.2 Preparation of samples and standards

6.3.2.1 Preparation of cell suspensions and seeding procedure

Cell suspension was diluted in supplemented media to give the appropriate cell density. The cell densities used were 5 x 10^5 cells/well. The desired cells were seeded into 6-well microtitre plates with 2 mL of the appropriate cell concentration. The cells were incubated for 24 h in order to attach to the plate. Drug stock solutions were prepared in DMSO (1%). Final test concentrations were prepared by diluting the stock solution with medium. The cells were exposed to drug concentrations, including a positive control for 5 different time points. Following exposure, the plates were incubated for the desired times.

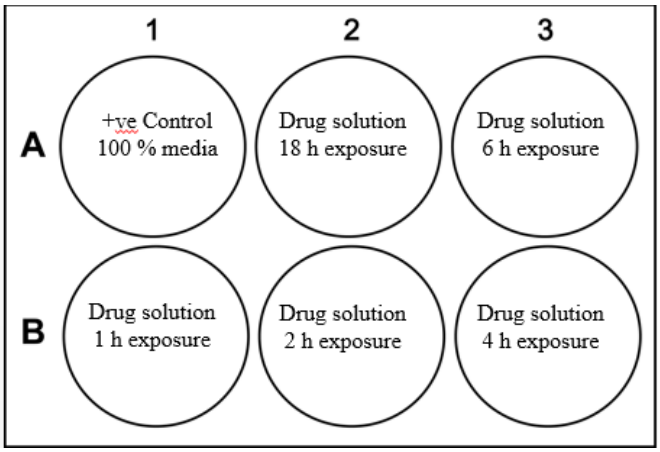

Figure 6.2: 6 well plate design for preparation of cell culture supernatant for ELISA assay.

6.3.2.2 Plate seeding procedure

a) 2 mL of the cell suspension was added to **each well** of each plate.

b) The plates were incubated at 37 ^{o}C in a humidified 5% CO_2 atmosphere for 24 hours to allow for attachment.

c) After 24 h, the media was discarded and each well rinsed with 2 mL sterile PBS

d) To **well A1, A3, B1, B2, B3** of the plate was added 2 mL supplemented media

e) To **well A2** was added the appropriate drug solution in supplemented media and the plate incubated.

f) After 12 hours, media was taken out of **well A3** and replaced with the appropriate drug concentration

g) After 2 hours, media was taken out of **well B3** and replaced with the appropriate drug concentration

h) After 2 hours, media was taken out of **well B2** and replaced with the appropriate drug concentration

i) After 1 hour, media was taken out of **well B1** and replaced with the appropriate drug concentration

j) After 1 hour, the plate was removed from the incubator and the media discarded

k) Each well was rinsed using sterile PBS and the cells trypsinised according to procedure 7.2.3. using 1 mL trypsin- EDTA and 5mL media.

l) The supernatant was collected for lysis.

6.3.2.3 Preparation of cell culture supernatant

The cell supernatant collected in section 7.3.2.2 was centrifuged @ 4 °C for 20 minutes at 2500 rpm. The supernatant was discarded and the cells rinsed using sterile PBS (2 * 2 mLs). The cell pellet was diluted in 2 mL PBS and lysis performed using a sonicator. (10 seconds blast and 10 seconds rest). The sonication was repeated three times. The cells were further centrifuged @ 4 °C for 20 minutes at 2500rpm to pellet the debris. The clear supernatant was transferred to a cryogenic vial and stored at -78 °C until required for use.

6.3.2.4 Preparation of drug solutions

Drug stock solutions were prepared in DMSO. All final drug solutions contained DMSO at a concentration no greater than 1%. The range of solutions were created by serial dilutions within the plates. Final test concentrations were prepared by diluting the stock solution with medium.

6.3.2.5 Preparation of standard and Assay Procedure

The standards and assay procedure were carried out as per manufacturers manual. The 96 well plate design is shown in Figure 6.3. Lanes 11 and 12 were removed and stored at -80 °C for future work.

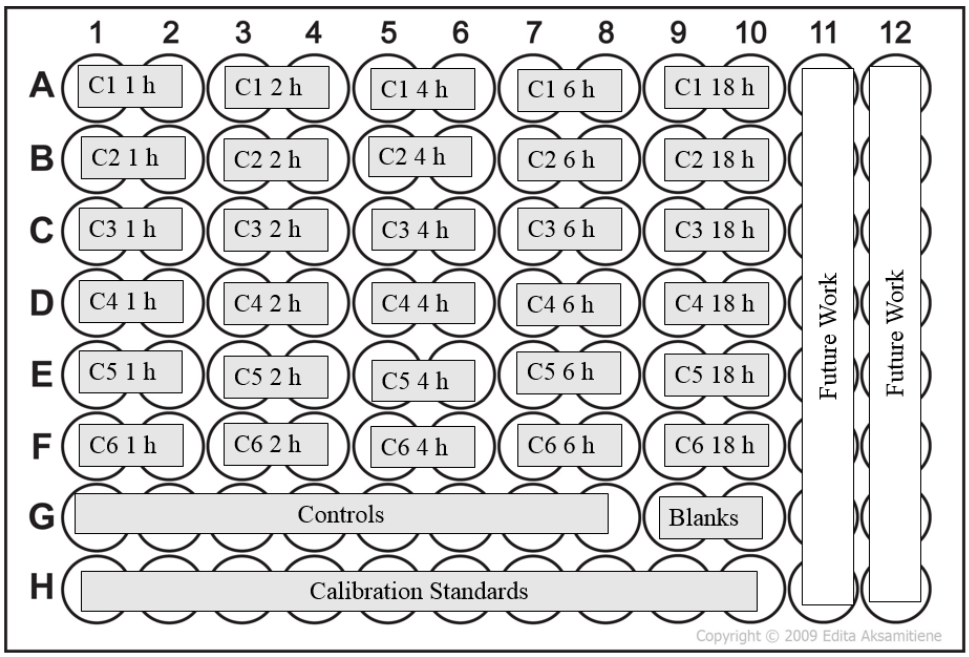

Figure 6.3: 96 well plate design for ELISA assay showing different drug solutions (C1-C6) and different time exposures (1, 2, 4, 6 and 18 hours), controls, calibration standards and blank wells.

A. Appendix

Results of the biological evaluation

Cytotoxicity data are the average of at least three experiments expressed as mean percentage viability relative to control (100 %) ± standard deviation (SD). The results have been statistically analysed using one-way analysis of variance (ANOVA) followed by a post-ANOVA Dunnett's test using GraphPad Prism software ®. Test results are considered relevant when $P < 0.05$(denoted with *) and very significant when $P < 0.01$ (denoted with #) for the Dunnets analysis. Statistical data were calculated using Microsoft excel. EC_{50} values were calculated using GraphPad Prism software ®.

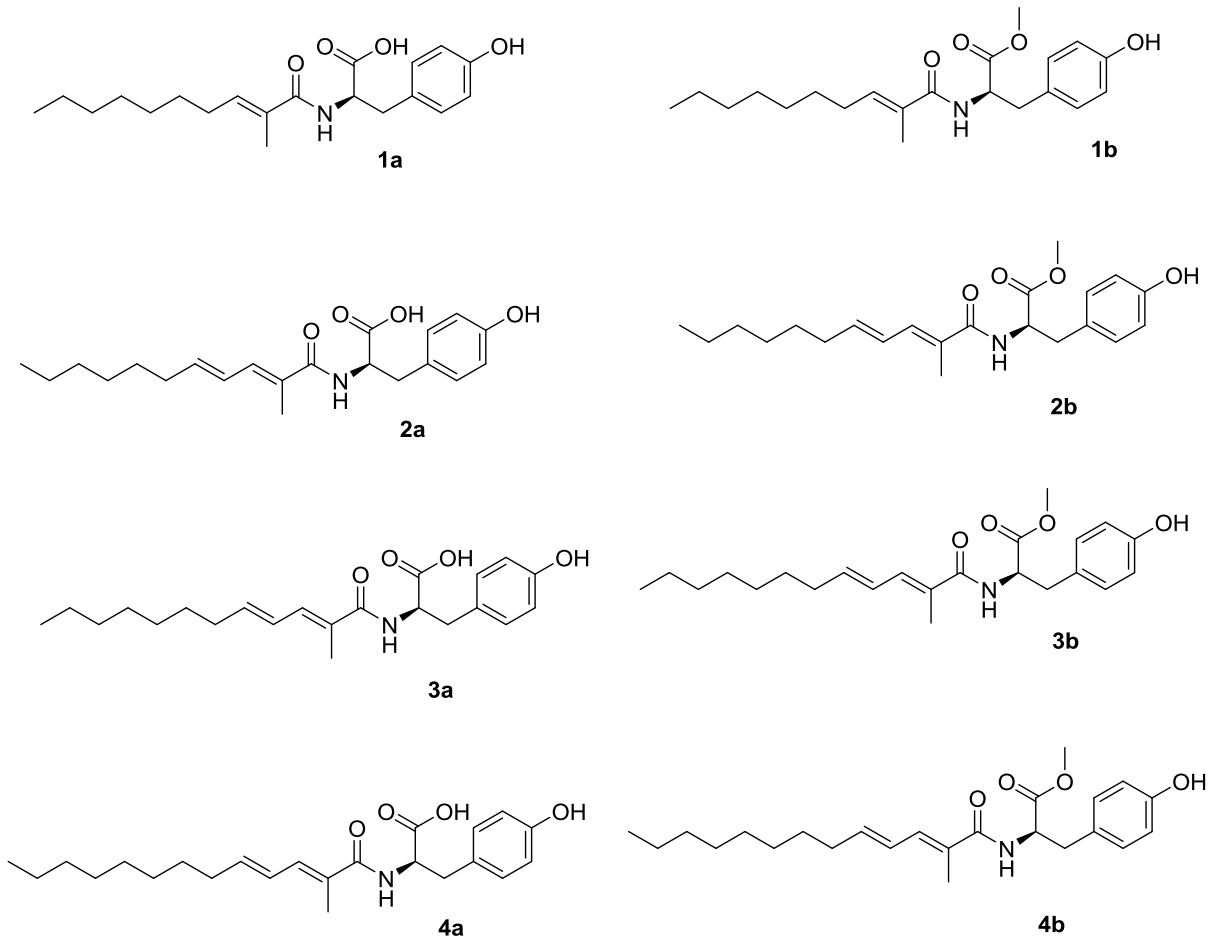

Figure A.1: Legend for Appendices

MTT Assay

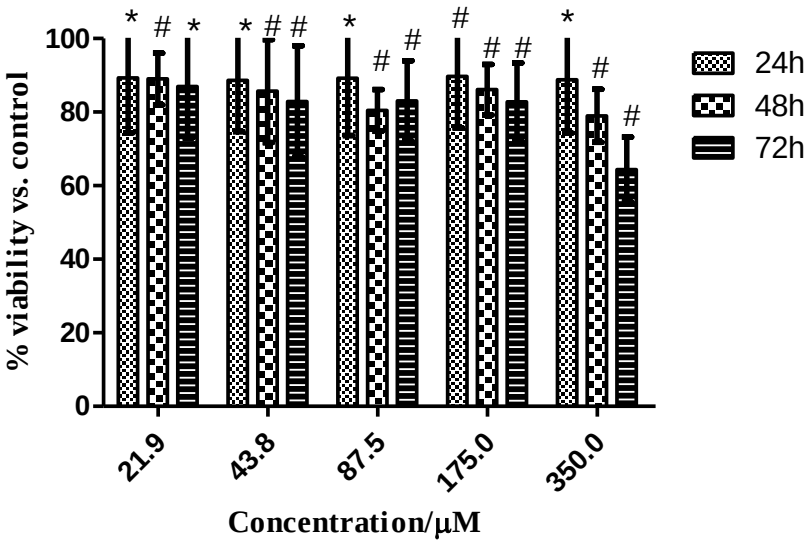

*Figure A.2: Viability of A549 versus concentration of **1a***

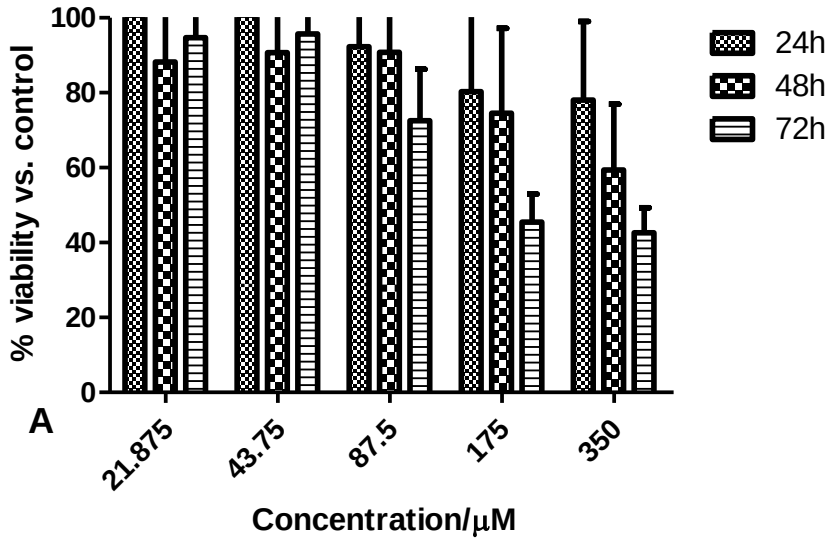

*Figure A.3: Viability of A549 versus concentration of **1b***

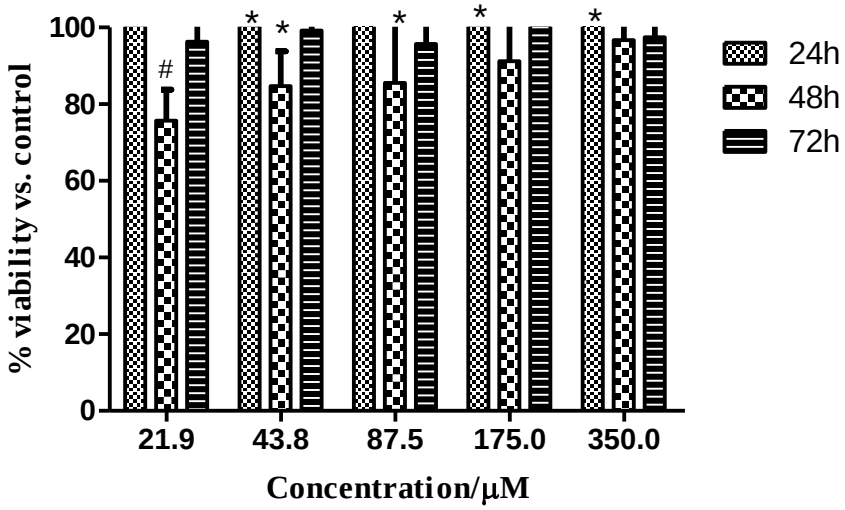

*Figure A.4: Viability of A549 versus concentration of **2a***

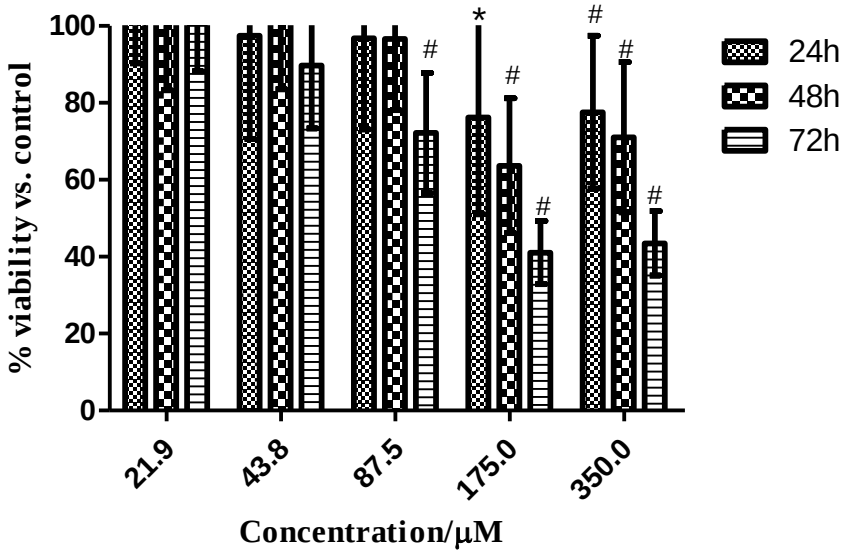

*Figure A.5: Viability of A549 versus concentration of **2b***

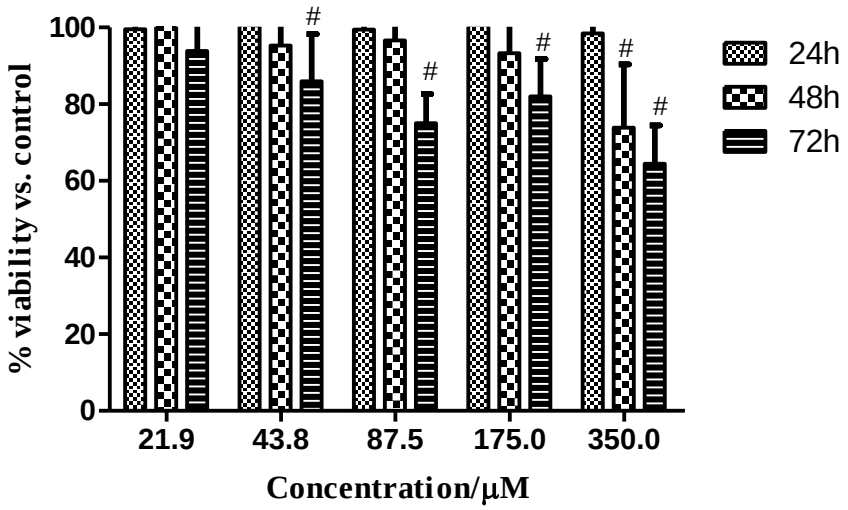

*Figure A.6: Viability of A549 versus concentration of **3a***

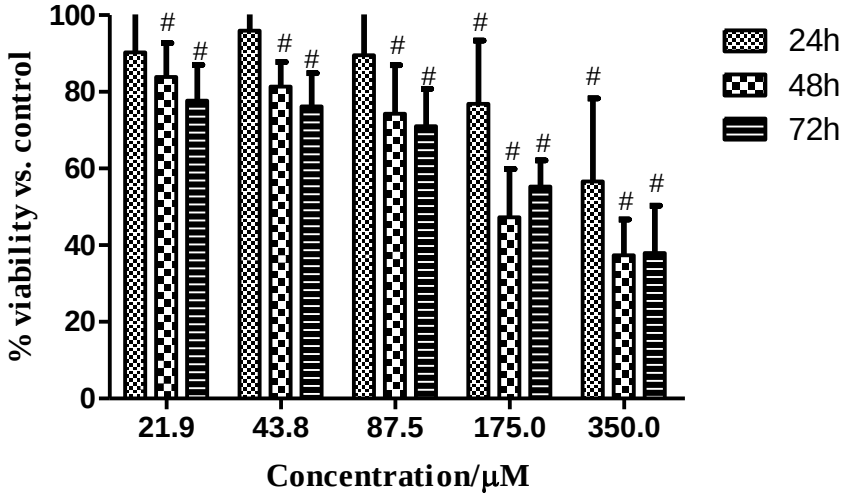

*Figure A.7: Viability of A549 versus concentration of **3b***

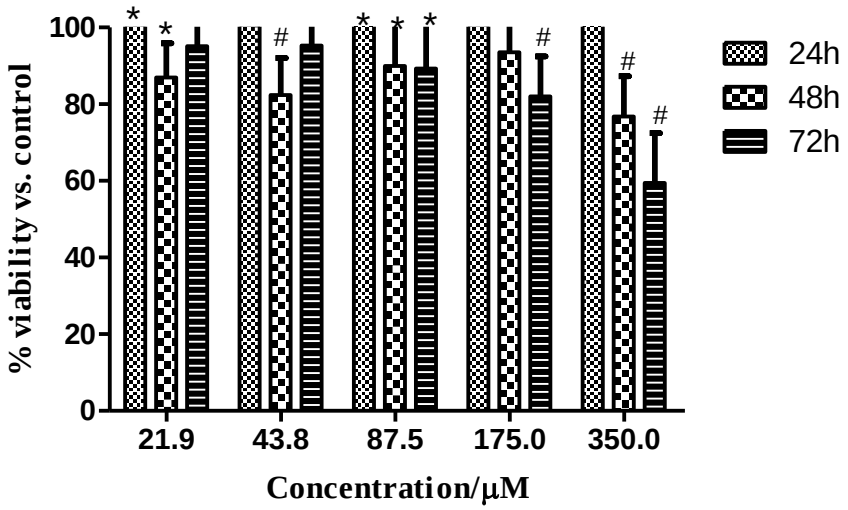

*Figure A.8: Viability of A549 versus concentration of **4a***

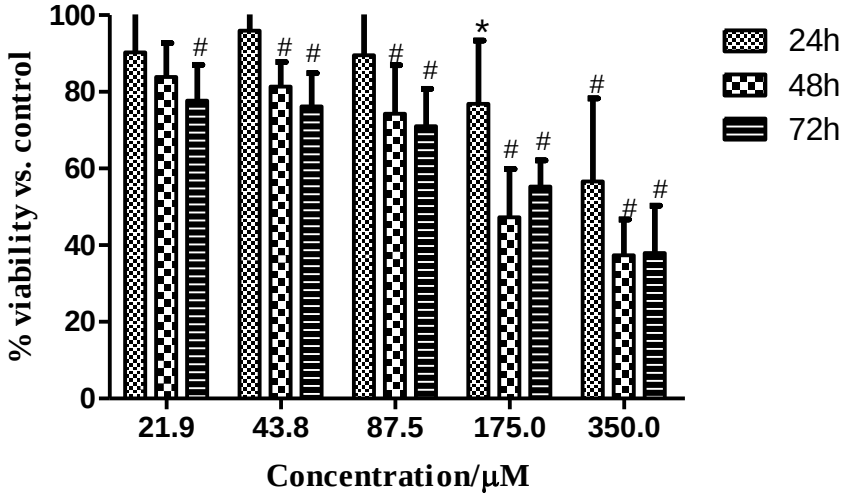

*Figure A.9: Viability of A549 versus concentration of **4b***

Alamar Blue Assay

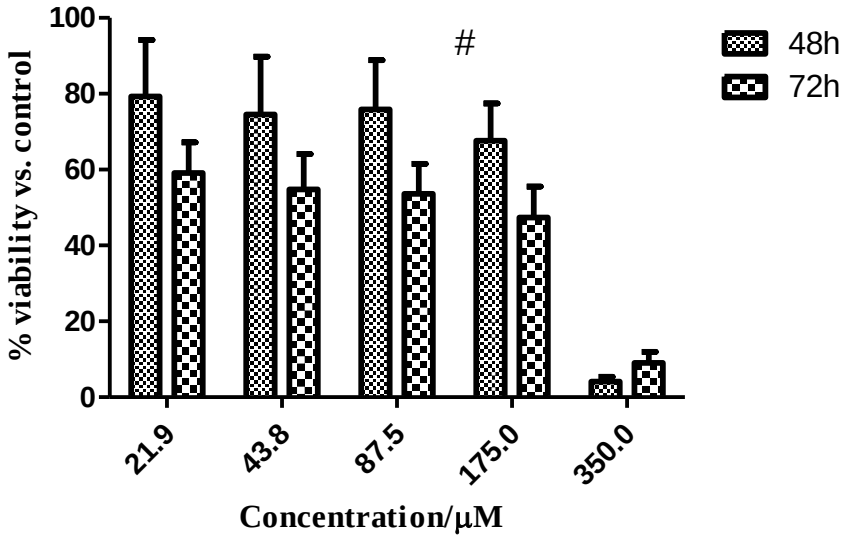

*Figure A.10: Viability of A549 versus concentration of **1b***

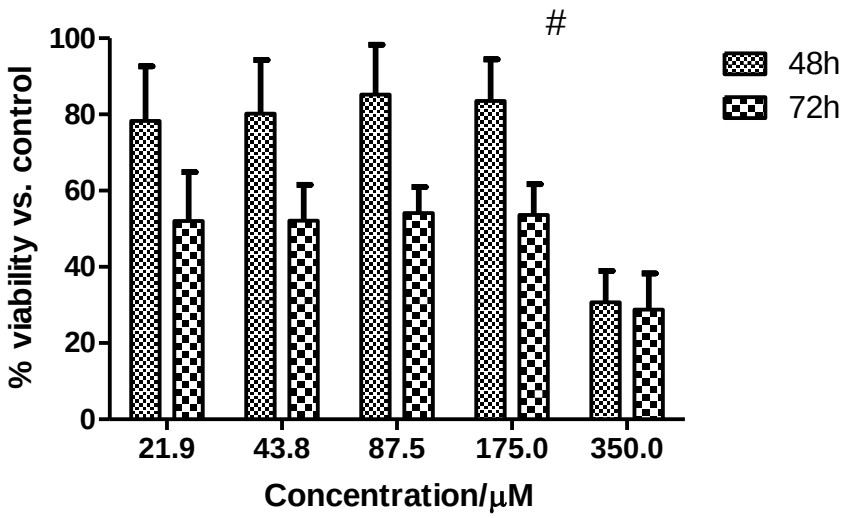

*Figure A.11: Viability of A549 versus concentration of **4a***

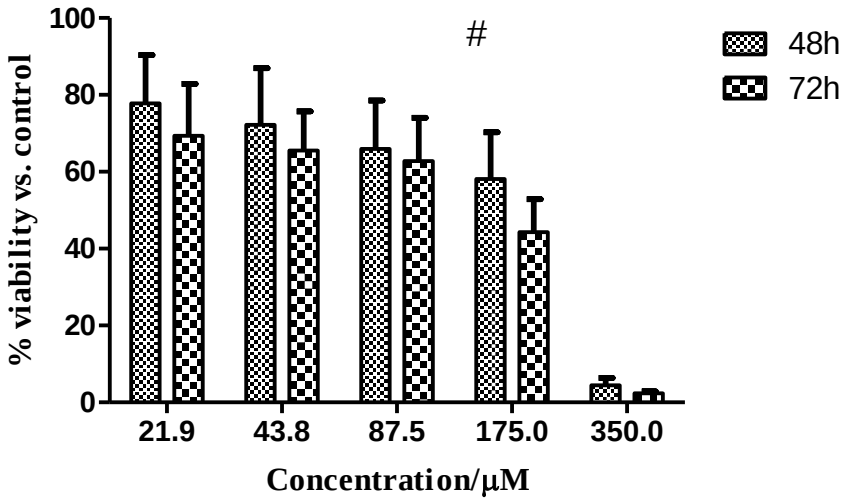

*Figure A.12: Viability of A549 versus concentration of **4b***